

Progressive Collapse of Ship Structures Under Cyclic Loading

By

Shen Li

Submitted for the degree of Doctor of Philosophy



Marine, Offshore and Subsea Technology Group

School of Engineering

Faculty of Science, Agriculture and Engineering

Newcastle University

Newcastle upon Tyne

United Kingdom

© 2021 Shen Li
Marine, Offshore and Subsea Technology Group
School of Engineering
Newcastle University
Newcastle upon Tyne
NE1 7RU
United Kingdom

“Success is not final, failure is not fatal: it is the courage to continue that counts” — Winston Churchill

Abstract

Following ultimate limit state philosophy, the structural safety of ships and ship-type floating structures are assessed by ensuring an acceptable margin between their maximum load-carrying capacity and the extreme design load. This ultimate limit state approach is established assuming that the structures are subjected to a monotonic load that leads to an elastoplastic buckling collapse. However, the environmental loads of most marine structures are of a cyclic nature. The evaluation procedure and analysis methodology for ship structures under extreme loads with multiple cycles is currently lacking.

Within this context, the aim of this research is to assess the collapse behaviour of ship structures, including plates, stiffened panels and ship hull girders, under combinations of cyclic loads and to investigate the influence of cyclic load on the ultimate strength of ship structures. Overall, four contributions have been achieved in this thesis.

A parametric nonlinear finite element study is first performed on a range of ship plates under multiple cycles of compression and tension. The outcomes of this investigation provides a new recognition, for the first time, of the buckling collapse behaviours of unstiffened plates under cyclic compression and tension. In particular the characteristic features that are relevant for ultimate limit state assessment of ship hull structures are demonstrated, such as a progressively reducing but converging compressive strength and stiffness in the reloading regime of structural members under cyclic loads as compared to those under monotonic loads.

Using observed response patterns from the numerical study, a response and updating rule methodology is proposed to predict the load-shortening curve of

structural component under cyclic load by updating the critical characteristics. The comparison with equivalent nonlinear finite element results shows an acceptable correlation. This novel method provides an efficient way to represent the cyclic buckling collapse response of structural members and is in an appropriate format for implementing in a Smith-type progressive collapse analysis for estimating the hull girder response.

Following the response and updating rule load-shortening curve methodology, an unique extension to the Smith method is introduced for predicting cyclic bending response. Case studies are completed out on several ship-type box girder structures under different combinations of cyclic loads. The validation with nonlinear finite element analysis shows the rationality of the proposed extension, and also demonstrates that the prediction of cyclic response is highly sensitive to structural component's post-collapse behaviour.

An uncertainty evaluation procedure is developed to analyse the effects of critical features of the load-shortening relationship on the hull girder response prediction. The influences of different load-shortening features, including elastic stiffness, ultimate compressive strength, ultimate strain and post-collapse stiffness, are quantified. It is indicated that the post-collapse stiffness of structural components have the largest influence as suggested by a sensitivity index. In addition, this procedure is not only useful for the cyclic response, but also the conventional assessment concerning monotonic load.

The outcome of this research work is a validated method which has the potential to improve the safety of ships by considering cyclic load effects.

Acknowledgement

In the past three years, I have received a great deal of support and assistance.

I would first like to express my greatest gratitude to my supervisor, Dr Simon Benson, who has expertly guided me throughout this doctoral research programme. His expertise in ship structural mechanics is invaluable in helping me to formulate the research topic and to develop the methodology. He has his unique style of supervision that most of his knowledges and experiences are philosophically delivered. This turns out to be an excellent approach for me to work with him, as it has unlimited myself to explore more prospective options, rather than being constrained by a certain direction. It is enjoyable to be his research student.

I would also like to thank my co-supervisor, Professor Zhiqiang Hu. I still remember three years ago, Professor Hu encouraged me that completing a PhD is all about persistence. His words always cheer me up when I am facing difficulty.

In addition, I would like to acknowledge Dr Do Kyun Kim, who has given me a new perspective in ship structural analysis. Dr Kim joined the university when I was in the final year of my study. His experience and also the passion in particular have enriched my way of thinking toward research as well as future career. A big thank to him.

Meanwhile, I would like to express my very best wishes to all the research students at the Marine Group of Newcastle University.

Last but not least, I need to thank my parents for their supports. It would be unthinkable to survive in this exhausted campaign without their love.

Table of Contents

| | |
|---|-------------|
| Abstract | i |
| Acknowledgement | iii |
| Table of Contents | iv |
| List of Figures | ix |
| List of Tables | xvi |
| List of Publications | xvii |
| Nomenclature | xx |
| Chapter 1 Introduction | xxi |
| 1.1 Background..... | 1 |
| 1.2 Ship Structural Response in Still Water..... | 2 |
| 1.3 Ship Structural Response in Wave..... | 2 |
| 1.4 Ship Structural Design Philosophy..... | 4 |
| 1.5 Recent Advances in Ultimate Limit State Design..... | 6 |
| 1.6 Motivation..... | 8 |
| 1.7 Aim and Objectives..... | 10 |
| 1.8 Thesis Layout..... | 11 |
| 1.9 Novelty and Contributions..... | 13 |
| Chapter 2 Literature Review | 15 |
| 2.1 Introduction..... | 15 |
| 2.2 Fundamentals of Ship Structures..... | 15 |
| 2.3 Buckling and Ultimate Collapse Mechanism..... | 17 |
| 2.3.1 Plates..... | 17 |

| | |
|---|----|
| 2.3.2 Stiffened Panels | 18 |
| 2.3.3 Ship Hull Girders | 19 |
| 2.4 Experimental Works | 24 |
| 2.5 Ultimate Strength Analysis Methods of Structural Members..... | 26 |
| 2.5.1 Analytical Approaches..... | 26 |
| 2.5.2 Numerical Simulation | 32 |
| 2.5.3 Empirical Formulation..... | 33 |
| 2.6 Ultimate Strength Analysis Methods of Hull Girders..... | 39 |
| 2.6.1 Empirical Method | 40 |
| 2.6.2 Presumed Stress Distribution-Based Method | 40 |
| 2.6.3 Structural Segment Collapse Strain-Based Method | 45 |
| 2.6.4 Simplified Progressive Collapse Method (Smith Method)..... | 47 |
| 2.6.5 Idealised Structural Unit Method (ISUM)..... | 53 |
| 2.6.6 Nonlinear Finite Element Method | 54 |
| 2.7 Initial Imperfection | 60 |
| 2.7.1 Measurements | 60 |
| 2.7.2 Practical Consideration (Shape/Distribution) | 62 |
| 2.7.3 Practical Consideration (Magnitude)..... | 66 |
| 2.8 Cyclic Loading | 69 |
| 2.8.1 Material Properties | 69 |
| 2.8.2 Structural Behaviour (Theoretical)..... | 72 |
| 2.8.3 Structural Behaviour (Experimental) | 73 |
| 2.9 Chapter Summary | 74 |

| | |
|---|------------|
| Chapter 3 Numerical Analysis on Ship Plating Under Cyclic Compression and Tension | 76 |
| 3.1 Rationale..... | 76 |
| 3.2 Test Matrix..... | 76 |
| 3.2.1 Geometric Dimensions and Material Properties | 76 |
| 3.2.2 Loading Protocol of Structural Member | 78 |
| 3.3 Finite Element Modelling | 80 |
| 3.4 Single-Cycle Response..... | 83 |
| 3.4.1 Load-Shortening Behaviour (Single-Cycle) | 83 |
| 3.4.2 Influence of the Combined Hardening Model..... | 89 |
| 3.4.3 Compressive Strength (Single-Cycle)..... | 90 |
| 3.5 Multi-Cycle Response | 98 |
| 3.5.1 Load-Shortening Behaviour (Multi-Cycle)..... | 98 |
| 3.5.2 Compressive Strength (Multi-Cycle)..... | 100 |
| 3.6 Chapter Summary | 104 |
| Chapter 4 Methodology For Predicting the Cyclic Load-Shortening Curves of Structural Members | 106 |
| 4.1 Rationale..... | 106 |
| 4.2 Principle..... | 107 |
| 4.3 Response Rule..... | 109 |
| 4.4 Updating Rule | 111 |
| 4.5 Rationality of the Response and Updating Rules | 115 |
| 4.6 Schematic Illustrations | 117 |

| | |
|---|------------|
| 4.7 Validation | 122 |
| 4.7.1 Plates – Single Cycle | 123 |
| 4.7.2 Plates – Multi Cycle | 125 |
| 4.7.3 Stiffened Panel..... | 126 |
| 4.8 Discussions on Further Enhancement..... | 132 |
| 4.9 Chapter Summary | 132 |
| Chapter 5 Extended Smith Method for Predicting the Progressive Collapse of Hull Girders Under Cyclic Bending | 134 |
| 5.1 Rationale | 134 |
| 5.2 Methodology | 135 |
| 5.3 Validation | 140 |
| 5.3.1 Model Characteristics | 141 |
| 5.3.2 Comparison of Load-Shortening Responses..... | 145 |
| 5.3.3 Comparison of Bending Moment Versus Curvature Relationship (Experimental Box Girder) | 153 |
| 5.3.4 Comparison of Bending Moment Versus Curvature Relationship (Numerical Box Girder) | 155 |
| 5.3.5 Discussions..... | 163 |
| 5.4 Chapter Summary | 165 |
| Chapter 6 Uncertainty Evaluation of the Extended Smith Method | 166 |
| 6.1 Rationale | 166 |
| 6.2 Methodology | 166 |
| 6.3 Scope of Evaluation | 169 |

| | |
|---|------------|
| 6.4 Effect of Elastic Stiffness | 170 |
| 6.5 Effect of Ultimate Compressive Strength | 171 |
| 6.6 Effect of Ultimate Strain | 172 |
| 6.7 Effect of Post-Collapse Stiffness | 173 |
| 6.8 Sensitivity Index | 174 |
| 6.9 Chapter Summary | 176 |
| Chapter 7 Conclusions and Recommendations | 177 |
| 7.1 Thesis Summary | 177 |
| 7.2 Conclusions | 178 |
| 7.3 Recommendations | 182 |
| 7.3.1 Further Improvement (Numerical Study) | 182 |
| 7.3.2 Further Improvement (Methodology for Predicting Load-Shortening Curve) | 185 |
| 7.3.3 Further Improvement (Extended Smith Method) | 187 |
| 7.3.4 Further Improvement (Uncertainty Evaluation) | 189 |
| 7.3.5 Potential Development (Structural Dynamic Analysis) | 189 |
| 7.3.6 Potential Development (Hydro-Structural Dynamic Analysis) | 191 |
| 7.3.7 Potential Development (Fracture and Cracking) | 191 |
| 7.3.8 Prospective Application of the Cyclic Method | 192 |
| References | 194 |

List of Figures

| | |
|--|----|
| Figure 1-1 Ship hull girder failure due to excessive longitudinal bending (Class NK, 2014; Rutherford and Caldwell, 1990) | 1 |
| Figure 1-2 Effects of the imbalanced distribution of still water loads..... | 2 |
| Figure 1-3 Effects of waves actions on ship hull girders | 3 |
| Figure 1-4 Ship structural design philosophy | 5 |
| Figure 1-5 Comparison of the mid-ship vertical bending moment (Lee et al., 2011)..... | 7 |
| Figure 1-6 Tests on mid-ship vertical bending moments in various sea states (Lee et al., 2012)..... | 8 |
| Figure 1-7 Illustration of the thesis layout..... | 12 |
| Figure 2-1 Typical plate slenderness ratio of ship plates (Zhang and Khan, 2009) | 16 |
| Figure 2-2 Typical column slenderness ratio of ship panels (Zhang and Khan, 2009)..... | 16 |
| Figure 2-3 Schematic illustration of the plate buckling mechanism..... | 17 |
| Figure 2-4 Pre- and post-buckling stress distribution of plate | 18 |
| Figure 2-5 Collapse mechanism of single hull VLCC under vertical bending .. | 20 |
| Figure 2-6 Collapse mechanism of double hull VLCC under vertical bending. | 21 |
| Figure 2-7 Collapse mechanism of bulk carrier under vertical bending | 22 |
| Figure 2-8 Collapse mechanism of container ship under vertical bending..... | 23 |
| Figure 2-9 Test data of welded simply supported unstiffened plates | 25 |
| Figure 2-10 Test data of stiffened panels..... | 25 |
| Figure 2-11 Effective width concept | 27 |
| Figure 2-12 Model idealisation of Dow and Smith method..... | 30 |
| Figure 2-13 Stress-strain distribution of beam-column cross sections..... | 31 |

Figure 2-14 Comparison of ultimate strength formula for unstiffened plates .. 35

Figure 2-15 A.R.E column collapse strength design charts..... 38

Figure 2-16 Comparison of the stiffened panel ultimate strength predictions by different empirical formulations..... 39

Figure 2-17 Nomenclature in presumed stress distribution-based method..... 41

Figure 2-18 Presumed stress distribution of Caldwell method..... 42

Figure 2-19 Presumed stress distribution of Wong method..... 43

Figure 2-20 Presumed stress distribution of Paik and Mansour method 44

Figure 2-21 Presumed stress distribution of modified Paik and Mansour method..... 45

Figure 2-22 Illustration of the critical segment collapse strain-based method. 47

Figure 2-23 Flow chart of the extended Smith method for multi-frame collapse 50

Figure 2-24 Flow chart of the extended Smith method combined vertical and torsional bending 52

Figure 2-25 Examples of finite element models for ship hull collapse strength analysis 57

Figure 2-26 Influence of different FE solvers on the collapse analysis..... 59

Figure 2-27 Schematic illustration of the initial imperfection in stiffened plating due to welding 61

Figure 2-28 Schematic view of the initial distortion of stiffened panels..... 62

Figure 2-29 Illustration of the local plate deflection profiles of different formulations..... 65

Figure 2-30 Idealisation of welding residual stress profiles 66

Figure 2-31 Comparison between maximum local plate deflection and Smith’s average-level estimate..... 67

Figure 2-32 Example stress-strain curve of Chaboche model..... 72

Figure 3-1 Schematic illustration of loading protocol 78

Figure 3-2 Boundary condition of the unstiffened plate model 81

Figure 3-3 Validation of the monotonic ultimate compressive strength..... 83

Figure 3-4 Load-shortening curves of ship plates ($\beta = 2.5$; compression init.) .84

Figure 3-5 Load-shortening curves of ship plates ($\beta = 2.0$; compression init.) .84

Figure 3-6 Load-shortening curves of ship plates ($\beta = 1.5$; compression init.) .85

Figure 3-7 Load-shortening curves of ship plates ($\beta = 2.0$; tension init.)..... 85

Figure 3-8 Load-shortening curves of ship plates (Varied amplitude) 86

Figure 3-9 Schematic illustration of the nonlinear tensile reloading response
(compression init.) 87

Figure 3-10 Schematic illustration of the nonlinear tensile reloading response
(tension init.) 88

Figure 3-11 Schematic illustration of the compressive reloading response..... 88

Figure 3-12 Comparison of load-shortening response with different material
models..... 90

Figure 3-13 The reloading ultimate compressive strength of different loading
protocols ($a/b = 1.0$, ID = 1~13) 92

Figure 3-14 The reloading ultimate compressive strength of different loading
protocols ($a/b = 2.0$, ID = 1~13) 93

Figure 3-15 The reloading ultimate compressive strength of different loading
protocols ($a/b = 3.0$, ID = 1~13) 94

Figure 3-16 The reloading ultimate compressive strength of different loading
protocols ($a/b = 4.0$, ID = 1~13) 95

Figure 3-17 Correlation between the unloading stress and maximum
compressive reloading strength (Black marker: perfectly plastic and constant
amplitude; Red marker: perfectly plastic and varied amplitude; Green marker:
hardening and constant amplitude) 97

Figure 3-18 Load-shortening curves of unstiffened plates (ID: 24) 99

Figure 3-19 Load-shortening curves of unstiffened plates (ID: 17) 99

Figure 3-20 Variation of the compressive strength in multi-cycle loading..... 100

Figure 3-21 Variation of the tensile strength in multi-cycle loading 101

Figure 3-22 Out-of-plane deflection profile (1st cycle)..... 102

Figure 3-23 Out-of-plane deflection profile (2nd cycle) 102

Figure 3-24 Out-of-plane deflection profile (3rd cycle)..... 102

Figure 3-25 Out-of-plane deflection variation 103

Figure 3-26 Post-collapse stiffness variation 104

Figure 4-1 Flowchart of the proposed method to predict the load-shortening curves of plates and stiffened panels under cyclic axial loads..... 108

Figure 4-2 Illustration of the critical points of a LSC..... 109

Figure 4-3 Illustration of the compressive response rule (Updated curve)..... 110

Figure 4-4 Illustration of the tensile response rule..... 111

Figure 4-5 Illustration of the updating rule 1 to 3..... 113

Figure 4-6 Illustration of the updating rule 4 to 5..... 113

Figure 4-7 Illustration of the updating rule 6 114

Figure 4-8 Illustration of the updating rule 8 114

Figure 4-9 Illustration of the updating rule 9 115

Figure 4-10 Schematic illustration of scenario 1 118

Figure 4-11 Schematic illustration of scenario 2 119

Figure 4-12 Schematic illustration of scenario 3..... 120

Figure 4-13 Schematic illustration of scenario 4 121

Figure 4-14 Schematic illustration of scenario 5 122

Figure 4-15 Single-cycle LSC validation ($a/b = 1.0$; $\beta = 2.0$; IDs = 9C & 11C) 123

Figure 4-16 Single-cycle LSC validation ($a/b = 2.0$; $\beta = 2.0$; IDs = 9C & 11C)
 124

Figure 4-17 Single-cycle LSC validation ($a/b = 3.0$; $\beta = 2.0$; IDs = 9C & 11C)
 124

Figure 4-18 Single-cycle LSC validation ($a/b = 4.0$; $\beta = 2.0$; IDs = 9C & 11C)
 124

Figure 4-19 Multi-cycle LSC of unstiffened plates 125

Figure 4-20 Statistical evaluation of the prediction of final compressive strength under multi-cycle loading between NLFEM and the proposed methodology 126

Figure 4-21 Stiffened panel model for NLFEM analysis 127

Figure 4-22 Comparison of single-cycle LSCs of stiffened panels..... 128

Figure 4-23 Multi-cycle load-shortening curves of stiffened panels (NLFEM)
 129

Figure 4-24 Multi-cycle load-shortening curves of stiffened panels (Proposed)
 130

Figure 4-25 Variation of the maximum compressive strength of Panel A 130

Figure 4-26 Variation of the maximum compressive strength of Panel B 131

Figure 4-27 Variation of the maximum compressive strength of Panel C 131

Figure 4-28 Variation of the maximum compressive strength of Panel D 131

Figure 5-1 Flowchart of the proposed extended Smith method 138

Figure 5-2 Illustration element subdivision in the Smith method..... 139

Figure 5-3 Sub-division techniques of stiffened panels 139

Figure 5-4 Cyclic loading protocol of ship hull girders..... 141

Figure 5-5 Cross section of the experimental model..... 142

Figure 5-6 Cross section of the single hull model for numerical validation.... 143

Figure 5-7 Cross section of the double hull model for numerical validation .. 144

Figure 5-8 Cross section of the bulk carrier model for numerical validation.. 144

Figure 5-9 Cross section of the container ship model for numerical validation
 145

Figure 5-10 Model extent and boundary conditions of plate–stiffener
 combination model 147

Figure 5-11 The effect of different cyclic loading on the post-ultimate strength
 stiffness in compression..... 149

Figure 5-12 Load-shortening curve comparison of deck/bottom stiffened panel
 (Experimental box girder model)..... 151

Figure 5-13 Load-shortening curve comparison of deck/bottom stiffened panel
 (Numerical box girder model)..... 152

Figure 5-14 Collapse modes of the stiffened panels of experimental and
 numerical models 152

Figure 5-15 Correlation of the compressive reloading strength prediction..... 153

Figure 5-16 Bending moment versus curvature relation of experimental model
 154

Figure 5-17 Correlation of the reloading strength of experimental model 155

Figure 5-18 Contour plot of double hull model under loading protocol 1..... 157

Figure 5-19 Contour plot of double hull model under loading protocol 2..... 157

Figure 5-20 Bending moment versus curvature relation of single hull model
 under loading protocol 1 159

Figure 5-21 Bending moment versus curvature relation of double hull model
 under loading protocol 1 160

Figure 5-22 Bending moment versus curvature relation of bulk carrier model
 under loading protocol 1 161

Figure 5-23 Bending moment versus curvature relation of container ship model
 under loading protocol 1 161

Figure 5-24 Bending moment versus curvature relation of case study models under loading protocol 2..... 162

Figure 5-25 Correlation of the reloading bending moment with numerical simulation 163

Figure 6-1 Overall procedure of uncertainty evaluation..... 167

Figure 6-2 Schematic illustration of the adaptable algorithm..... 168

Figure 6-3 Example load-shortening curve developed by the adaptable algorithm 170

Figure 6-4 The effects of elastic stiffness on the cyclic and monotonic bending moment versus curvature response of double hull model 171

Figure 6-5 The effects of ultimate compressive strength on the cyclic and monotonic bending moment versus curvature response of double hull model .. 172

Figure 6-6 The effects of ultimate strain on the cyclic and monotonic bending moment versus curvature response of double hull model 173

Figure 6-7 The effects of post-collapse stiffness on the cyclic and monotonic bending moment versus curvature response of double hull model..... 174

List of Tables

| | | |
|------------------|--|-----|
| Table 2-1 | Coefficients of Xu formula..... | 37 |
| Table 2-2 | Fourier coefficients of British naval design initial distortion | 64 |
| Table 2-3 | Fourier coefficients of hungry-horse initial distortion | 64 |
| Table 2-4 | Maximum magnitude of column-type distortion | 68 |
| Table 2-5 | Material property (Krolo et al., 2016)..... | 71 |
| Table 2-6 | Material property (Jia and Kuwamura, 2015) | 72 |
| Table 3-1 | Geometric dimension of the tested ship plating | 77 |
| Table 3-2 | Material property | 77 |
| Table 3-3 | Loading protocols of unstiffened plates | 80 |
| Table 3-4 | Validation of the monotonic ultimate compressive strength | 82 |
| Table 3-5 | Statistical correlation between the unloading stress and maximum compressive reloading strength..... | 96 |
| Table 4-1 | Dimension and material property of the stiffened panels..... | 127 |
| Table 4-2 | Dimensionless parameters of the stiffened panels..... | 127 |
| Table 4-3 | Loading protocols of stiffened panels | 127 |
| Table 5-1 | Dimension and material property of the experimental model | 141 |
| Table 5-2 | Dimension and material property of the numerical model | 143 |
| Table 5-3 | Different LSCs used in the numerical validation..... | 147 |
| Table 6-1 | Mean values of each critical features..... | 175 |
| Table 6-2 | Summary of the sensitivity index ($\times 10^{-2}$) | 176 |

List of Publications

During the doctoral research in the past three years, a number of publications are disseminated in several peer-reviewed journals, magazine and conferences. A list of publications is summarised as follows:

Peer-reviewed journals:

- Li, S., Benson, S.D., 2019. A re-evaluation of the hull girder shakedown limit states. *Ships and Offshore Structures*, 14: sup1, 239-250.
- Li, S., Hu, Z.Q., Benson, S.D., 2019. An analytical method to predict the buckling and collapse behaviour of plates and stiffened panels under cyclic loading. *Engineering Structures*, 199, 109627.
- Li, S., Hu, Z., Benson, S.D., 2020. Progressive collapse analysis of ship hull girders subjected to repeated longitudinal bending. *Marine Structures*, 73, 102803.
- Li, S., Kim, D.K., Benson, S.D., 2020. An adaptable algorithm to predict the load-shortening curves of stiffened panels in compression. *Ships and Offshore Structures* (Under review).
- Li, S., Kim, D.K., Benson, S., 2020. A probabilistic approach to assess the computational uncertainty of ship hull ultimate strength. *Reliability Engineering and System Safety* (Under review).
- Li, S., Kim, D.K., Benson, S., 2021. The influence of residual stress on the ultimate strength of longitudinally compressed stiffened panels. *Ocean Engineering* (Under review)

Peer-reviewed conferences:

Li, S., Benson, S.D., 2018. A re-evaluation of the hull girder shakedown limit states. In: 3rd International Conference on Ships and Offshore Structures (ICSOS), Gothenburg, Sweden.

Li, S., Hu, Z.Q., Benson, S.D., 2019. A cyclic progressive collapse method to predict the bending response of a ship hull girder. In: 7th International Conference on Marine Structures (MARSTRUCT), Dubrovnik, Croatia.

Li, S., Hu, Z., Benson, S.D., 2019. Bending response of a damaged ship hull girder predicted by the cyclic progressive collapse method. In: 8th International Conference on Collision and Grounding of Ships and Offshore Structures (ICCGS), Lisbon, Portugal.

Li, S., Hu, Z., Benson, S.D., 2020. Ultimate strength performance of a damaged container ship. In: International Conference on Damaged Ship, London, UK.

Li, S., Hu, Z., Benson, S.D., 2020. The sensitivity of ultimate ship hull strength to the structural component load-shortening curve. In: 30th International Ocean and Polar Engineering Conference (ISOPE), Shanghai, China.

Li, S., Kim, D.K, Benson, S.D., 2020. An adaptable algorithm to predict the load-shortening curves of stiffened panels in compression. In: 5th International Conference on Ships and Offshore Structures (ICSOS), Glasgow, UK.

Li, S., Benson, S.D., 2020. The effects of welding-induced residual stress on the buckling collapse behaviours of stiffened panels. In: 5th International Conference on Marine Technology and Engineering (MARTECH), Lisbon, Portugal.

Li, S., Benson, S.D., 2020. Probabilistic evaluation of the computational uncertainty in ultimate ship hull strength prediction. In: 5th International

Conference on Marine Technology and Engineering (MARTECH), Lisbon, Portugal.

Li, S., Benson, S., 2021. A Timoshenko beam finite element formulation for thin-walled box girder considering inelastic buckling. In: 8th International Conference on Marine Structures (MARSTRUCT), Trondheim, Norway (Under review).

Georgiadis, D.G., Samuelides, M.S., Li, S., Benson, S., 2021. Influence of stochastic geometric imperfection on the ultimate strength of stiffened panel in compression. In: 8th International Conference on Marine Structures (MARSTRUCT), Trondheim, Norway (Under review).

Peer-reviewed magazine:

Li, S., Hu, Z.Q., Benson, S., 2020. Ultimate strength performance of a damaged container ship. The Naval Architect, RINA.

Nomenclature

β : Plate slenderness ratio

λ : Column slenderness ratio

a : Plate length

b : Plate width

t_p : Plate thickness

h_w : Height of stiffener web

t_w : Thickness of stiffener web

b_f : Width of stiffener flange

t_f : Thickness of stiffener flange

σ_Y : Material yield stress of plating

σ_{Yeq} : Equivalent material yield stress of stiffened panel

E : Material Young's modulus

ν : Poisson's ratio

r : Radius of gyration

σ_x : Longitudinal resultant stress

ε_x : Longitudinal resultant strain

σ_{xu} : Longitudinal ultimate strength

ε_{xu} : Longitudinal ultimate strain

M_u : Ultimate bending moment of cross section

M_p : Plastic bending moment of cross section

χ : Curvature of cross section

w_{opl} : Local plate distortion

w_{oc} : Column-type distortion

w_{os} : Stiffener sideway distortion

w_{opl}^{max} : Maximum local plate distortion

w_{oc}^{max} : Maximum column-type distortion

w_{os}^{max} : Maximum stiffener sideway distortion

m : Number of half-waves of critical buckling mode shape

A_{0i} : Fourier coefficient of Hungry-horse mode deflection

σ_{rcx} : Compressive residual stress

σ_{rtx} : Tensile residual stress

b_t : Width of tensile residual stress

σ_{unload} : Unloading stress

ε_{unload} : Unloading strain

φ_1 : Compressive post-collapse stiffness reduction factor

φ_2 : Tensile strength reduction factor

D_{HH} : Horizontal bending stiffness

D_{VV} : Vertical bending stiffness

D_{HV} : Interactive horizontal and vertical bending stiffness

D_{VH} : Interactive horizontal and vertical bending stiffness

NLFEM: Nonlinear finite element method

CSR: Common Structural Rule

COV: Coefficient of variation

IACS: International Association of Classification Society

ISSC: International Ships and Offshore Structures Congress

ISUM: Idealised Structural Unit Method

ULS: Ultimate limit state

Chapter 1 Introduction

1.1 Background

The suitability of ship structures should be assessed by considering their responses to the most likely extreme environment with a safety margin. In structural analysis, ships are usually viewed as a beam-like hull girder. While in service, the ship hull girders are primarily subjected to longitudinal bending moment, which includes the still water component and the wave-induced component.

In an unusual circumstance, the excessive longitudinal bending moment would lead to the catastrophic ship structural failure of “breaking its back”, such as the failure of *MOL Comfort* and *Energy Concentration* (Figure 1-1). Hence, one of the fundamental tasks in the safety design of ship structures is to minimise the risk of this kind.

Within this context, ship structural design currently follows the ultimate limit state philosophy. This design approach explicitly calculates the maximum load-carrying capacity of ship structures and the safety margin evaluation is conducted by comparing the ultimate strength and the most probable extreme load. The current ultimate limit state approach only assumes monotonic loading. However, the extreme loads applied on ships are associated with a cyclic nature.



Figure 1-1 Ship hull girder failure due to excessive longitudinal bending (Class NK, 2014; Rutherford and Caldwell, 1990)

1.2 Ship Structural Response in Still Water

In still water, the weight and the buoyancy of a ship constitute the two major load components. Whilst the total weight and the buoyancy are in equilibrium, the imbalanced distribution along the ship's length will result in bending moment and shear force of the ship hull girder, as schematically shown in Figure 1-2. Generally, the maximum bending moment occurs at the mid-ship region, whereas the maximum shear force occurs at the quarter positions. As the still water load is a resultant of the weight and buoyancy, it is predominately determined by the cargo loading cases, i.e. full departure load case, full arrival load case, ballast departure and ballast arrival. The worst scenario may be used for the structural integrity assessment. As a standard naval architecture design procedure, the evaluation of the still water load is normally part of the hydrostatic calculation.

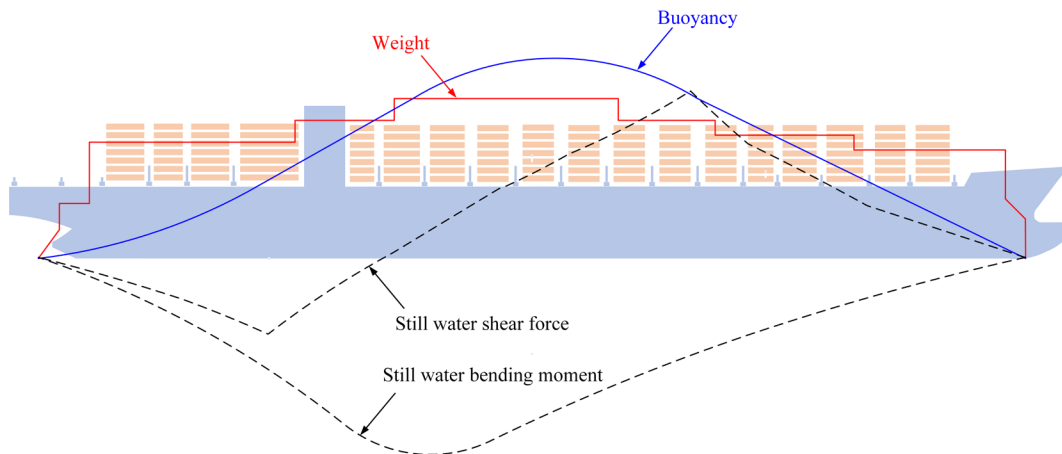


Figure 1-2 Effects of the imbalanced distribution of still water loads

1.3 Ship Structural Response in Wave

Due to the dynamic wave-body interaction, the response of a vessel in waves is far more complex than that in still water. From a structural engineers' point of view, the most important task is to estimate the wave-induced load comprising the wave-induced bending moment and shear force acting on the ship hull girders. This was initially tackled with a static load assumption (John, 1874). The calm

water surface is replaced by imposing a static wave with assumed profile, as shown in Figure 1-3. If the wave crest presents at the mid-ship region and the wave trough occurs at the bow and stern, there will be an increase in buoyancy at midship and loss in buoyancy at bow and stern. This effectively produces a bending moment to hog the vessel. Similarly, a sagging moment is produced if the wave crest occurs at the bow and stern and the mid-ship region is in the wave trough.

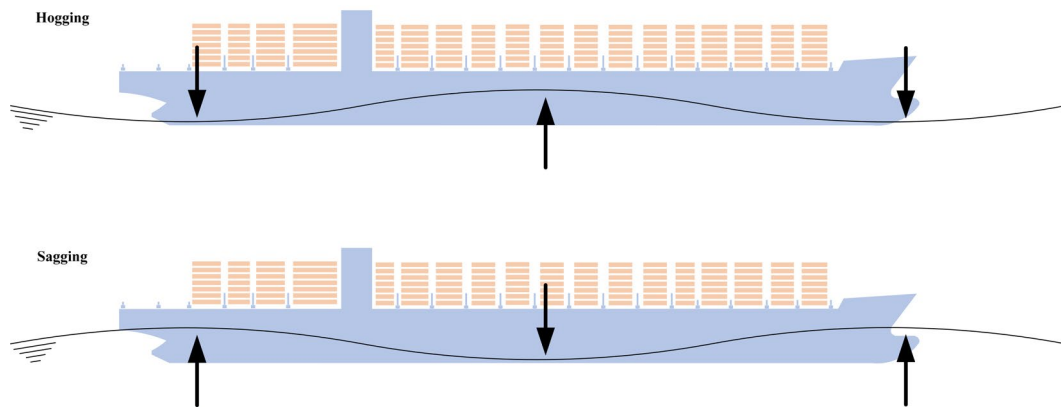


Figure 1-3 Effects of waves actions on ship hull girders

The static assumption to calculate the wave-induced load has led to the development of empirical formulae as a function of the principal particulars of the vessels. The first formula of this kind was developed by John (1874), which was simply given in terms of the displacement and ship's length. Whist being more refined, this fundamental concept is still adopted in contemporary design guidelines, such as Common Structural Rules (CSR) (IACS, 2019).

However, the static approach neglects the dynamic nature of wave actions. In this regard, the theory of Rigid Body Dynamics is employed to predict the ship response in waves and to estimate the wave-induced loads for structural design. An established methodology may refer to strip theory (Salvesen et al., 1970). Assuming that no deformation of the ship structures will take place (only six degrees of freedom), the rigid body dynamics deals with prediction of ship's

response in wave by setting up the dynamic equilibrium equation in terms of fluid-structure mass, fluid-structure damping, hydrostatic force and the excitation force.

Whilst conventional hydrodynamic analysis is applicable for ships such as bulk carrier and oil tankers, the elastic deformation of ship hulls may also be taken into account, particularly for slender hull girders such as container ships. To this end, elastic body dynamics can be employed. This type of analysis is usually termed hydroelasticity, and was pioneered by Bishop and Price (1979) with a two-dimensional theory which was later extended to three-dimensional (Bishop et al., 1986) by combining the finite element method with the boundary element method. The major advancement of elastic body dynamics is to account for the elastic deflection modes of the ship hull girder in addition to the six degrees of freedom rigid body motions. With the use of hydroelasticity theory, the elastic structural response at different frequencies can be evaluated, as compared with the conventional hydrodynamic analysis where only the response at the encounter frequency is estimated.

1.4 Ship Structural Design Philosophy

Ship structural design has evolved significantly owing to the development in various disciplines, such as material science, structural engineering and fluid dynamics. As shown in Figure 1-4, the principle design philosophy for ship structures has progressed from the allowable stress criterion (stress-based) to the ultimate limit state assessment (strength-based).

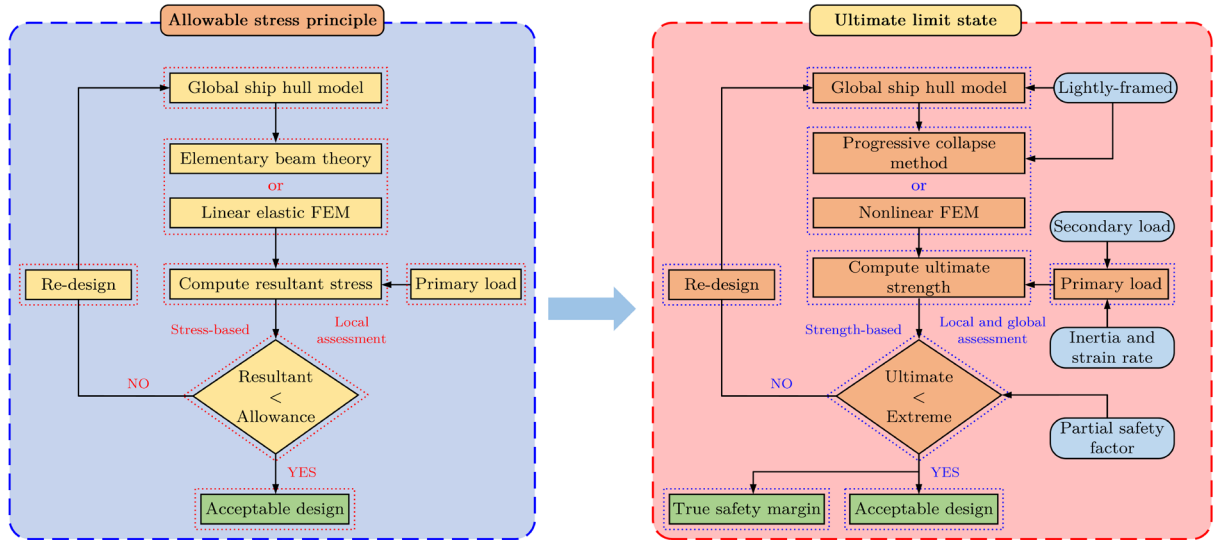


Figure 1-4 Ship structural design philosophy

The principle of the allowable stress criterion is first to calculate the resultant stress of ship structures under a specific load case, which is then compared to a required stress level. This used to be the material tensile fracture stress and was later modified to the material yield stress and critical buckling stress. Thus, the allowable stress principle is essentially a stress-based philosophy, with an overall aim to constrain the stress level in different parts of the structures. The evaluation of resultant stress may be performed by various methods, from elementary beam theory to three-dimensional finite element analysis. However, they are usually based on a linear elastic assumption. This assessment philosophy is usually accused of two drawbacks in the contemporary design practice. Firstly, the linear elastic assumption may be invalid due to the re-distribution of the internal stress after the onset of nonlinear response. This could lead to an overestimation of the resultant stress. Therefore, the structural design based on the allowable stress principle tends to be conservative. Secondly, in calculating the resultant stress, the analyst has no information regarding the maximum capacity of the overall structures and therefore the true safety margin with reference to the extreme load scenario cannot be evaluated.

In this regard, the ultimate limit state assessment has become the preferred ship structural methodology in recent years. Compared with the allowable stress principle, the ultimate limit state approach is effectively a strength-based philosophy where the ultimate strength of ship structures under certain loading actions are explicitly evaluated considering geometric and material nonlinearity. It may also be known as Load Resistance Factor Design (LRFD). In terms of ship hull girders, it is usually the ultimate bending strength against longitudinal bending and in terms of structural components, it is primarily the in-plane compression and tension. As the ultimate strength is explicitly evaluated, the safety margin of ship hull girder can be assessed with reference to the extreme design load.

1.5 Recent Advances in Ultimate Limit State Design

Within the ultimate limit state philosophy, there have been several advancements in recent years. These advancements are usually driven by novel structural design, special operational requirement and enhanced load prediction methods.

For instance, the large deck opening of container ships, which results in a low torsional rigidity, has drawn attention to account for the adverse effect of torsional bending. The analysis methodology to calculate the ultimate bending strength has therefore been progressed from dealing with pure vertical bending to the combined vertical and torsional bending (Tanaka et al., 2015; Syrigou et al., 2017). Similar examples may refer to the construction of lightweight ship structures, which are usually lightly-framed as compared with the stocky transverse frames in conventional merchant ships. This issue has resulted in the development of a compartment-level analysis methodology dedicated for multi-frame buckling failure (Benson et al., 2013). In addition, the recent failure of container ship MOL Comfort suggested the inability of the conventional calculation method to deal

with double bottom structures, which therefore has led to the development of an extended Smith-type method (Tatsumi and Fujikubo, 2020; Tatsumi et al., 2020).

In addition, advancements are recently motivated by special operational requirements, such as those dedicated for arctic environment and fire protection. A series of full-scale collapse tests were performed by Paik et al. (2020) on stiffened grillages subjected to low temperature and high temperature. Ship hull girder strength in arctic environment was investigated by Kim et al. (2019).

More often, progress has been driven by an enhanced understanding on the external loads. A comparison of linear hydrodynamic analysis, nonlinear hydrodynamic analysis and hydro-elastic analysis on the prediction of mid-ship vertical bending moment is shown in Figure 1-5.

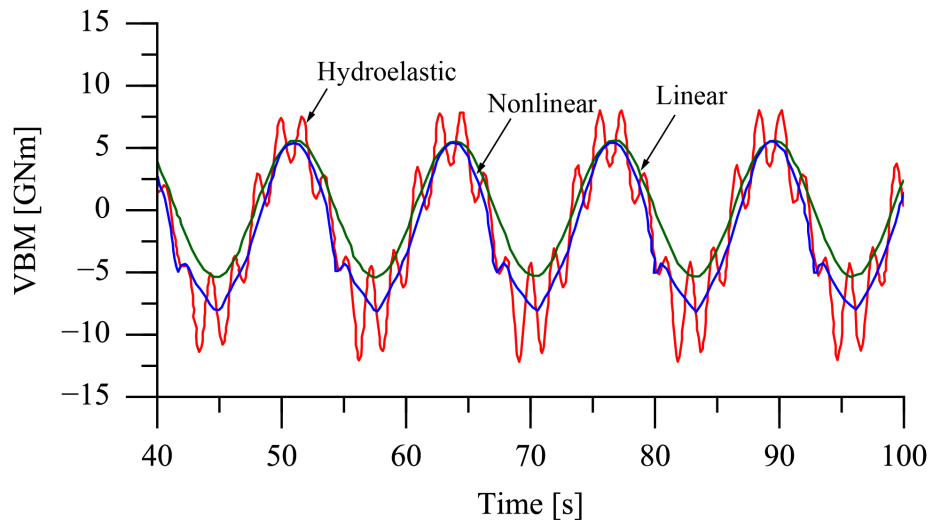


Figure 1-5 Comparison of the mid-ship vertical bending moment (Lee et al., 2011)

As in many instances, predictions by nonlinear hydrodynamic analysis and hydro-elastic analysis are higher than linear rigid-body hydrodynamic analysis. This finding has led to a refined calibration of partial safety in the limit state equation. Besides, the use of hydroelasticity theory indicates that the magnitude of high-

frequency dynamic stress components, which is likely induced by impact loading, is of a similar order as compared with the magnitude of quasi-static stress component which is predominately induced by wave actions. This issue has triggered a large body of research in the dynamic ultimate strength of ship structures, such as Jagite et al. (2019; 2020).

1.6 Motivation

Under the framework of ultimate limit states, the research reported in this thesis is motivated by the cyclic nature of the applied loads on ship structures. The ultimate limit state assessment usually assumes a monotonic loading. However, as demonstrated in Figure 1-6, it is likely that the ship hull girder is subjected to multiple cycles of extreme load. After the first excursion with extreme magnitude, the subsequent loading, which may be associated with some vibratory ship hull response, appears to be equally severe as compared with the initial load.

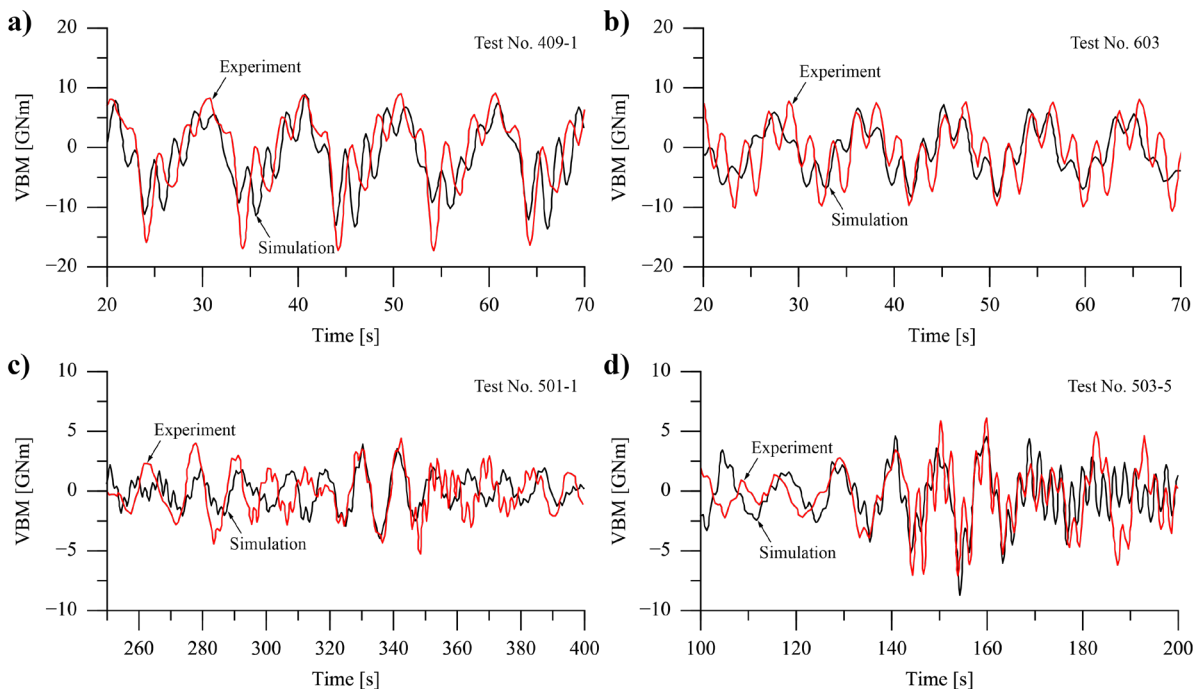


Figure 1-6 Tests on mid-ship vertical bending moments in various sea states (Lee et al., 2012)

Although most ultimate strength failures of ships are considered as distinct single events, their causes may be rooted in accumulative elastoplastic buckling degradation within highly loaded areas of the hull structure until the ultimate strength is surpassed and the hull girder fails. In these scenarios, the magnitudes of the load cycles contributing to the degradation may be significantly less than the nominal ultimate hull girder strength. For instance, in the failure analysis of an inland waterway oil bunker barge (Hess, 1997), the collapse was largely attributed to progressive damage, which resulted in inelastic behaviours during repeated cycles of loading. In the aftermath of the *MOL Comfort* disaster, a repeated load between the still water bending moment and 90% of the ultimate bending moment was applied to verify the buckled bottom plating found on the sister ships (Sumi et al., 2015). An accumulatively increased distortion was reproduced, which may have had an adverse effect on the eventual ultimate ship hull strength performance.

The cyclic loading may continue to act on a ship hull even after the ultimate hull girder strength is exceeded, in which case the response may also surpass the nominal ultimate capacity. This series of extreme cyclic loading may eventually result in the destructive final event, with fracture induced in the highly loaded panels that leads to the hull girder “breaking its back”. Within this context, Iijima and Fujikubo (2015) experimentally investigated the cumulative damage and collapse extent of a small-scale ship model under a series of extreme waves. A hydro-elastoplasticity method was proposed to simulate the post-ultimate strength behaviour of a ship where both the fluid-structural coupling and nonlinear structural stiffness are accounted for (Iijima et al., 2011).

The issue of extreme cyclic loading has also been raised by the Ultimate Strength Committee of ISSC (ISSC, 2000; 2003). There were several works presented in the 1990s on the collapse behaviour of unstiffened plating under extreme cyclic loading.

Recently, a four-point bending test was conducted by Cui and Yang (2018) to investigate the failure characteristics of box girder. Full-scaled collapse test on stiffened panels under cyclic axial compression was reported by Paik et al. (2020). However, as compared with the extensive research in ultimate strength of ship structures under monotonic load, little efforts were devoted to cyclic loading.

In particular, no verified analysis methodology is established to predict the structural collapse behaviour of local members and ship hull girders under cyclic loads. Additionally, numerical and physical testing are insufficient. Calibration of material data is lacking for modelling the material cyclic behaviour.

In this regard, a systematic research is attempted in this project to better understand the buckling and collapse behaviours of ship and ship-type floating structure under extreme cyclic load.

1.7 Aim and Objectives

The aim of this research is to assess the collapse behaviour of ship structures, including plates, stiffened panels and ship hull girders, under combinations of cyclic loads and to investigate the influence of cyclic load on the ultimate strength of ship structures. To achieve this, the following objectives will be completed:

1. Analyse the critical load-shortening response features of ship plates under different combinations of cyclic compression and tension. This will be completed by conducting nonlinear finite element analysis on ship plates with four different aspect ratios and three different slenderness ratios.
2. Develop a methodology to predict the load-shortening curves of ship structural members under cyclic in-plane load, which is suitable for implementing in the Smith-type progressive collapse method. The method is deduced on the basis of the concluded critical response characteristics from the numerical study in Objective One.

3. Propose and validate a methodology to predict the bending moment versus curvature relationship of ship hull girders subjected to cyclic longitudinal bending. This is achieved by extending the simplified progressive collapse method (Smith method). The extension is attributed to the re-formulation of structural member's load shortening curve, which is enabled by the methodology developed in Objective Two.
4. Evaluate the computational uncertainty of the ship hull girder response prediction using the extended Smith method proposed in Objective Three. This is completed by developing a load-shortening curve formulation, which is formed of four critical features, i.e. elastic stiffness, ultimate compressive strength, ultimate strain and post-collapse stiffness. The four critical features are adaptable which allows for the evaluation of their respective influence on the overall hull girder response.

1.8 Thesis Layout

This thesis is formed of seven chapters, as illustrated by Figure 1-7.

Chapter one sets out the context of the research by giving an introduction to ship structural design philosophy and its recent advancements. More importantly, the motivation of this research is highlighted.

Chapter two provides a comprehensive literature review in ultimate limit state assessment of ship structures, including analytical and experimental works on plates, stiffened panels and ship hull girders.

Chapter three presents a parametric study on ship plates under cyclic compression and tension by applying nonlinear finite element method. A series of plating scantlings under different loading profiles are analysed. The critical response characteristics of structural components under cyclic in-plane load are summarised.

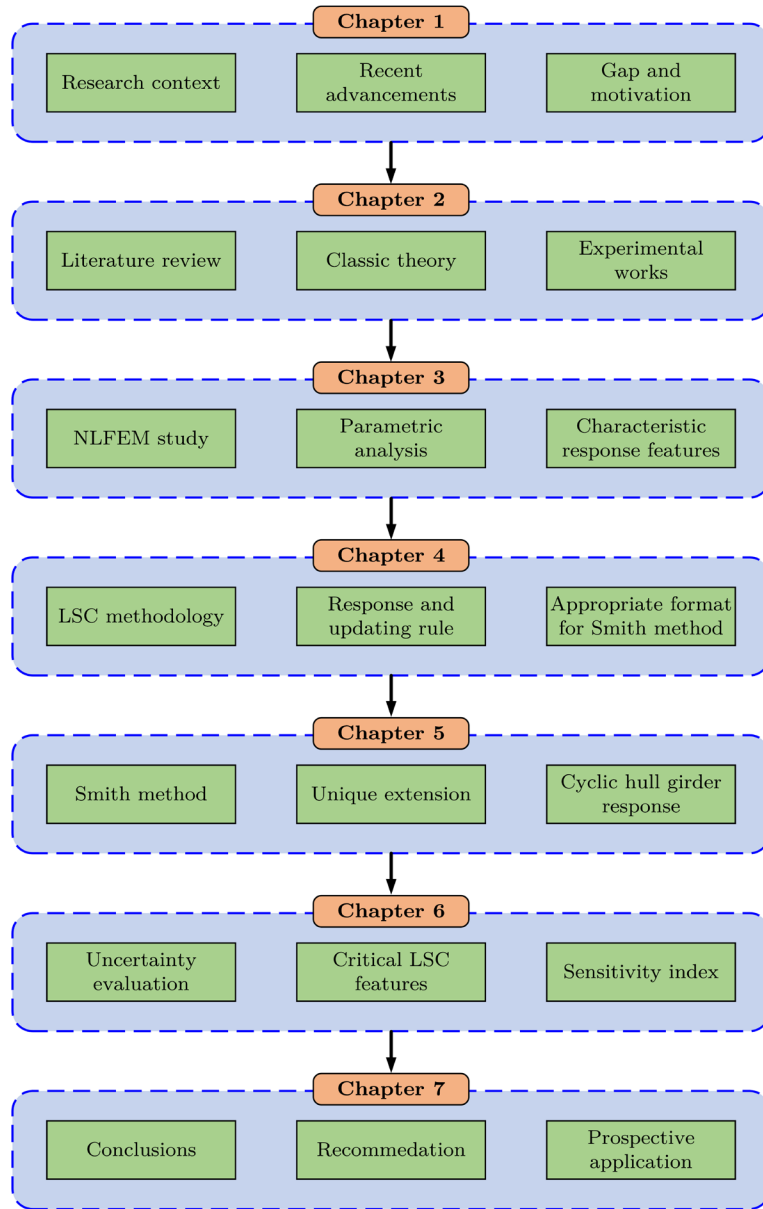


Figure 1-7 Illustration of the thesis layout

Chapter four deals with a methodology to predict the load-shortening response of structural members under cyclic in-plane load. The development and validation of the method are fully documented.

Chapter five introduces an extended Smith-type progressive collapse method to predict the bending response of ship hull girder under cyclic extreme loads. Validation is presented for extreme scenarios where the load magnitude has surpassed the nominal ultimate strength.

Chapter six carries out an uncertainty assessment for the extended Smith method to demonstrate the most critical load-shortening characteristics of structural members.

Chapter seven summarises the key insights and conclusions obtained from this research. Meanwhile, a recommendation of future work is suggested.

1.9 Novelty and Contributions

Four novel developments are contributed to the research field of buckling and ultimate strength of ship structures.

The numerical study on the load-shortening behaviour of ship plates under cyclic loads demonstrates the strength and stiffness reduction due to repeated loading. Meanwhile, the distinctive features of compressive and tensile responses as compared to those under monotonic load are illustrated. For the first time, these features have been quantified across a large parametric range of plate slenderness ratio, which have contributed to an improved understanding on the fundamental progressive collapse behaviour of ship structures subjected to combination of in-plane cyclic load.

The response and updating rule methodology developed for generating the load-shortening curve of ship structural member is a novel model for cyclic response simulation. The capability of existing monotonic load-shortening prediction approach is extended, as the proposed methodology enables the subsequent load cycles to utilise information from previous cycle to define the load-shortening characteristics.

The implementation of response and updating rule methodology in the simplified progressive collapse method (Smith method) is an unique development that enables the simulation of cyclic response prediction of ship hull girders. The extension is based on the established approach codified in the Common Structural

Rule, which means it has the potential for practical application. Besides, it can be further extended to a dynamic analysis procedure coupling with load prediction method.

The uncertainty evaluation procedure is a new approach for analysing the influence of the load-shortening relationship on the overall ship hull girder response. By the use of this approach, the effects of the ultimate compressive strength and post-collapse stiffness of structural members are quantified. This is not only useful for the cyclic response, but also the conventional progressive collapse assessment in monotonic loading.

Chapter 2 Literature Review

2.1 Introduction

The research reported in the thesis is conducted under framework of ultimate limit state assessment of ship structures. There have been a wide range of experimental and theoretical research efforts devoted in this field. These have enabled a progressively improved understanding of the buckling collapse mechanism and robust prediction of such phenomenon. In this chapter, the fundamentals of ship structures are first summarised. A review is then presented to the major advancements in this research area. In addition, the investigations concerning the buckling collapse response under cyclic loading are outlined.

2.2 Fundamentals of Ship Structures

Ship hull structure is a thin-walled box girder composed of plates and stiffeners (Yao and Fujikubo, 2016). Long plates are usually adopted, with an aspect ratio from 2.0 to 6.0 (Smith et al., 1987). Ship plates are normally characterised by the plate slenderness ratio (Equation 2-1), which is a dimensionless parameter embedded with the plating dimension and material property. According to Zhang and Khan's survey (2009), the most common range of the plate slenderness ratio is around 1.5 to 2.5, as shown in Figure 2-1. Typical stiffener types include tee-bar, angle bar and flat bar. The stiffener is usually considered in association with the attached plating as a plate-stiffener combination (column structure) and is characterised by a column slenderness ratio (Equation 2-2). Following Zhang and Khan's survey, the most common range of the column slenderness ratio is around 0.2 to 0.8, as shown in Figure 2-2.

$$\beta = \frac{b}{t_p} \sqrt{\frac{\sigma_Y}{E}} \tag{2-1}$$

$$\lambda = \frac{a}{\pi r} \sqrt{\frac{\sigma_{Ye q}}{E}} \tag{2-2}$$

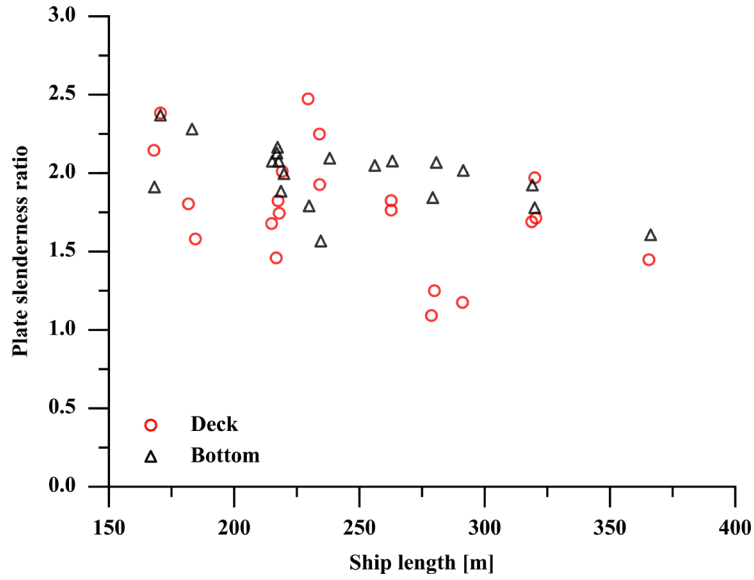


Figure 2-1 Typical plate slenderness ratio of ship plates (Zhang and Khan, 2009)

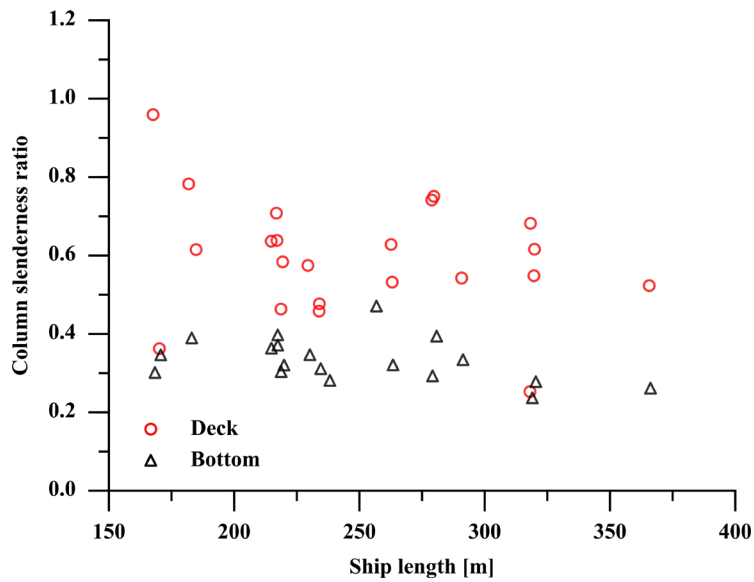


Figure 2-2 Typical column slenderness ratio of ship panels (Zhang and Khan, 2009)

2.3 Buckling and Ultimate Collapse Mechanism

2.3.1 Plates

The collapse mechanism of ship plating under axial compression may refer to a description by Winter (1947). Considering an edge supported long plate under longitudinal compression, it deforms into a non-developable and wavy surface after the onset of buckling, which continues to resist the increasing stress. As shown in Figure 2-3, the compressed bars (strips) would not fail as simple columns by continued deflection because of the restraint by the transverse bars. In addition, the load distribution is not equal among the compressed bars. In view of the variation of deflection, the bars near the edge would carry more load than those near the centre. Thus, the stress distribution after the onset of buckling may be shown as Figure 2-4.

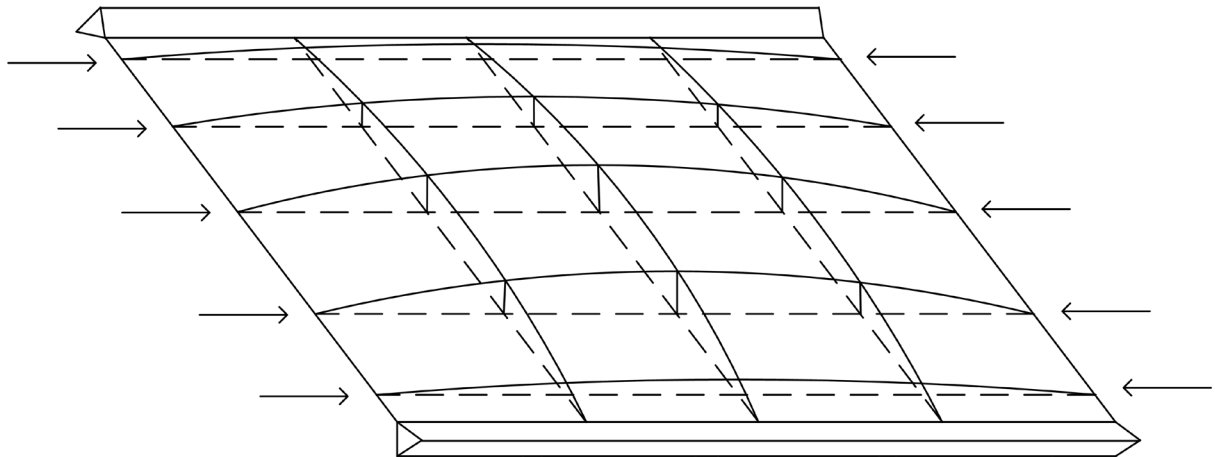


Figure 2-3 Schematic illustration of the plate buckling mechanism

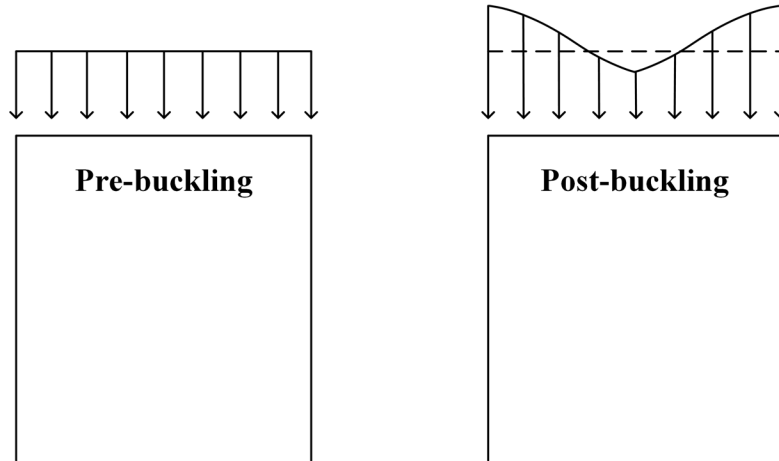


Figure 2-4 Pre- and post-buckling stress distribution of plate

2.3.2 Stiffened Panels

As introduced by Smith (1975), the collapse mechanism of a stiffened panel formed of attached plating and stiffeners may primarily take one of the following failure modes:

- **Plate failure:** in this case the maximum plate load is exceeded and is followed by significant unloading of the plate, leading to the collapse of the stiffened panel before significant yield occurs in the stiffeners. This type of failure is likely to occur in nearly perfect plating or in hybrid structures with high-strength stiffeners and low-strength plating.
- **Interframe flexural buckling:** this form of failure, also known as the beam-column collapse, involves yielding of the stiffeners accelerated by the loss of stiffness due to the yielding and buckling of the plating. Depending on the direction of buckling, a plate-induced flexural failure where the panel deflects away the plate or a stiffener-induced flexural buckling where the panel buckles toward the plate may occur. The failure of this type is highly sensitive to the interaction with adjacent panels.
- **Lateral torsional buckling of stiffeners:** this form of failure can occur in panels with torsionally weak stiffeners (e.g. flat bars) or stiffeners which

are very short relative to their depth. Lateral torsional instability can occur in association with the plate-induced flexural failure where the panel buckles away the stiffener outstand.

- **Overall grillage instability:** this form of failure, involving the bending of transverse frames and longitudinal stiffeners, is likely to occur at the superstructure panels or lightly framed structures such as a weight-critical high speed vessel.

2.3.3 Ship Hull Girders

The buckling collapse of ship hull girders are typically governed by the collapse of the compressed critical structural segments. Under extreme sagging, the failure of the deck panels normally signifies the overall collapse of conventional ship hull girders, as the neutral axis translates toward the bottom after the deck panel failure which therefore further increases the imposed strain at the compressed portion and the overall failure would rapidly take place. Under extreme hogging, the progressive collapse may occur in a similar manner as that in sagging for a single hull configuration. However, a double bottom design, which is more common nowadays due to the ocean environment protection regulation, may lead to a different progressive collapse behaviour. As the initial elastic neutral axis is close to the double bottom, the yielding of deck panels may also greatly affect the overall collapse of the ship hull, and even become the first failure region such as that in a container ship. The collapse mechanism of several ISSC benchmark ship hull girders are illustrated from Figure 2-5 to Figure 2-8.

In terms of the single hull VLCC (Figure 2-5), the buckling first occurs at the upper longitudinal bulkhead and the deck girders, which results in the gentle downward translation of the neutral axis when the hull girder is submitted to sagging. The first failure takes place at the deck panel and subsequently deck girder, upper bulkhead and the upper side shell panels. Soon after that, the hull

girder reaches its ultimate limit state against longitudinal bending. In hogging, the onset of buckling bottom panel and bottom girders leads to upward translation of the neutral axis. However, the first failure occurs at the deck and upper side shell panels due to tensile yielding, which therefore results in a sudden drop of the neutral axis. With further applied curvature, the buckling collapse of the bottom panel and bottom girder take place. Soon after that, the hull girder reaches its ultimate limit state against longitudinal bending.

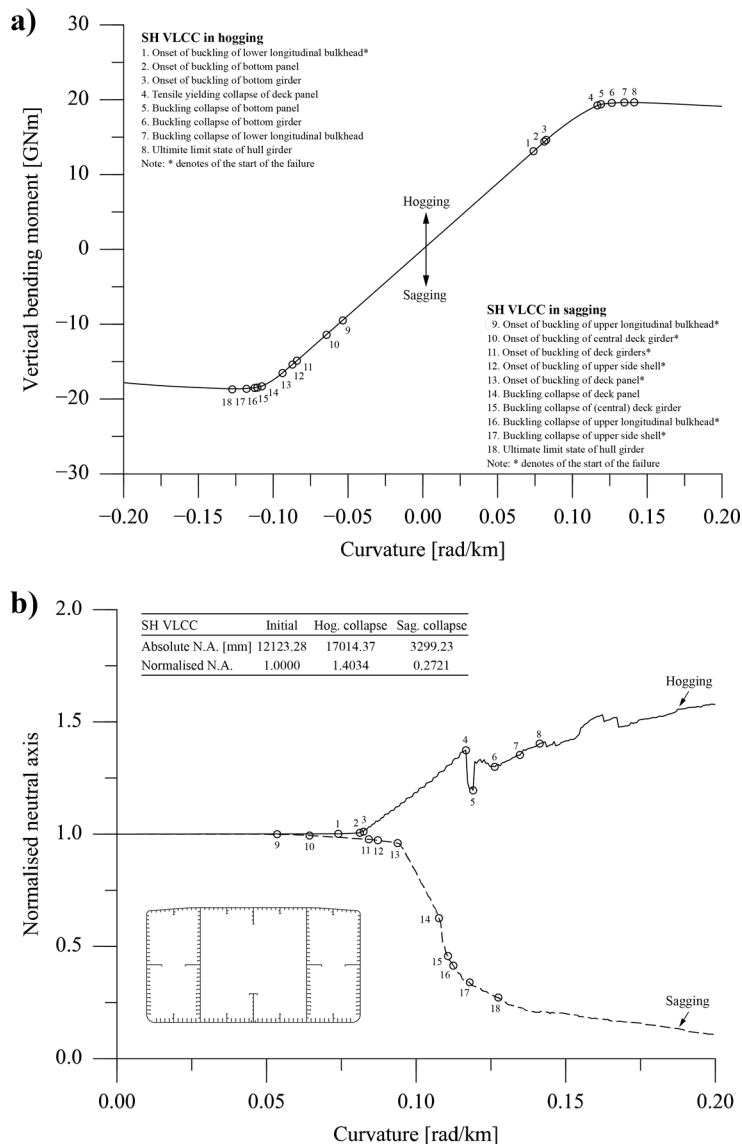


Figure 2-5 Collapse mechanism of single hull VLCC under vertical bending

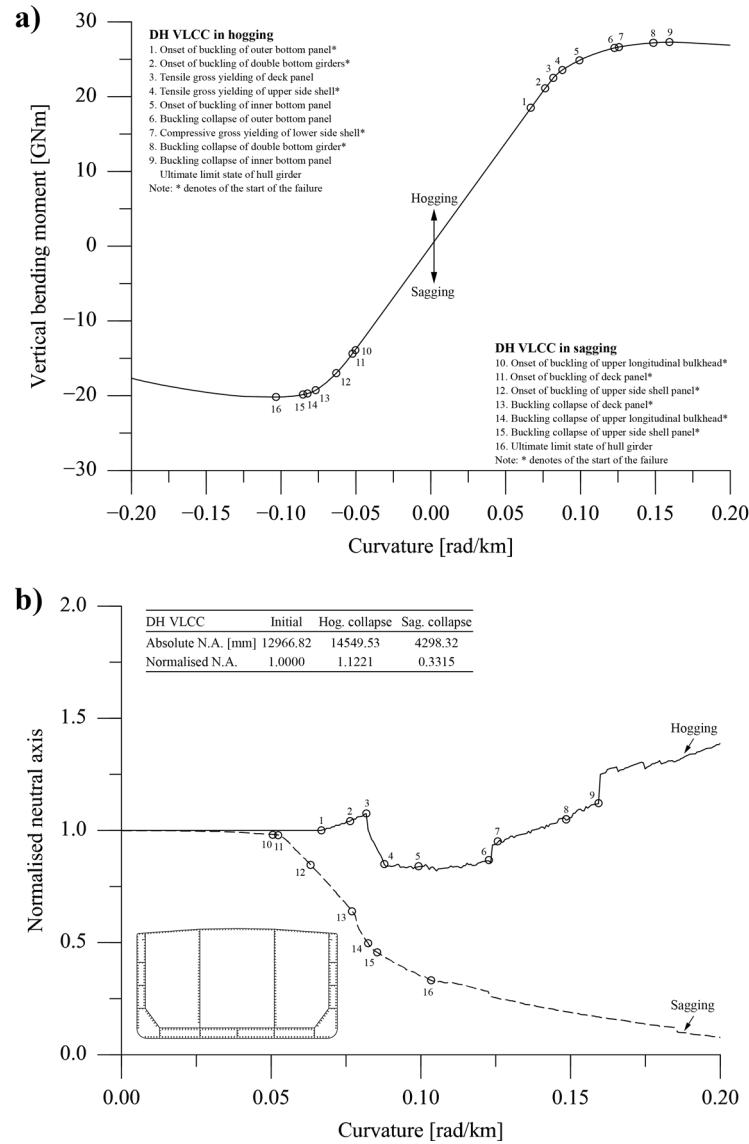


Figure 2-6 Collapse mechanism of double hull VLCC under vertical bending

Regarding the double hull VLCC shown in Figure 2-6, the collapse of the vessel in sagging is triggered by the buckling failure of the deck panel, which is then followed by the buckling collapse of the upper panels of the longitudinal bulkhead. The failure spreads in sequence along the vertical direction of the bulkhead until the ultimate limit state of the hull girder is attained. Relatively large tensile stress is developed in the bottom panels and lower part of the longitudinal bulkhead. However, no tensile yielding collapse took place even at the ultimate limit state as the neutral axis keeps moving downward. In hogging, the onset of buckling outer bottom panel and double bottom girders leads to upward translation of the

neutral axis. However, the first failure occurs at the deck and upper side shell panels due to tensile yielding, which therefore results in a sudden drop of the neutral axis. With further applied curvature, the buckling collapse of the outer bottom panel takes place. The ultimate limit state of the hull girder is attained soon after the buckling collapse of the inner bottom panels.

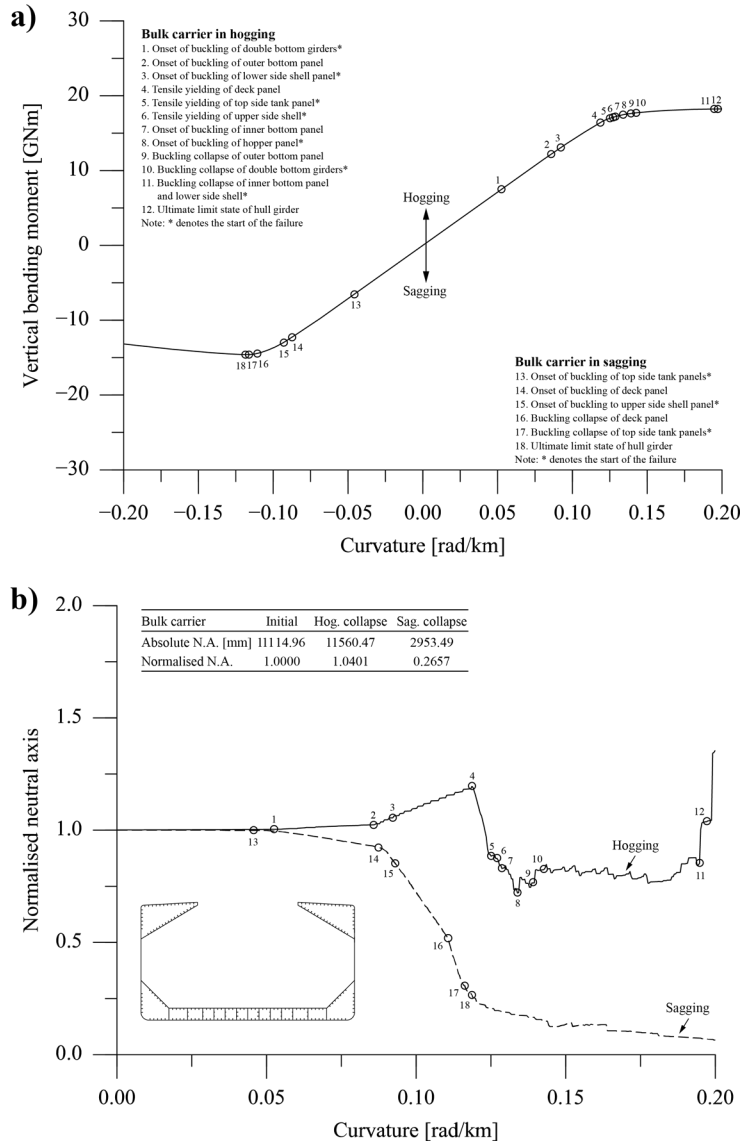


Figure 2-7 Collapse mechanism of bulk carrier under vertical bending

As for the bulk carrier and container ship with large deck opening (Figure 2-7 and Figure 2-8), the collapse in sagging takes place due to the buckling collapse of

deck panel, upper side shell as well as the top side tank panel. No tensile yielding is observed at the sagging collapse state.

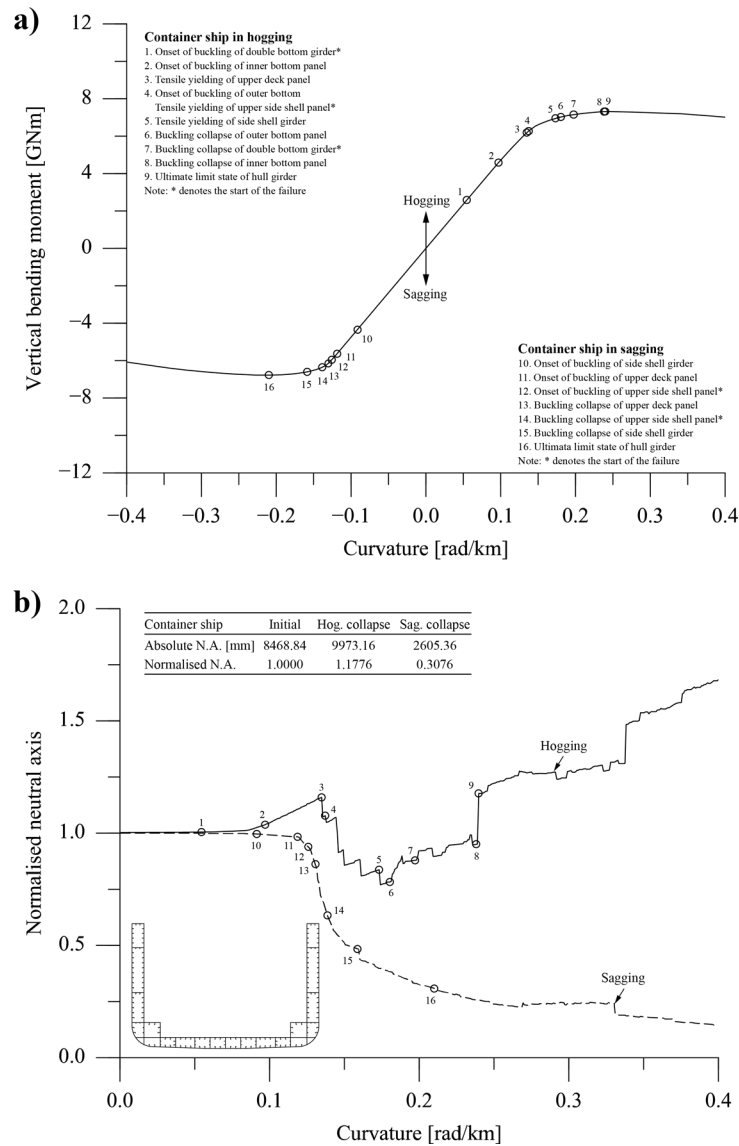


Figure 2-8 Collapse mechanism of container ship under vertical bending

In hogging, the collapse mechanisms of bulk carrier and container ship are similar to VLCC. After the buckling collapse of the outer bottom, the cross section is still able to sustain further rotational displacement, although no significant bending moment is accumulated. This is because the neutral axis is still close to the double bottom of the cross section even the outer bottom panel has failed, which means a further curvature application would result in fairly small strain increment on

the inner bottom and lower side shell panels, the collapse of which marked the final failure of the hull girder.

2.4 Experimental Works

Concerning the buckling collapse behaviour of unstiffened plates, physical testing was conducted by Dwight and Ractliffe (1967), Moxham (1971), Bradfield (1980), Nielsen et al. (1980) and Fukumoto et al. (1984). The test data is presented as a function of the plate slenderness ratio β in Figure 2-9 for the welded simply support plates which might be the most relevant scenario in ship structure application. Deviation between the test results can be attributed to the differences in welding quality, individual plate versus a square corner tube configuration, definition of the material strength and the boundary conditions of the testing rig. Nevertheless, a clear relation between the plating collapse strength and the slenderness ratio β could be identified.

In terms of the stiffened panels, the physical experiments on the collapse behaviours in longitudinal compression may refer to Smith (1975), Faulkner (1977), Horne et al. (1976, 1977), Niho (1978), Yao (1980), Tanaka and Endo (1988) and Paik and Thayamballi (1997). Tee-bar, angle-bar and flat-bar stiffened panels were covered in these testing. Collecting from Paik and Thayamballi (1997), a summary of the test data is illustrated in Figure 2-10. Smith's large-scale multi-bay testing indicated that the beam-column collapse behaviour might be the most representative failure mode of ship-type structures.

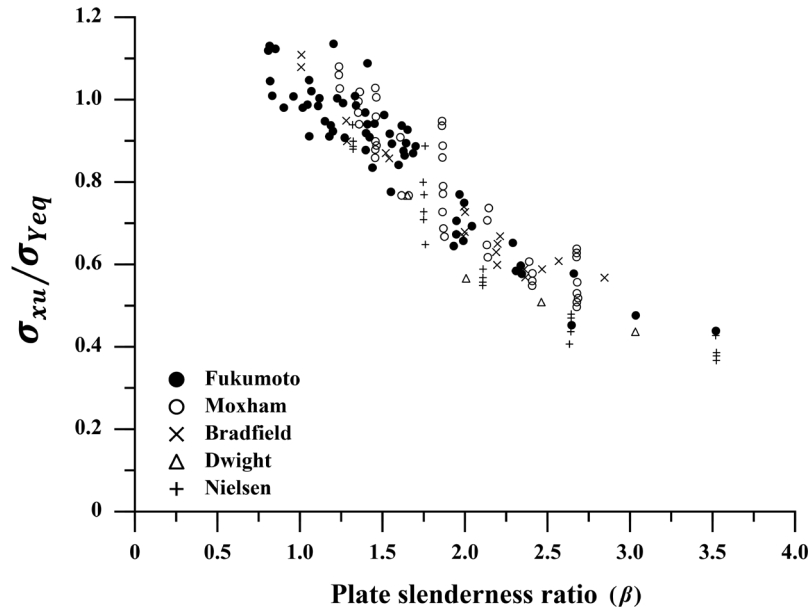


Figure 2-9 Test data of welded simply supported unstiffened plates

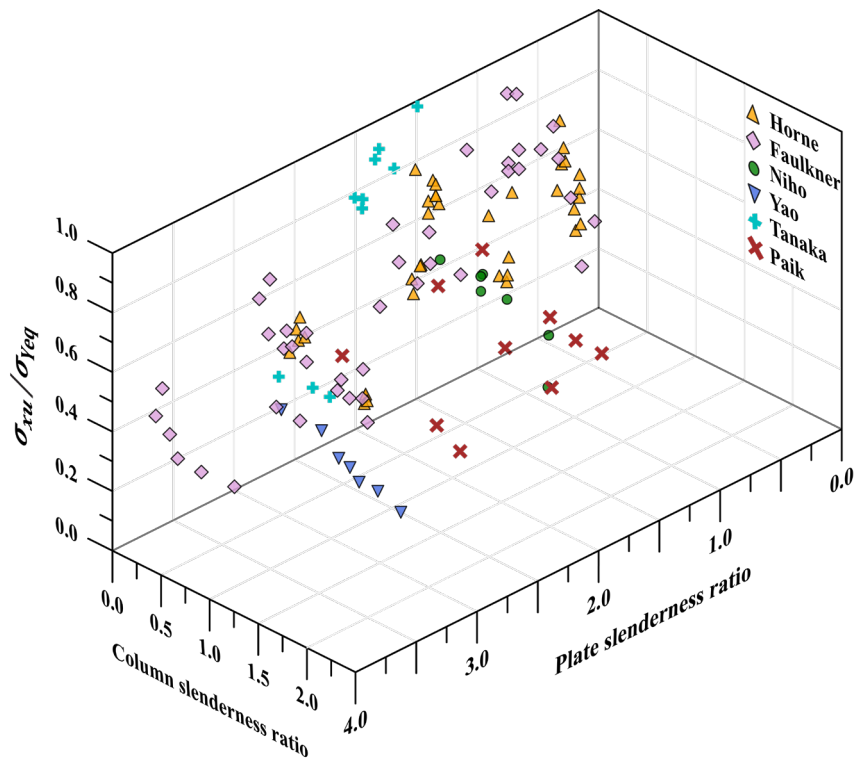


Figure 2-10 Test data of stiffened panels

Regarding to the ship hull girders, full-scale testing on actual ship girders under vertical bending were conducted by the US Navy in the 1930s and the UK Royal Navy in the 1950s. All these experiments indicated that the buckling of the compressed panels dominated the overall collapse of the ship hulls. However, it should be noted that all the tests were conducted on riveted ships and may be of less relevance for the assessment of modern ships that are primarily constructed by welding. Unfortunately, full-scale testing was absent ever since and hence there is no full-scale data of the collapse strength available for a welded ship hull. Conversely, the scaled-model experiments on welded box girders and ship hulls were conducted by Dowling et al. (1973), Nishihara (1983), Reckling (1979), Gordo and Guedes Soares (2013) under longitudinal bending. Recently, a testing on container ship model was carried out by Tanaka et al. (2015) to investigate the effect of combined vertical and torsional bending. Among these scaled-model tests, the most classical one might be the 1/3 scaled frigate test by Dow (1991), which has been subjected to several benchmark studies (ISSC, 2000; ISSC, 2012).

2.5 Ultimate Strength Analysis Methods of Structural Members

To assist with the design and appraisal of ship structures, various theoretical analysis methods are developed to predict the collapse strength of plates, stiffened panels and ship hull girders. Based on their fundamental principles, these methods may be separated into three distinct types: analytical approaches, numerical simulations and empirical formulations.

2.5.1 Analytical Approaches

- **Effective Width Concept (Plate)**

An effective width concept was proposed by von-Karman assuming that the stress distribution of a buckled plate may be idealised as Figure 2-11 (Timoshenko and Woinowsky, 1959). This model assumes that the middle buckled part has no load-

carrying capacity, whereas the effective part carries all the applied load. As the overall applied force increases, the effective part will be progressively narrowed by the progressive buckling of the middle part. This approach allows for the determination of edge stress and total post-buckling force through the relationship given by Equation (2-3). It was postulated that the plate will collapse when the edge stress reaches yield and thus the von-Karman model of the ultimate strength of plates under compression is given by Equation (2-4).

$$F = \int_0^b \sigma dy = \sigma_e b_e = \sigma_{ave} b \quad (2-3)$$

$$\frac{\sigma_{xu}}{\sigma_{Yeq}} = \frac{1.9}{\beta} \quad (2-4)$$

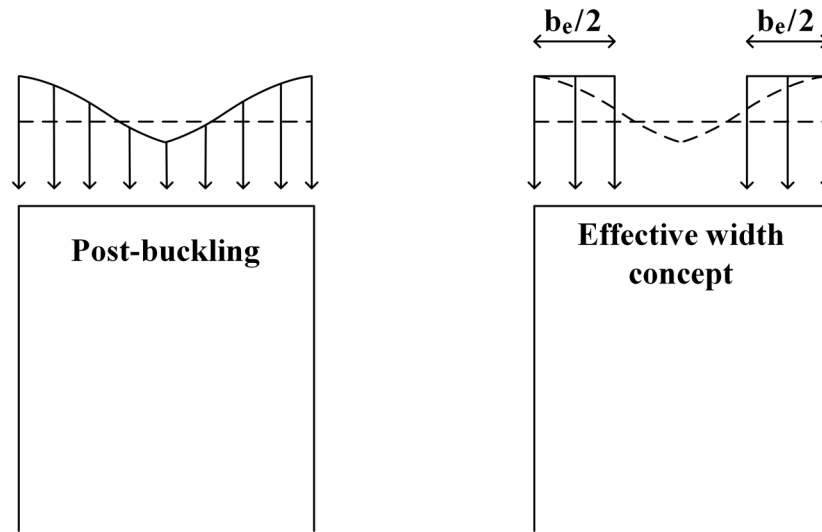


Figure 2-11 Effective width concept

- **Elastic Large Deflection Theory (Plate)**

The elastic large deflection theory was generalised from the small deflection formulation of elastic plate to account for both bending and membrane actions. Originally formulated by von-Karmon, the equilibrium relation and compatibility relation of an imperfect plate with initial deflection w_0 are given as Equation (2-

5) and Equation (2-6) respectively. Solution to Equation (2-5) and (2-6) may be achieved assuming that the plate is simply supported and the total deflection w and initial deflection w_0 take the form of Equation (2-7) and Equation (2-8).

$$\nabla^4(w - w_0) = \frac{t}{D} \left[\frac{\partial^2 F}{\partial y^2} \frac{\partial^2 w}{\partial x^2} - 2 \frac{\partial^2 F}{\partial x \partial y} \frac{\partial^2 w}{\partial x \partial y} + \frac{\partial^2 F}{\partial x^2} \frac{\partial^2 w}{\partial y^2} \right] \quad (2-5)$$

$$\nabla^4 F = E \left[\left(\frac{\partial^2 w}{\partial x \partial y} \right)^2 - \left(\frac{\partial^2 w}{\partial x^2} \right) \left(\frac{\partial^2 w}{\partial y^2} \right) - \left(\frac{\partial^2 w_0}{\partial x \partial y} \right)^2 + \left(\frac{\partial^2 w_0}{\partial x^2} \right) \left(\frac{\partial^2 w_0}{\partial y^2} \right) \right] \quad (2-6)$$

$$w = A_m \sin \left(\frac{m\pi x}{a} \right) \sin \left(\frac{\pi y}{b} \right) \quad (2-7)$$

$$w_0 = A_{0m} \sin \left(\frac{m\pi x}{a} \right) \sin \left(\frac{\pi y}{b} \right) \quad (2-8)$$

By the application of Galerkin method, such as in Paik and Hughes (2010), a cubic equation in terms of the unknown maximum total deflection A_m (Equation 2-9) can be derived.

$$C_1 A_m^3 + C_2 A_m^2 + C_3 A_m + C_4 = 0 \quad (2-9)$$

where

$$C_1 = \frac{\pi^2 E}{16} \left(\frac{m^4}{a^4} + \frac{1}{b^4} \right)$$

$$C_2 = 0$$

$$C_3 = \frac{m^2}{a^2} \sigma_x + \frac{\pi^2 D}{t_p} \left(\frac{m^2}{a^2} + \frac{1}{b^2} \right)^2 - A_{0m}^2 \frac{\pi^2 E}{16} \left(\frac{m^4}{a^4} + \frac{1}{b^4} \right)$$

$$C_4 = -A_{0m} \frac{\pi^2 D}{t_p} \left(\frac{m^2}{a^2} + \frac{1}{b^2} \right)^2$$

The solution to Equation (2-9) may be obtained using Cardano method given Equation (2-10) to (2-19). Note that an unique solution may not exist for a cubic function and only real positive solution is relevant for elastic large deflection analysis.

$$P = \frac{C_3}{C_1} \quad (2-10)$$

$$Q = \frac{C_4}{C_1} \quad (2-11)$$

$$\Delta = \left(\frac{Q}{2}\right)^2 + \left(\frac{P}{3}\right)^3 \quad (2-12)$$

$$S = 2\sqrt[3]{R} \quad (2-13)$$

$$R = \sqrt{-\left(\frac{P}{3}\right)^3} \quad (2-14)$$

$$\theta = \frac{1}{3}\cos^{-1}\left(-\frac{Q}{2R}\right) \quad (2-15)$$

$$A_m = 0 \quad \text{if } Q = 0 \text{ and } P \geq 0 \quad (2-16)$$

$$A_m = -\sqrt{P} \quad \text{if } Q = 0 \text{ and } P < 0 \quad (2-17)$$

$$A_m = \sqrt[3]{-\frac{Q}{2} + \sqrt{\Delta}} + \sqrt[3]{-\frac{Q}{2} - \sqrt{\Delta}} \quad \text{if } Q < 0 \text{ and } \Delta > 0 \quad (2-18)$$

$$A_m = \max(A_m^1, A_m^2, A_m^3) \quad \text{if } Q < 0 \text{ and } \Delta \leq 0 \quad (2-19)$$

$$A_m^1 = S\cos\theta; A_m^2 = S\cos(\theta + 120); A_m^3 = S\cos(\theta + 240)$$

• **Dow and Smith Method (Stiffened Panel)**

An analytical method was developed by Dow and Smith (1986) to predict the ultimate strength and the complete load-shortening curve of stiffened panels. In this approach, a beam-column idealisation was adopted to model the behaviours of stiffened grillages on the assumption of a wide panel containing a large number of parallel stiffeners which behave identically. The interaction between two adjacent spans was accounted and the transverse frame was assumed to be flexural rigid and torsional weak. Therefore a simple support condition was imposed. The idealised structure is subdivided along the length into 20 beam-column elements, which are further discretised over the depth into fibres (Figure 2-12). The attached plating is treated as a single fibre with stiffness estimated from pre-defined stress-strain curves. A finite element procedure was employed to solve the incremental force-displacement equation with an iteration by the modified Newton-Raphson method at each incremental step for equilibrium correction. The method is incorporated in the computer code FABSTRAN. Note that this approach is limited to a beam-column buckling failure mode.

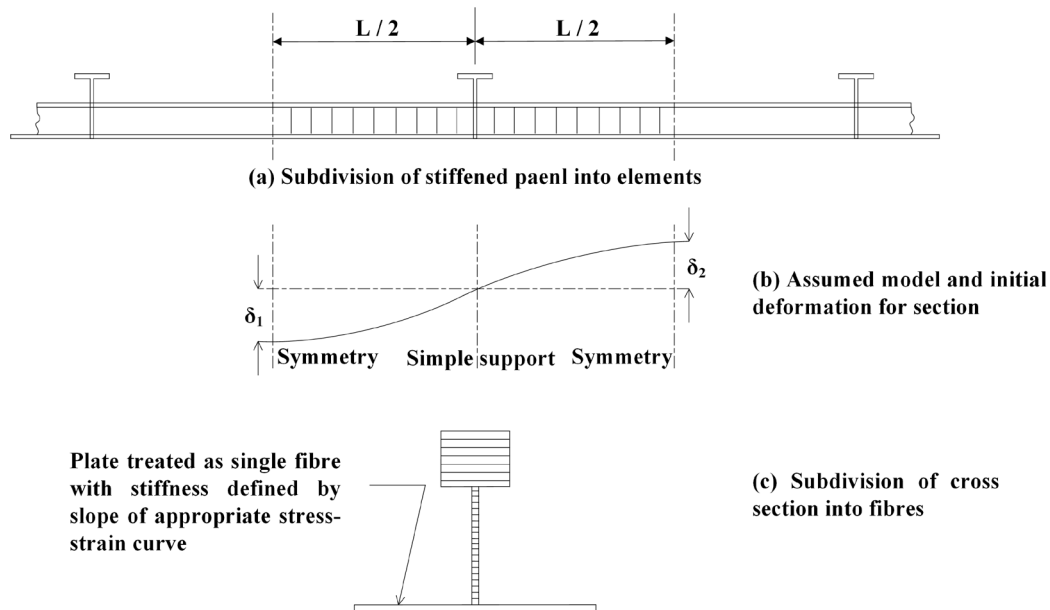


Figure 2-12 Model idealisation of Dow and Smith method

• **Yao and Nikolov Method (Stiffened Panel)**

A similar beam-column model concept was employed by Yao and Nikolov (1991) to develop an analytical method for predicting the plastic/buckling collapse and full load-shortening response of stiffened panels. Instead of a pre-evaluation, a combination of elastic large deflection analysis and rigid-plastic mechanism analysis is applied to predict the effectiveness of the attached plating. By contrast, a set of stress and strain distribution was pre-defined for stiffener under in-plane compression considering large deflection (Figure 2-13). The overall beam-column response is predicted incrementally with iterative check for the force and moment equilibrium at the cross sections.

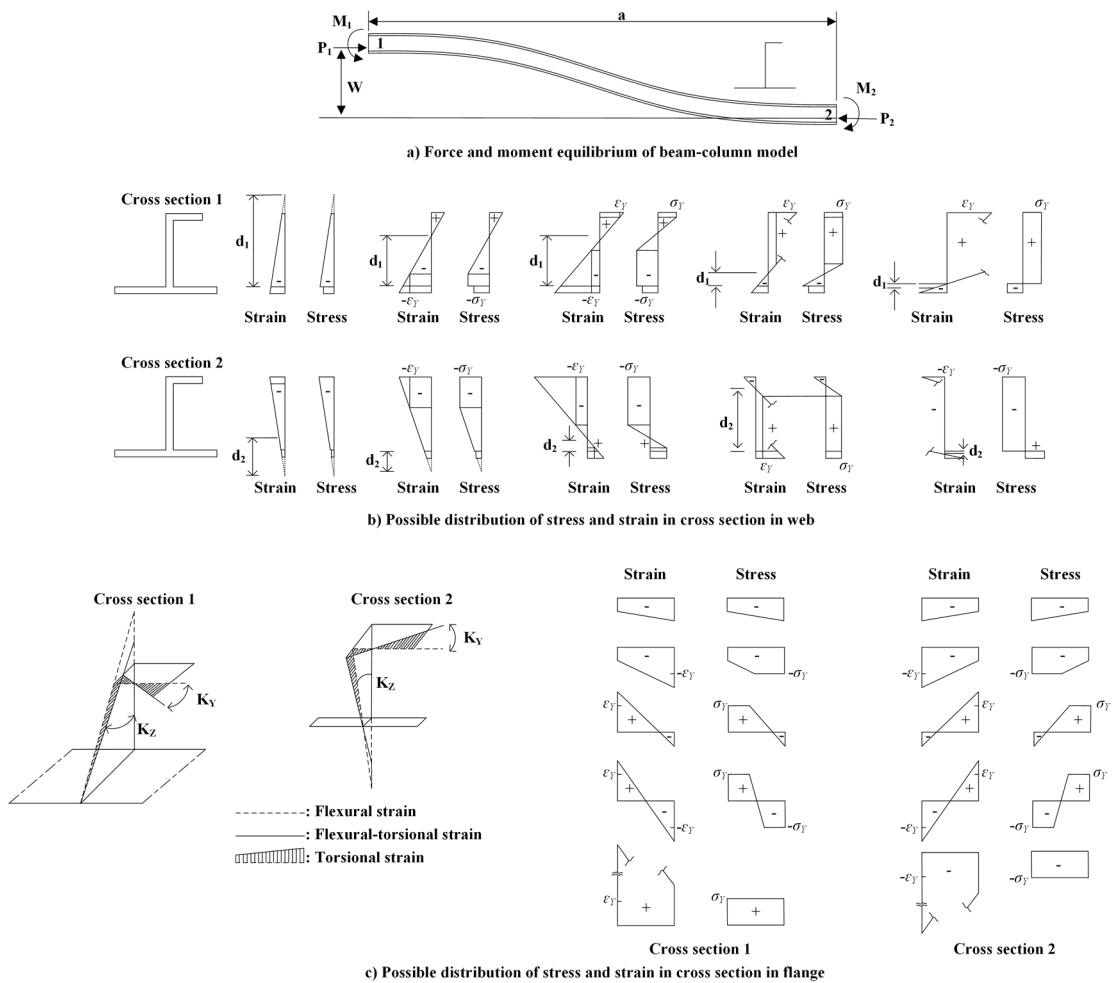


Figure 2-13 Stress-strain distribution of beam-column cross sections

- **Gordo and Guedes Soares Method (Stiffened Panel)**

Gordo and Guedes Soares (1993) developed an analytical approach considering local plate buckling failure, flexural column buckling and stiffener tripping. This approach generalised Faulkner's effective width concept (Faulkner et al., 1973) to consider the loss of effectiveness of local plating caused by buckling. No iteration is required in this method.

- **IACS Common Structural Rule method (Stiffened Panel)**

A highly accessible approach was readily available in the Common Structural Rule (IACS, 2019). The CSR method is established in a similar way as Gordo and Guedes Soares' approach, but embedded with the Frankland formula (Frankland, 1940) to consider the loss of effectiveness caused by buckling using an effective width concept. Meanwhile, the local buckling of stiffener web is also taken into account in the CSR method.

- **Adapted Orthotropic Method (Stiffened Panel)**

An adapted large deflection orthotropic plate methodology was proposed by Benson et al. (2015), with a capability to account for both inter-frame and multi-frame buckling collapse modes of an orthogonal stiffened panel. This method is useful for the strength assessment of lightly framed grillages typical for lightweight vessels.

2.5.2 Numerical Simulation

Numerical simulation, based usually on finite element method has been a capable approach for buckling and ultimate strength analysis. The use of nonlinear finite element method enables the evaluation of various parameters of influence, including initial imperfections, secondary loadings, in-service degradations and different materials. Dow and Smith (1984) employed the finite element method to

analyse the effects of localised imperfection on the compressive strength of rectangular long plates. Gordo (2015) analysed the influence of initial imperfection on the strength of restrained plating with the aid of finite element analysis. Benson et al. (2011, 2013a) investigated the ultimate collapse strength and load-shortening characteristics of marine-grade aluminium alloy plates in compression. Syrigou and Dow (2018) analysed the collapse behaviour of steel and aluminium plates under combined compression/tension and shear. An introduction to nonlinear finite element methods and approaches for marine structures was given by Benson and Collette (2017). Paik and Seo (2009a, 2009b) discussed the modelling techniques and practical procedure for ultimate strength analysis of plate and stiffened panels under combined biaxial compression and lateral pressure.

2.5.3 Empirical Formulation

A number of empirical formulation are developed, typically by regression analysis on experimental or numerical dataset to predict the ultimate strength of plates and stiffened panels. These formulation provide highly efficient first-cut estimation of the buckling performance of structural segments, as only the basic dimensionless parameters are needed for computation.

- **Frankland Formula (Plate)**

Frankland formula (Equation 2-20) was derived based on test data on unwelded constrained plates to predict the ultimate compressive strength of unstiffened plates. The formula follows the von-Karman model given as a function of the plate slenderness ratio, but includes a second-order term. Note that Frankland formula is embedded in the IACS-CSR methodology for predicting the ultimate strength and load-shortening curves of stiffened panels.

$$\frac{\sigma_{xu}}{\sigma_{Yp}} = \frac{2.25}{\beta} - \frac{1.25}{\beta^2} \quad \text{if } \beta > 1.25$$

$$\frac{\sigma_{xu}}{\sigma_{Yp}} = 1.0 \quad \text{if } \beta \leq 1.25 \quad (2-20)$$

- **Faulkner Formula (Plate)**

Faulkner formula was formulated using the experimental data on unwelded unconstrained plates and was given in the same second-order form as Frankland formula with revised coefficients (Equation 2-21). Note that Faulkner formula is incorporated in the Gordo and Guedes Soares method for predicting the ultimate strength and load-shortening curves of stiffened panels. A comparison between the Frankland formula, Faulkner formula and von-Karman formula is shown in Figure 2-14. It is clear that Faulkner formula is more conservative in full range of plate slenderness ratio than Frankland and von-Karman formulae.

$$\frac{\sigma_{xu}}{\sigma_{Yp}} = \frac{2.0}{\beta} - \frac{1.0}{\beta^2} \quad \text{if } \beta > 1.0$$

$$\frac{\sigma_{xu}}{\sigma_{Yp}} = 1.0 \quad \text{if } \beta \leq 1.0 \quad (2-21)$$

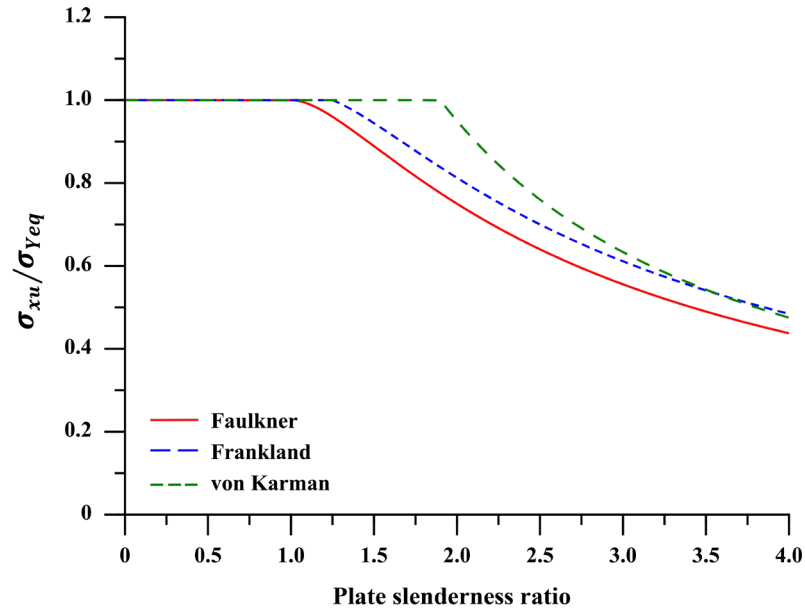


Figure 2-14 Comparison of ultimate strength formula for unstiffened plates

- **Lin Formula (Stiffened Panel)**

A polynomial form was proposed by Lin (1984) to develop a design formula for predicting the ultimate strength of stiffened plating in terms of plate slenderness ratio β and column slenderness ratio (Equation 2-22). Least-square method was employed for the regression analysis with the aid of dataset produced by a numerical method using a finite difference procedure. An average-level initial distortion and welding-induced residual stress were considered.

$$\frac{\sigma_{xu}}{\sigma_{Yeq}} = \frac{1}{\sqrt{0.960 + 0.765\lambda^2 + 0.176\beta^2 + 0.131\lambda^2\beta^2 + 1.046\lambda^4}} \quad (2-22)$$

- **Paik and Thayamballi Formula (Stiffened Panel)**

Paik and Thayamballi formula (1997) adopted the same polynomial form of Lin's formula with a modification of the empirical constants to improve the prediction accuracy for stiffened panels with high column slenderness ratio (Equation 2-23). The supporting dataset was generated by experimental measurement. Hence, the

initial distortion and welding-induced residual stress may implicitly be taken into account in an as-built condition.

$$\frac{\sigma_{xu}}{\sigma_{Yeq}} = \frac{1}{\sqrt{0.995 + 0.936\lambda^2 + 0.176\beta^2 + 0.188\lambda^2\beta^2 - 0.067\lambda^4}} \quad (2-23)$$

- **Zhang and Khan Formula (Stiffened Panel)**

Zhang and Khan formula (2009) was developed on the basis of ABAQUS nonlinear finite element solutions (Equation 2-24). The finite element analysis was performed on three-bay/one-span stiffened panels with ten longitudinal stiffeners. The initial distortion was incorporated in the form of local mode and global mode. The local mode includes the plate and stiffener's web multi-waves deflection with a maximum magnitude of $b/200$ for the plate where b is the plate width, and $h_w/200$ for the stiffener's web where h_w is the web height of stiffener. The welding-induced residual stress is excluded in Z-K formula.

$$\frac{\sigma_{xu}}{\sigma_{Yeq}} = \frac{1}{\beta^{0.28}} \frac{1}{\sqrt{1 + \lambda^{3.2}}} \text{ for } \lambda < \sqrt{2} \text{ and } \beta = 1.0 \text{ if } \beta < 1.0 \quad (2-24)$$

- **Kim Formula (Stiffened Panel)**

Kim et al. formula (2017) was proposed based on ANSYS nonlinear finite element results (Equation 2-25). The finite element analysis was conducted on the three-bay/three-span stiffened panel model with eight longitudinal stiffeners between the longitudinal girders. Three types of initial distortions were considered, namely the local plate deflection, column-type deflection and stiffener sideways deflection. The maximum magnitude of each deflection was $0.1\beta^2t$, $0.0015a$, $0.0015a$ where β , t and a are plate slenderness ratio, plate's thickness and panel's length respectively. No residual stress was modelled.

$$\frac{\sigma_{xu}}{\sigma_{Yeq}} = \frac{1}{0.8884 + e^{\lambda^2}} + \frac{1}{0.4121 + e^{\sqrt{\beta}}} \quad (2-25)$$

• **Xu Formula (Stiffened Panel)**

Xu et al. formula (2018) was established with the aid of ANSYS nonlinear finite element prediction (Equation 2-26). A three bay/three span model with two stiffeners on a single span was adopted for the finite element analysis. The formula was given in the form similar to Lin and P – K formula with an increased number of coefficients. The coefficients are summarised in Table 2-1 and are given separately for different types of stiffener profiles (Flat-bar, angle-bar and tee-bar).

$$\frac{\sigma_{xu}}{\sigma_{Yeq}} = \frac{1}{\sqrt{C_0 + C_1\lambda + C_2\beta + C_3\lambda\beta + C_4\lambda^2 + C_5\beta^2 + C_6\lambda^2\beta^2 + C_7\lambda^3 + C_8\beta^3 + C_9\lambda^3\beta^3 + C_{10}\lambda^4}} \quad (2-26)$$

Table 2-1 Coefficients of Xu formula

| | C_0 | C_1 | C_2 | C_3 | C_4 | C_5 |
|-------|-------|-------|-------|-------|----------|-------|
| Flat | 1.11 | -4.91 | 0.49 | 0.77 | 10.07 | -0.11 |
| Angle | 1.19 | -1.58 | -0.36 | 0.29 | 3.41 | 0.46 |
| Tee | 3.56 | -3.58 | -3.42 | 1.00 | 4.80 | 1.81 |
| | C_6 | C_7 | C_8 | C_9 | C_{10} | |
| Flat | -0.14 | -7.09 | 0.00 | 0.01 | 1.56 | |
| Angle | -0.02 | -2.26 | -0.08 | 0.00 | 0.46 | |
| Tee | -0.22 | -2.58 | -0.28 | 0.02 | 0.46 | |

• **A.R.E Design Charts (Stiffened Panel)**

As given in Figure 2-15, column collapse strength design charts were developed by the Admiralty Research Establishment (A.R.E.) by regression on a series of

numerical results computed FABSTRAN. Both initial distortion and welding residual stress were considered with three different levels of severity. Interpolation may be applied on the design charts. A comparison of empirical formulation reviewed above with the IACS-CSR method on the prediction of ultimate compressive strength of typical stiffened panels is given in Figure 2-16.

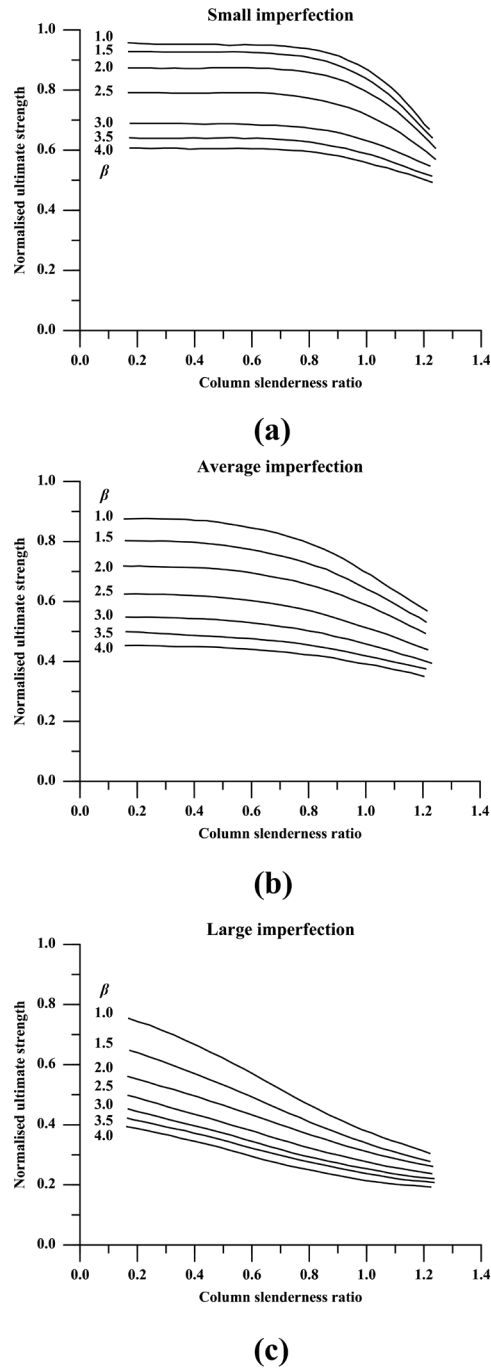


Figure 2-15 A.R.E column collapse strength design charts

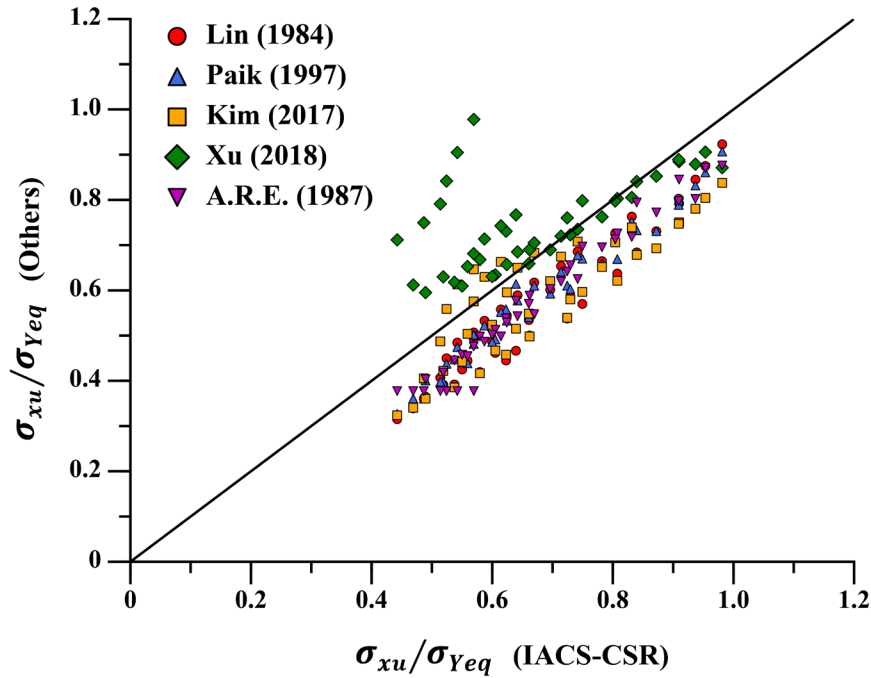


Figure 2-16 Comparison of the stiffened panel ultimate strength predictions by different empirical formulations

It is clear that most empirical formulations are conservative in predicting the ultimate compressive strength of stiffened panels, as compared with the IACS-CSR approach. Whilst the discrepancy could be caused by the difference in assumed imperfection (shape and magnitude), it is likely that the deviation is driven by the relatively optimistic effective width model (Frankland formula) adopted in IACS-CSR. This is also demonstrated by Figure 2-14, in which the Frankland formula overestimate the strength of unstiffened plate in comparison with Faulkner formula.

2.6 Ultimate Strength Analysis Methods of Hull Girders

Several methodologies for the theoretical prediction of ultimate ship hull strength are available. These includes direct calculation approaches with closed-form expression restricted to the ultimate hull girder strength only and the rigorous incremental approach which is able to trace the full bending moment/curvature relationship.

2.6.1 Empirical Method

An empirical formula was proposed by Frieze and Lin (1991) to estimate the ultimate bending capacity of ship hull girders in terms of the compressive strength of critical panel (Equation 2-27 & 2-28). The formula was developed based upon a series of calculation using a methodology similar to Smith method, which will be introduced later. The critical panels are normally deck panels in sagging and bottom panels in hogging.

This empirical method provides a fast estimation on the ultimate ship hull girder strength. However, like most of the empirical formulation, its accuracy and applicability are subject to the database upon which it was developed. For the regression of empirical constants of the sagging expression, ten results were employed. For the regression of empirical constants of the hogging expression, six results were adopted. In addition, although no indication was made on its applicability, this formula was developed from the results of longitudinally-framed naval ships.

$$\frac{M_u}{M_p} = -0.172 + 1.548 \frac{\sigma_{xu}}{\sigma_{Yeq}} - 0.368 \left(\frac{\sigma_{xu}}{\sigma_{Yeq}} \right)^2 \quad \text{for sagging} \quad (2-27)$$

$$\frac{M_u}{M_p} = 0.003 + 1.459 \frac{\sigma_{xu}}{\sigma_{Yeq}} - 0.461 \left(\frac{\sigma_{xu}}{\sigma_{Yeq}} \right)^2 \quad \text{for hogging} \quad (2-28)$$

2.6.2 Presumed Stress Distribution-Based Method

The presumed stress distribution-based method usually refers to a direct calculation methodology based on a presumption on the stress distribution on the ship hull cross section at the moment of collapse. An integration of the resultant stress gives the ultimate bending moment of the cross section. This class of methods may be originated from the calculation of plastic bending moment of a simple beam with generalisation to a box girder cross section (Figure 2-17).

Relevant nomenclature are given in Equation (2-29) to (2-32). The presumed stress distribution-based methods are usually developed as closed-form formulae. It thus enables a fast approximation of the ultimate ship hull girder strength in the early stage of design (Paik and Mansour, 1995). However, its accuracy is largely dominated by the assumed stress distribution profile.

$$A = A_D + 2A_S + A_B \quad (2-29)$$

$$\alpha_D = A_D/A \quad (2-30)$$

$$\alpha_S = A_S/A \quad (2-31)$$

$$\alpha_B = A_B/A \quad (2-32)$$

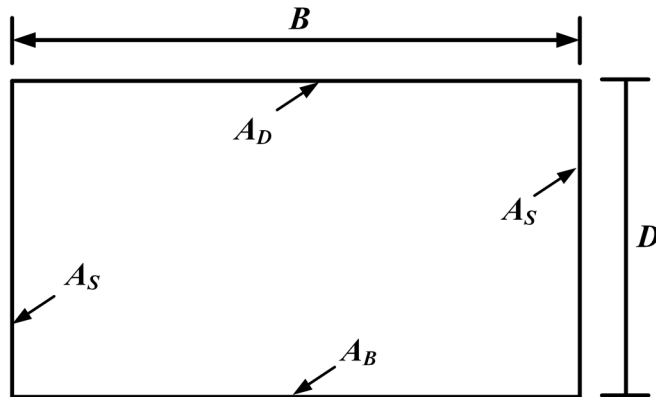


Figure 2-17 Nomenclature in presumed stress distribution-based method

- **Caldwell Method**

Caldwell (1965) proposed a stress distribution shown in Figure 2-18 taking into account of the buckling reduction at the compressed part and the fully developed yielding of the tensile part. The expression of Caldwell method is given by Equation (2-33). However, this method assumes that the collapse of all panels take place simultaneously and no consideration is given for the reduction of the

post-ultimate capacity of structural components, which therefore would give an overestimation of the ultimate bending moment.

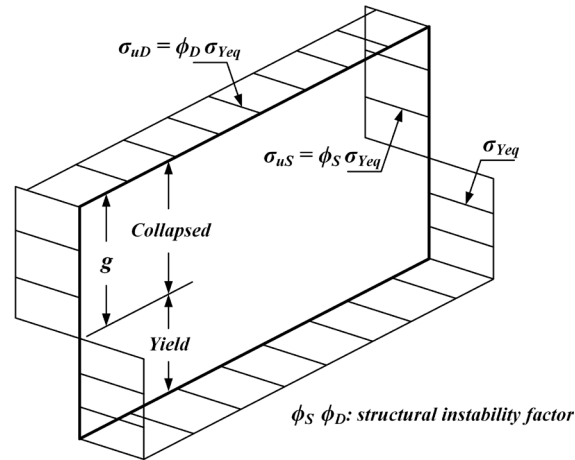
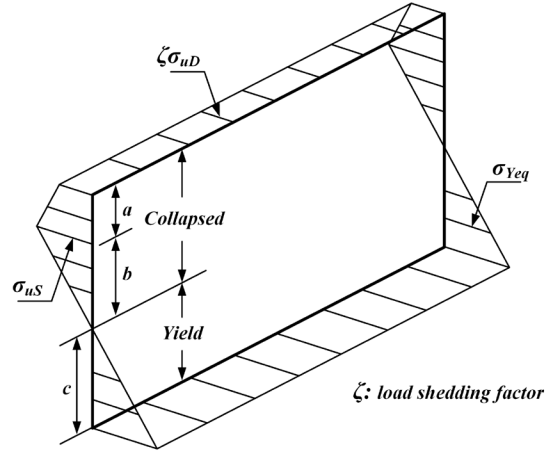


Figure 2-18 Presumed stress distribution of Caldwell method

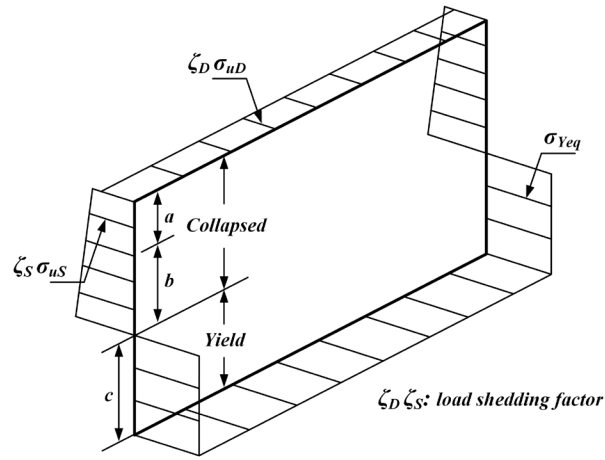
$$M_u = \sigma_{Yeq} AD \left\{ \phi_D \alpha_D \gamma + 2\alpha_S \left[\frac{1}{2} - \gamma + \gamma^2 \frac{(1 + \phi_S)}{2} \right] + \alpha_B (1 - \gamma) \right\} \quad (2-33)$$

- **Wong Method**

Wong (1977) proposed two patterns of stress distribution at the moment of collapse to consider the effects of post-collapse load-shedding between the failed and intact stiffened panels (Figure 2-19). The expressions of ultimate bending moment are given by Equation (2-34) and (2-35) for type 1 and type 2 respectively.



(a) Type 1



(b) Type 2

Figure 2-19 Presumed stress distribution of Wong method

$$M_u = \sigma_{Yeq}AD \left\{ \alpha_D \phi_D (\gamma_a + \gamma_b) + \alpha_S \phi_S \left[\frac{\gamma_a^2}{3} (1 + 2\zeta) + \gamma_a \gamma_b (1 + \zeta) + \frac{2}{3} \gamma_b^2 \right] + \frac{2}{3} \alpha_S \gamma_c^2 + \alpha_B \gamma_c \right\} \quad (2-34)$$

$$M_u = \sigma_{Yeq}AD \left\{ \alpha_S \left(\frac{\phi_S}{3} + \frac{2}{3} \phi_S \zeta_S + 1 \right) \gamma^2 + \gamma (\alpha_D \zeta_D \phi_D - 2\alpha_S - \alpha_B) + \alpha_S + \alpha_B \right\} \quad (2-35)$$

- **Modified Paik and Mansour Method**

To allow for the propagation of the yielded zone, a modified Paik and Mansour method was developed by Paik et al. (2013), in which the presumed stress distribution is shown in Figure 2-21. In contrast to the original method, this modified formulation involves two unknowns h_C and h_Y . Hence, an iterative procedure was employed to ensure the force equilibrium condition of the cross section.

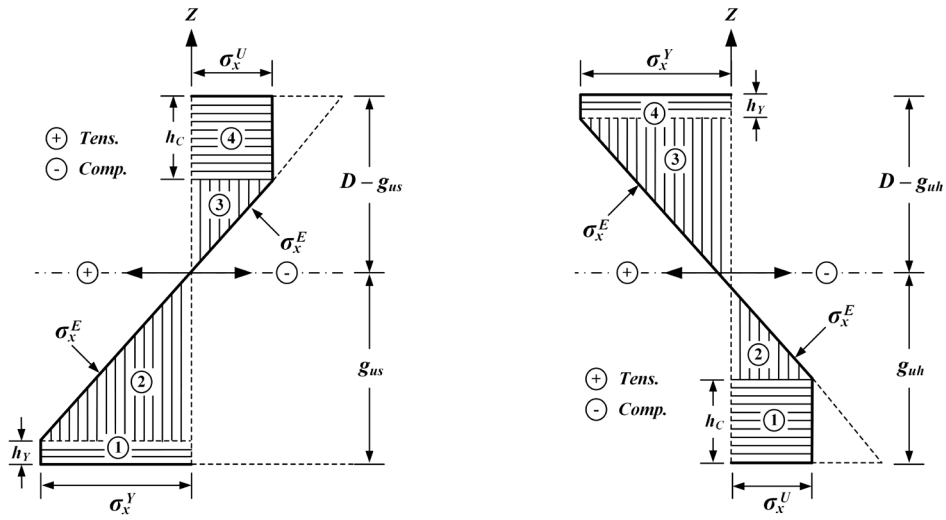


Figure 2-21 Presumed stress distribution of modified Paik and Mansour method

2.6.3 Structural Segment Collapse Strain-Based Method

Apart from using the resultant stress at collapse state to derive an expression of ultimate bending strength, an alternative method was proposed by Hughes (1988) utilising the collapse strain of structural segment to establish an equilibrium state at failure (Figure 2-22).

The first step is to calculate the first failure curvature ϕ_0 and corresponding bending moment M_0 without equilibrium check as given by Equation (2-38) and (2-39) where ε_{xu}^i is the compressive collapse strain of panel i , ε_{Yeq}^i is the tensile collapse strain of panel i , y_i is the distance between the panel centroid and the

neutral axis, ϕ is the bending curvature at collapse and EI_0 is the elastic stiffness of the intact cross section. The subscripts in ϕ_0 and M_0 indicate the current incremental step.

$$\phi_0 = \min \left(\left| \frac{\varepsilon_{xu}^i}{y_i} \right|, \left| \frac{\varepsilon_{Yeq}^i}{y_i} \right| \right) \quad \text{for } i = 1 \sim N_p \quad (2-38)$$

$$M_0 = EI_0 \phi_0 \quad (2-39)$$

In most cases, the first failure is triggered by the compressive collapse of critical components. As a result of the compressive failure and the subsequent load-shedding, the equilibrium of the hull girder would be disturbed. To this end, the hull girder properties such as y_i and EI_0 should be updated considering the capacity loss of the failed panels. The new curvature corresponding to the potential equilibrium point may be calculated as Equation (2-40).

$$\phi_0^{(1)} = \frac{M_0}{EI_0^{(1)}} \quad (2-40)$$

It is necessary to check for the failure of other panels because of the increase in curvature and the translation of neutral axis. After establishing the first failure equilibrium, an incremental procedure could be commenced with an incremental curvature given by Equation (2-41). The procedure just outlined is repeated until equilibrium can no longer be established. In most ships, only a limited incrementation is required.

$$\Delta\phi_1^{(0)} = \min \left(\left| \frac{(\varepsilon_{xu}^i) - (\varepsilon_{ave}^i)_1^{(0)}}{(y_i)_1^{(0)}} \right|, \left| \frac{(\varepsilon_{Yeq}^i) - (\varepsilon_{ave}^i)_1^{(0)}}{(y_i)_1^{(0)}} \right| \right) \quad \text{for } i = 1 \sim N_p \quad (2-41)$$

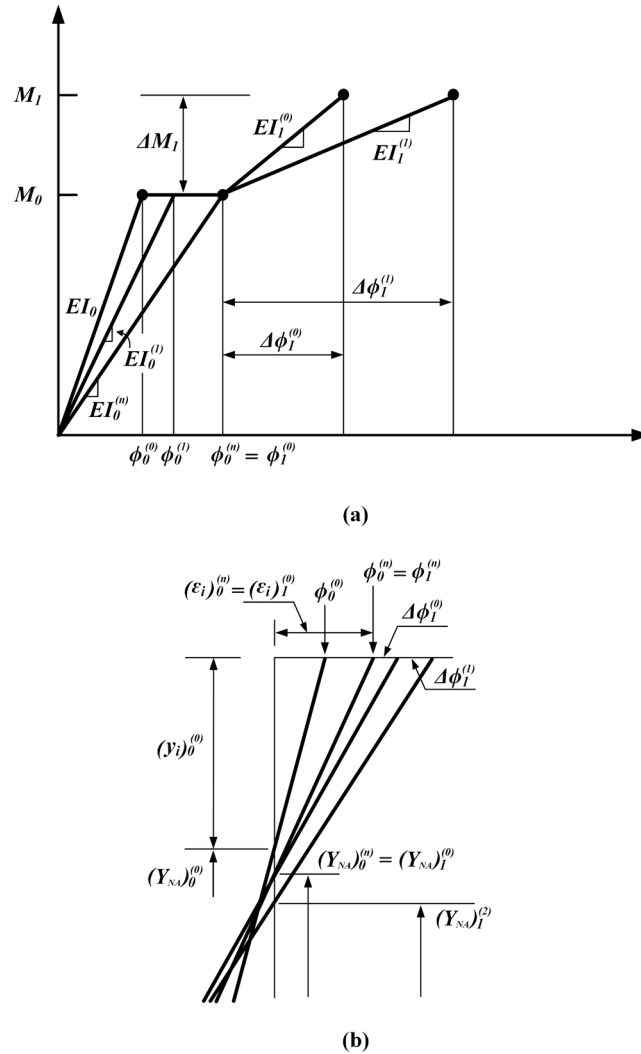


Figure 2-22 Illustration of the critical segment collapse strain-based method

2.6.4 Simplified Progressive Collapse Method (Smith Method)

The foregoing methodologies are only able to predict the ultimate bending capacity. A simplified progressive collapse method originally proposed by Smith (1977) can predict the full bending moment/curvature relationship. There are equivalent formulations developed by Gordo and Guedes Soares (1996) and Adamchak (1982). The Smith method has now become an established approach in the ultimate strength assessment. Through experimental testing such as Dow (1991) and numerical simulation such as Guedes Soares et al. (2008), it is well-validated and therefore has been codified in the Common Structural Rule. In principle, the Smith method is a generalisation of the Euler-Bernoulli beam

bending theory. In the following, an introduction to the original formulation and its extensions is presented.

- **Original Formulation**

The original formulation of Smith method was proposed to solve the pure vertical bending. As introduced by Smith (1977), three assumptions were made:

1. Beam assumption: the cross section remains plane throughout the progressive collapse and its behaviour follows the Euler-Bernoulli beam bending theory, which thereby gives a linearly varying distribution of the applied strain as the resultant of curvature increment;
2. Independency assumption: there is no interaction between the adjacent structural elements. Hence, their behaviour can be predicted independently;
3. Inter-frame assumption: the failure of the cross section is constrained to occur between frames, assuming that the transverse supports are sufficiently stocky.

- **Extended Formulation for Combined Vertical and Horizontal Bending**

Extending upon the original method, Dow and Smith (1986) derived a revised formulation to deal with combined vertical and horizontal bending (Equation 2-42). The solution may be given taking either the bending moment or the curvature as a controlling variable. However, to predict the post-collapse response, a curvature control must be used in the currently established formulation.

$$\begin{Bmatrix} \Delta M_H \\ \Delta M_V \end{Bmatrix} = \begin{bmatrix} D_{HH} & D_{HV} \\ D_{VH} & D_{VV} \end{bmatrix} \begin{Bmatrix} \Delta \chi_H \\ \Delta \chi_V \end{Bmatrix} \quad (2-42)$$

- **Extended Formulation for Multi-Frame Collapse**

An extended Smith method formulation was proposed by Benson et al. (2013) to address the overall instability failure involving multiple transverse frames. This extended capability is of importance for the strength assessment of lightweight vessels. The extended method follows the principle assumptions of the original approach where elements are subdivided into small segments as the original approach. However, the independency assumption is removed and the element length stretches over the entire compartment rather than inter-frame. The elements are grouped into “panel set” to define the overall extent of the orthogonal grillages, the load-shortening behaviour of which is predicted using the adapted orthotropic plate theory (Benson et al., 2015). A flow chart is given in Figure 2-23 highlighting the extension of this method with respect to the original approach.

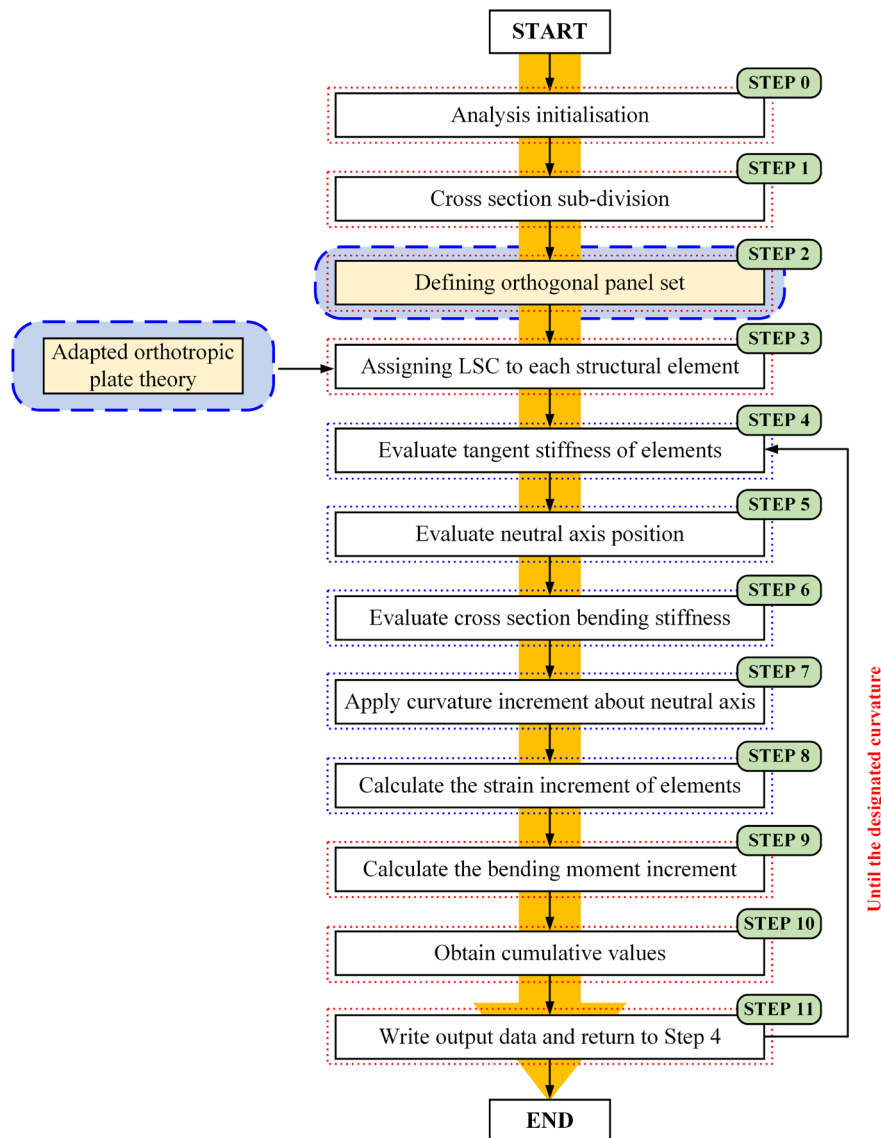


Figure 2-23 Flow chart of the extended Smith method for multi-frame collapse

- **Extended Formulation for Combined Vertical and Torsional Bending**

To account for the adverse effect of torsional bending which might be critical for ships with large opening such as container ships, an extended Smith method formulation was developed by Syrigou (2018). This extended capability allows for the prediction of an interactive diagram of the ultimate capacity under combined vertical and torsional bending. For a given torsional load, this method first calculates the shear flow distribution on each cells of the cross section. A series of

interactive diagrams are introduced for typical ship plates under combined compression and shear. These diagrams provides an estimation of the knock-down effect on the load-shortening curves of structural components. Once the load-shortening curves of each element with reduced capacity due to shear are derived, the incremental procedure is then invoked to predict the ultimate bending strength under vertical bending combined with a certain amount of torsion, which constitutes one estimation point in the interactive diagram. A flow chart is given in Figure 2-24 highlighting the extension of this formulation with respect to the original approach.

- **Extended Formulation for Combined Vertical Bending and Local Bottom Loads**

An extended Smith method was introduced by Tatsumi et al. (2020) to consider the effect of bottom local loads. The double bottom is idealized as a plane grillage and the rest part of the cross section as a prismatic beam. An average stress-average strain relationship of plate/stiffened plate elements employed in Smith's method is transformed into an average stress-average plastic strain relationship, and implemented in the conventional beam finite element as a pseudo strain hardening/softening behaviours. The extended Smith's method is validated through a comparison with nonlinear finite element analysis, which shows a good agreement between two methods.

- **Integrated Formulation Between the Smith Method and Finite Element Method**

An integrated formulation between the original Smith method and finite element method was proposed by Tanaka et al. (2015). The original Smith method and its extension reviewed above can only deal with the prediction of the bending moment/curvature relationship, which is the cross sectional behaviour. However,

no information can be given to the global flexural response of a ship hull girder. The integrated formulation proposed by Tanaka et al. (2015) is able to re-solve this issue, in which the finite beam element is utilised to simulate the global flexural behaviour and the Smith method is adopted to evaluate the nonlinear structural response.

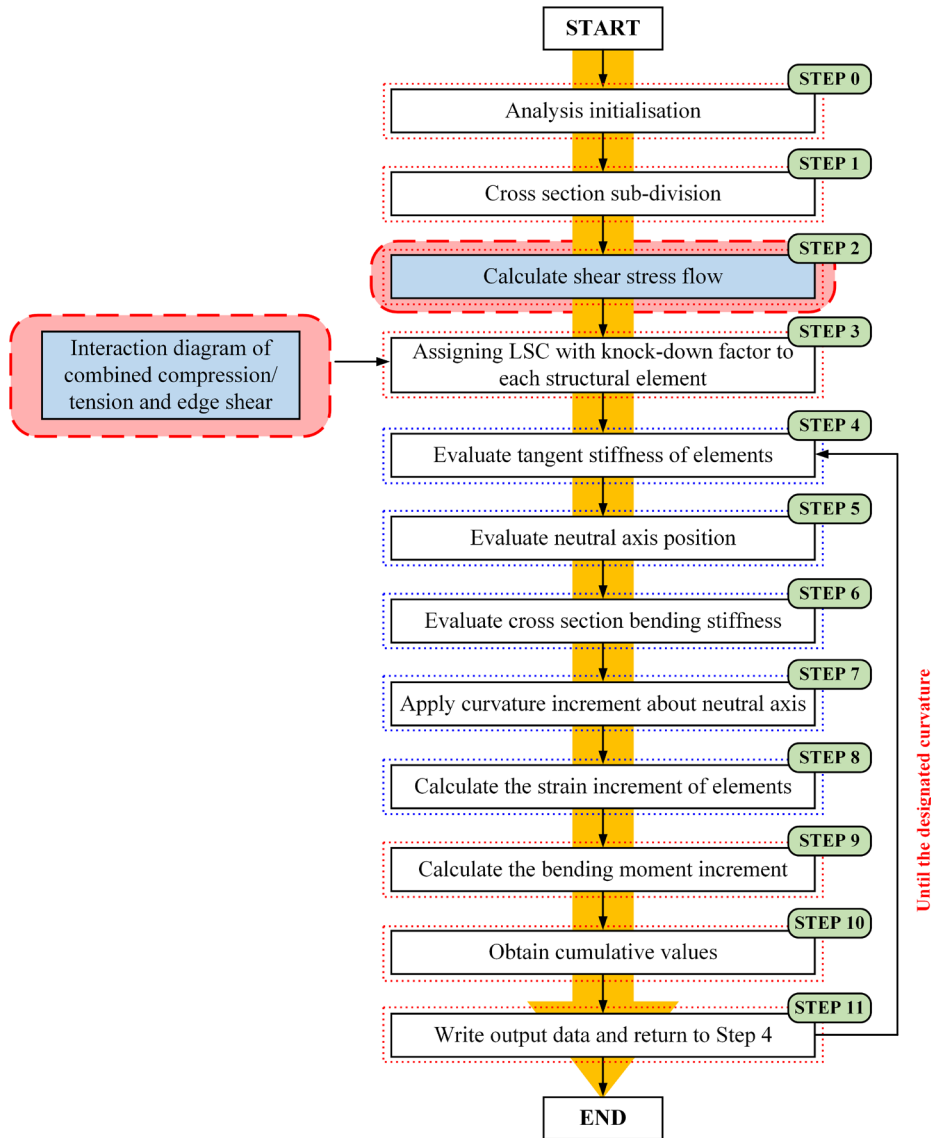


Figure 2-24 Flow chart of the extended Smith method combined vertical and torsional bending

2.6.5 Idealised Structural Unit Method (ISUM)

The idealised structural unit method (ISUM) is an alternative to simulate the elastoplastic buckling collapse behaviour of ship structures, which intended to tackle of the large computational effort of conventional finite element method. Originally proposed by Ueda et al. (1984), there is a significant development in ISUM elements with various capabilities. According to their fundamental basis, ISUM elements can be classified as three generations.

- **First Generation**

The first ISUM element was proposed by Ueda et al. (1984) to simulate the collapse behaviour of a transverse girder. The effective width concept was introduced to consider the loss of in-plane stiffness caused by buckling. The buckling and ultimate strength interaction relationship in terms of sectional forces were employed. Similar concepts were applied to develop plate element and stiffened panel element. However, as indicated by Ueda in the discussion to ISSC (2000) Ultimate Strength report, the first generation of ISUM was rather complex and difficult to understand. Special intuition and engineering judgement were required.

- **Second Generation**

The most important progress in the development of the second generation of ISUM element was to adopt eigen-function to model deflection field in an element (Ueda and Masaoka, 1995). A buckling mode deflection shape was usually employed and it was assumed that the same deflection shape was developed even in the post-ultimate strength range.

- **Third Generation**

A more realistic collapse behaviour of steel plate involves the localisation of elastoplastic buckling deformation, rather than a perfectly periodic pattern. To this end, the third generation of ISUM element was proposed by using new lateral shape functions on the basis of a series of finite element analyses (Fujikubo et al., 2000). Several element were used for modelling of a long plate, which enabled the simulation of buckling nucleation. Although more degrees of freedom were introduced, it was still highly efficient compared with the ordinary FEM.

2.6.6 Nonlinear Finite Element Method

As all buckling failure modes and their interaction can be taken into account, the use of nonlinear finite element method is more common recently for the prediction of hull girder responses. A number of studies applying NLFEM on the ultimate strength analysis can be found in the literature, such as (Sumi et al., 2015; Paik et al., 2013; Kim et al., 2014; Darie and Rörup, 2017; Benson et al., 2013; Mohammed et al., 2016).

However, a significant modelling and computational effort is required in the collapse analysis using NLFEM. The generation of a three-dimensional finite element model is usually time-consuming, especially for complex structures such as a ship hull. Moreover, the application of structural initial imperfection into the finite element model is a challenging task. This is normally because extra care must be taken for structural components that are neither vertical nor horizontal with respect to the reference plane. A nodal coordinate transformation should be used in the application of initial imperfection for these components, which often leads to an error and several attempts may be needed. In addition, a relatively fine mesh is adopted in the collapse analysis applying NLFEM, which leads to the creation of a large matrix. Consequently, the computational time is dramatically

increased. Whilst the computational time of one NLFEM analysis is significant, several trials may be needed to obtain a reliable result. This uncertainty is normally induced by the parameters setting, such as the incremental size. By changing the incremental size, a FEM solution might eventually be obtained. However, in some cases, the whole model should be modified including the mesh size and the initial imperfection. For example, in the buckling analysis on slender structures, the snap-back phenomenon with an undesirable load reversal may be observed. This is often associated with the significant and abrupt change in the distortion shape. When a complex initial distortion shape is employed, it might be problematic as compared with only applying the critical buckling mode shape, in which case the sudden change of distortion may be prevented and a solution can be obtained. However, the accuracy of this solution should be critically assessed.

Thus, NLFEM is usually employed for the research purpose, for example as a validation tool for the simplified methods introduced in previous sections. Different finite element model extents can be adopted, typically including single-frame model, multi-frame model, compartment model and full ship model. Besides, NLFEM also differs in the choice of solvers. For the collapse analysis, the static arc-length solver, dynamic explicit solver and dynamic implicit solver can be employed.

2.6.6.1 Finite Element Model Extent

- **Single Frame Analysis**

Single frame finite element model may be the simplest case for ship hull girder analysis. As shown in Figure 2-25(a), this model extent only includes the effective longitudinal members and no transverse supports are modelled. Examples of applying this model extent include Paik et al. (2013) and Kim et al. (2014). The

single frame finite element model is substantially more efficient than a larger model extent. However, the interaction with the adjacent members in longitudinal direction is omitted. Moreover, replacing the transverse frames with the direct application of boundary conditions may lead to a considerable uncertainty in the final result. As found in the panel analysis (ISSC, 2012), an inappropriate boundary condition on the transverse frame location, such as restraining the end-rotation of stiffener, would cause an overestimation on the ultimate capacity of stiffened panel. This suggests that a strengthening effect may be induced in the single-frame hull girder analysis.

- **Multi Frames Analysis**

The disadvantages of single frame analysis may be resolved by adopting a multi-frame model. As shown in Figure 2-25(b), a $1/2+1+1/2$ model would be an efficient example of this kind. This extent includes the modelling of transverse frames. Therefore the interaction between longitudinal members could be considered and the strengthening effects of the boundaries may be eliminated. A $1/2+1+1/2$ model is suitable for the analysis of pure vertical bending.

If the transverse frames of the hull girder are sufficiently stocky, the pre-mature failure of transverse frames prior to the collapse of longitudinal members can be prevented. In this case, the single-frame and multi-frame models are equivalent to the original formulation of Smith method, which assumes that the collapse zone is constrained to occur within the transverse frames. In addition, the $1/2+1+1/2$ model is relatively computationally efficient as compared with the compartment model.

- **Compartment Level Analysis**

A compartment level analysis employs a full compartment as the finite element model (Figure 2-25c), which is computationally intensive. However, in the case of

overall collapse involving multiple frames and the analysis of combined vertical and torsional bending a compartment model is necessary. For the former, it is essential to include several transverse frames for the prediction of overall grillage instability (Benson et al., 2013). For the latter, a compartment model is useful to prevent the restraint of the warping which may induced significant stress concentration (Mohammed et al., 2016).

- **Full Ship Analysis**

It is scarce that a complete ship is modelled for nonlinear buckling and ultimate strength analysis due to the long computational time. Example analysis can be found in the study on the progressive collapse of bulk carrier in alternate hold loading condition (Amlashi and Moan, 2008) and the ultimate strength analysis on container ship in oblique sea (Darie and Rörup, 2017). It should be noted that only the midship section is applied with fine mesh while a coarse meshing is used in the other parts.

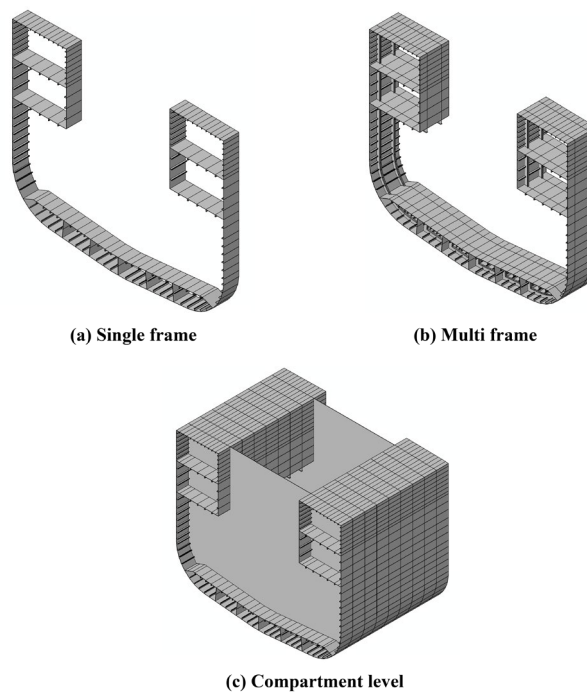


Figure 2-25 Examples of finite element models for ship hull collapse strength analysis

Overall, the selection of FE model extents is based on different analysis purpose. In this thesis, the cyclic vertical bending is the only type of external load and the case study models are all conventionally designed. Hence, there is no need to employ a compartment level FE model. In addition, the cyclic load would significantly increase the total computational time. Thus, a $1/2+1+1/2$ model is employed in this thesis for NLFEM analysis.

2.6.6.2 Finite Element Solver

There are several choices of the finite element solvers, such as static explicit, static implicit, dynamic explicit and dynamic implicit. Although the progressive collapse process is a dynamic event, the ultimate strength analysis of ship structures applying NLFEM is usually taken as a static evaluation. This also matches the assumption of the simplified progressive collapse method where the governing equation is formulated as a static relationship.

The most common finite element solver in the collapse analysis is the arc-length (Riks) solver, as it is a static solution scheme which is able to predict the post-collapse behaviour. Alternatively, the dynamic explicit and dynamic implicit solvers can be employed. To achieve a quasi-static equivalence, it is a common practice to keep the simulated time as long as possible. The load-shortening curve of a stiffened panel is compared in Figure 2-26 to illustrate the influence of different finite element solver. Additionally, different simulated time is adopted in the dynamic solvers. Through this test case, it can be seen that the arc-length solver, the dynamic explicit solver and the dynamic implicit solver can provide equivalent prediction. Whilst using the dynamic solver in the ultimate collapse analysis, it might be important to make a few comparison with the equivalent static solution and also the simplified calculation such as the empirical formulae such that the validity of the dynamic solution can be confirmed.

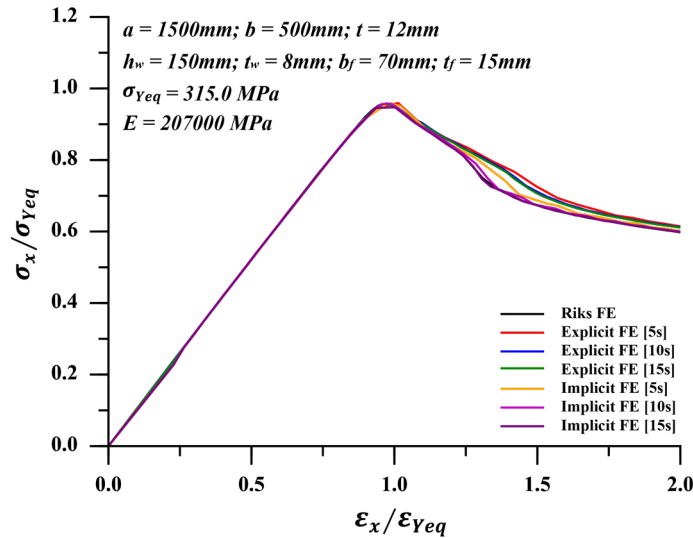


Figure 2-26 Influence of different FE solvers on the collapse analysis

In this thesis, the NLFEM analyses on the cyclic response are conducted with the dynamic solvers, while some analyses on the monotonic response are performed with the arc-length solver. The use of dynamic solver is primarily to allow for the application of cyclic loading protocol. In the cyclic response analyses of stiffened panels, the FE solver is switched between the dynamic explicit and the dynamic implicit. This is because the simulation of stiffened panel's behaviour is simultaneously affected by the choice of material model and FE solver. It is found that, if the elastic-perfectly plastic material model is utilised, the dynamic implicit solver in ABAQUS fails to predict the post-collapse tensile response due to convergence issue, whereas an unstable response path is predicted in the second cycle of loading when using the dynamic explicit solver. Therefore, the explicit solver is adopted to predict the response under single-cycle loading, in which the influence of two different material models are examined. On the other hand, the implicit solver is adopted for the prediction of multi-cycle response where only the combined hardening material model is incorporated.

2.7 Initial Imperfection

As demonstrated by Smith (1981), it is well recognised that the initial imperfection is the governing parameter of influence on the buckling and ultimate strength performance of ship structures that otherwise have the same slenderness properties. In the fabrication, the welding metal is melted with the adjacent plates until solidification. As a result, a considerable distortions of the plating and stiffeners are developed. Meanwhile, tensile stress is induced in the solidified part and compressive stress is developed at the neighbouring part so as to achieve an equilibrium condition. The initial imperfection is detrimental to the buckling and ultimate strength performance of ship structures. Thus, it is crucial to better characterise the initial imperfection of ship structures including their shapes and magnitude.

2.7.1 Measurements

A schematic illustration of the initial imperfection in stiffened ship plating is given by Figure 2-27. The initial distortion is typically in the form of a single barrel-shaped half-wave of amplitude w_{o1} , on which may be superimposed by shorter wavelength components including localised dents with amplitude w_{ob} . A more general expression of the initial distortion may be given as a Fourier series (Equation 2-43). The welding residual stress normally develops as tensile blocks near the intersection of plates and supporting members, and compressive blocks distributed over the rest of the plate.

$$w_o = \sum_{i=1}^M \sum_{j=1}^N A_{oij} \sin\left(\frac{i\pi x}{a}\right) \sin\left(\frac{j\pi y}{b}\right) \quad (2-43)$$

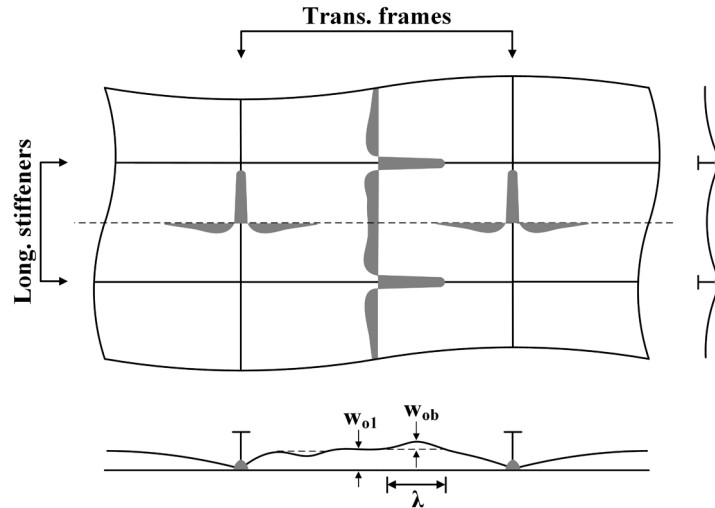


Figure 2-27 Schematic illustration of the initial imperfection in stiffened plating due to welding

A measurement of the initial deflection of ship plating was reported by Carlsen and Czujko (1978), which indicated that the maximum deflection appeared to be independent on the material yield stress and the aspect ratio of the plate. Hence, it was suggested that the maximum deflection of ship plating w_{omax} may be expressed as a function of slenderness b/t .

Measurement on bulk carrier and car carrier plating was conducted by Ueda et al. (1983), Ueda and Yao (1985) and Yao et al. (1992). It was indicated that every Fourier components would contribute to the buckling behaviour of the plating. Hence, the measured deflection was decomposed into eleven components by applying Least Square Method.

In addition to the full-scaled measurement, the initial imperfection of a series of scaled model was summarised by Paik and Thayamballi (1997), including the imperfection data of experiments conducted by Smith (1975), Faulkner (1977), Horne et al. (1976, 1977), Niho (1978), Yao (1980), Tanaka and Endo (1988).

Apart from physical measurements, Gannon et al. (2016) applied a thermo-mechanical finite element analysis to simulate the initial imperfection on stiffened panels with different stiffener profiles. The numerical simulation showed a comparable imperfection shape and magnitude with the experimental measurement.

2.7.2 Practical Consideration (Shape/Distribution)

Following the measurements on stiffened plating, the shape of the initial distortion of a stiffened panel in practice is usually separated into three different types, namely local plate distortion w_{opl} , column-type distortion w_{oc} and stiffener sideways distortion w_{os} as shown in Figure 2-28.

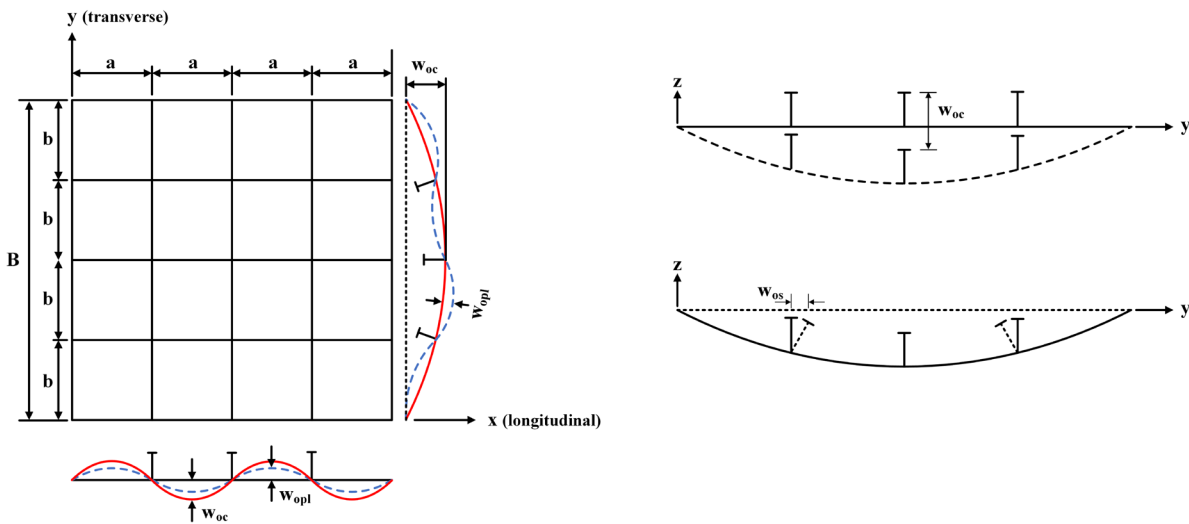


Figure 2-28 Schematic view of the initial distortion of stiffened panels

The column types distortion and stiffener sideways distortion are generally realised as Equation (2-44) and (2-45), which constitutes a single half-wave Fourier component. Conversely, the shape of local plate distortion differs between different literature. In general, three different shapes are adopted, i.e. critical buckling shape (Equation 2-46), A.R.E. shape (Equation 2-47) and hungry shape (Equation 2-48).

$$w_{oc} = w_{oc}^{max} \sin\left(\frac{\pi x}{a}\right) \sin\left(\frac{\pi y}{B}\right) \quad (2-44)$$

$$w_{os} = w_{os}^{max} \frac{z}{h_w} \sin\left(\frac{\pi x}{a}\right) \quad (2-45)$$

$$w_{opl} = w_{opl}^{max} \sin\left(\frac{m\pi x}{a}\right) \sin\left(\frac{\pi y}{b}\right) \quad (2-46)$$

$$w_{opl} = w_{opl}^{max} \left\{ A_{o1} \sin\left(\frac{\pi x}{a}\right) + A_{om} \sin\left(\frac{m\pi x}{a}\right) + 0.01 \sin\left[\frac{(m+1)\pi x}{a}\right] \right\} \sin\left(\frac{\pi y}{b}\right) \quad (2-47)$$

$$w_{opl} = w_{opl}^{max} \sum_{i=1}^{11} A_{oi} \sin\left(\frac{i\pi x}{a}\right) \sin\left(\frac{\pi y}{b}\right) \quad (2-48)$$

The critical buckling shape takes account of the primary buckling deflection mode that primarily leads to the failure of the plating. The number of half-wave could be determined using Equation (2-49). However, with the same maximum deflection magnitude, the critical buckling shape would generally lead to an underestimation of the stiffness and strength of the plating in the pre-collapse range. This is because any other deflection shapes would result in certain strengthening of the plating by inhibiting it from deflecting in a preferred mode. On the other hand, the nucleation of distortion after attaining the ultimate strength would not occur, which leads to an optimistic prediction of the post-collapse strength decay.

$$m = \text{int}\left(\frac{a}{b}\right) + 1 \quad (2-49)$$

An alternative way for modelling the initial distortion is to include a limited Fourier components in the distortion formulation. Typically, a single half-wave component is combined with the critical buckling component, while a higher order term with small amplitude may also be included as given by Equation (2-47). The

first two modes represents a realistic distortion of critical buckling and the high-order mode ensures that the nucleation of out-of-plane deflection occurs at one part of the plate. The ratio between the single half-wave mode and the critical buckling mode is usually taken as $A_{o1}/A_{om} = 4$ in accordance with the British Naval Design recommendation (Benson, 2011). A list of A_{o1} and A_{om} for different critical half-wave number is given in Table 2-2.

Table 2-2 Fourier coefficients of British naval design initial distortion

| | m=3 | m=4 | m=5 | m=6 | m=7 | m=8 |
|----------|------|------|------|------|------|------|
| A_{o1} | 1.12 | 0.84 | 0.80 | 0.82 | 1.12 | 0.80 |
| A_{om} | 0.28 | 0.21 | 0.20 | 0.21 | 0.28 | 0.20 |

The hungry-horse deflection shape with eleven Fourier components was developed based on full-scaled measurement. A recommendation of the Fourier coefficients is listed in Table 2-3 for different ranges of aspect ratios (Yao and Fujikubo, 2016). A relatively large portion of the single half-wave component exists in all cases. A comparison of the distortion profile between different local plate deflection formulation is given in Figure 2-29.

Table 2-3 Fourier coefficients of hungry-horse initial distortion

| Aspect ratio | A_{01} | A_{02} | A_{03} | A_{04} | A_{05} | A_{06} |
|-------------------------------|----------|----------|----------|----------|----------|----------|
| $1 < a/b < \sqrt{2}$ | 1.1158 | -0.0276 | 0.1377 | 0.0025 | -0.0123 | -0.0009 |
| $\sqrt{2} < a/b < \sqrt{6}$ | 1.1421 | -0.0457 | 0.2284 | 0.0065 | 0.0326 | -0.0022 |
| $\sqrt{6} < a/b < \sqrt{12}$ | 1.1458 | -0.0616 | 0.3079 | 0.0229 | 0.1146 | -0.0065 |
| $\sqrt{12} < a/b < \sqrt{20}$ | 1.1439 | -0.0677 | 0.3385 | 0.0316 | 0.1579 | -0.0149 |
| $\sqrt{20} < a/b < \sqrt{30}$ | 1.1271 | -0.0697 | 0.3483 | 0.0375 | 0.1787 | -0.0199 |
| Aspect ratio | A_{07} | A_{08} | A_{09} | A_{10} | A_{11} | |
| $1 < a/b < \sqrt{2}$ | -0.0043 | 0.0008 | 0.0039 | -0.0002 | -0.0011 | |
| $\sqrt{2} < a/b < \sqrt{6}$ | -0.0109 | 0.0010 | -0.0049 | -0.0005 | 0.0027 | |
| $\sqrt{6} < a/b < \sqrt{12}$ | 0.0327 | 0.0000 | 0.0000 | -0.0015 | -0.0074 | |
| $\sqrt{12} < a/b < \sqrt{20}$ | 0.0743 | 0.0059 | 0.0293 | -0.0012 | 0.0062 | |
| $\sqrt{20} < a/b < \sqrt{30}$ | 0.0995 | 0.0107 | 0.0537 | -0.0051 | 0.0256 | |

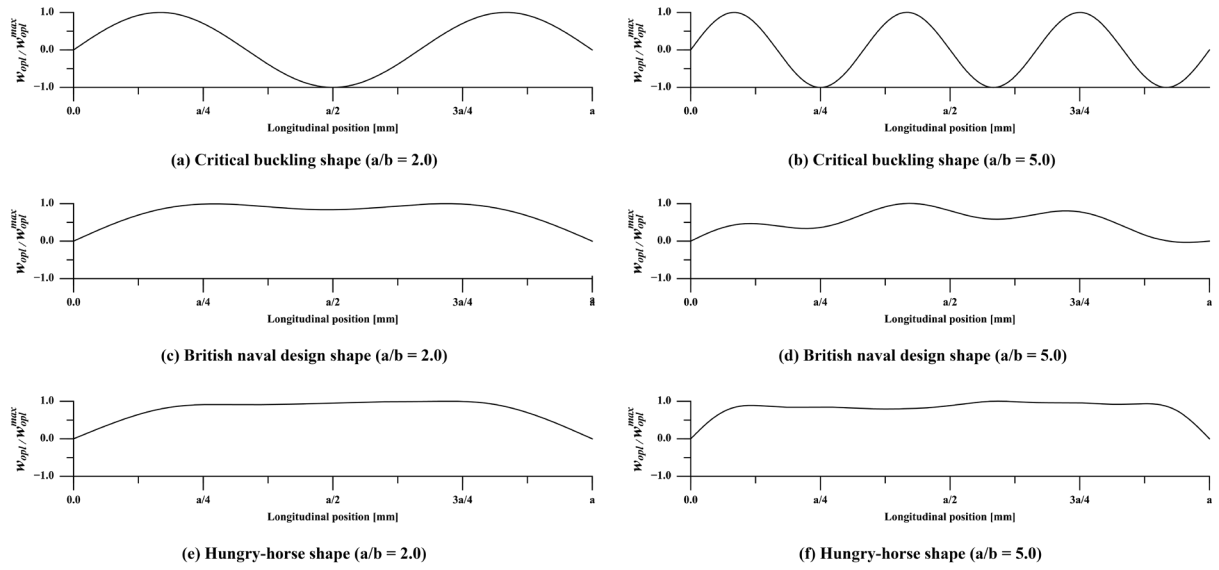


Figure 2-29 Illustration of the local plate deflection profiles of different formulations

Regarding to the distribution of welding residual stress, Smith et al. (1991) suggested a simplified welding-induced residual stress distribution for stiffened panels (Figure 2-30a), in which the residual stress field was idealised as tension and compression blocks. In addition, a triangular distribution shape was assumed for the compressive stress field of stiffener's web, while the tensile stress field was taken as a rectangular strip near the intersection with plating. Similar distribution was given by Yao and Fujikubo (2016) for fillet welding (Figure 2-30b). However, an uniform distribution was assumed for the compressive stress field along the height of the stiffener's web. A more elaborated distribution pattern for the plating was given by Paik and Thayamballi (2003) considering the residual stress in both longitudinal and transverse directions (Figure 2-30c). Due to the self-equilibrium of the welding residual stress, the tensile stress and compressive stress fields follow the relationship of Equation (2-50).

$$2b_t \sigma_{rtx} = (b - 2b_t) \sigma_{rcx} \quad (2-50)$$

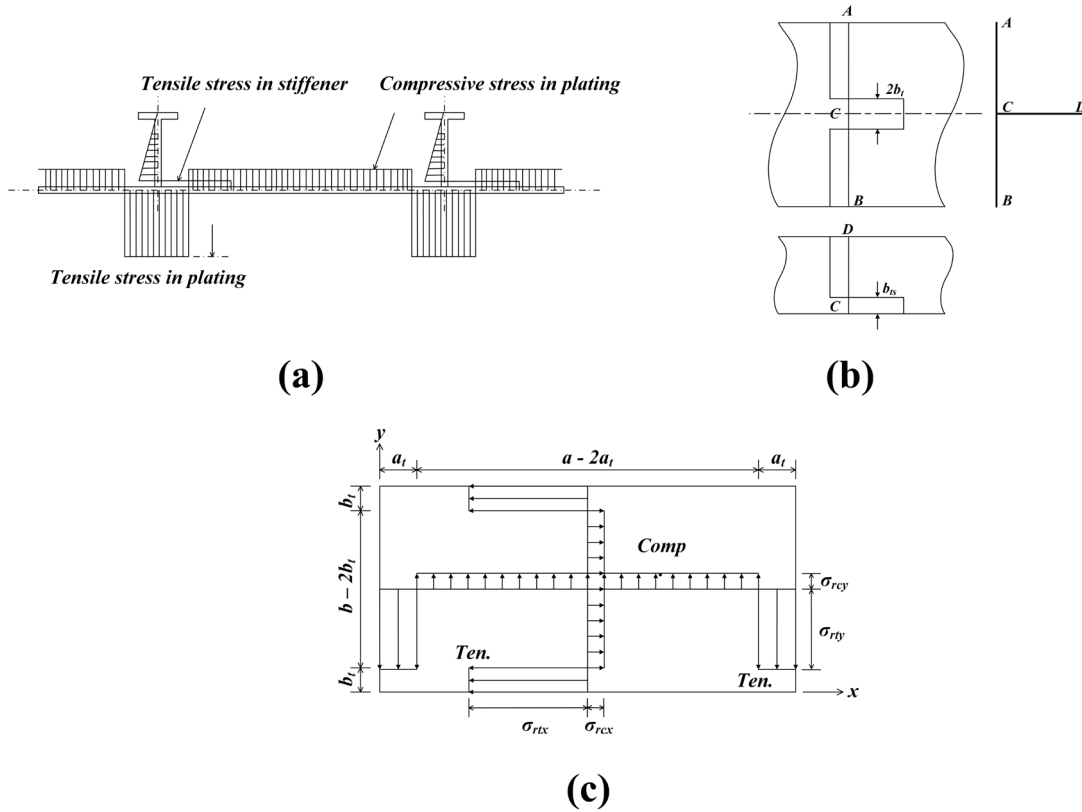


Figure 2-30 Idealisation of welding residual stress profiles

2.7.3 Practical Consideration (Magnitude)

According to measurements, several recommendations have been proposed for the magnitude characterisation of the initial imperfection. In terms of the initial distortion, a maximum magnitude is normally adopted as the characteristic parameter. A summary of the maximum magnitude for different distortion types is given as follows.

Smith et al. (1987) suggested three levels of severity, namely slight, average and severe, for maximum local plate initial deflection as a function of plate slenderness ratio and plate thickness as given by Equation (2-51). A comparison of Smith's average-level magnitude with scaled model measurement is shown in Figure 2-31.

$$w_{opl}^{max} = 0.025\beta^2t \quad (\text{Slight})$$

$$w_{opl}^{max} = 0.1\beta^2t \quad (\text{Average}) \tag{2-51}$$

$$w_{opl}^{max} = 0.3\beta^2t \quad (\text{Severe})$$

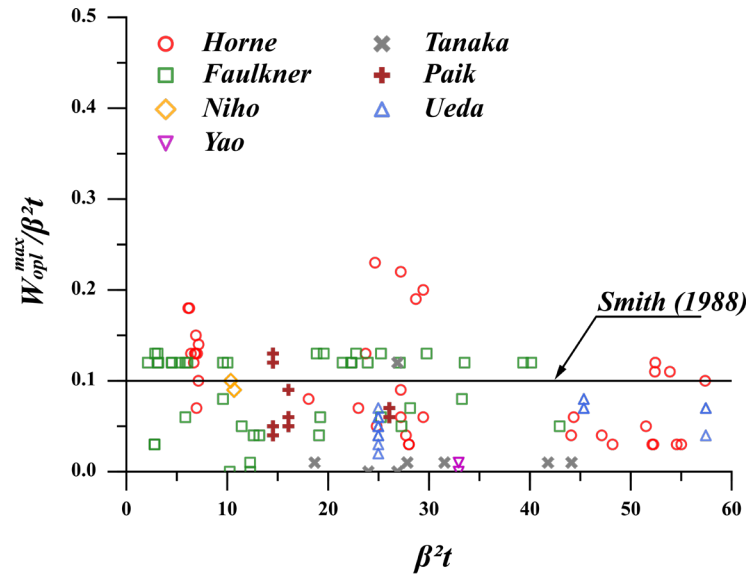


Figure 2-31 Comparison between maximum local plate deflection and Smith’s average-level estimate

Alternatively, Dowling et al. (1977) suggested Equation (52) as an estimate of the maximum local plate deformation magnitude in terms of the plating breadth. Carlsen and Czujko (1978) proposed Equation (53) as a function of b/t on the basis of mean value + 2 × standard deviation of the measurement. Similar expressions were introduced by Antoniou (1980) (Equation 54) and Kmiecik (1981) (Equation 55). All these estimates may be considered as equivalent with the average-level specified by Smith et al. (1987).

$$w_{opl}^{max} = \frac{b}{200} \tag{2-52}$$

$$w_{opl}^{max} = \frac{b}{100} \tag{2-53}$$

$$w_{opl}^{max} = 0.238\beta t - 0.177t \tag{2-54}$$

$$w_{opl}^{max} = 0.0065b + 0.022t \tag{2-55}$$

In terms of the column-type distortions, the maximum distortion magnitude is generally given as a function of the panel length. Table 2-4 summarises the recommendation by Smith (1991) and ISSC (2012).

Table 2-4 Maximum magnitude of column-type distortion

| | | Slight | | Average | | Severe | |
|-------------|-----------------------|----------------|---------------------|----------------|---------------------|----------------|---------------------|
| λ | | w_{oc}^{max} | w_{oc}^1/w_{oc}^2 | w_{oc}^{max} | w_{oc}^1/w_{oc}^2 | w_{oc}^{max} | w_{oc}^1/w_{oc}^2 |
| Smith | $\lambda \leq 0.2$ | 0.00025a | 0.25 | 0.0008a | 0.25 | 0.0020a | -1.0 |
| | $0.2 < \lambda < 0.6$ | 0.00025a | 0.25 | 0.0012a | 0.25 | 0.0038a | -1.0 |
| | $\lambda \geq 0.6$ | 0.00025a | 0.25 | 0.0015a | 0.25 | 0.0046a | -1.0 |
| ISSC (2012) | | | | 0.0015a | | | |

Regarding to the magnitude of welding residual stress, Yao (1980) suggested that the width of tensile block can be expressed as a function of plating thickness, web thickness and the weld heat input. Meanwhile, the tensile yield stress is equal to the material yield stress in the case of ordinary steel (Yao et al., 1998). An empirical formula was given by Smith et al. (1991) to estimate the compressive residual stress (Equation 2-56). Three different severities (slight, average and severe) were suggested.

$$\begin{aligned}\sigma_{rcx} &= -0.05\sigma_{Yp} && \text{(Slight)} \\ \sigma_{rcx} &= -0.15\sigma_{Yp} && \text{(Average)} \\ \sigma_{rcx} &= -0.30\sigma_{Yp} && \text{(Severe)}\end{aligned}\tag{2-56}$$

In this thesis, the A.R.E. distortion shape is employed for modelling the initial deflection with an average-level magnitude following Smith’s recommendation (Equation 2-49). Asymmetric shape is considered for the adjacent panel. The welding-induced residual stress is not considered. In the case of cyclic loading, the residual stress may undergo a relaxation due to the shakedown phenomenon. Moreover, this also matches the current CSR approach where the residual stress is neglected.

2.8 Cyclic Loading

The foregoing sections review the advancement in the research of buckling and ultimate collapse of ship structures principally subjected to extreme monotonic loading. A literature survey is documented in the following on the research works concerning the response under extreme cyclic loads.

2.8.1 Material Properties

The material property of the constructional steel for ship structures is conventionally considered as elastic-perfectly plastic for the assessment of buckling and ultimate strength under monotonic extreme loads. In general, no hardening phenomenon is taken into account. This is because the ultimate strength problem is dominated by the buckling failure and the maximum capacity usually attains at a relatively low strain. Hence, it is reasonable to neglect the hardening effect. However, in terms of cyclic loading, it might be important to evaluate the effects of cyclic hardening and the Bauschinger phenomenon.

Cyclic hardening refers to a phenomenon where the peak stress is increased in magnitude when the metal is cycled between equal positive and negative strain limits. On the other hand, the Bauschinger effect is associated with the condition where the yield strength of the metal is decreased when the direction of strain is reversed. Johnson-Cook plasticity theory (Johnson and Cook, 1985) is a commonly used material model with hardening. However, it is not able to consider the cyclic hardening and the Bauschinger phenomenon. To account for the combination of cyclic hardening and Bauschinger effect, a combined hardening model may be adopted where the isotropic rule is used to simulate the cyclic hardening and the kinematic rule is used to model the Bauschinger effect (Chaboche, 1986).

In the formulation of the combined hardening model, the yield surface is defined as follows:

$$F = f(\sigma - \alpha) - \sigma_Y \quad (2-57)$$

where

$f(\sigma - \alpha)$ = Equivalent von-Mises with respect to backstress α

$$= \sqrt{\frac{3}{2} (S - \alpha^{dev}) : (S - \alpha^{dev})}$$

σ_Y = Yield stress

The kinematic hardening model is defined to be an additive combination of a purely kinematic term and a relaxation term, which introduces nonlinearity (Equation 2-58). In addition, several kinematic hardening components (backstresses) can be superposed to obtain the overall backstress (2-59).

$$\dot{\alpha}_k = C_k \frac{1}{\sigma_Y} (\sigma - \alpha) \dot{\epsilon}^{pl} - \gamma_k \alpha_k \dot{\epsilon}^{pl} \quad (2-58)$$

$$\alpha = \sum_{k=1}^N \alpha_k \quad (2-59)$$

where

C_k = Initial kinematic hardening modulus

γ_k = The rate at which the kinematic hardening modulus decreases with the plastic deformation

The isotropic hardening rule defines the evolution of the yield surface size as a function the equivalent plastic strain $\bar{\epsilon}^{pl}$, which can be expressed by an exponential law as follows:

$$\sigma^0 = \sigma|_0 + Q_\infty (1 - e^{-b\bar{\epsilon}^{pl}}) \quad (2-60)$$

where

$\sigma|_0$ = Initial isotropic hardening modulus

Q_∞ = Maximum change in the size of the yield surface

b = Changing rate of yield surface

The calibrations of the material constants of combined hardening model were conducted Krolo et al. (2016) and Jia and Kuwamura (2015), as summarised in Table 2-5 and Table 2-6. An example stress/strain curve is shown in Figure 2-32.

Table 2-5 Material property (Krolo et al., 2016)

| Kinematic hardening | | | | | |
|---------------------|------------|-------------|------------|-------------|------------|
| C_1 (MPa) | γ_1 | C_2 (MPa) | γ_2 | C_3 (MPa) | γ_3 |
| 13921 | 765 | 4240 | 52 | 1573 | 14 |
| Isotropic hardening | | | | | |
| Q_∞ (MPa) | | | b | | |
| 25.6 | | | 4.4 | | |

Table 2-6 Material property (Jia and Kuwamura, 2015)

| Kinematic hardening | | | | | |
|---------------------|------------|-------------|------------|-------------|------------|
| C_1 (MPa) | γ_1 | C_2 (MPa) | γ_2 | C_3 (MPa) | γ_3 |
| 26.9 | 0 | 1617.2 | 10.7 | 26.9 | 0 |
| Isotropic hardening | | | | | |
| Q_∞ (MPa) | | | b | | |
| 227.8 | | | 5.8 | | |

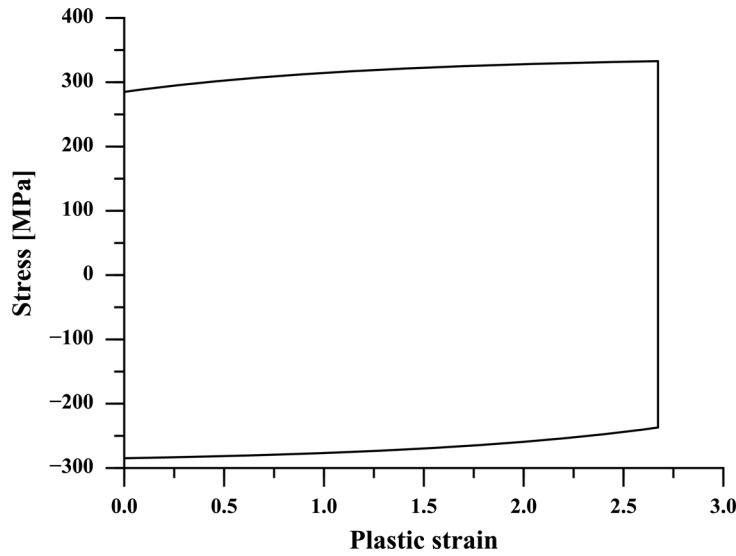


Figure 2-32 Example stress-strain curve of Chaboche model

2.8.2 Structural Behaviour (Theoretical)

Yao and Nikolov (1990) performed a series of elastoplastic large deflection analyses using the nonlinear finite element method on an unstiffened short plate (800mm×1000mm) subjected to cyclic in-plane load. The responses under single-cycle and multi-cycle loadings were investigated. It was found that the load-shortening curve tends to converge to a certain loop, but a complete convergence was not observed.

Extended from the work of Yao and Nikolov (1990), an analytical method was proposed by Yao et al. (1995). The analytical method was developed based upon a combination of the elastic large deflection theory and the rigid plastic

mechanism analysis. However, the proposed method was only validated on a short plate under a single-cycle loading protocol.

Fukumoto and Kusama (1985) described the theoretical behaviour of a simply supported square plate under alternating uniaxial forces with the aid of an elastic and perfectly plastic large deflection-small strain analysis. It was suggested that the unloading curve was almost parallel to the elastic portion of the initial curve and the peak stress of the reloading curve was close to the stress of the starting point of unloading.

Goto et al. (1995) investigated the localization of plastic buckling pattern on a simply supported plate under cyclic loading. The study revealed that the strength deterioration due to the deflection localization under cyclic loading was more evident on plates with larger b/t and a/b ratio. Further, it was indicated that the plate with a bilinear constitutive model exhibited a larger strength deterioration rate than that with a two-surface cyclic plasticity model. This was probably caused by the abrupt change of material stiffness in the bilinear model, which led to a localized unstable behaviour of the structural system.

2.8.3 Structural Behaviour (Experimental)

A limited number of experimental programmes were performed to investigate the buckling and ultimate collapse behaviour of small-scaled box girder models under cyclic vertical bending.

Masaoka et al. (2006) performed a cyclic four-point bending test on a stiffened plated box girder structure. After several load cycles, the load-carrying capacity of the box girder dropped rapidly and a crack was initiated at the location where the plastic deformation concentrated.

Four-point bending tests were also carried out by Cui and Yang (2018) on several box girders. The measurement of the bending moment-curvature relationship were

documented. It was reported that the box girder failed by an incremental collapse where the permanent deformation accumulated at each cycle. The initiation of crack, which was classified as the low-cycle fatigue crack due to large magnitude reversing straining, was also reported as one of the failure characteristics. In the initial phase of the cyclic loading, the reduction of ultimate strength is caused by the failure induced by elastoplastic buckling. In the later phase of the cyclic loading, cracks occur in some parts of the box girder leading to a further deterioration of the ultimate strength. There is no indication from the reference about the predominate failure mode in the later phase of loading. But it is postulated that the occurrence of cracking would weaken the structural resistance against the extreme loading, resulting in a greater inelastic deformation. This in turn would cause further cracking initiated in the structures. Therefore, the inelastic buckling and cracking may interactively lead to the final catastrophic failure, such as “breaking of its back” for ship hull girder.

2.9 Chapter Summary

A review is presented in this chapter to discuss the recent progress in the buckling and ultimate strength of ship structures. Both theoretical analysis methods and experimental works have been covered. It is clear that a considerable advancement has been achieved in understanding the collapse mechanism of ship structures under extreme monotonic loading, and a vast number of theoretical approach are available to predict the progressive collapse and ultimate strength of plates, stiffened panels and hull girders.

Regarding the response under extreme cyclic loading, however, only a limited number of works were documented in the open literature. Theoretical prediction method has not yet been established for a tractable prediction. Thus, a systematic investigation is needed to reveal the characteristic features of buckling collapse behaviours under extreme cyclic loading. Moreover, efficient computational

methods should be developed for a robust prediction. In light of this, this research work has completed a parametric analysis to investigate the load-shortening characteristics of ship plating under cyclic compression and tension. Practical computational methods are proposed and validated to evaluate the response of structural segments and hull girders under combinations of cyclic loads, which will be presented in the following chapters.

Chapter 3 Numerical Analysis on Ship Plating Under Cyclic Compression and Tension

3.1 Rationale

Ship structures are essentially a network of plates and stiffeners. To assess the ultimate strength of ship hull girders using a Smith-type method, it is essential to investigate and define the load-shortening relationship of structural components under in-plane loading. This has been well analysed for monotonic loading, as reviewed in Chapter 2. However, a robust methodology for defining the load-shortening behaviour under cyclic compression and tension is lacking in the literature. A systematic NLFEM analysis is thus conducted. The main purposes are to:

- 1) investigate the influence of structural dimensions (e.g. slenderness) on the elastoplastic buckling collapse responses under cyclic in-plane loading;
- 2) investigate the influence of material plasticity models on the structural response under cyclic load;
- 3) provide a dataset to develop the response and updating methodology in Chapter 4.

3.2 Test Matrix

3.2.1 Geometric Dimensions and Material Properties

The scope of the numerical test is confined to four aspect ratios ($a/b = 1, 2, 3, 4$) and three plate slenderness ratios ($\beta = 1.5, 2.0, 2.5$). In relation to the classic plate theory, these aspect ratios correspond to the lowest buckling strength in the case of simply supported plate. In terms of the plate slenderness, the chosen slenderness ratios correspond to the transition region of the von-Karman plate ultimate strength equation, in which the plating strength would substantially deviate at $\beta = 1.9$. Meanwhile, these scantlings are typical in cargo ship structural design

according to Zhang and Khan (2009). The tested plate has a constant width of 1000mm. The material yield stress is 285MPa and Young’s modulus is 207000MPa. The yield stress and Young’s modulus are specified following the material testing by Krolo et al. (2016) to utilise their combined hardening model data. The variance in aspect ratios and slenderness ratios are achieved by changing the plate length or the thickness. A summary of the geometric dimension is given in Table 3-1. The material property is given in Table 3-2.

Table 3-1 Geometric dimension of the tested ship plating

| a (mm) | b (mm) | t (mm) | α | β |
|----------|----------|----------|----------|---------|
| 1000 | 1000 | 25.0 | 1.0 | 1.5 |
| 1000 | 1000 | 18.5 | 1.0 | 2.0 |
| 1000 | 1000 | 15.0 | 1.0 | 2.5 |
| 2000 | 1000 | 25.0 | 2.0 | 1.5 |
| 2000 | 1000 | 18.5 | 2.0 | 2.0 |
| 2000 | 1000 | 15.0 | 2.0 | 2.5 |
| 3000 | 1000 | 25.0 | 3.0 | 1.5 |
| 3000 | 1000 | 18.5 | 3.0 | 2.0 |
| 3000 | 1000 | 15.0 | 3.0 | 2.5 |
| 4000 | 1000 | 25.0 | 4.0 | 1.5 |
| 4000 | 1000 | 18.5 | 4.0 | 2.0 |
| 4000 | 1000 | 15.0 | 4.0 | 2.5 |

Table 3-2 Material property

| Elastic behaviour | E (MPa) | | ν | | σ_Y (MPa) | |
|-------------------|---------------------|------------|-------------|------------|------------------|------------|
| | 207000 | | 0.3 | | 285 | |
| | Kinematic hardening | | | | | |
| | C_1 (MPa) | γ_1 | C_2 (MPa) | γ_2 | C_3 (MPa) | γ_3 |
| Plastic behaviour | 13921 | 765 | 4240 | 52 | 1573 | 14 |
| | Isotropic hardening | | | | | |
| | Q_∞ (MPa) | | | | b | |
| | 25.6 | | | | 4.4 | |

3.2.2 Loading Protocol of Structural Member

A loading protocol is defined to describe the applied load history of the structure under analysis, which refers to the in-plane compression and tension and is given in terms of the dimensionless average strain (edge displacement) for ship structural members. A schematic illustration of the loading protocol of structural components is given in Figure 3-1. The example loading protocol represents a five-cycle in-plane loading with equal magnitude of in both compression and tension. Note that only the magnitude and the number of loading cycles are represented in the loading protocol. A protocol time is used to indicate the progress within a prescribed loading history, which should be distinguished with the “real time”, i.e. If the protocol time equals to two, the second-cycle loading is started. The corresponding resultant stress is computed based on the input of the loading protocol so that the load-shortening response is predicted.

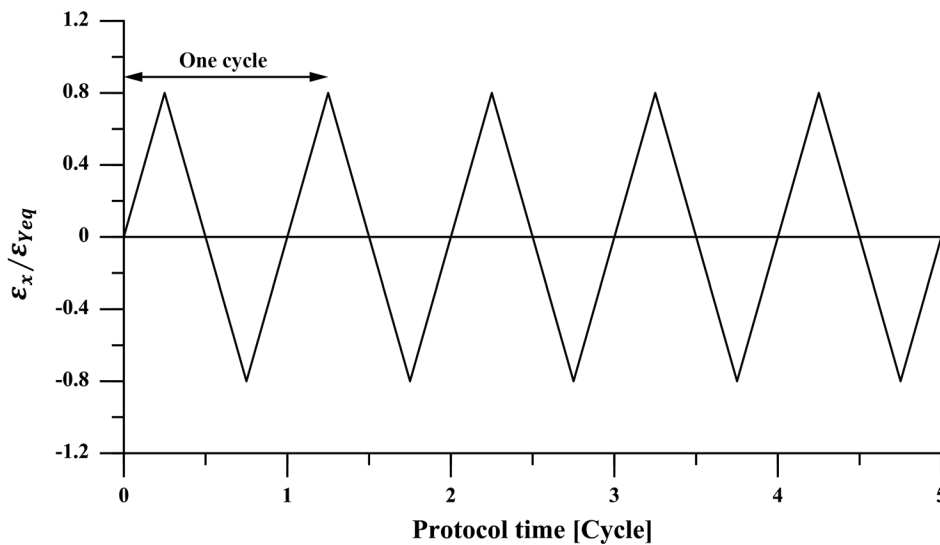


Figure 3-1 Schematic illustration of loading protocol

Regarding to the loading protocols, the unstiffened plates are subjected to single-cycle loading and multi-cycle loading. Despite named as ‘single-cycle’ for brevity, this loading protocol actually consists of one plus a quarter cycle, i.e. one cycle completes one reloading. This is to meet one of the objectives of the present

analysis as stated before that to investigate the influence of a combined hardening material model compared with the elastic-perfectly plastic model conventional for ultimate strength analysis. It was found that, if the elastic-perfectly plastic material model is utilised, the dynamic implicit solver in ABAQUS fails to predict the post-collapse tensile response due to convergence issue, whereas an unstable response path is predicted in the second cycle of loading when using the dynamic explicit solver. Therefore, the explicit solver is adopted to predict the response under single-cycle loading, in which the influence of two different material models are examined. On the other hand, the implicit solver is adopted for the prediction of multi-cycle response where only the combined hardening material model is incorporated. The simulation time of each cycle is $5 \times 16 = 80$ seconds. As shown by Figure 2-26, the loading period would not lead to a substantial difference for the analysis of this kind.

For each plate, the applied loading protocols are summarised in Table 3-3. The loading protocols are given in terms of the applied strain range. Loading protocols 1 to 11 and 14 to 24 are constant amplitude loadings, while the loading protocols 12 and 13 are varied amplitude loadings. The remark column indicates the initial loading direction of each loading protocol where “C” represents the compression and “T” represents the tension. For loading protocols 1 to 11, the initial load direction is in either compression or tension. For the remaining loading protocols, the initial load is only in the compressive direction.

Table 3-3 Loading protocols of unstiffened plates

| | ID | Applied strain range | Remark |
|---|----|--|----------|
| Single-cycle (Constant amplitude) | 1 | $-1.0\varepsilon_{Yeq} < \varepsilon < 1.0\varepsilon_{Yeq}$ | (C & T) |
| | 2 | $-1.1\varepsilon_{Yeq} < \varepsilon < 1.1\varepsilon_{Yeq}$ | (C & T) |
| | 3 | $-1.2\varepsilon_{Yeq} < \varepsilon < 1.2\varepsilon_{Yeq}$ | (C & T) |
| | 4 | $-1.3\varepsilon_{Yeq} < \varepsilon < 1.3\varepsilon_{Yeq}$ | (C & T) |
| | 5 | $-1.4\varepsilon_{Yeq} < \varepsilon < 1.4\varepsilon_{Yeq}$ | (C & T) |
| | 6 | $-1.5\varepsilon_{Yeq} < \varepsilon < 1.5\varepsilon_{Yeq}$ | (C & T) |
| | 7 | $-1.6\varepsilon_{Yeq} < \varepsilon < 1.6\varepsilon_{Yeq}$ | (C & T) |
| | 8 | $-1.7\varepsilon_{Yeq} < \varepsilon < 1.7\varepsilon_{Yeq}$ | (C & T) |
| | 9 | $-1.8\varepsilon_{Yeq} < \varepsilon < 1.8\varepsilon_{Yeq}$ | (C & T) |
| | 10 | $-1.9\varepsilon_{Yeq} < \varepsilon < 1.9\varepsilon_{Yeq}$ | (C & T) |
| | 11 | $-2.0\varepsilon_{Yeq} < \varepsilon < 2.0\varepsilon_{Yeq}$ | (C & T) |
| Single-cycle (Varied amplitude) | 12 | $-1.0\varepsilon_{Yeq} < \varepsilon < 1.5\varepsilon_{Yeq}$ | (C only) |
| | 13 | $-1.0\varepsilon_{Yeq} < \varepsilon < 2.0\varepsilon_{Yeq}$ | (C only) |
| Multi-cycle (Ten cycles) (Constant amplitude) | 14 | $-1.0\varepsilon_{Yeq} < \varepsilon < 1.0\varepsilon_{Yeq}$ | (C only) |
| | 15 | $-1.1\varepsilon_{Yeq} < \varepsilon < 1.1\varepsilon_{Yeq}$ | (C only) |
| | 16 | $-1.2\varepsilon_{Yeq} < \varepsilon < 1.2\varepsilon_{Yeq}$ | (C only) |
| | 17 | $-1.3\varepsilon_{Yeq} < \varepsilon < 1.3\varepsilon_{Yeq}$ | (C only) |
| | 18 | $-1.4\varepsilon_{Yeq} < \varepsilon < 1.4\varepsilon_{Yeq}$ | (C only) |
| | 19 | $-1.5\varepsilon_{Yeq} < \varepsilon < 1.5\varepsilon_{Yeq}$ | (C only) |
| | 20 | $-1.6\varepsilon_{Yeq} < \varepsilon < 1.6\varepsilon_{Yeq}$ | (C only) |
| | 21 | $-1.7\varepsilon_{Yeq} < \varepsilon < 1.7\varepsilon_{Yeq}$ | (C only) |
| | 22 | $-1.8\varepsilon_{Yeq} < \varepsilon < 1.8\varepsilon_{Yeq}$ | (C only) |
| | 23 | $-1.9\varepsilon_{Yeq} < \varepsilon < 1.9\varepsilon_{Yeq}$ | (C only) |
| | 24 | $-2.0\varepsilon_{Yeq} < \varepsilon < 2.0\varepsilon_{Yeq}$ | (C only) |

3.3 Finite Element Modelling

Four-node shell element with reduced integration (SR4) are used. A one bay/one span model extent of the unstiffened plate is adopted. The boundary condition is illustrated in Figure 3-2. For the loading application, a reference point is created, at which the displacement-controlled loading is applied such that the loaded edge is kept straight. On the contrary, the opposite end is constrained in the longitudinal loading direction. The unloaded edges are constrained in the transverse direction. In terms of the element size, the number of elements in the

longitudinal direction is dependent on the aspect ratio ($20 \times a/b$), whereas 20 elements are used in the transverse direction, resulting in a $50\text{mm} \times 50\text{mm}$ characteristic mesh size. The initial plating distortion follows the A.R.E. recommendation as described in Chapter 2. The initial plating distortion profile is defined by Equation (3-1) and its magnitude is given by Equation (3-2). No residual stress is considered.

$$w_{opl} = w_{opl}^{max} \left\{ 0.8 \sin\left(\frac{\pi x}{a}\right) + 0.2 \sin\left(\frac{m\pi x}{a}\right) + 0.01 \sin\left[\frac{(m+1)\pi x}{a}\right] \right\} \sin\left(\frac{\pi y}{b}\right) \quad (3-1)$$

$$w_{opl}^{max} = 0.1\beta^2 t \quad (3-2)$$

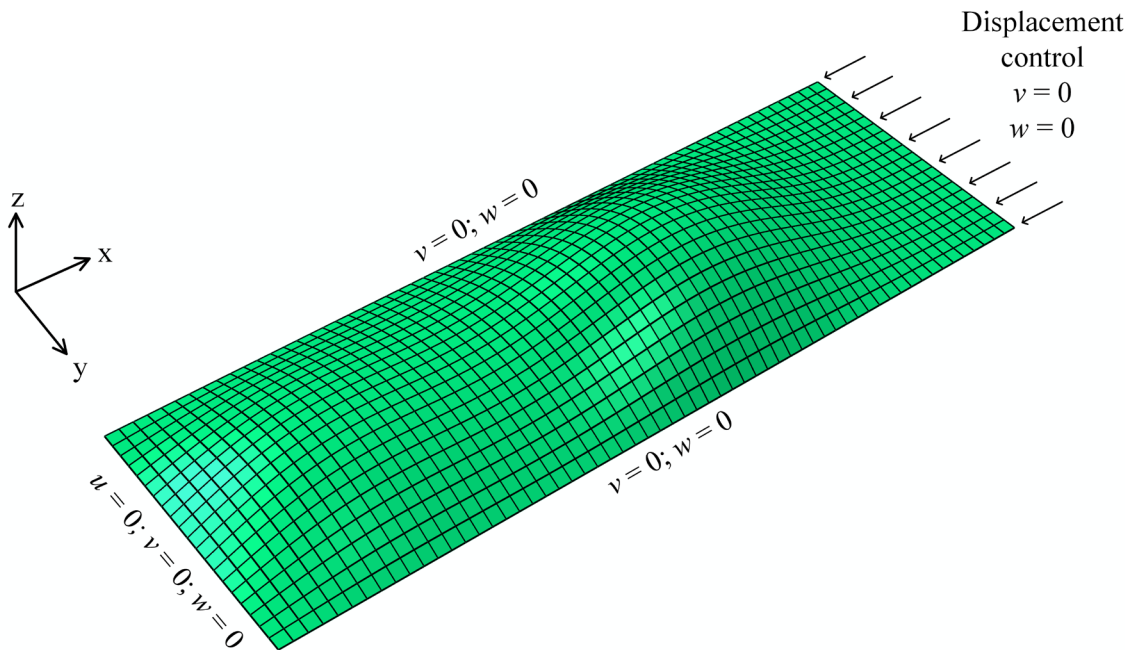


Figure 3-2 Boundary condition of the unstiffened plate model

As a validation of the finite element modelling, a comparison with the Faulkner and Frankland formulae is shown in Figure 3-3 and summarised in Table 3-4 for the monotonic ultimate compressive strength. The comparison is indicated using

a mean value and its coefficient of variance (COV). The mean value refers to the average ratio between predictions by different methods, while the COV is defined as standard deviation divided by the mean value. The former quantity usually indicates the overall prediction accuracy (optimistic or conservative) while the latter quantity is used to evaluate its uncertainty (large fluctuation or small fluctuation). Normally, a COV less than 0.10 corresponds to a robust comparison with little uncertainty (Collette, 2005). A reasonable comparison is presented where the present NLFEM is slightly overestimated with respect to Faulkner formula and slightly underestimated with respect to Frankland formula. This discrepancy is mainly due to the plating boundary conditions in each formulae. The former was developed from unconstrained plates whereas the latter was derived from constrained plates.

Table 3-4 Validation of the monotonic ultimate compressive strength

| α | β | NLFEM | Frankland | Faulkner |
|----------|---------|--------|-----------|----------|
| 1.0 | 1.5 | 0.8768 | 0.9444 | 0.8889 |
| 1.0 | 2.0 | 0.7596 | 0.8125 | 0.7500 |
| 1.0 | 2.5 | 0.6388 | 0.7000 | 0.6400 |
| 2.0 | 1.5 | 0.8498 | 0.9444 | 0.8889 |
| 2.0 | 2.0 | 0.8145 | 0.8125 | 0.7500 |
| 2.0 | 2.5 | 0.7087 | 0.7000 | 0.6400 |
| 3.0 | 1.5 | 0.9656 | 0.9444 | 0.8889 |
| 3.0 | 2.0 | 0.7813 | 0.8125 | 0.7500 |
| 3.0 | 2.5 | 0.6510 | 0.7000 | 0.6400 |
| 4.0 | 1.5 | 0.9703 | 0.9444 | 0.8889 |
| 4.0 | 2.0 | 0.7992 | 0.8125 | 0.7500 |
| 4.0 | 2.5 | 0.6563 | 0.7000 | 0.6400 |

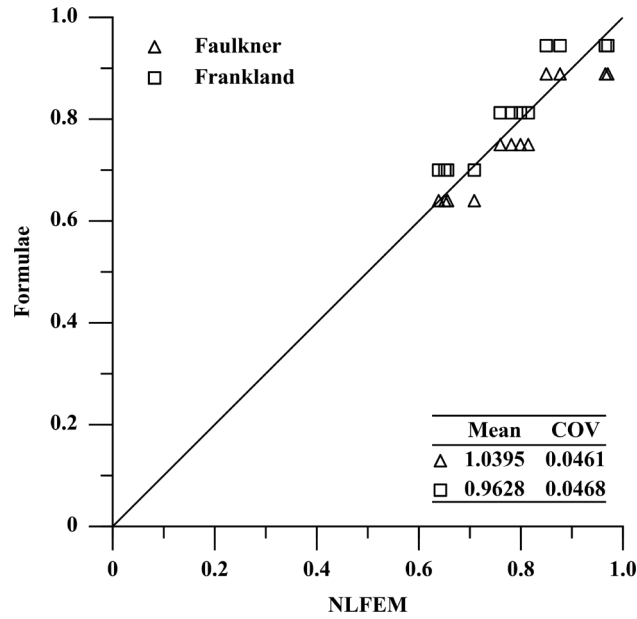


Figure 3-3 Validation of the monotonic ultimate compressive strength

3.4 Single-Cycle Response

3.4.1 Load-Shortening Behaviour (Single-Cycle)

Figures 3-4 to 3-7 show examples of single-cycle load-shortening curves under constant amplitude loading protocol (IDs 7 and 11) with the initial load direction in compression (Figures 3-4 to 3-6) and in tension (Figure 3-7). Figure 3-8 shows the example single-cycle load-shortening curves under varied amplitude loading protocol (IDs 12 and 13). In each single-cycle load-shortening curve, 8000 data points are output. The data should be sufficient to represent the load-shortening response and are not illustrated to keep the readability of the plots. The characteristics within the examples shown are consistent with the results observed for all cases tested in this study.

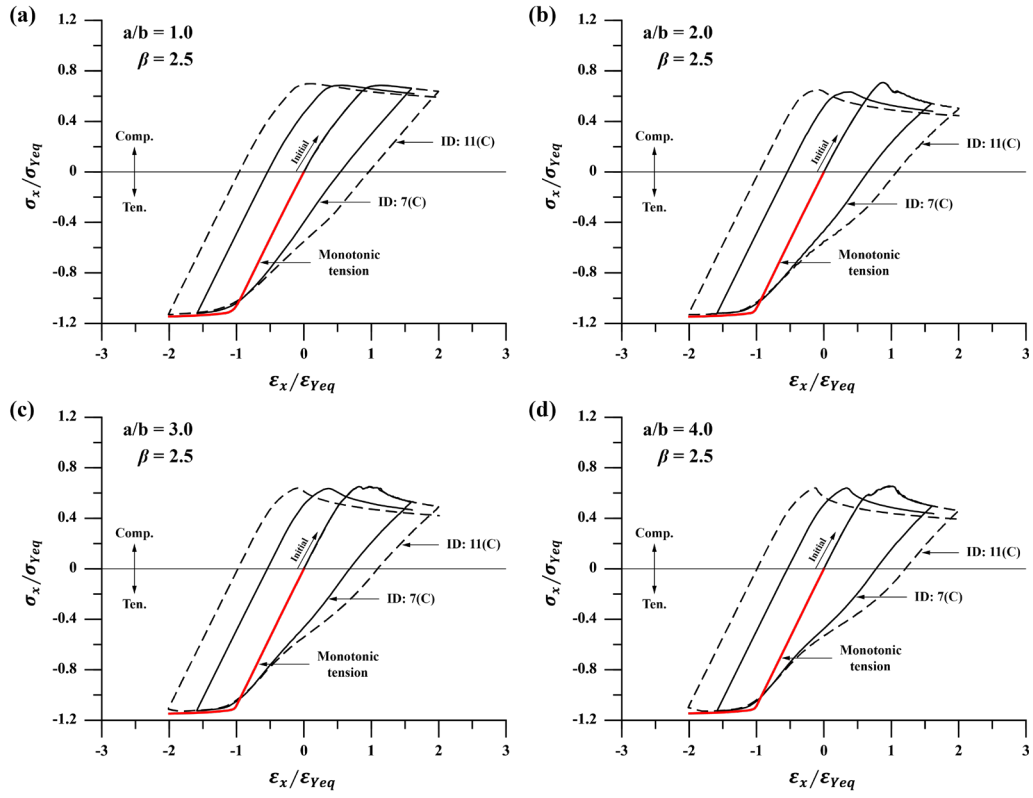


Figure 3-4 Load-shortening curves of ship plates ($\beta = 2.5$; compression init.)

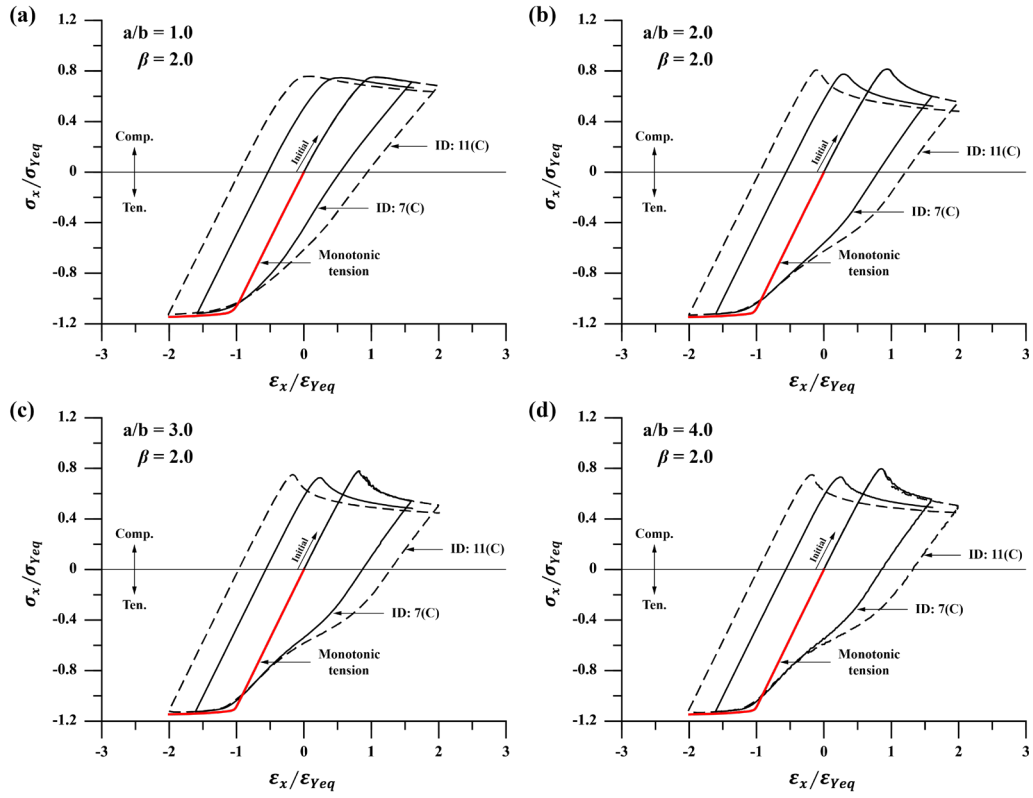


Figure 3-5 Load-shortening curves of ship plates ($\beta = 2.0$; compression init.)

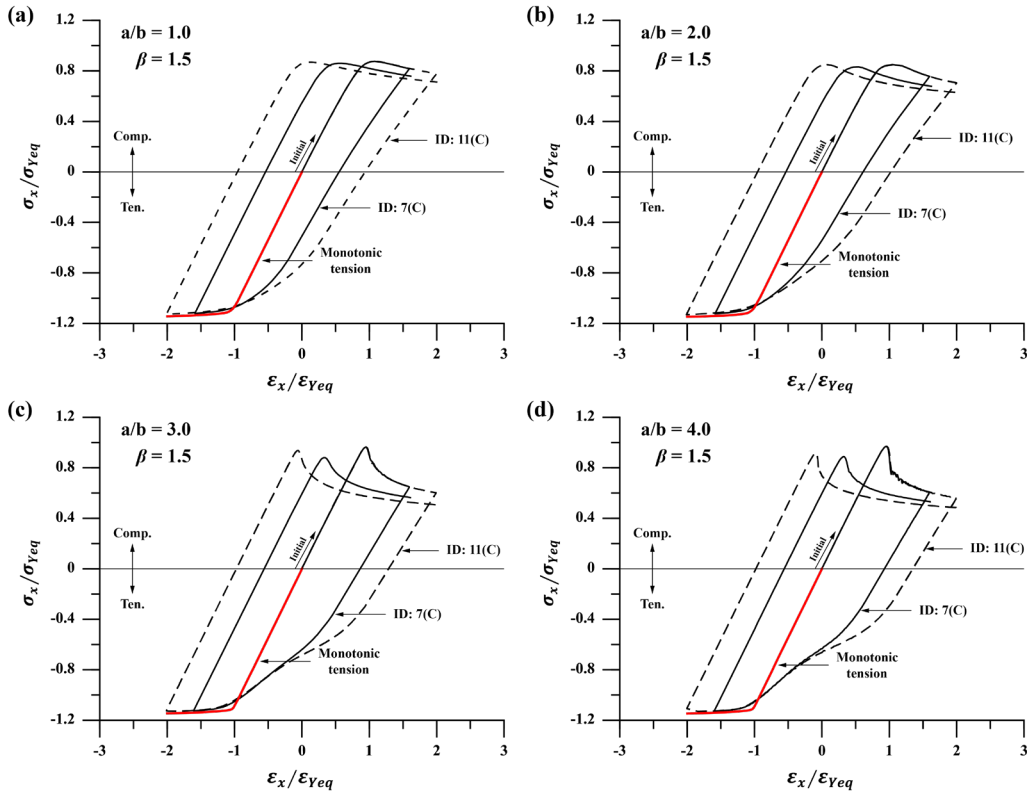


Figure 3-6 Load-shortening curves of ship plates ($\beta = 1.5$; compression init.)

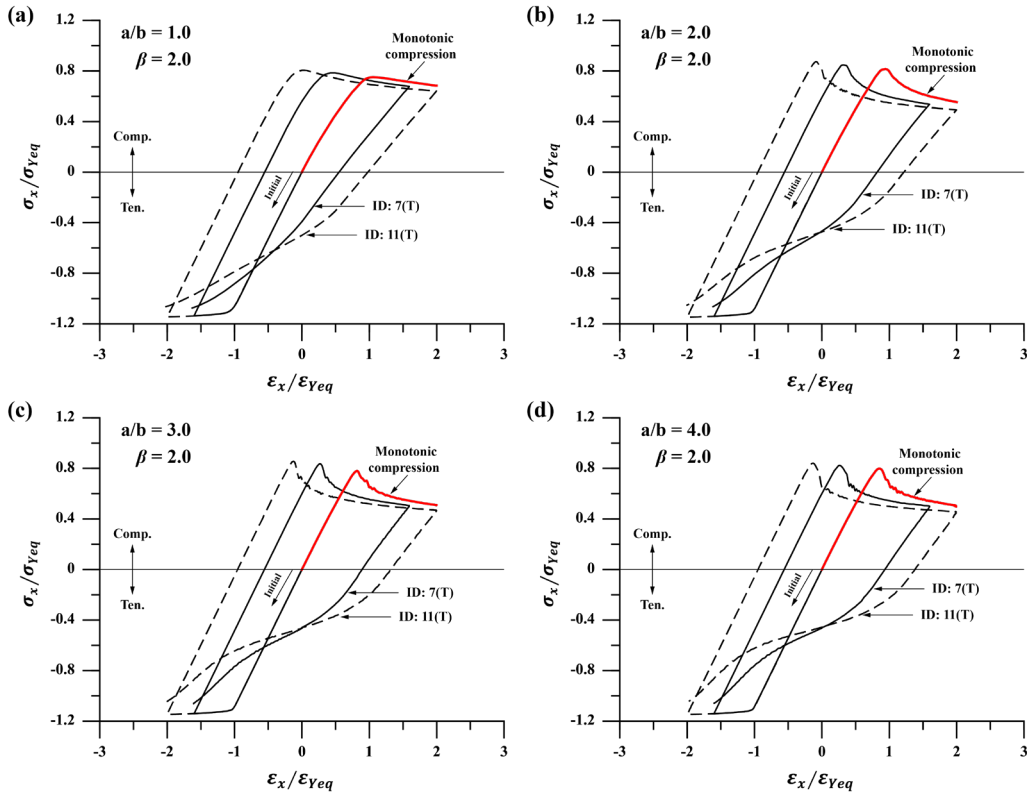


Figure 3-7 Load-shortening curves of ship plates ($\beta = 2.0$; tension init.)

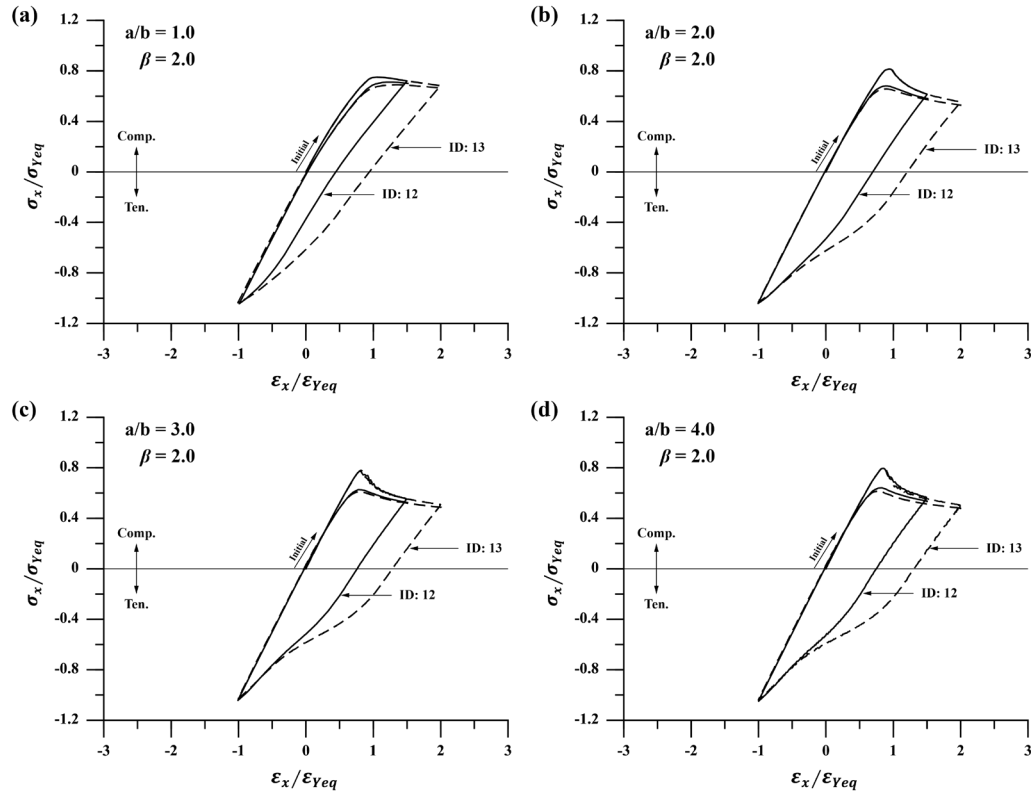


Figure 3-8 Load-shortening curves of ship plates (Varied amplitude)

The single-cycle load-shortening curve results show four important insights:

- Nonlinearity from compression to tension;
- The reduced stiffness in tensile reloading;
- The shift of the compressive failure point;
- Correlation between the compressive reloading strength and unloading stress.

It is universal in all plates that the transition from compression to tension results in a nonlinear response with an in-plane stiffness much lower than the common assumption in monotonic tensile loading, such as CSR. For longer plates, this nonlinearity becomes more significant. This is attributed for the fact that under the same averaged strain, more significant localization of the buckling/plastic deformation in the post-compressive failure regime would occur in longer plates as compared with shorter plates. This leads to earlier re-yielding and larger

nonlinearity when the plate is re-loaded to tension. A schematic illustration of this feature is shown in Figure 3-9.

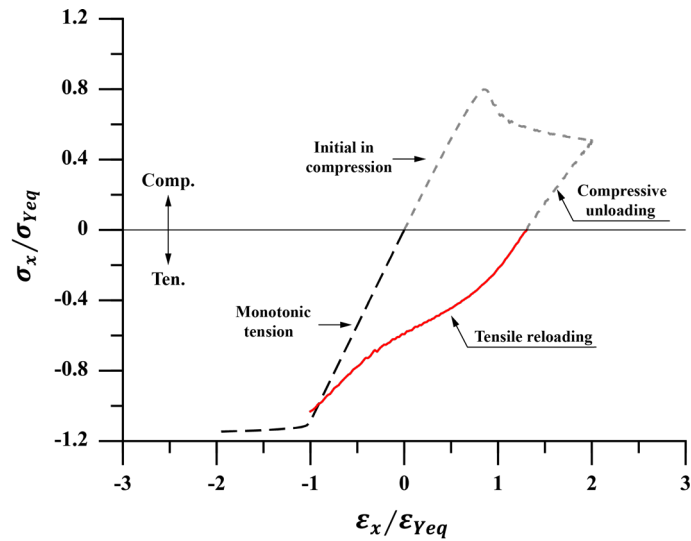


Figure 3-9 Schematic illustration of the nonlinear tensile reloading response (compression init.)

If no tensile load that surpass the elastic limit has been previously applied (i.e. initial in compression), it appears that the failure point in tension is close to the failure point under a monotonic tensile loading, which is approximately $\varepsilon_{xu}/\varepsilon_{Yeq} = -1$ as indicated by the red line showing the monotonic tensile curve in Figures 3-4 to 3-6. However, if a tensile unloading has taken place previously, the reloading path under tensile load tends to approach the previous tensile unloading point. At the previous tensile unloading strain, a smaller resultant stress (in magnitude) is obtained. A schematic illustration of this behaviour is shown in Figure 3-10. This is probably due to the residual deformation and stress developed in the previous compressive loading.

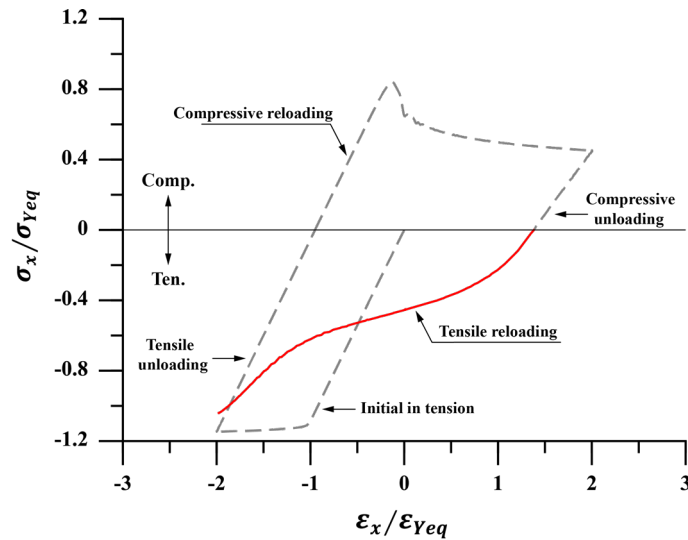


Figure 3-10 Schematic illustration of the nonlinear tensile reloading response (tension init.)

Unlike the tensile response, the compressive failure point will be shifted in accordance with the change of the permanent deformation point (zero resultant stress). Therefore, the general shape of the compressive curve remains similar under the single-cycle loading. A schematic illustration of these characteristics is shown in Figure 3-11.

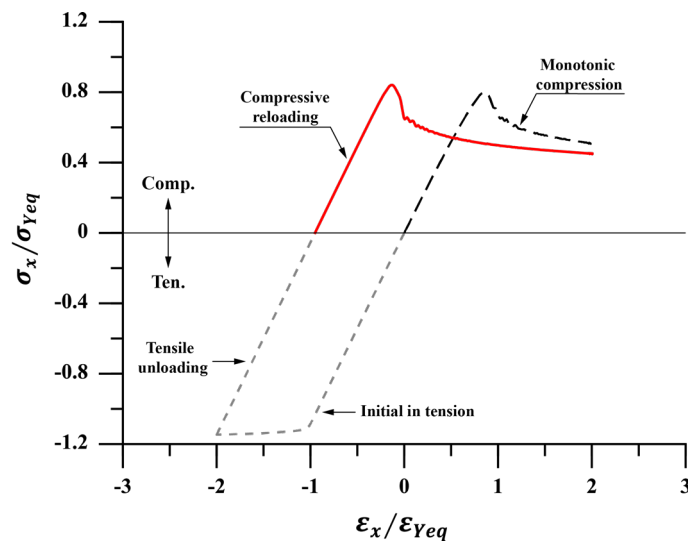


Figure 3-11 Schematic illustration of the compressive reloading response

Regarding to the unloading response, the tensile unloading is almost linear and its stiffness approximately equals to the material Young's modulus, being independent on the unloading strain. As for the compressive unloading, there is generally a reduced stiffness compared to the average initial compressive stiffness.

3.4.2 Influence of the Combined Hardening Model

Figure 3-12 shows a comparison of the load-shortening curve with two different material plasticity models, namely the elastic-perfectly plastic model and the combined hardening model (Chaboche model) as defined in Section 2.8.1.

It is evident that the choice of material model leads to a significant difference in the post-collapse behaviour. Since the hardening effect is accounted for in the material model, the loss of the load-carrying capacity in the compressive post-collapse regime is less than that predicted by the elastic-perfectly plastic model. The initial ultimate compressive strength is not affected, whereas the tensile strength is slightly higher. For long plates with a relatively steep initial post-collapse stiffness (Figure 3-12 & d), the post-collapse behaviour will become more stable during compressive reloading when the combined hardening model is employed. On the contrary, the post-collapse behaviour in compressive reloading still exhibits a steep capacity loss when the elastic-perfectly plastic material model is employed. When the combined hardening model is employed, the ultimate compressive reloading strength is close to the stress at which the compressive unloading is started.

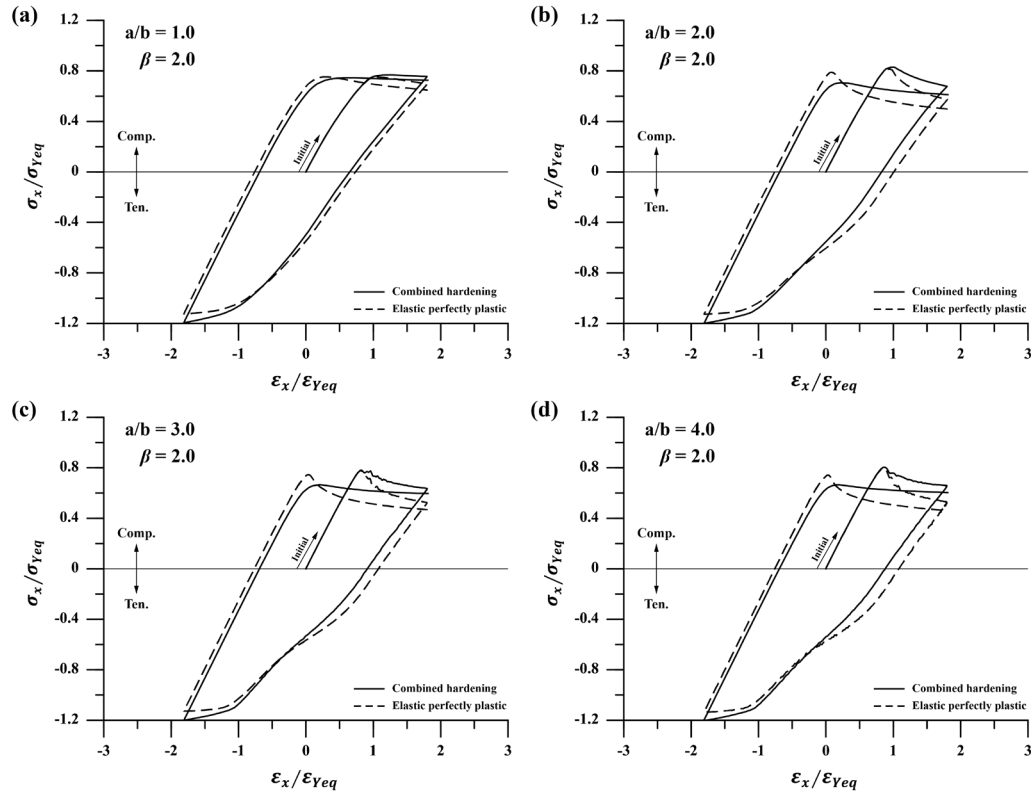


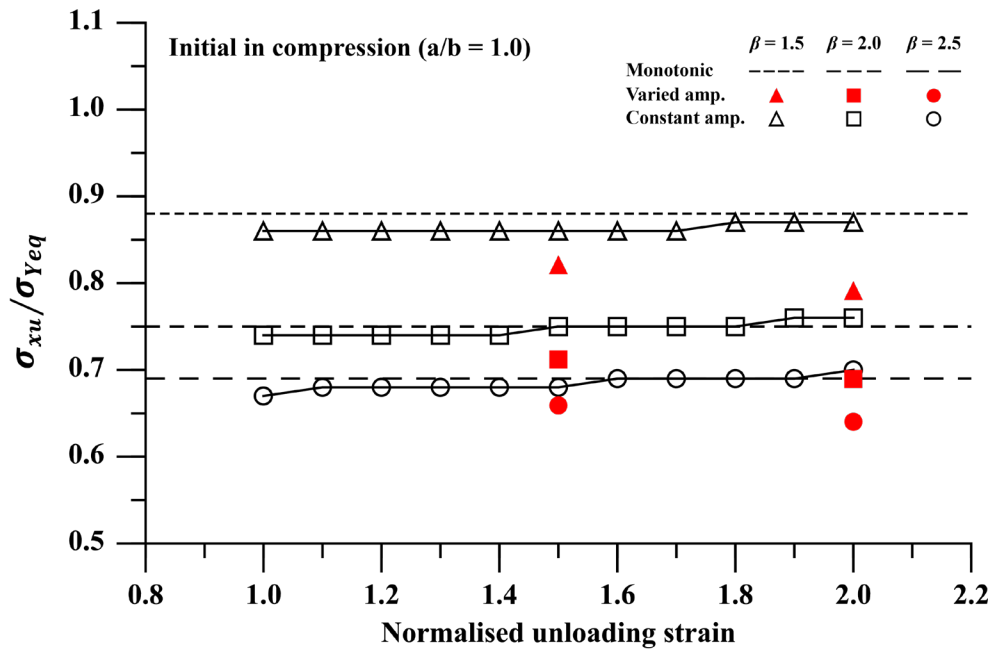
Figure 3-12 Comparison of load-shortening response with different material models

3.4.3 Compressive Strength (Single-Cycle)

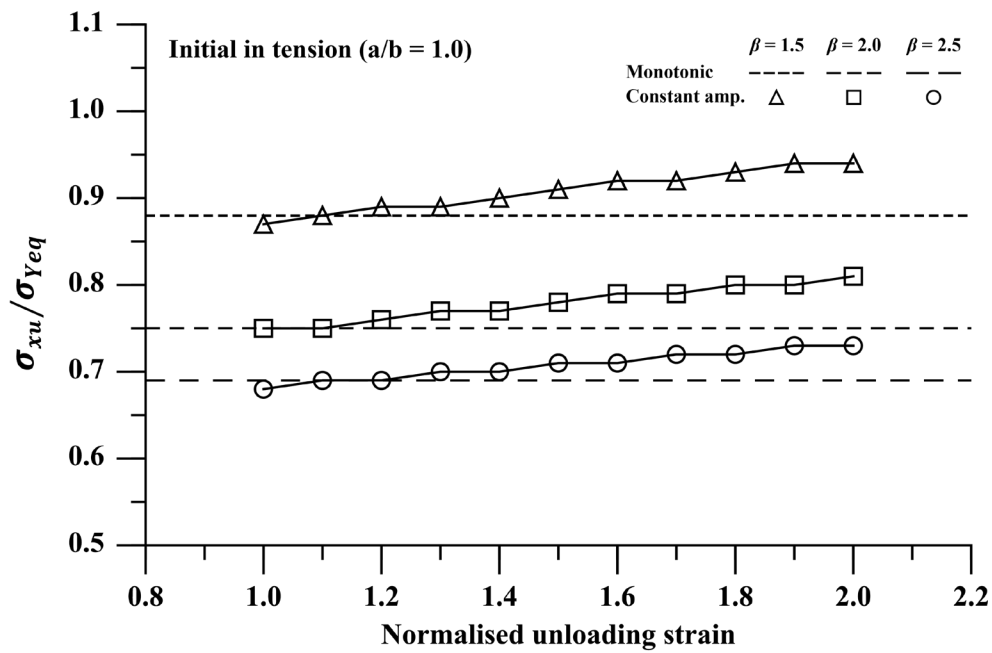
Figure 3-13 to Figure 3-16 show the reloading ultimate compressive strength after single-cycle loading with constant and varied amplitude loading protocols. The black markers indicate the results obtained under constant amplitude loading protocols (IDs 1-11) whilst the red markers are for varied amplitude loading protocols (IDs 12-13). The ultimate compressive strength under monotonic loading is also plotted as dashed lines for comparison.

It is apparent for all aspect ratio plates analysed that there is a reduction of the ultimate compressive reloading strength when the plate is initially loaded in compression. The reduction seems to be dependent on the unloading strain, but the pattern is not clear. This may be explained in association with the responses when initially loaded in tension, where the reloading ultimate compressive

strength will be increased compared with the initial compressive strength, as indicated from Figure 3-13(b), Figure 3-14(b), Figure 3-15(b) and Figure 3-16(b). Hence, the reduction of the ultimate compressive strength under constant amplitude loading protocol with constant strain range may be smaller than that with a smaller strain range. Further, this may also explain that the compressive strength reduction caused by the varied amplitude loading is larger than that caused by the constant amplitude loading.

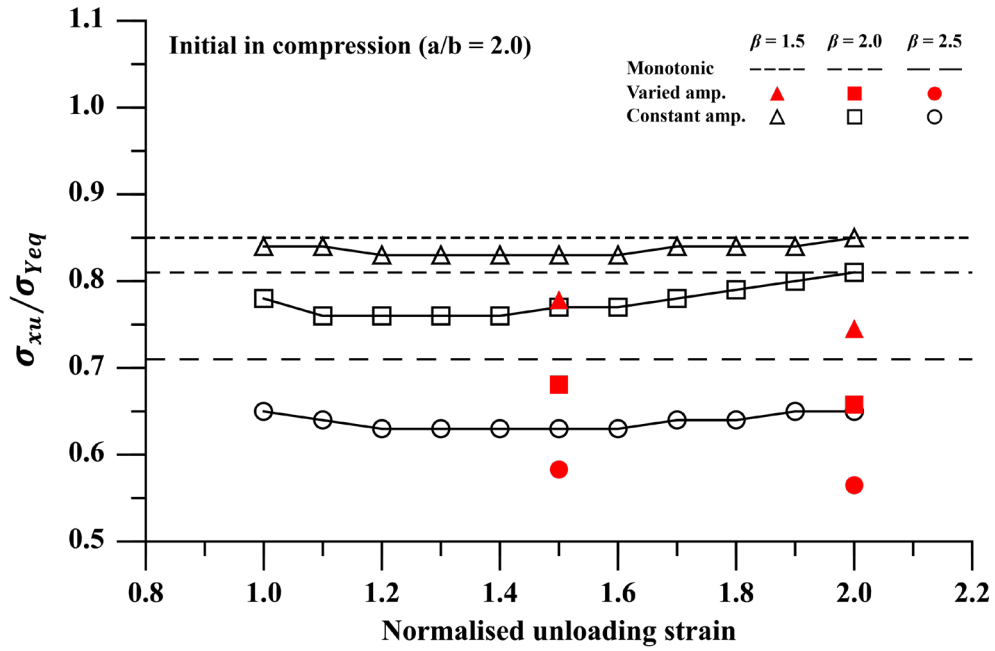


(a)

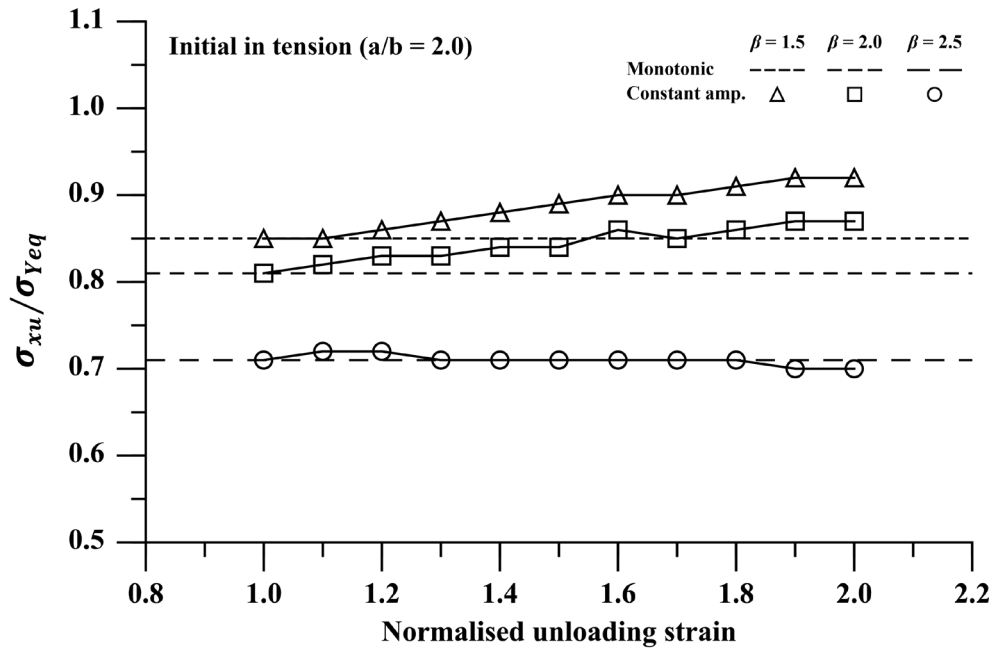


(b)

Figure 3-13 The reloading ultimate compressive strength of different loading protocols (a/b = 1.0, ID = 1~13)

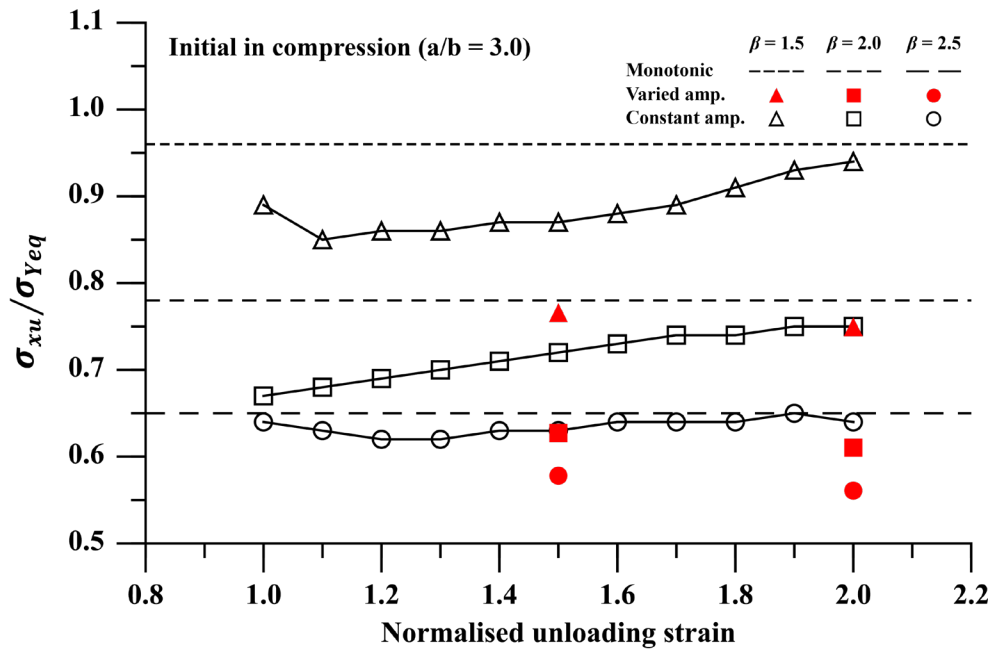


(a)

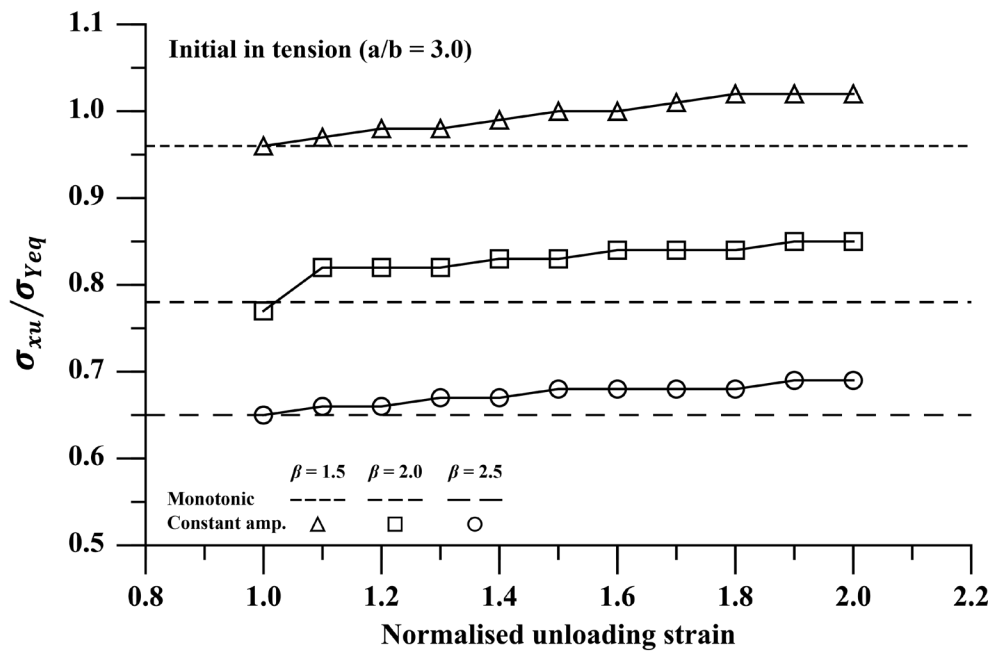


(b)

Figure 3-14 The reloading ultimate compressive strength of different loading protocols (a/b = 2.0, ID = 1~13)

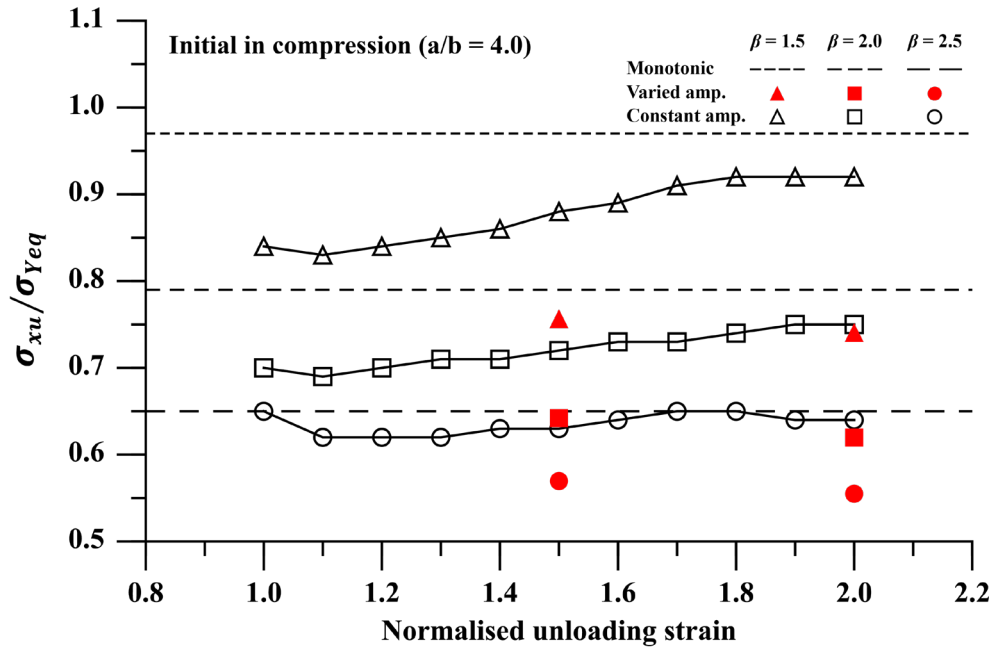


(a)

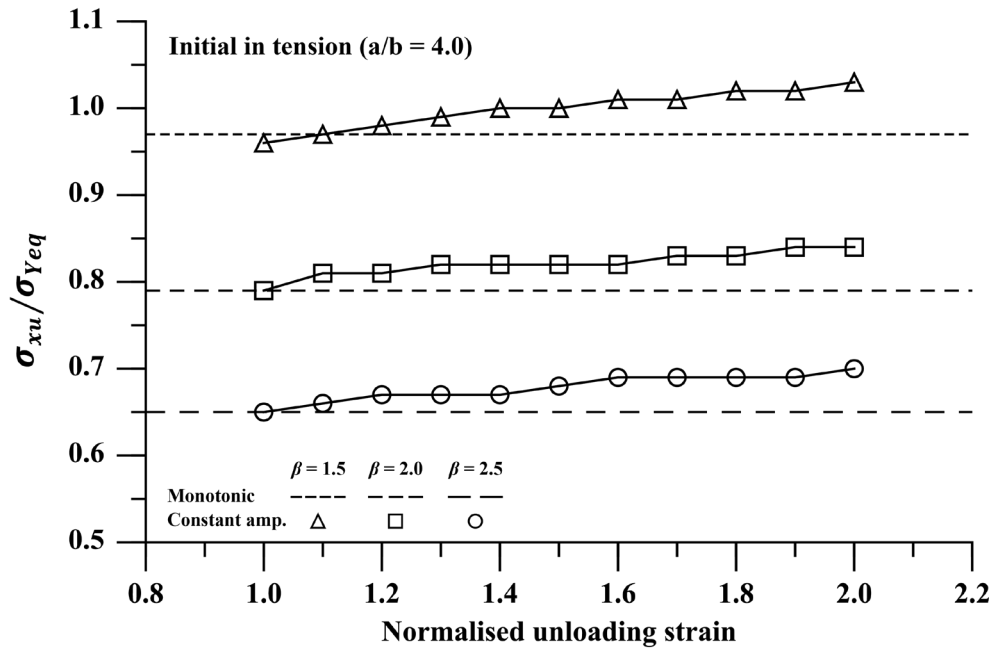


(b)

Figure 3-15 The reloading ultimate compressive strength of different loading protocols (a/b = 3.0, ID = 1~13)



(a)



(b)

Figure 3-16 The reloading ultimate compressive strength of different loading protocols (a/b = 4.0, ID = 1~13)

Figure 3-17 illustrates the correlation between the unloading stress and reloading ultimate compressive strength. In addition to the constant and varied amplitude loading protocols with elastic-perfectly plastic material model, the results obtained using the Chaboche hardening model under constant amplitude are also illustrated (green marker). A statistical comparison is summarised in Table 3-5. When the elastic-perfectly plastic model is adopted, the reloading strength under constant amplitude loading is higher than the stress of the unloading starting point with a mean bias of 1.18 and a coefficient of variation (COV) of 0.14. Conversely, a higher correlation is obtained when the varied amplitude loading is applied (Mean bias = 1.11 and COV = 0.09). When the material hardening model is used, highly correlated results are obtained. The unloading stress and the maximum reloading compressive strength are nearly the same with a mean bias of 1.00 and COV of 0.02. This comparison agrees with Fukumoto and Kusama (1985), showing that the compressive reloading strength is close to the stress at the starting point of unloading. Note that a varied amplitude loading protocol was applied in Fukumoto and Kusama's study (1985) where the tensile unloading took place at $\varepsilon_{xu}/\varepsilon_{Yeq} = -1$. From these comparisons, a close correlation between the unloading stress and the reloading ultimate compressive strength may be concluded.

Table 3-5 Statistical correlation between the unloading stress and maximum compressive reloading strength

| Material Model | Loading Protocol | Mean Bias | COV |
|-------------------|--------------------|-----------|------|
| Perfectly plastic | Constant amplitude | 1.18 | 0.14 |
| Perfectly plastic | Varied amplitude | 1.11 | 0.09 |
| Hardening | Constant amplitude | 1.00 | 0.02 |

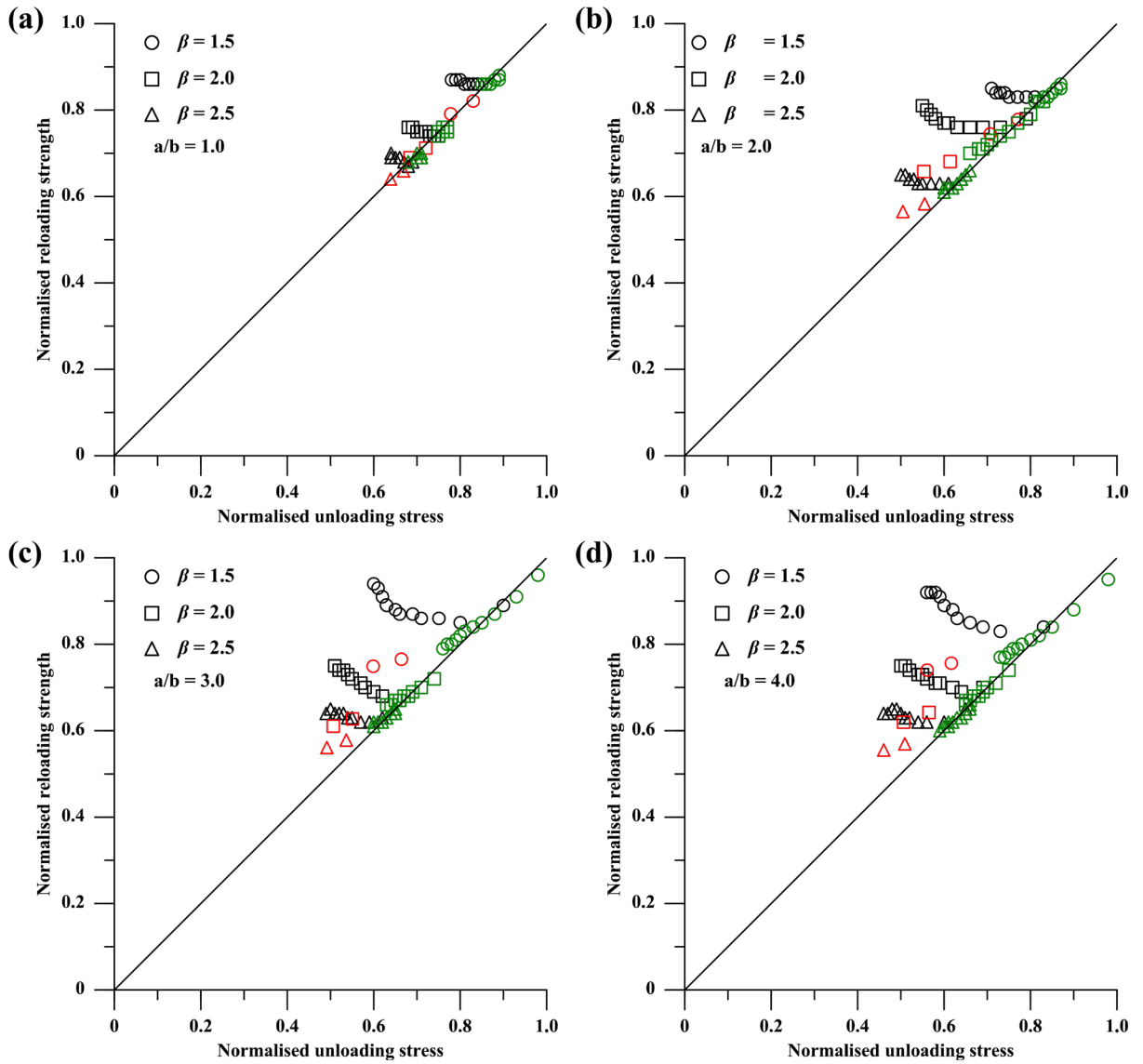


Figure 3-17 Correlation between the unloading stress and maximum compressive reloading strength (Black marker: perfectly plastic and constant amplitude; Red marker: perfectly plastic and varied amplitude; Green marker: hardening and constant amplitude)

3.5 Multi-Cycle Response

3.5.1 Load-Shortening Behaviour (Multi-Cycle)

Figures 3-18 and 3-19 show the typical load-shortening curves of two different multi-cycle loading protocols (i.e. ID: 24 & ID: 17). The response characteristics of the examples presented are similar with all other test cases. The monotonic curves predicted by IACS-CSR are also included for comparison.

The multi-cycle load-shortening curve results show three important insights:

- Converging reduction of the compressive strength;
- Continuous reduction of the tensile strength reduction;
- Response plateau of the compressive post-collapse regime.

As stated before, the tensile reloading path is expected to approach the previous tensile unloading point, while the compressive failure point would be shifted following the permanent deformation point so that the compressive path retains the same characteristic shape as that of the monotonic curve. Within the ten-cycles of loading, there is continuous reduction of the tensile strength. By contrast, the compressive strength reduction tends to converge. Meanwhile, the relatively drastic decay of the compressive strength in the post-collapse regime is absent after a few loading cycles, whereas a response plateau represented by a horizontal post-collapse curve in the LSC occurs.

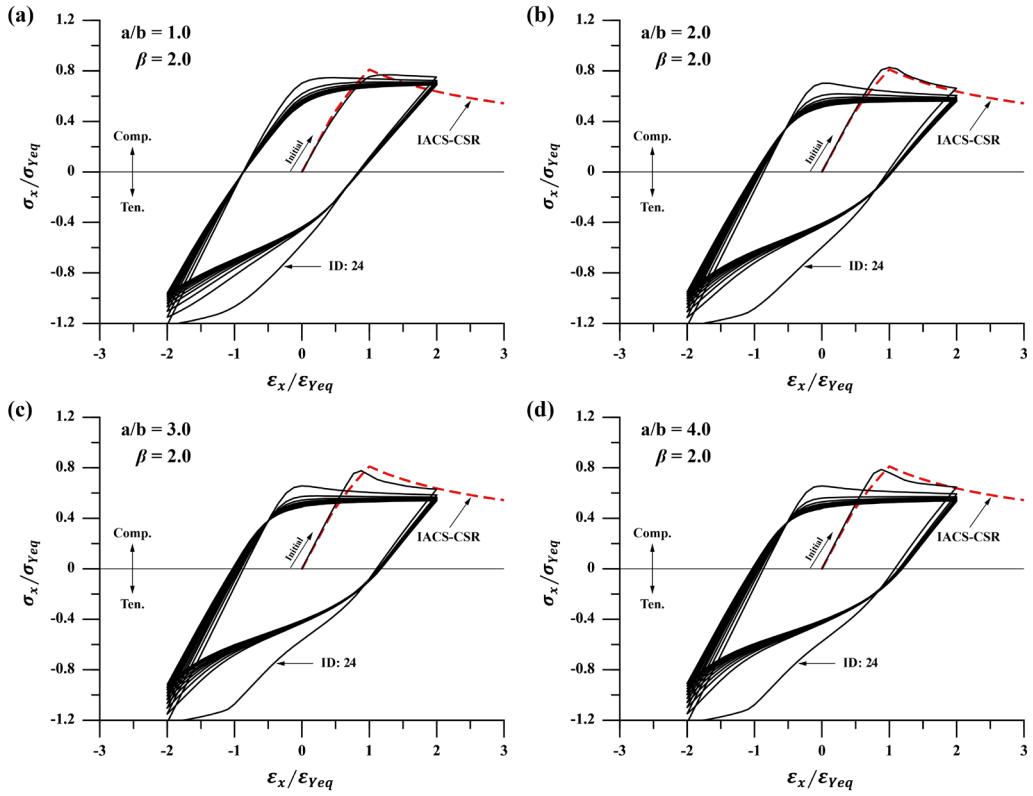


Figure 3-18 Load-shortening curves of unstiffened plates (ID: 24)

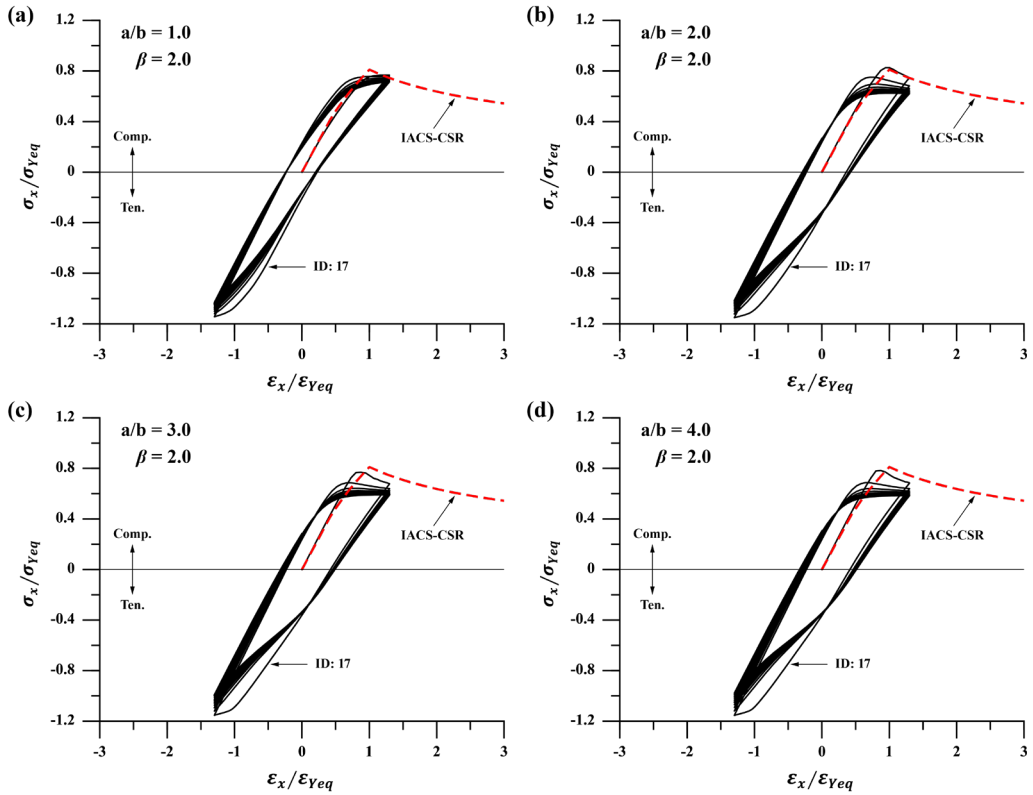


Figure 3-19 Load-shortening curves of unstiffened plates (ID: 17)

3.5.2 Compressive Strength (Multi-Cycle)

The compressive response convergence phenomenon is evident, which is consistent with Yao and Nikolov (1990). As illustrated in Figure 3-20, the ultimate compressive strength tends to converge to a constant value after three cycles of loading, although there is no complete convergence within the applied loading cycles. Conversely, at the same applied strain, the tensile strength continues to decrease during the cyclic loading, indicating a progressive reduction of the tensile stiffness. The decreasing rate of tensile strength is illustrated in Figure 3-21. Both loading protocols show a linear decrease of the tensile strength, in which a larger applied strain results in a larger decreasing rate. Once the response has converged, the value of the compressive strength appears to depend on the applied strain range. With a larger applied strain range, this value converges to a smaller compressive strength.

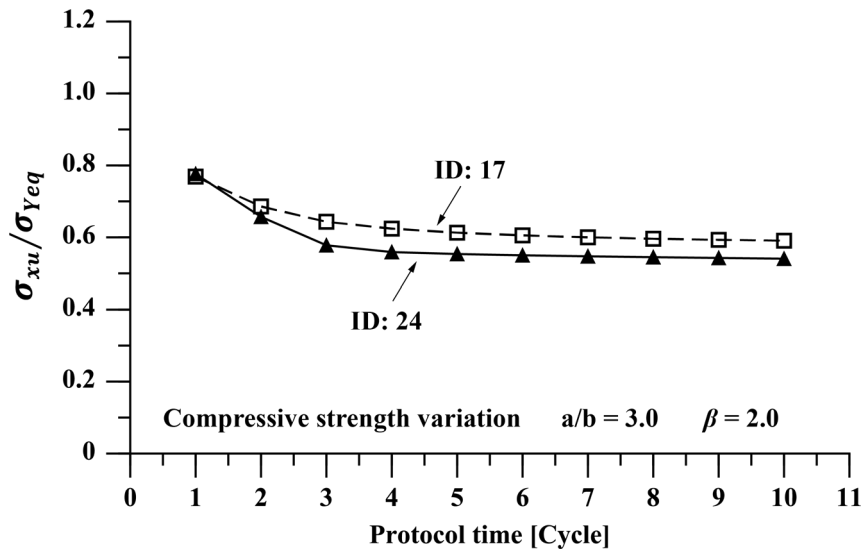


Figure 3-20 Variation of the compressive strength in multi-cycle loading

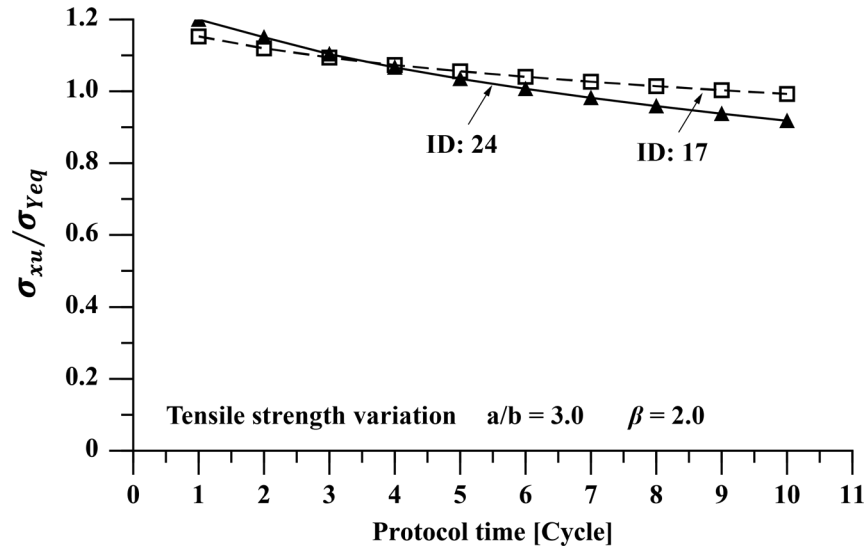


Figure 3-21 Variation of the tensile strength in multi-cycle loading

The compressive strength convergence behaviour is accompanied by the level-off of out-of-plane deflection and post-collapse stiffness of the plates. Typical out-of-plane deflection contour plots are shown in Figures 3-22 to 3-24. These show that in the post-ultimate regime, the out-of-plane deflection nucleates at the end of the plate. The variation of deflection nucleation is generally in alignment with the change of compressive strength. As shown in Figure 3-25, after three cycles of loading, the out-of-plane deflection stabilizes with a similar magnitude at the end of compression loading (start of unloading).

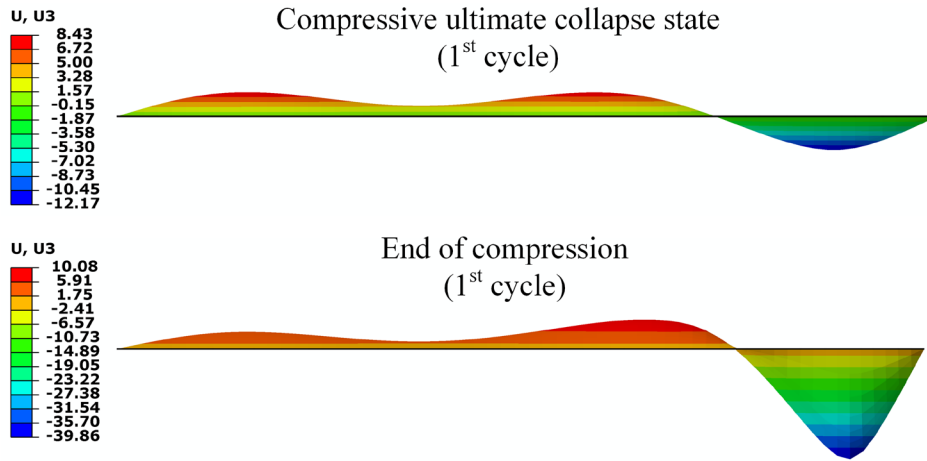


Figure 3-22 Out-of-plane deflection profile (1st cycle)

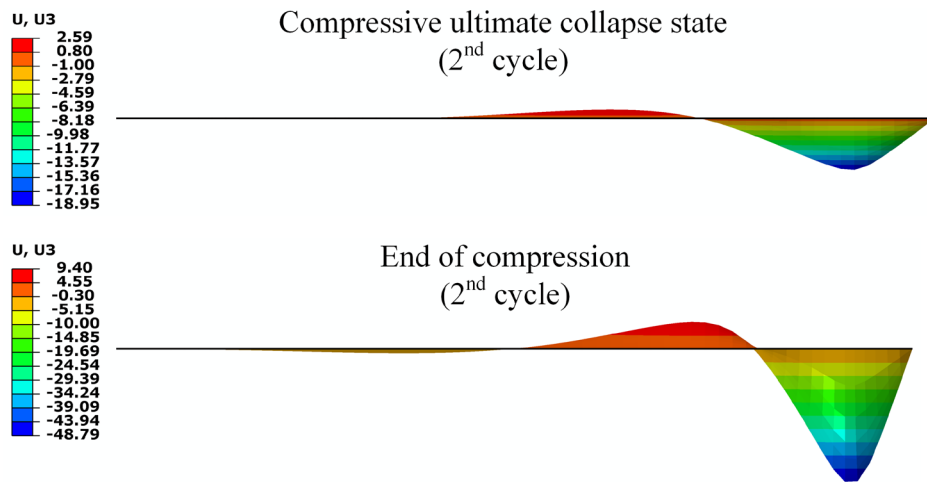


Figure 3-23 Out-of-plane deflection profile (2nd cycle)

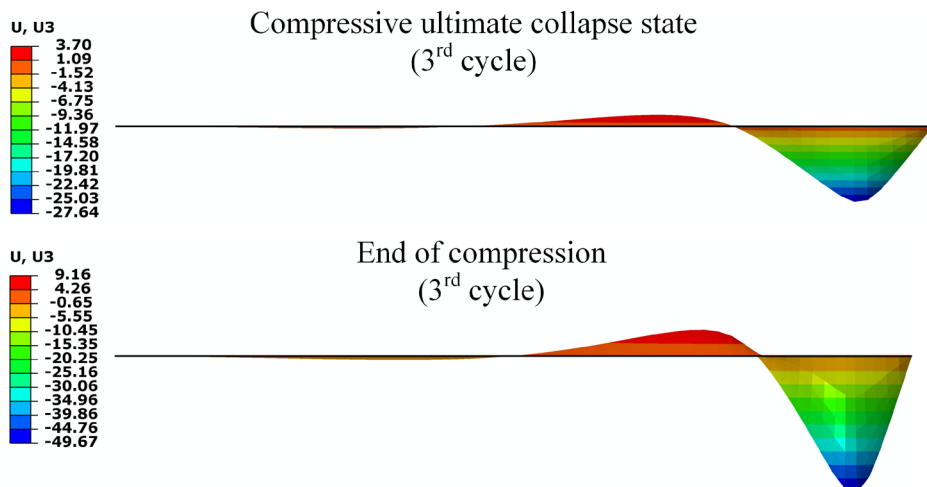


Figure 3-24 Out-of-plane deflection profile (3rd cycle)

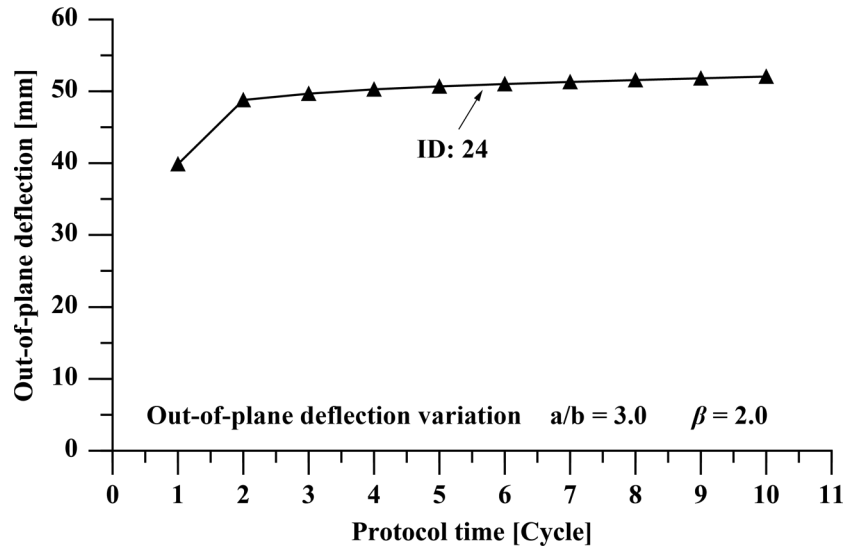


Figure 3-25 Out-of-plane deflection variation

Figure 3-26 shows the variation of the average post-ultimate stiffness normalised by the Young’s modulus for the first three cycles. It is evident that the post-collapse stiffness (the absolute value) reduces under the cyclic loading and approaches to zero after three cycles of loading. In association with the previous discussion that the ultimate compressive reloading strength is close to the unloading stress at each cycle, it can be suggested that the variation of the post-collapse stiffness leads to response convergence to a constant compressive strength, as the unloading stress will be similar to maximum strength when the post-collapse stiffness is close to zero.

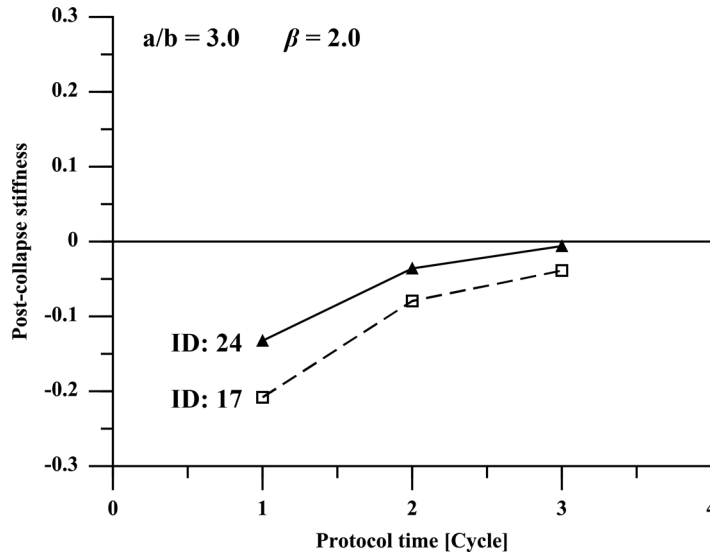


Figure 3-26 Post-collapse stiffness variation

3.6 Chapter Summary

To analyse the elastoplastic buckling collapse behaviour of local structural components under cyclic compression and tension, a systematic NLFEM analysis is conducted on a series of unstiffened plates subjected to idealised loading protocols. Through this, insights of the load-shortening behaviour of unstiffened plates under cyclic compression and tension are obtained. The typical characteristics are summarised as follows:

- The load-shortening responses of unstiffened plates under cyclic in-plane load markedly differ from the monotonic responses;
- When reloading from compression to tension, the tensile path is nonlinear with a considerably lower stiffness compared with the Young's modulus;
- The strain value of the tensile ultimate point is dependent upon the previous unloading in tension. If no unloading previously taken place in tension, the strain value remains the same as that under monotonic tensile loading. If unloading previously taken place in tension, the strain value becomes close to the tensile unloading point;

- The general shape of the compressive load-shortening curve remains similar, as the compressive ultimate point will be shifted in accordance with the change of the permanent deformation point;
- Under multi-cycle loading, the constant ultimate compressive strength converges to a nearly constant value, which commences after three loading cycles. This convergence behaviour is accompanied with the level-off of the out-of-plane deflection and the post-collapse stiffness. Conversely, the maximum tensile strength under the same given strain decreases at each cycle, which leads to the progressive reduction of tensile stiffness.

The outcomes of this investigation provides us with a new recognition of the buckling collapse behaviours of unstiffened plates under cyclic compression and tension, in particular the characteristic features that are relevant for ultimate limit state assessment of ship hull structures. The observed response patterns are beneficial for developing an efficient methodology to predict the structural components in Chapter 4 and further provide input data to the hull girder response analysis in Chapter 5.

Chapter 4 Methodology For Predicting the Cyclic Load-Shortening Curves of Structural Members

4.1 Rationale

The primary objective in this chapter is to describe an efficient methodology for predicting the load-shortening response of structural components under cyclic axial loading. The rationale of developing this method may be summarised as follows:

- 1) Smith-type progressive collapse method is an established method to predict the collapse response of ship hull girders under longitudinal bending. To employ Smith-type approach, a methodology to trace the load-shortening curves of structural components should be first developed.
- 2) There have been many well established methods and widely adopted in monotonic loading analysis. However, for the monotonic loading analysis, the applied load simply takes the form of starting from null to a prescribed value surpassing the ultimate limit state. In this case, the loading protocols of all structural components normally follow the same loading path, although their magnitudes may be different. Thus, their load-shortening behaviours can be predicted in advance and be taken as an input data for the hull girder progressive collapse analysis using the Smith-type method. By contrast, under cyclic loading, the loading protocol of structural elements are unknown a priori. When the load reversal takes place in a hull girder, the structural members are at different strain states because of the difference in the vertical locations with respect to the cross section neutral axis. Therefore the load-shortening curves cannot be prepared in advance as an input data for the hull girder analysis using the Smith-type

progressive collapse method. An efficient approach that is suitable to be integrated with the Smith's method is needed.

- 3) Although the NLFEM is a capable approach for evaluating load-shortening behaviours of structural segments, the required computational efforts are considerable and would be significantly amplified as a result of the application of cyclic loads. In the meantime, it is sometimes difficult to obtain a reliable and converged solution. Thus, it may not be appropriate for incorporating with Smith-type progressive collapse method and a more efficient approach is necessary.

4.2 Principle

As shown in Figure 4-1, the prediction of cyclic behaviour is driven by a loading protocol which can either be an incremental output from the hull girder progressive collapse method or an independently prescribed cyclic load. An initial compressive LSC is first pre-defined. Any approach can be employed and is independent on the proposed methodology for cyclic response prediction. Through this way, the proposed methodology is compatible with the existing approach used for the buckling and ultimate strength assessment, such as CSR. The subsequent simulation of the cyclic behaviour is determined by a response rule and an updating rule which adapts the initial compressive LSC input to an updated LSC due to the corresponding load reversals.

The novelty is the response and updating rules, which are derived based upon the observations on a systematic analysis using NLFEM as reported in Chapter 3. The response rule is utilised for the incremental prediction following the critical points of the current LSC. When the load reversal takes place, the updating rule is then called to update the critical points, which are then used by the response rule for subsequent incremental predictions until the next load reversal.

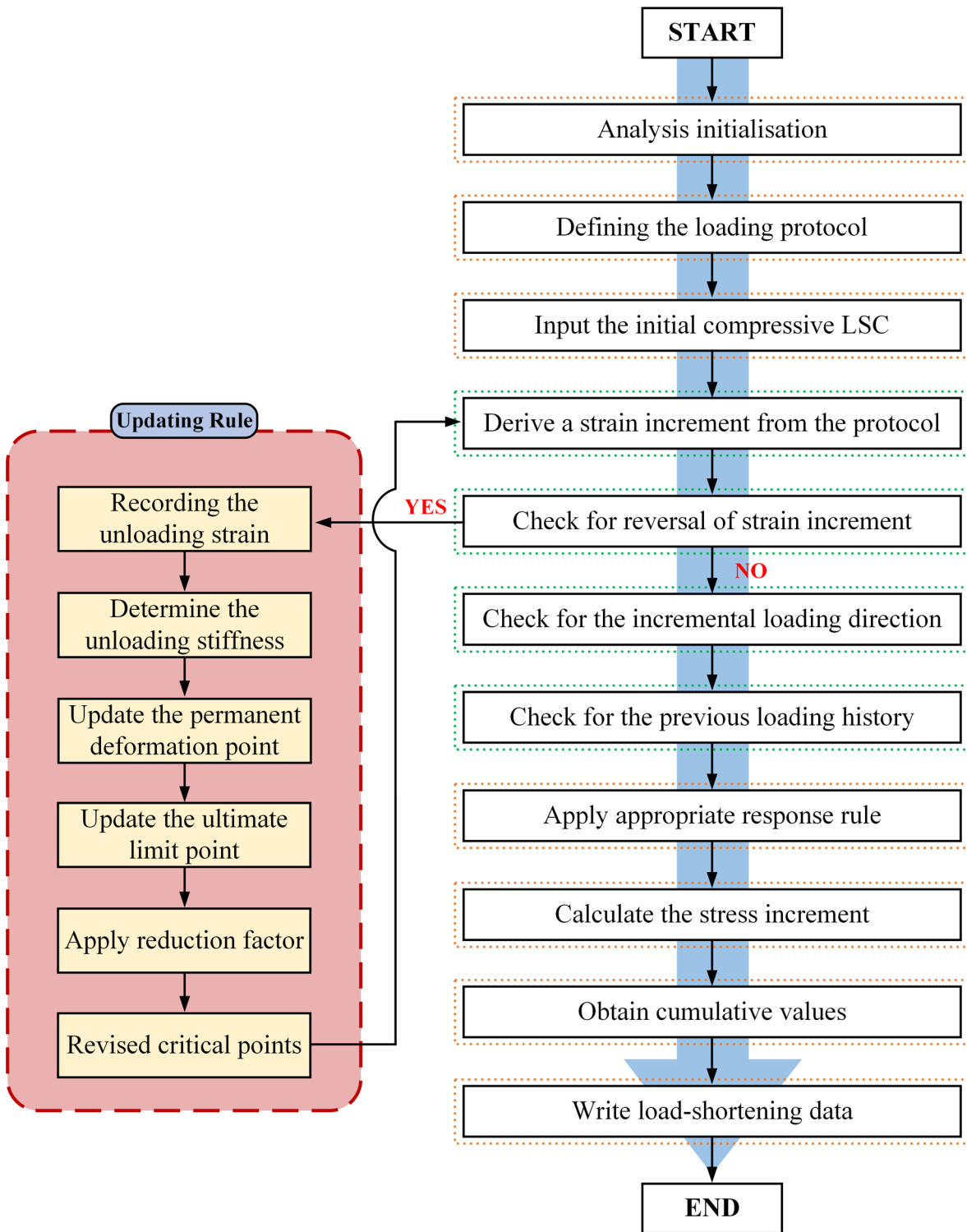


Figure 4-1 Flowchart of the proposed method to predict the load-shortening curves of plates and stiffened panels under cyclic axial loads

4.3 Response Rule

As illustrated in Figure 4-2, the following critical points which are regarded as the most important characteristics are defined for a LSC of structural component in both compression and tension:

- The compressive and tensile ultimate points, at which the ultimate strength is attained, i.e. point a & c respectively;
- The permanent deformation point, at which the resultant stress is zero, i.e. point b;
- The compressive and tensile unloading point, at which the load reversal is started, i.e. point d or point e.

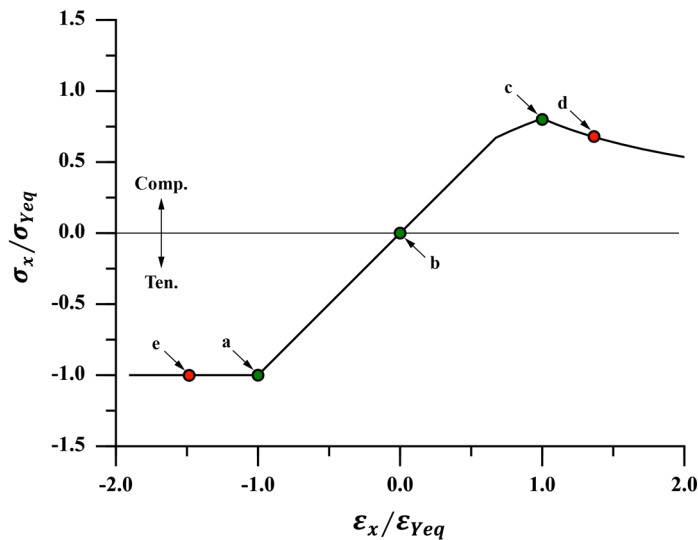


Figure 4-2 Illustration of the critical points of a LSC

The response rule follows a different approach for compression and tension:

Compression:

1. The initial compressive response is predicted by any established method applicable for monotonic loading (e.g. CSR method or NLFEM);
2. The updated compressive response is idealised as piece-wise linear (Figure 4-3):
 - a) The pre-ultimate strength response path follows ‘permanent deformation point --> compressive ultimate point’;
 - b) The post-ultimate strength response follows a constant stiffness determined in the latest update due to the compressive unloading.

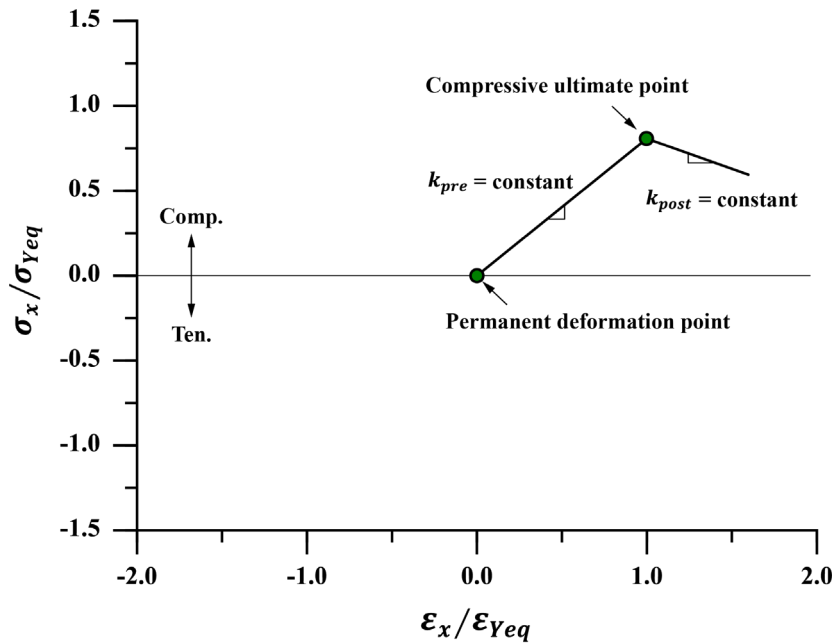


Figure 4-3 Illustration of the compressive response rule (Updated curve)

Tension:

1. The tensile response is always assumed as piece-wise linear (Figure 4-4):
 - a) If unloading has not taken place in tension, the pre-ultimate strength response path follows ‘permanent deformation point --> tensile ultimate point’;
 - b) If unloading has previously taken place in tension, the pre-ultimate strength response follows the path ‘permanent deformation point --> tensile unloading point --> tensile ultimate point’.
2. The tensile ultimate stress and strain are initialised as the material yield stress and yield strain respectively;
3. In the post-ultimate strength range, the tensile stiffness is taken as zero.

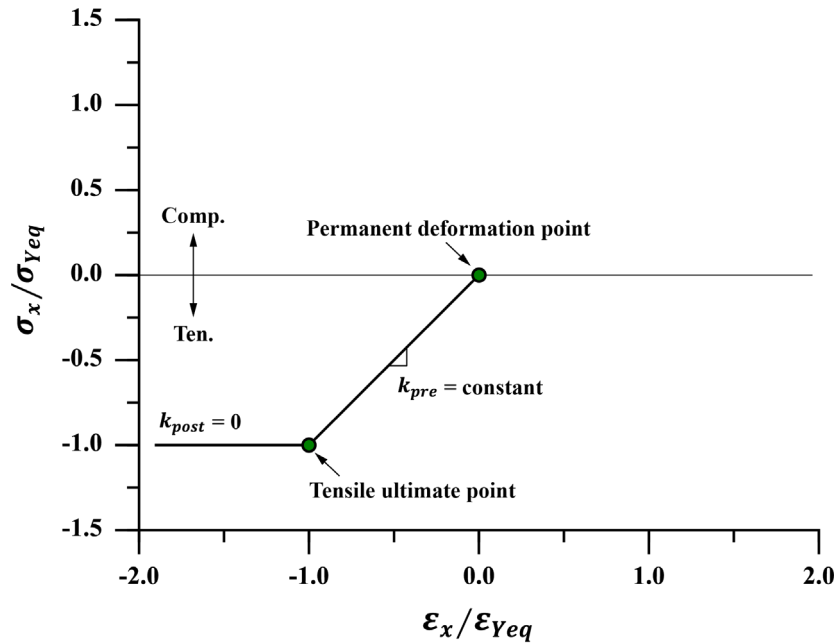


Figure 4-4 Illustration of the tensile response rule

4.4 Updating Rule

Once the applied strain is reversed, the last applied strain and resultant stress will be recorded as the unloading strain and stress respectively. The following rules describes the update of relevant data used in the response rule.

1. The compressive unloading stiffness is estimated as $k = (\sigma_{xu}/\sigma_{Yeq}) \times E$ where σ_{xu} is the initial ultimate compressive strength, σ_{Yeq} is the material yield stress and E is the material Young's modulus (Figure 4-5);
2. The tensile unloading stiffness is taken as the material Young's modulus (Figure 4-5);
3. The permanent deformation point is updated based on corresponding unloading stiffness (Figure 4-5);
4. For the unloading in compression, it is assumed that the permanent deformation point remains the same if the unloading strain does not exceed the ultimate strain (Figure 4-6);
5. If the permanent deformation point is unchanged, the update procedure is terminated and all of the LSC data remain the same (Figure 4-6);
6. If unloading takes place in compression, the post-collapse stiffness in compression k_{post} will be updated as $k_{post} = \varphi_1 (\sigma_u - \sigma_{unload}) / (\varepsilon_u - \varepsilon_{unload})$ where φ_1 is the compressive post-collapse stiffness reduction factor (Figure 4-7);
7. If the unloading takes place beyond the ultimate point, the ultimate point is updated as the unloading point;
8. If the unloading takes place from compression, the tensile ultimate strain should be updated in accordance with the tensile strength reduction factor φ_2 to cover the effects of the distortion and residual stress amplified by the previous loading in compression;
9. If the unloading takes place from tension, the critical points relevant to compression remain the same except for the compressive ultimate strain, which should be updated considering the change of the permanent deformation point.

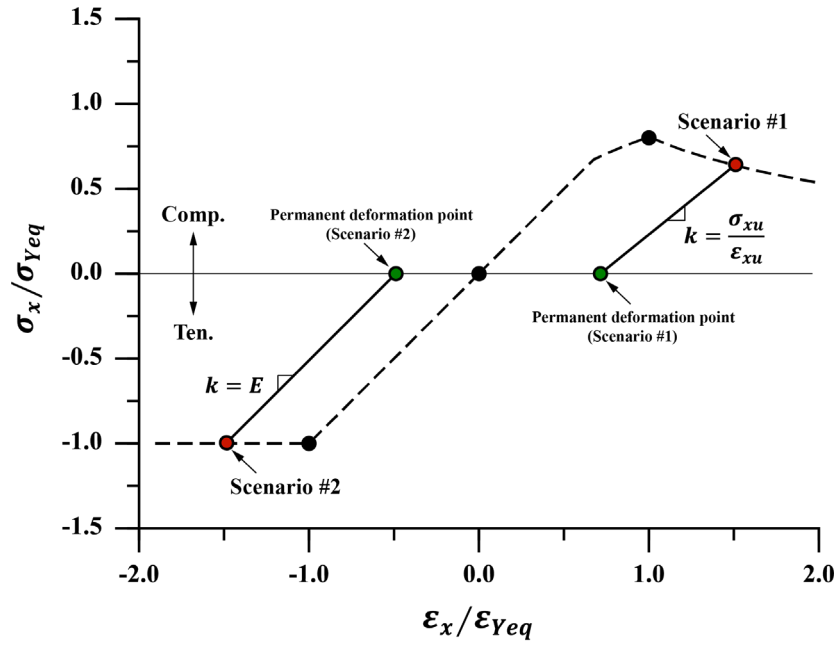


Figure 4-5 Illustration of the updating rule 1 to 3

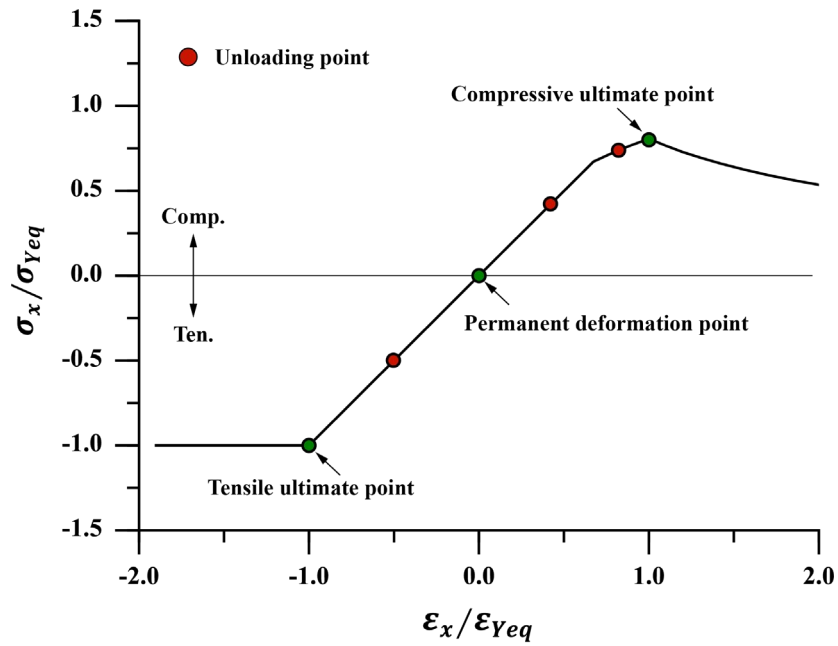


Figure 4-6 Illustration of the updating rule 4 to 5

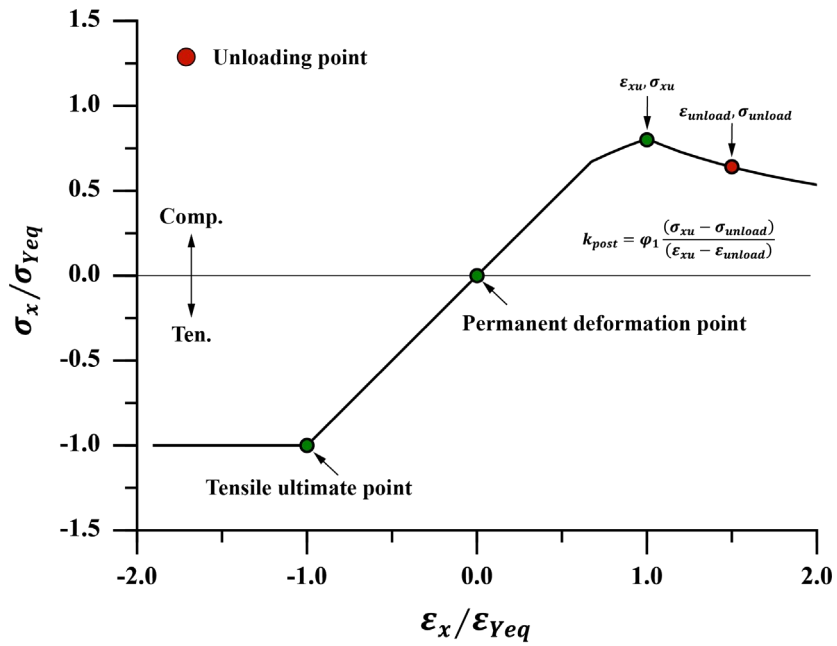


Figure 4-7 Illustration of the updating rule 6

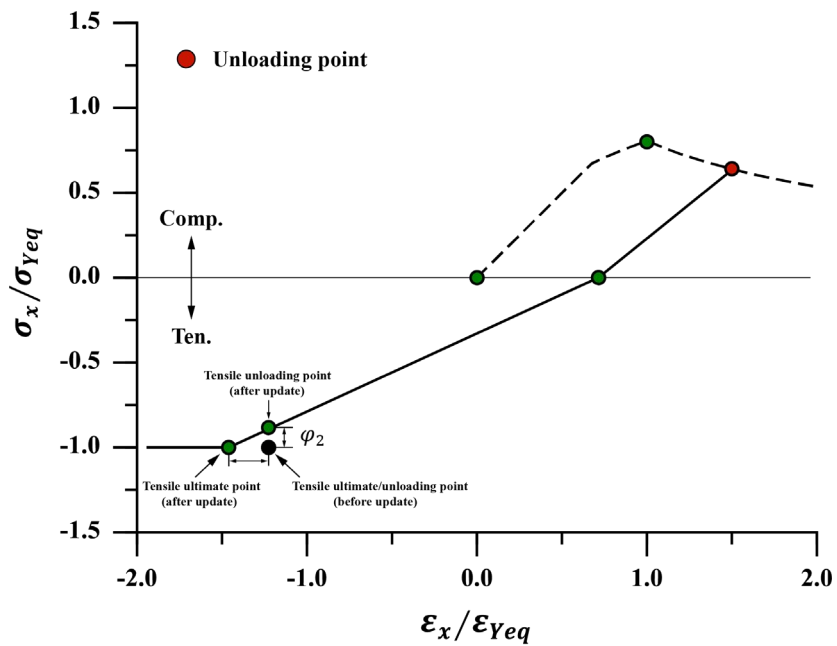


Figure 4-8 Illustration of the updating rule 8

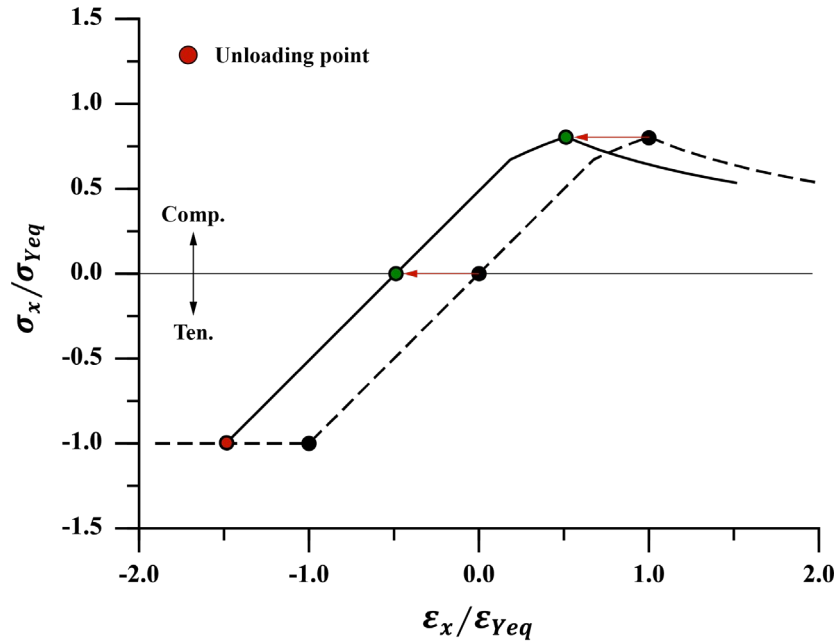


Figure 4-9 Illustration of the updating rule 9

4.5 Rationality of the Response and Updating Rules

The fundamental concept of the response and updating rules is that the load-shortening behaviour of ship structural member under in-plane loading is characterised by specific features within the LSC, i.e. critical points. The relative relationships of these critical features within the LSC are independent of the applied load. These critical features are subject to updating depending on the load reversals. The response rule is developed to describe the former (relative relationship) and the updating rule is introduced to govern the latter (updating).

The permanent deformation point is specified in the response rule as it is an indication of whether the applied load prior to the reversal has an adverse effect on the structural member, which may permanently alter the “initial imperfection” and consequently its load-shortening behaviour. The compressive/tensile ultimate points are specified since they represent the maximum load-carrying capacity. The compressive/tensile unloading points are specified to track the load reversal history of the structural member. It is separately defined for compression and

tension since an unloading in different direction would lead to a different influence on the load-shortening behaviour.

The compressive response rule #1 is developed to ensure the compatibility of the proposed scheme with the existing approaches for deriving monotonic LSCs. The proposed response and updating rule would serve as an extension to the existing approach for predicting the cyclic response. The assumption of piece-wise linear in the compressive response rule #2 is a simplified behaviour compared to the numerical simulation as shown in the latter validation and also Section 3.5 of Chapter 3. However, it can increase the efficiency and robustness when incorporating with the Smith method at a relatively small cost of losing accuracy. A difference between the tensile response rule #1(a) and #1(b) is that in the latter the tensile unloading point is taken in the response path. This is attempted to accommodate the scenario where the unloading point and ultimate point are different. This scenario will be illustrated in the next section. The tensile response rule #2 and #3 follows the usual practice in the collapse analysis of ship-type structures.

The updating rule is developed in a step-by-step procedure where the first general step (Updating rule #1 to #5) is to calculate the new permanent deformation point. With this updated information, one can determine whether the updating procedure should be continued or terminated (Updating rule #3). If there is no change on the permanent deformation, which may imply no alteration of the “initial imperfection” of the structural member, an updating of the LSC is therefore not needed. The assumption of the compressive/tensile unloading stiffness in updating rule #1 and #2 is based on NLFEM observations. As discussed in Section 3.5.1 of Chapter 3, the compressive unloading stiffness is usually smaller than the initial stiffness. Hence, the ratio between the original compressive ultimate point and original permanent deformation point is a

reasonable approximation. Conversely, the tensile unloading is very close to the Young's modulus. A reduction factor φ_1 is applied in updating rule #6 when evaluating the post-ultimate strength stiffness in compression in order to cater for the convergence phenomenon of the ultimate compressive strength and the post-collapse stiffness. The other reduction factor φ_2 is applied in updating rule #8 in order to accommodate the tensile strength reduction. The calibration of these factors may be best determined on the a case-by-case basis. Alternatively, a unified expression may be developed with the aid of a large body simulation. However, it could be difficult not only because various scantlings of panels should be covered, but also different loading protocols.

4.6 Schematic Illustrations

To demonstrate the response rule and updating rule, schematic illustrations are presented for typical responses to cyclic loads.

Scenario 1: Initial in compression and unloading from compression

In Figure 4-10, the unloading first takes place in compression at Point e. The updating rule will then be called and, as stated by updating rule 1, the permanent deformation point is calculated as Point g assuming that the compressive unloading stiffness is taken as the slope between the initial permanent deformation point and the initial compressive ultimate point, i.e. Point c and Point d. The compressive ultimate point is updated as Point e according to updating rule 7. Since the compressive unloading has taken place, the compressive LSC will be idealised as piece-wise linear according to the compressive response rule 2. The compressive post-ultimate stiffness (slope e-f) is calculated following updating rule 6. Since there is no tension being applied previously, the critical points relevant to tension do not require an update and the tensile pre-ultimate response follows the path 'permanent deformation point --> tensile ultimate point' (path

g-b) as stated in the tensile response rule 1a. Overall, the compressive LSC is updated as g-e-f and the tensile LSC is updated as g-b-a.

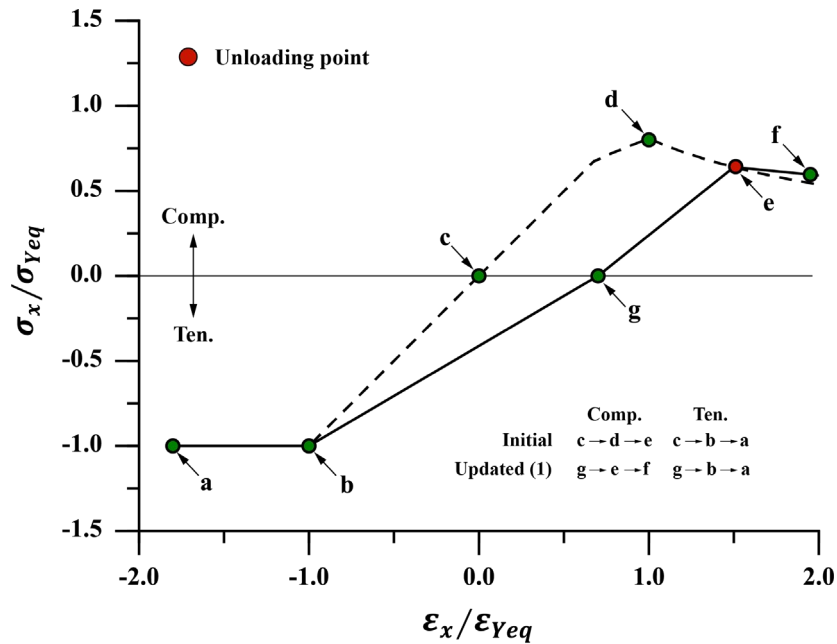


Figure 4-10 Schematic illustration of scenario 1

Scenario 2: follow-up of scenario 1 and unloading from tension (surpass elastic limit)

Figure 4-11 is the follow-up of the response shown in Figure 4-10 and the unloading takes place at Point b in the post-ultimate strength regime of tension. The updating rule is called to calculate the permanent deformation point (Point g) assuming that the unloading stiffness takes the value of Young’s modulus in accordance with updating rule 2. The tensile ultimate point is updated as Point b following updating rule 7 and the tensile response follows the path ‘permanent point --> tensile unloading point --> tensile ultimate point’ in accordance with the tensile response rule 1(b). Note that the tensile ultimate point and tensile unloading point at this stage are effectively identical. Following updating rule 9, the compressive LSC is modified as the permanent deformation point shifted from Point d to Point g. No change is needed for the ultimate compressive strength

and the post-ultimate strength stiffness, but the ultimate strain. Overall, the compressive LSC is updated as g-h-i and the tensile LSC is updated as g-b-a.

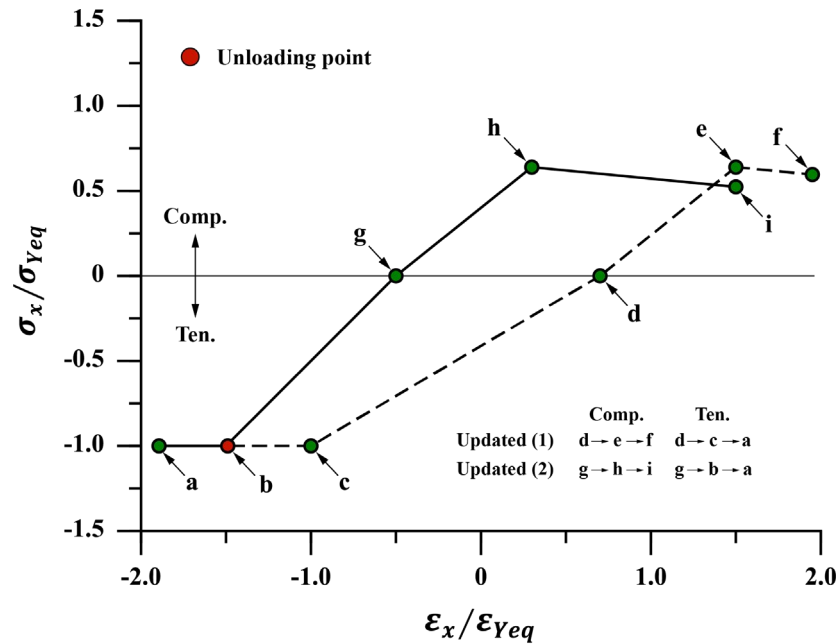


Figure 4-11 Schematic illustration of scenario 2

Scenario 3: follow-up of scenario 1 and unloading from tension (within elastic limit)

Figure 4-12 is a variant of the load reversal scenario shown in Figure 4-11. This scenario is also originated from the illustration shown in Figure 4-10, but the unloading in tension takes place at pre-ultimate strength regime in tension (Point c). Since the unloading takes place prior to surpassing the tensile ultimate point, the tensile ultimate point remains as Point b. The tensile response follows the path ‘permanent point --> tensile unloading point --> tensile ultimate point’ in accordance with the tensile response rule 1(b). Note that the tensile ultimate point and tensile unloading point at this stage are different. As in updating of scenario 2, the compressive LSC is modified as the permanent deformation point shifted from Point d to Point g. No update is needed for the ultimate compressive strength

and the post-ultimate strength stiffness, but the ultimate strain. Overall, the compressive LSC is updated as g-h-i. The tensile LSC is updated as g-c-b-a.

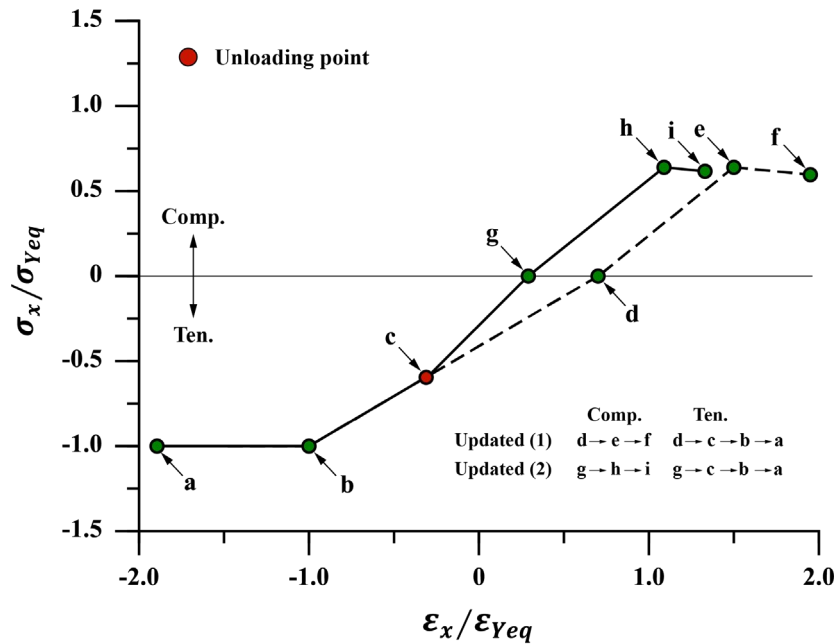


Figure 4-12 Schematic illustration of scenario 3

Scenario 4: initial in tension and unloading from tension

In Figure 4-13, an illustration is given for a typical scenario where the load-shortening response is started in tension. Similar to Figure 4-11, the unloading occurs Point b in the post-ultimate strength regime of tension. The updating procedure is nearly identical with the illustration in Figure 4-11, except that the compressive LSC follows the initial input which is derived by any established methods as specified by the compressive response rule 2(a) since no compressive unloading has previously taken place. Note that the modification of compressive LSC to accommodate the shift of permanent deformation point still applies. Overall, the compressive LSC is updated as g-h-i and the tensile LSC is updated as a-b-g.

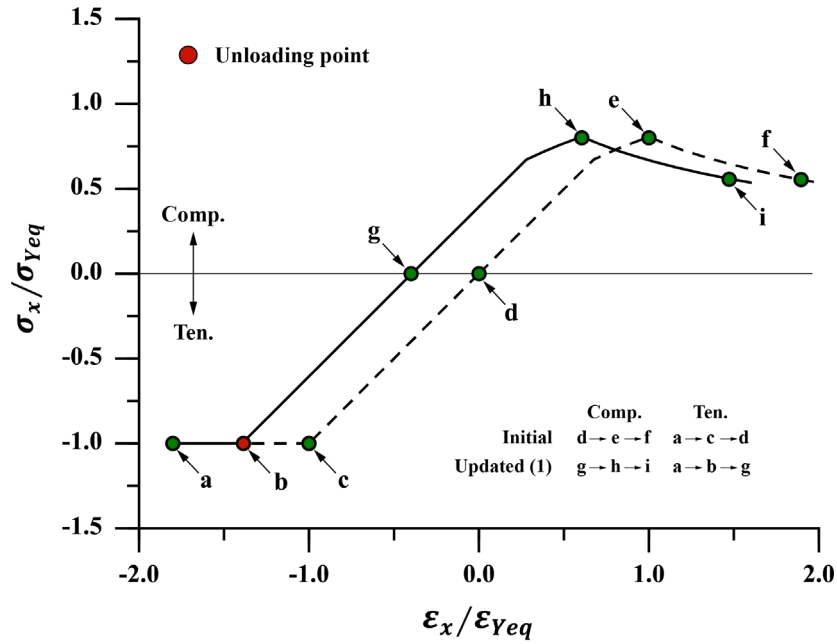


Figure 4-13 Schematic illustration of scenario 4

Scenario 5: follow-up of scenario 4 and unloading from compression

Figure 4-14 follows the scenario shown in Figure 4-13, in which the unloading occurs at Point f in the post-ultimate strength regime of compression. The update of compressive LSC critical points follows the same procedure in Figure 4-10, whereas the update of tensile LSC follows the updating rule 8 where a reduction factor φ_2 is applied to cover the effects of amplified residual stress and distortion. The tensile unloading point is therefore updated from Point c to Point h and the tensile ultimate point is updated from Point c to Point b. Overall, the compressive LSC is updated as i-f-j and the tensile LSC is updated as i-h-b-a.

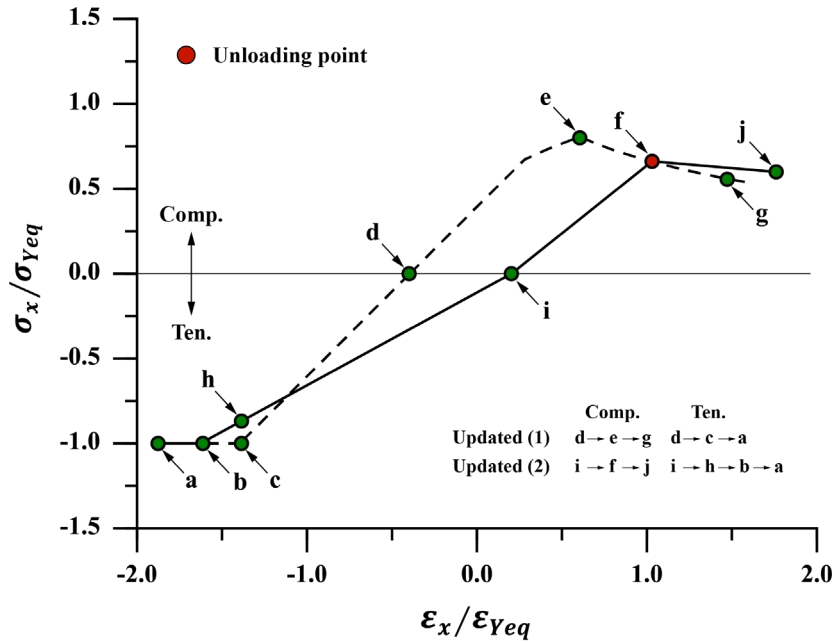


Figure 4-14 Schematic illustration of scenario 5

4.7 Validation

To examine the accuracy of the proposed analytical method, two validations are performed, firstly on all unstiffened plates tested in the systematic analysis of Chapter 3 (Table 3-1) and secondly a selection of stiffened panels typical of ship structures.

Following the systematic study, the validation on unstiffened plating is divided into single-cycle and multi-cycle predictions (Table 3-3), in which the definition of a single-cycle is consistent to that in Chapter 3. The initial compressive LSC input for the proposed method are given by NLFEM (single-cycle only) and IACS-CSR (single-cycle and multi-cycle). The full cyclic LSC for validation is given by dynamic implicit NLFEM. In either case, the NLFEM analyses consider the cyclic plasticity using Chaboche model. The reduction factors φ_1 of 0.3 and φ_2 of 0.98 are taken for the proposed method as provisional values.

4.7.1 Plates – Single Cycle

A selection of single-cycle LSC comparison is shown from Figure 4-15 to Figure 4-18 for the unstiffened plating ($\beta = 2.0$) with different aspect ratios and loading protocols. Since the initial compressive LSCs are derived by NLFEM which therefore leads to identical initial paths, highlights are given in the LSC plots for the subsequent response after the load reversals, i.e. initial LSC in grey and subsequent response in colour. Most of the validation results show a reasonable agreement in terms of the unloading and reloading responses. Although the NLFEM predicted curve exhibits some nonlinearities in the unloading and reloading path whereas the analytical curves are all assumed as piece-wise linear, they should be sufficient for further incorporating into the progressive collapse method to predict the bending response of a box girder since the maximum compressive strength and post-ultimate strength stiffness predictions, which are the most critical features, are well correlated.

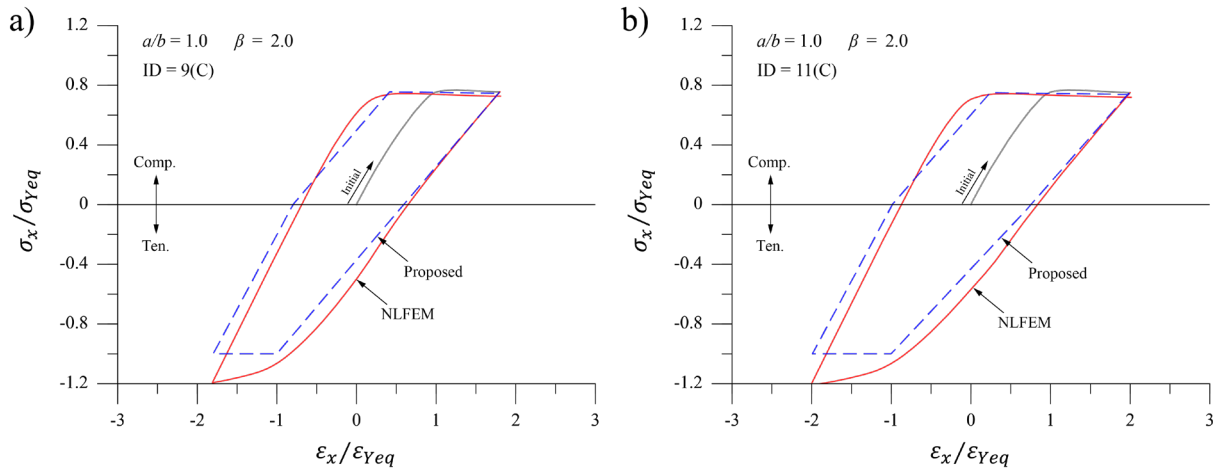


Figure 4-15 Single-cycle LSC validation ($a/b = 1.0$; $\beta = 2.0$; IDs = 9C & 11C)

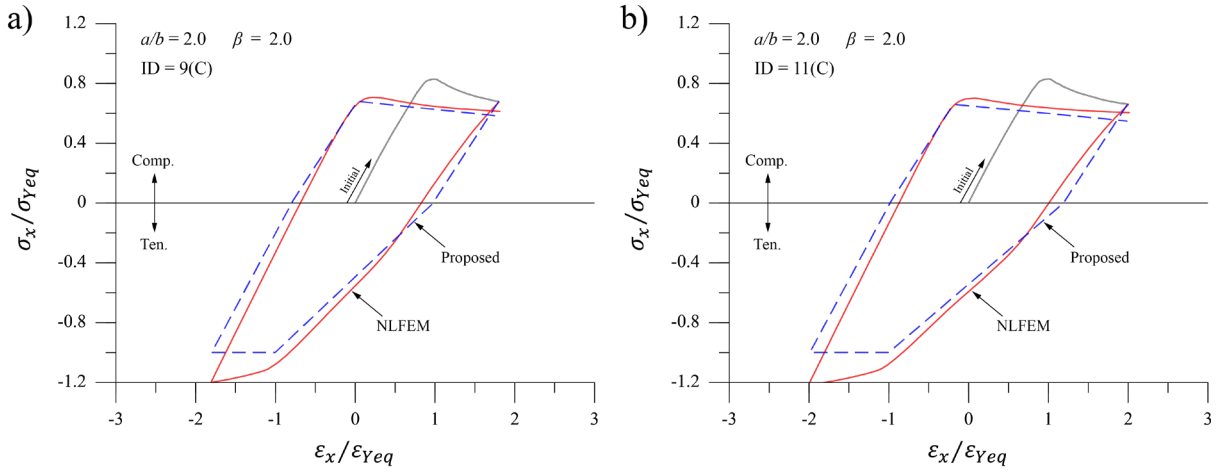


Figure 4-16 Single-cycle LSC validation ($a/b = 2.0$; $\beta = 2.0$; IDs = 9C & 11C)

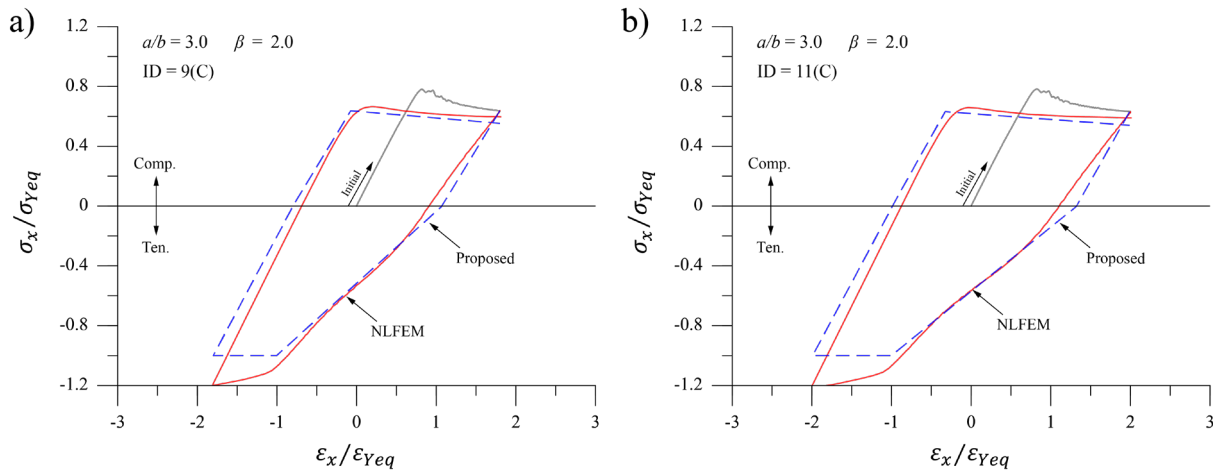


Figure 4-17 Single-cycle LSC validation ($a/b = 3.0$; $\beta = 2.0$; IDs = 9C & 11C)

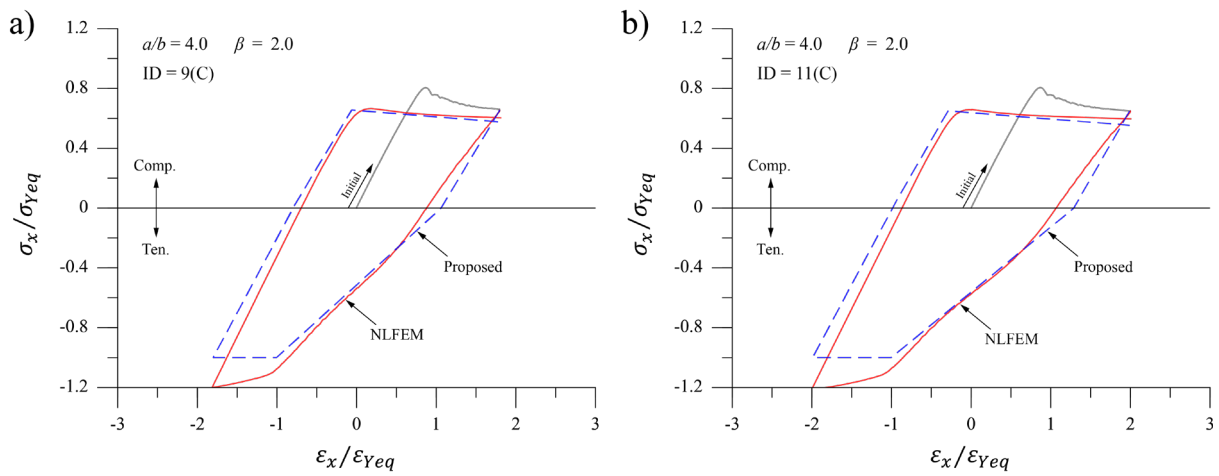


Figure 4-18 Single-cycle LSC validation ($a/b = 4.0$; $\beta = 2.0$; IDs = 9C & 11C)

4.7.2 Plates – Multi Cycle

Regarding to the validation on unstiffened plates under multi-cycle loading, a comparison of the typical LSC behaviour is shown in Figure 4-19. As revealed in Chapter 3, the typical characteristics of multi-cycle LSC includes the compressive strength convergence where the reduction of compressive strength levels-off to a certain value accompanied by the post-collapse stiffness approaching to zero, and the linearly reducing tensile strength where a reduction of tensile strength is seen during each cycle. Through the use of reduction factor φ_1 for post-ultimate strength stiffness in compression and φ_2 applied to the tensile critical points, these features have been captured in the prediction by the proposed methodology. Meanwhile, it is also observed that the prediction of in-plane stiffness may be subject to further development. As seen from the NLFEM results, after several cycles of loading, the compressive in-plane stiffness in both unloading and reloading regimes and the tensile unloading stiffness keeps reducing. However, these are assumed as fixed values regardless of the number of cycles. It is a reasonable assumption when the load cycle numbers are small, but the consideration of their reduction may be needed for more loading cycles.

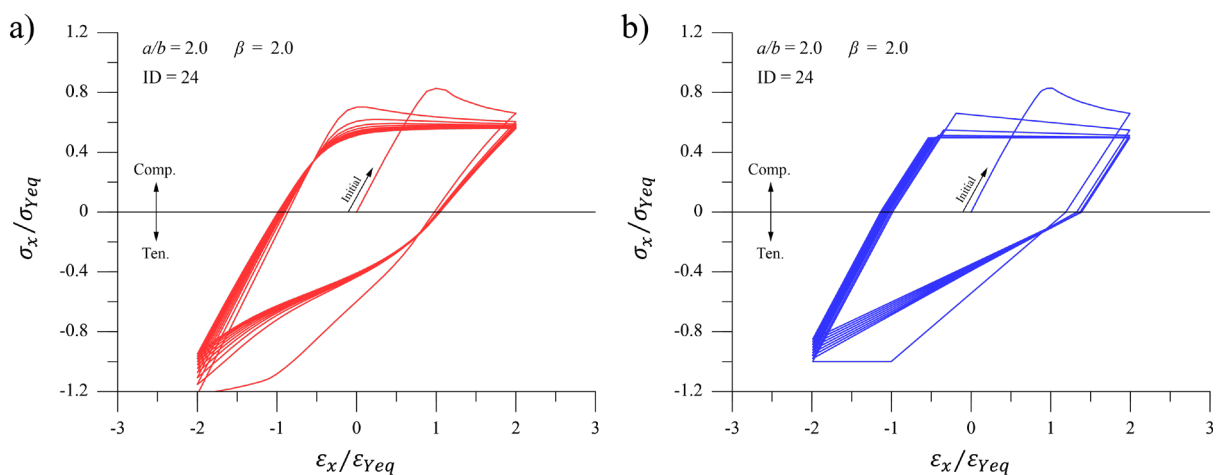


Figure 4-19 Multi-cycle LSC of unstiffened plates

In terms of the correlation of the predicted compressive strength, Figure 4-20 shows the probability of prediction ratio between the NLFEM and the proposed method for the compressive strength in the final cycle. In each plot, 132 cases are included. Both FEM-based and CSR-based prediction have a highly correlated mean value with the NLFEM, i.e. 1.0325 and 0.9924 respectively. Nevertheless, the variance of the CSR-based prediction is higher the FEM-based prediction where the former COV is 0.1462 and the latter COV is 0.0769.

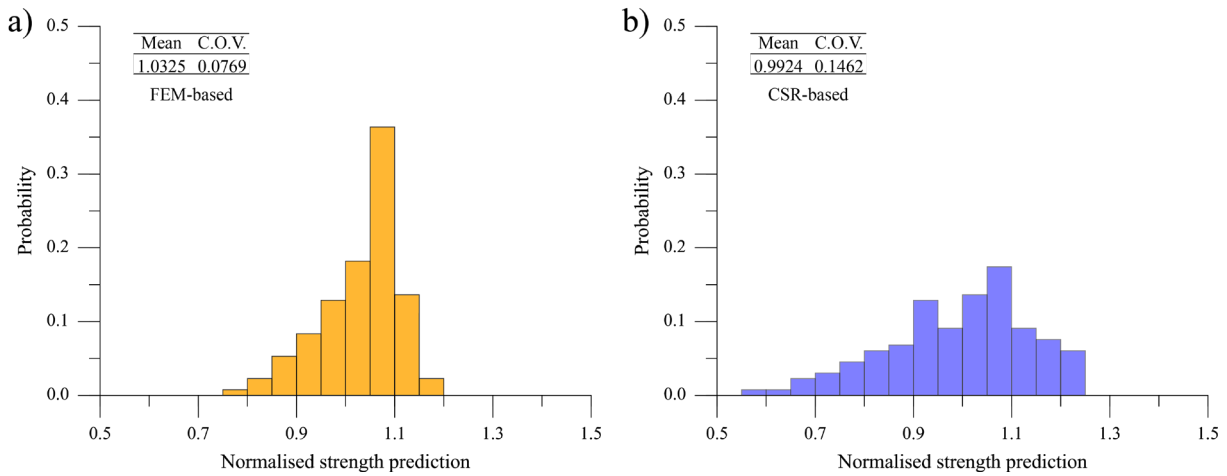


Figure 4-20 Statistical evaluation of the prediction of final compressive strength under multi-cycle loading between NLFEM and the proposed methodology

4.7.3 Stiffened Panel

To extend the application of the proposed method, four stiffened panels are chosen for a further validation. These stiffened panels are the benchmark cases adopted by Smith et al. (2008). The properties of these stiffened panels are listed in Table 4-1 and Table 4-2. A summary of the applied loading protocol is given in Table 4-3. In this section, the initial compressive response is predicted by the finite element method considering the combined hardening model. The finite element model with a characteristic mesh size of 25mm × 25mm is shown in Figure 4-21 with boundary conditions and loading application. Asymmetric ARE mode for local plate, column-type and stiffener sideway imperfections are considered.

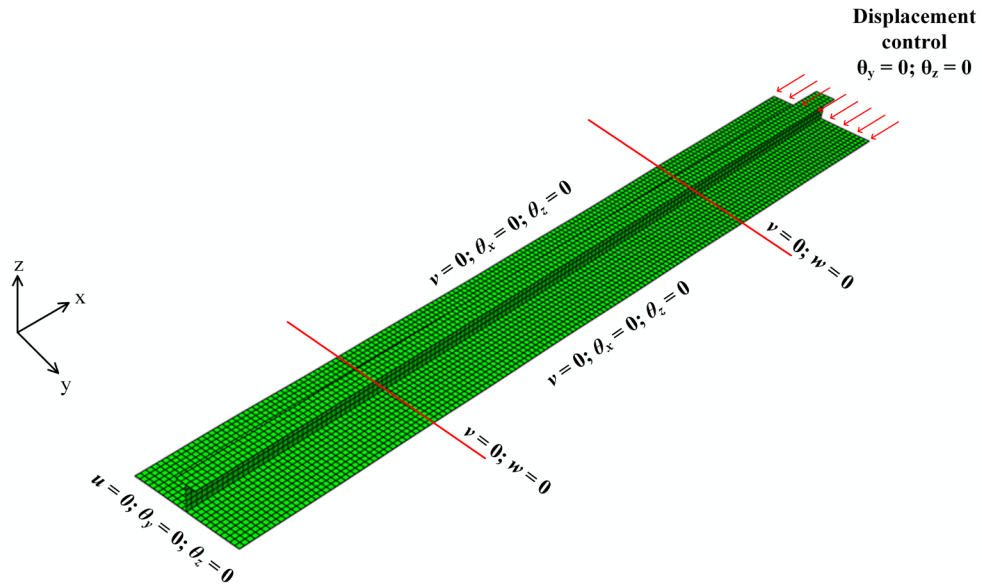

Figure 4-21 Stiffened panel model for NLFEM analysis

Table 4-1 Dimension and material property of the stiffened panels

| ID | a | b_p | t_p | Beam section | σ_{Yp} | σ_{Ys} |
|----|------|-------|-------|--|---------------|---------------|
| | | | | $h_w \times b_f \times t_w \times t_f$ | | |
| A | 1000 | 350 | 9 | 200×140×6.4×8.8 T | 350 | 350 |
| B | 2000 | 350 | 9 | 200×140×6.4×8.8 T | 350 | 350 |
| C | 2000 | 550 | 9 | 128×102×6.1×8.4 T | 350 | 350 |
| D | 1000 | 450 | 9 | 128×102×6.1×8.4 T | 350 | 350 |

Table 4-2 Dimensionless parameters of the stiffened panels

| ID | λ | β |
|----|-----------|---------|
| A | 0.1472 | 1.6037 |
| B | 0.2944 | 1.6037 |
| C | 0.5268 | 2.5202 |
| D | 0.2502 | 2.0620 |

Table 4-3 Loading protocols of stiffened panels

| Case No. | Load cycle | Applied strain range |
|----------|--------------|--|
| 1 | Single-cycle | $-1.5\varepsilon_{Yeq} < \varepsilon_x < 2.0\varepsilon_{Yeq}$ |
| 2 | Multi-cycle | $-1.0\varepsilon_{Yeq} < \varepsilon_x < 1.5\varepsilon_{Yeq}$ |

Figure 4-22 compares the single-cycle load shortening curves of stiffened panels. A reasonable agreement is presented in terms of the unloading and reloading paths of all four panels. However, the reloading compressive strength of Panel C is notably underestimated by the proposed method compared to the NLFEM. This may be due to the fact that Panel C, with a column slenderness ratio over 0.5, is much more slender than the other tested panels. Its reloading strength appears to be less correlated with the unloading stress.

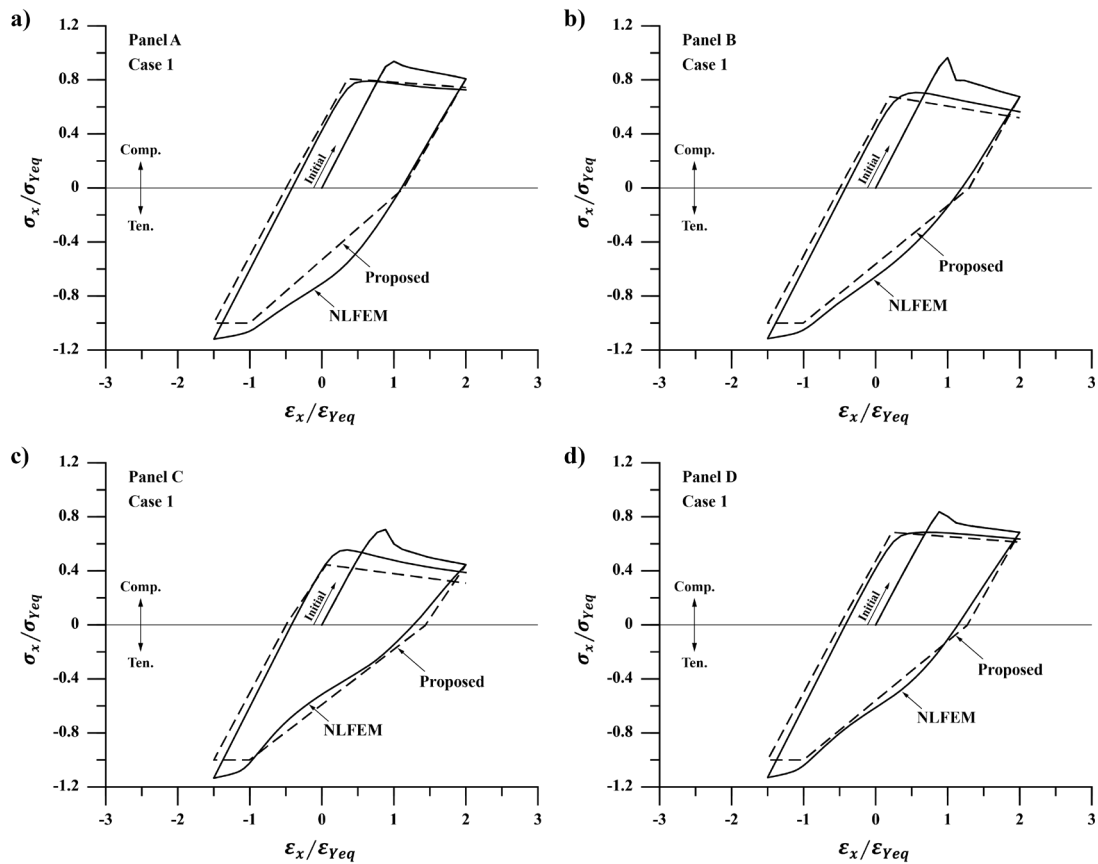


Figure 4-22 Comparison of single-cycle LSCs of stiffened panels

Figure 4-23 and Figure 4-24 show the multi-cycle load-shortening curves of stiffened panels predicted by NLFEM and the proposed methodology respectively. The variations of compressive strength during the multi-cycle loading are shown from Figure 4-25 to Figure 4-28 for the four panels. Similar to the unstiffened plate, whilst a complete convergence is not observed within the applied loading

cycles, the compressive strength of the stiffened panel tends to converge to a constant value after three loading cycles. The compressive strength of Panel B & D are well predicted by the analytical method. However, the predicted converged strength of Panel A is overestimated and the predicted converged strength of Panel C is underestimated. As shown in Figure 4-22, the proposed method gives a well validated result under single-cycle. However, the NLFEM result of Panel A illustrates that the compressive strength still exhibits an evident reduction even after three loading cycles. This might lead to an overestimation using the analytical method for multi-cycle prediction. Conversely, the NLFEM result of Panel C indicates that the compressive strength starts to converge after two loading cycles. Also, the analytical method prediction already gives a lower compressive reloading strength under single-cycle loading. The combination of these two factors may result in the conservative estimation of Panel C.

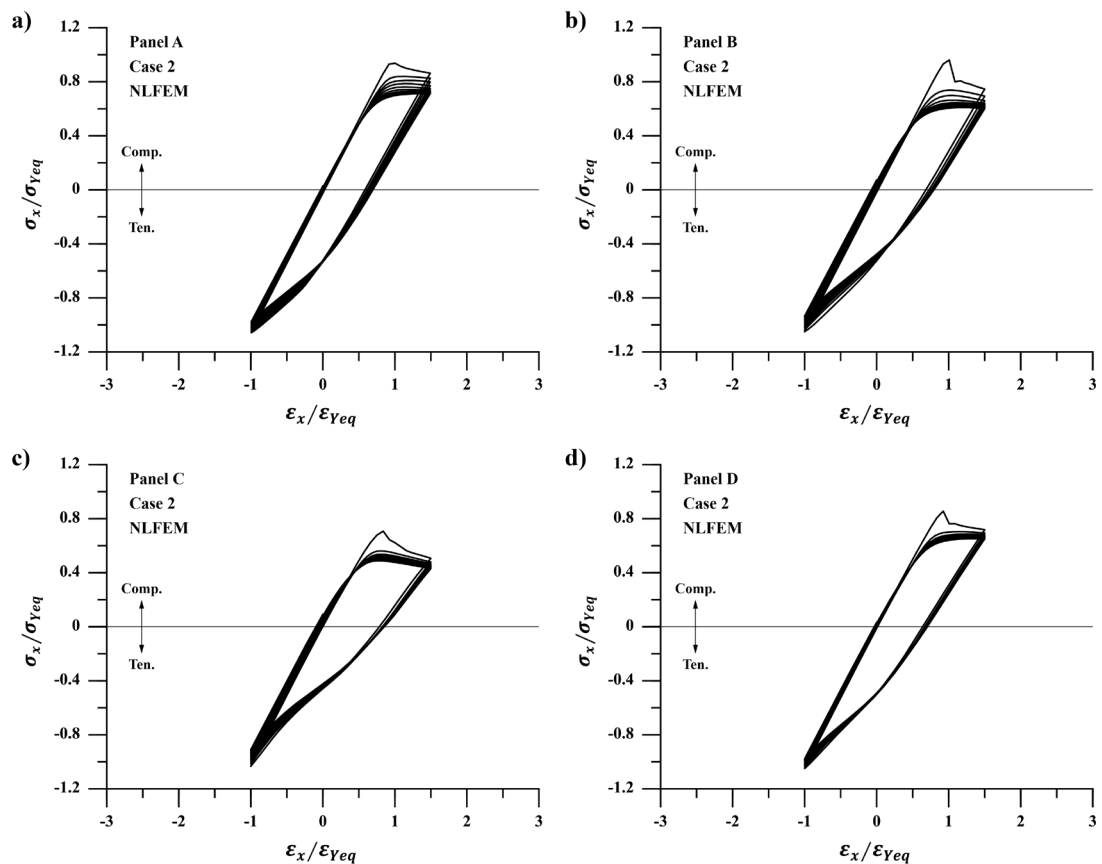


Figure 4-23 Multi-cycle load-shortening curves of stiffened panels (NLFEM)

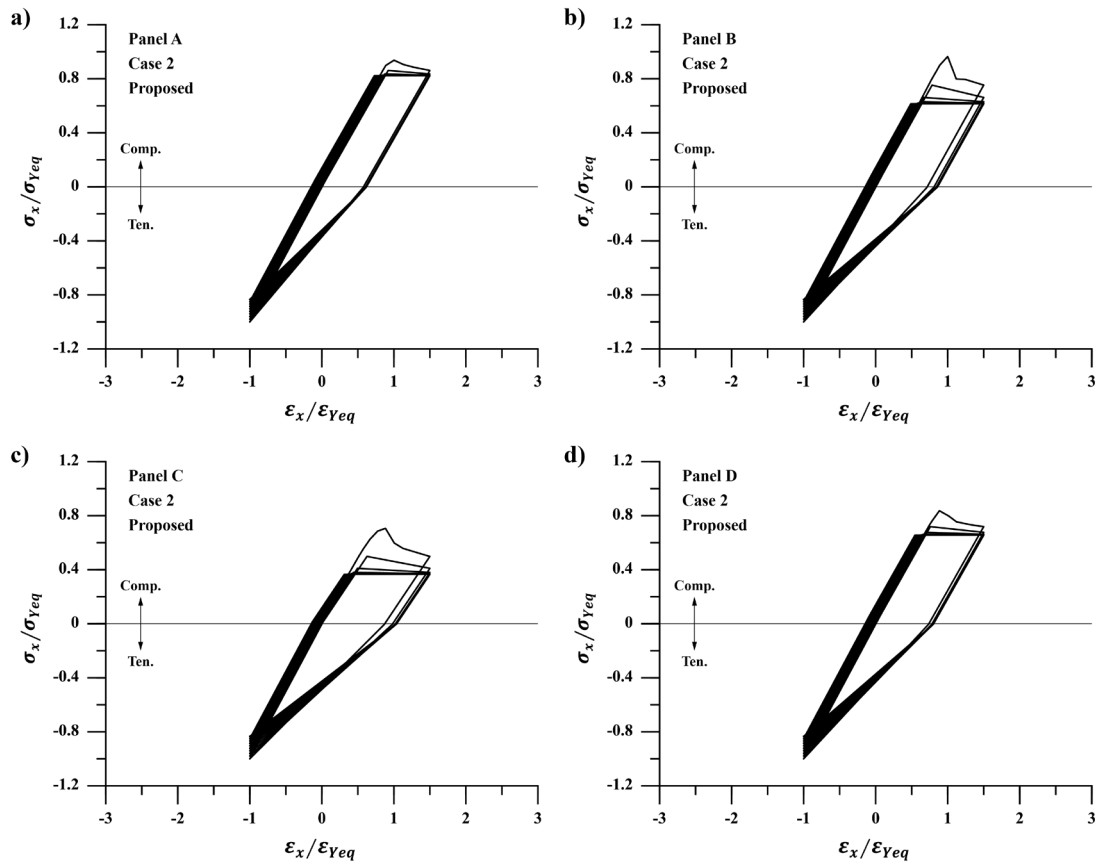


Figure 4-24 Multi-cycle load-shortening curves of stiffened panels (Proposed)

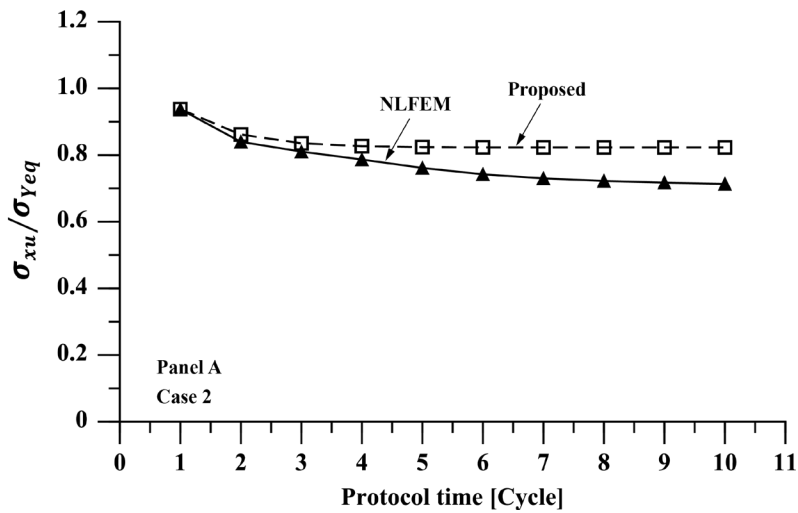


Figure 4-25 Variation of the maximum compressive strength of Panel A

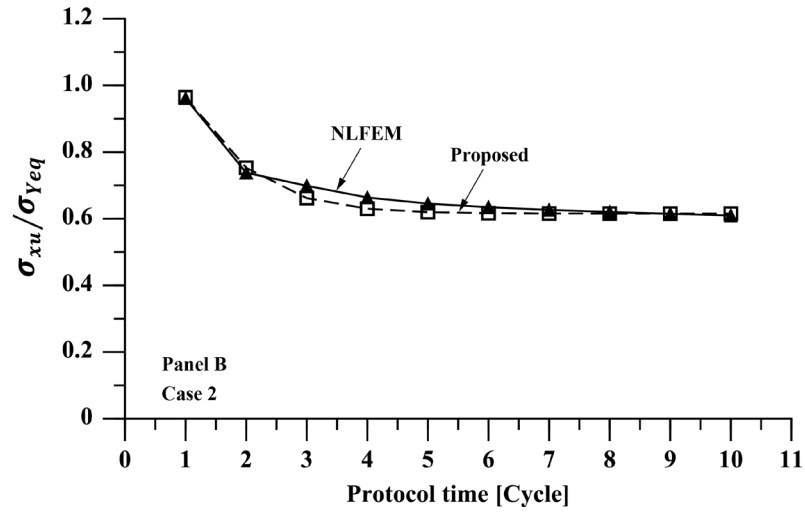


Figure 4-26 Variation of the maximum compressive strength of Panel B

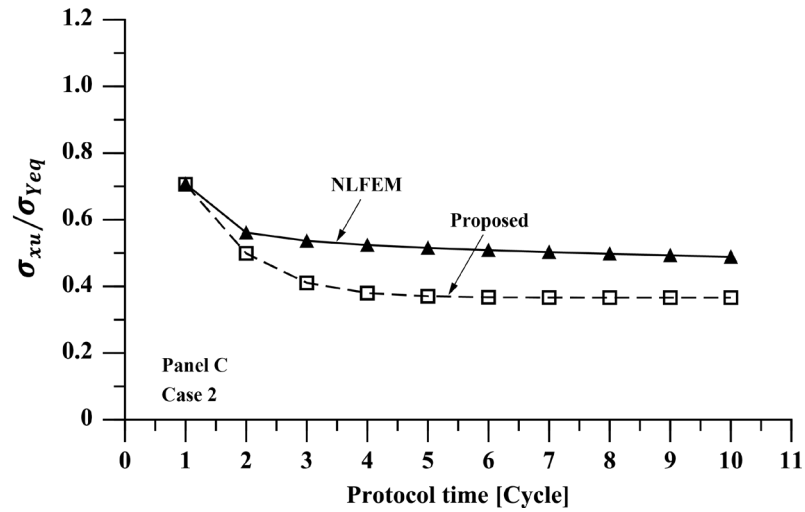


Figure 4-27 Variation of the maximum compressive strength of Panel C

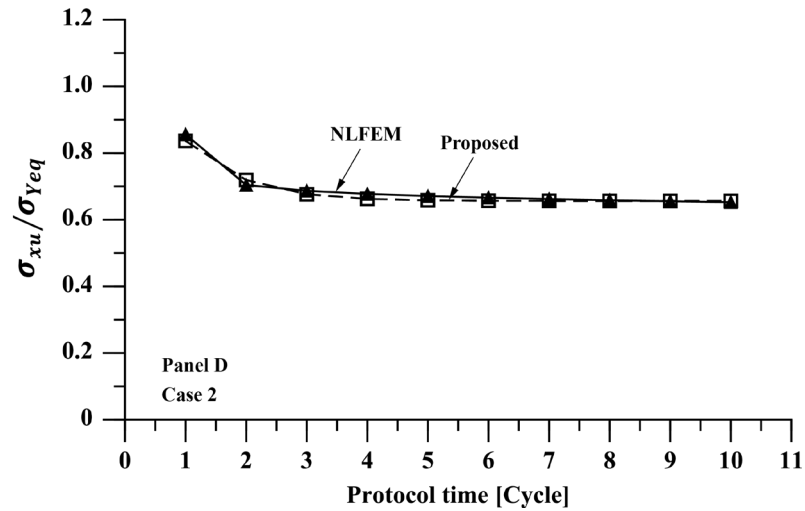


Figure 4-28 Variation of the maximum compressive strength of Panel D

4.8 Discussions on Further Enhancement

The capability of the proposed analytical method to predict the load-shortening curve of structural components is demonstrated through validation. In general, a reasonable agreement can be obtained in terms of the maximum compressive strength and its variation. Whilst the tensile strength is less correlated, its variation with respect to the loading cycle is well predicted. Therefore, it can be concluded that the proposed response rule and updating rule are valid for generating LSC with sufficient accuracy. In the meantime, the validation also suggests that the results are highly sensitive to the input of the initial load-shortening curve, which is also associated to the post-ultimate stiffness reduction factor and the tensile strength reduction factor. The use of these two coefficients is intended to simulate the variation of compressive post-collapse stiffness as well as the reduction of compressive and tensile strength during loading cycle. However, these are specified in the present study regardless of the initial load-shortening curve and different unloading strain. Further research can be directed to calibrate these coefficients, which could lead to an enhanced strength prediction under cyclic load. Another further improvement could relate to the in-plane compressive stiffness prediction under cyclic load. The proposed analytical method only addresses this issue for single-cycle loading. The in-plane compressive stiffness will be decreased at each loading cycle and the response and updating methodology only considers the reduction at the first compressive unloading. Further study can be conducted to account for the reduction caused by multi-cycle loading.

4.9 Chapter Summary

In this chapter, a method to predict the load-shortening behaviour of structural members of ship structures is proposed. It is developed as a combination of response rule and updating rule, which are derived by the observation of characteristic response patterns from a systematic NLFEM. In essence, they are

a set of behaviour rules with a prescribed initial response to predict the unloading and reloading behaviours following a load reversal event.

Validations are completed on plates and stiffened panels, showing a reasonable agreement with equivalent NLFEM analysis on the prediction of the load-shortening curves and the ultimate strength variation. From this point of view, the proposed methodology is appropriate for implementing in a Smith-type progressive collapse method to predict the progressive collapse response of hull girders under cyclic bending. Several further improvements may require in future works, such as the calibration of reduction factors and the reduction of in-plane compressive stiffness in multi-cycle loading.

Chapter 5 Extended Smith Method for Predicting the Progressive Collapse of Hull Girders Under Cyclic Bending

5.1 Rationale

The primary objective in this chapter is to propose and validate an extended Smith method with a capability to predict the progressive collapse of ship-type thin-walled box girders under cyclic longitudinal bending. The rationale of this development may be summarised as follows:

- 1) The current ship structural design principle aims to ensure that the maximum load-carrying capacity is not exceeded by the extreme load, in which case the monotonic ultimate limit state assessment is sufficient. However, the uncertainty in both strength (e.g. age-related degradation) and load predictions (e.g. unexpected extreme events) still leads to ship hull girder collapse accidents from time to time. In these cases, a ship hull girder is probably to be exposed to a series of extreme cyclic loads which has surpassed the nominal ultimate strength.
- 2) To simulate the complex collapse behaviour of ship hull girder in waves, it requires a coupling between the structural response method and load prediction approach. For the former, NLFEM is the only option at the moment. However, its inefficiency will impose significant challenges in the coupling with the load prediction method;
- 3) The Smith-type progressive collapse method is a well established approach codified in contemporary structural rules governing the ultimate limit state assessment of a ship hull girder. However, its capability is limited to the prediction of the response under monotonic load. An extension to the analysis procedure should be proposed to incorporate cyclic loading;

- 4) An extension to Smith method may be essential for incorporated with dynamic analysis procedure to take into account of the fluid-structure interaction so that the collapse behaviour in a given sea state could be simulated.

5.2 Methodology

The extended Smith method continues to follow the same major assumptions and general procedure, but re-formulates the load-shortening curve (LSC) to account for the accumulated degradation during cycles of extreme load. The overall methodology can be described with reference to Figure 5-1, in which the extension to the original Smith method is highlighted. The re-formulation of the LSC is driven by a loading protocol which allows the direction of each curvature increment to be controlled. When the direction of curvature increment is reversed, the re-formulation algorithm will be activated. This updated LSC will be utilised for the subsequent Smith method calculations until the next curvature increment reversal. As detailed in Chapter 4, the re-formulation algorithm is formed of a response rule and updating rule. Whilst the assumption of the method is given in Chapter 2 and the incremental formulation is given by Equation (5-1), the extended analysis procedure for the solution may be summarised as follows:

- Step 1:** The ship hull cross section is sub-divided into structural elements;
- Step 2:** A loading protocol is defined for the hull girder in terms of the curvature;
- Step 3:** A load-shortening curve (LSC) characterising the response under monotonic in-plane load is assigned to each element;
- Step 4:** Evaluate the tangent stiffness k_i of each element at present strain using the load-shortening curve;
- Step 5:** Calculate the position of instantaneous neutral axis (y_G, z_G) using Equation (5-2) to (5-3);

- Step 6:** Evaluate the bending stiffness of the cross section with respect to the instantaneous neutral axis Equation (5-4) to (5-6);
- Step 7:** Check for the reversal of curvature increment;
- Step 8a:** If no reversal takes place: Apply the curvature increment about the instantaneous neutral axis and proceed to step 9;
- Step 8b:** If reversal takes place: Return to step 3 to carry out a re-formation applying the response rule and updating and to re-assign the LSC;
- Step 9:** Calculate the strain increment of each element (5-7);
- Step 10:** Calculate the bending moment increment using Equation (5-8);
- Step 11:** Obtain the cumulative bending moment and curvature;
- Step 12:** Return to step 4.

$$\begin{Bmatrix} \Delta M_H \\ \Delta M_V \end{Bmatrix} = \begin{bmatrix} D_{HH} & D_{HV} \\ D_{VH} & D_{VV} \end{bmatrix} \begin{Bmatrix} \Delta \chi_H \\ \Delta \chi_V \end{Bmatrix} \quad (5-1)$$

$$y_G = (\sum_{i=1}^n y_i k_i A_i) / (\sum_{i=1}^n k_i A_i) \quad (5-2)$$

$$z_G = (\sum_{i=1}^n z_i k_i A_i) / (\sum_{i=1}^n k_i A_i) \quad (5-3)$$

$$D_{HV} = D_{VH} = \sum_{i=1}^n k_i A_i (y_i - y_G)(z_i - z_G) \quad (5-4)$$

$$D_{HH} = \sum_{i=1}^n k_i A_i (y_i - y_G)^2 \quad (5-5)$$

$$D_{VV} = \sum_{i=1}^n k_i A_i (z_i - z_G)^2 \quad (5-6)$$

$$\Delta \varepsilon_i = (y_i - y_G) \Delta \chi_H + (z_i - z_G) \Delta \chi_V \quad (5-7)$$

where

i denotes the number of the elements

A_i = Cross sectional area of the element i

y_i, z_i = Horizontal and vertical coordinate of the element i

y_G, z_G = Horizontal and vertical coordinate of the neutral axis

The subdivision of a ship hull cross section is illustrated in Figure 5-2. Since the ship structure is essentially a network of plates and stiffened panels, there are generally two ways to subdivide the cross section (Figure 5-3). Conventionally, a plate-stiffener combination is employed where the stiffener and its attached plate are taken as one element, for example as recommended by IACS-CSR. Alternatively, the local plating between the longitudinal stiffeners or individual stiffener can be considered as one element, which is called the plate-stiffener separation subdivision. All these elements take into account the elastoplastic buckling effect under compression, whilst the tensile response is usually assumed as the material stress/strain behaviour. In this thesis, the plate-stiffener combination subdivision technique is adopted. Apart from these stiffened panel elements, there are certain areas in the cross section, occurring at deck edges and at intersections of deck and shell panels with superstructure sides, longitudinal bulkheads and deep girders, that will resist buckling and effectively follow the material stress/strain curve up to and beyond collapse. These areas are termed “hard corner” elements. In this thesis, the subdivision of stiffened panel element is completed first. For those near the panel intersections, a hard corner element is assigned. This extent, for the case study model shown later, is equivalent to the CSR recommendation.

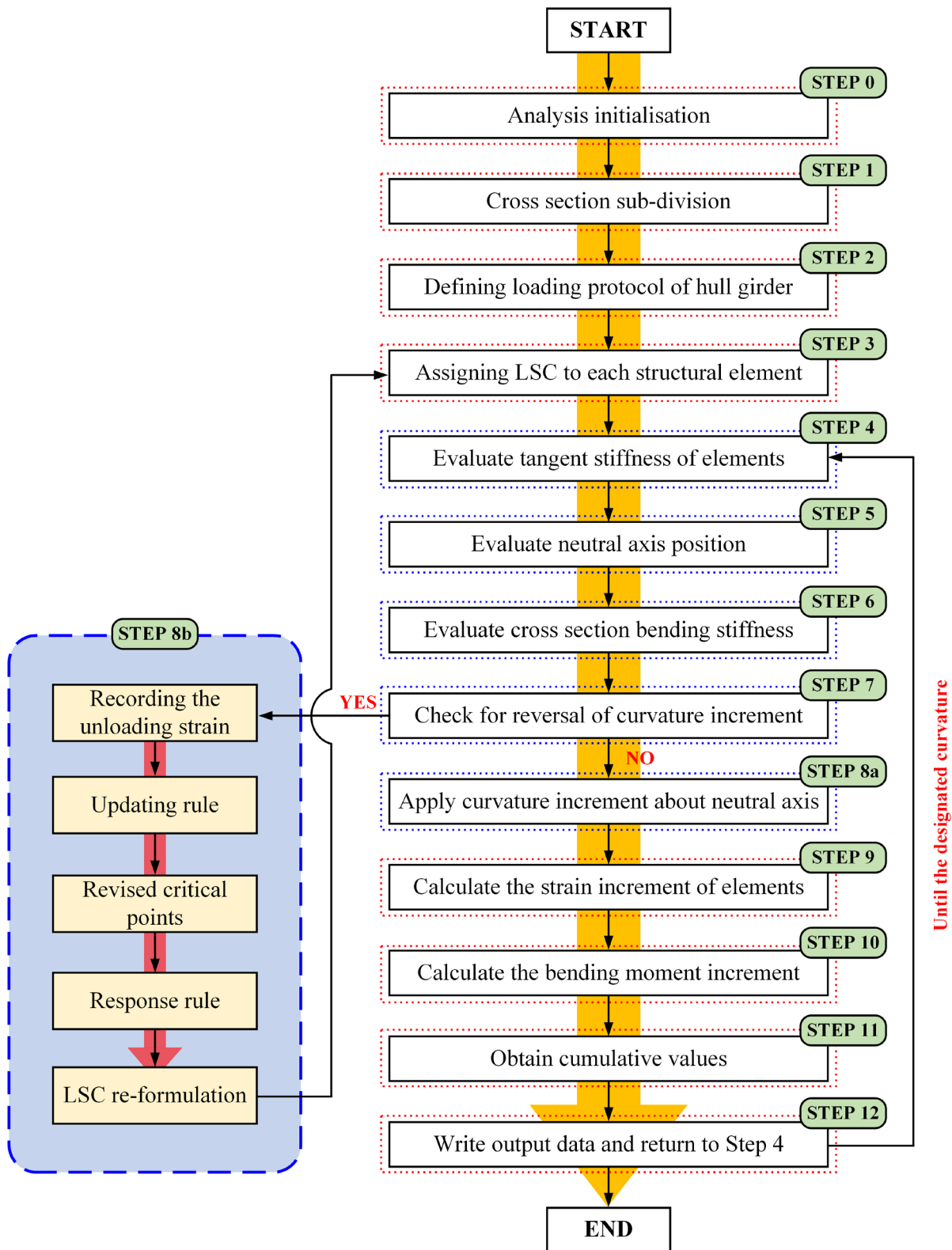


Figure 5-1 Flowchart of the proposed extended Smith method

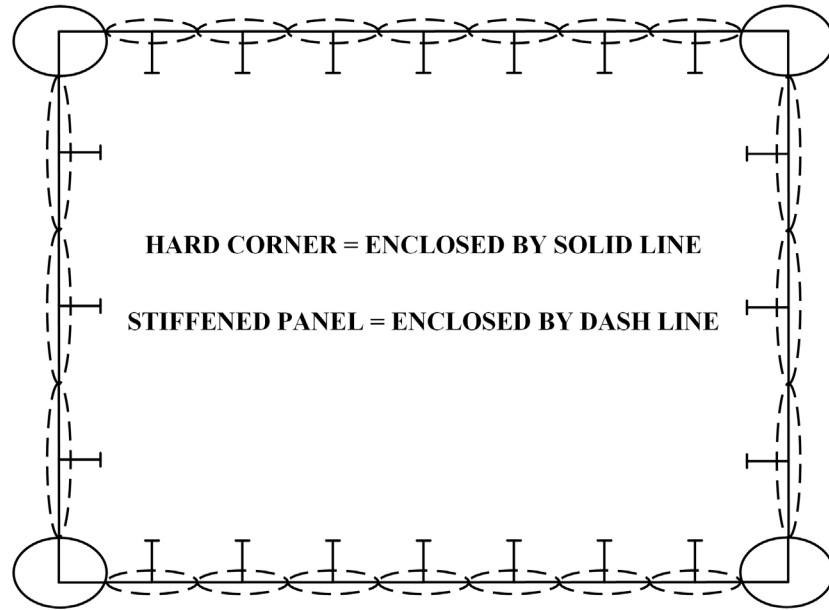


Figure 5-2 Illustration element subdivision in the Smith method

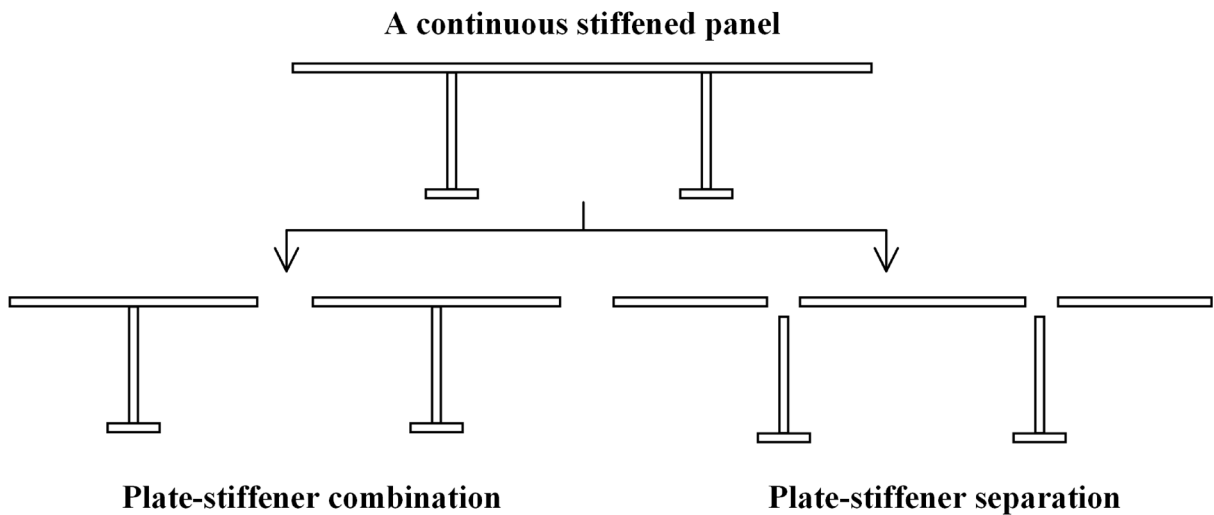


Figure 5-3 Sub-division techniques of stiffened panels

Once the sub-division of the cross section is completed, an average stress-average strain relationship (load-shortening curve) is assigned to each of these elements. This relationship characterises the structural response of an element under in-plane compression/tension, which is the primary loading arising from the global longitudinal bending of hull girder. The effect of secondary loadings, such as lateral pressure and shear force, may be incorporated by the application of knock-

down factors (Syrigou, 2017). The load-shortening curves of each structural elements are usually numerically represented in advance, and are taken as input data for the Smith-type progressive collapse analysis.

5.3 Validation

To validate the extended Smith method, a comparison on prediction of cyclic bending moment versus curvature curves with previously published experimental data and numerical simulations is conducted.

The progressive collapse method is derived by either curvature or bending moment incrementation. However, the load must be defined in terms of curvature if the cycle extends beyond the ultimate strength (Dow, 1997). In this validation a simple cyclic loading protocol with the same magnitude in both initial and reversed directions is applied for all numerical simulations (e.g. Figure 5-4). The protocol is chosen to demonstrate the validity of the proposed method, causing an unusually extreme load which surpasses the monotonic ultimate strength of the case-study girders. The purpose of this loading protocol is to represent a complex series of extreme load events in an efficient way for numerical simulations.

As the loading protocol induces unusually large bending moments on the case study box girders that exceed the nominal ultimate strength, these represent more severe scenarios than would be predicted by design guidelines such as the CSR. The insights developed in this validation associated with the implications for ship structures should be taken within the scope of this choice of load protocol. The implications and extension of these findings to normal operational loading conditions requires further research, as summarised in Section 5.3.5.

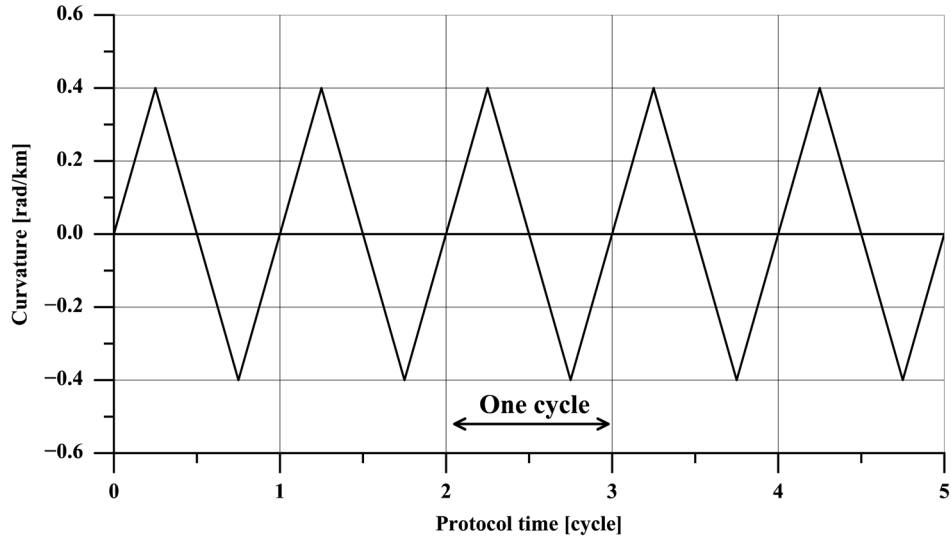


Figure 5-4 Cyclic loading protocol of ship hull girders

5.3.1 Model Characteristics

- **Experimental Model**

The experimental test result reported by Cui and Yang (2018) is utilised for the experimental validation. The experiment was performed on a small-scaled single-skin box girder model under alternating sagging and hogging. The tested specimen is 497.9 mm long with a plating thickness of 2.76 mm. Flat-bar stiffeners with a web height of 50mm and thickness of 3.78mm are employed. The cross section of the experimental model is shown in Figure 5-5 with scantlings and material properties listed in Table 5-5.

Table 5-1 Dimension and material property of the experimental model

| | | | | |
|----------|-----------|------------|------------------|------------|
| Geometry | a [mm] | t_p [mm] | h_w [mm] | t_w [mm] |
| | 497.8 | 2.76 | 50.0 | 3.78 |
| Material | E [MPa] | E' [MPa] | σ_Y [MPa] | ν |
| | 210300 | 5123 | 273.3 | 0.3 |

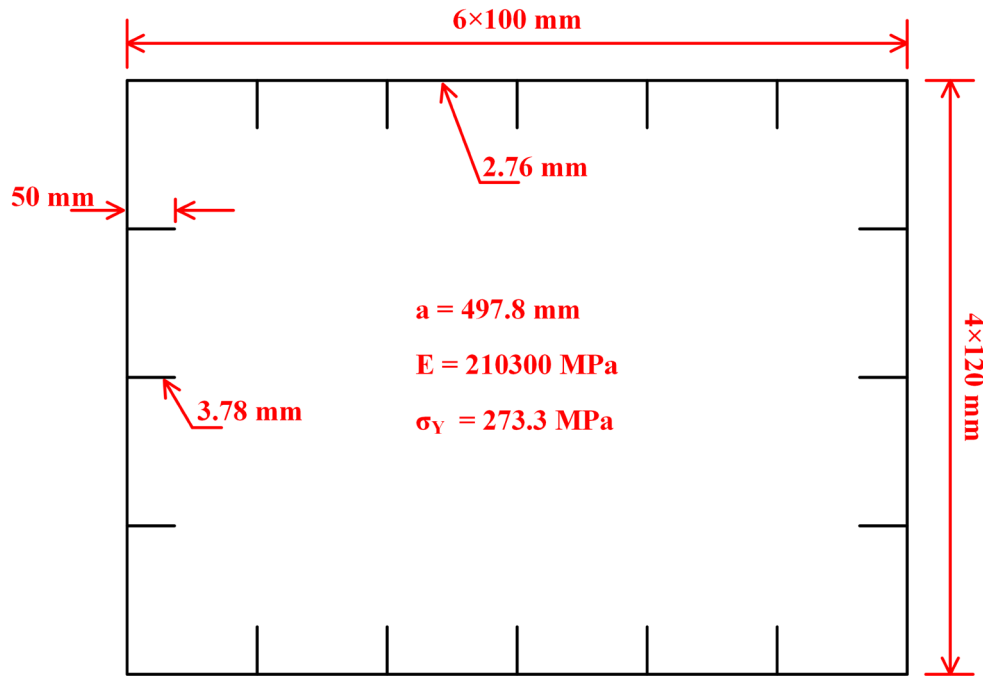


Figure 5-5 Cross section of the experimental model

- **Numerical Model**

Four box girder models are adopted for the numerical validation. These box girders are simplified representations of conventional midship cross sections for a single hull, double hull, bulk carrier and container ship (Figure 5-6 to Figure 5-9). With these simplified cross sections, the computational demand is considerably reduced while representative ship structural responses can be predicted. Each cross section has a width of 12000 mm and a height of 8000 mm . The thicknesses of the outer and the inner plating are 12 mm and 10 mm respectively. Except for the stiffening of the longitudinal girders in the double bottom where flat-bar stiffeners are utilised, the cross section is longitudinally stiffened by tee-bar stiffeners with the same scantling. In addition, each model is transversely framed at a spacing of 1500 mm . In the deck and the bottom, all four models effectively have the same plate-stiffener combination. The scantlings and material properties of the numerical models are summarised in Table 5-2.

Table 5-2 Dimension and material property of the numerical model

| | | a (mm) | h_w (mm) | t_w (mm) | b_f (mm) | t_f (mm) |
|----------|------------|-----------|------------------|------------|------------|------------|
| Geometry | Tee-bar | 1500 | 150 | 8 | 70 | 15 |
| | Flat-bar | 1500 | 100 | 10 | / | / |
| | Transverse | / | 300 | 16 | 140 | 30 |
| Material | | E [MPa] | σ_Y [MPa] | ν | | |
| | | 207000 | 315 | 0.3 | | |

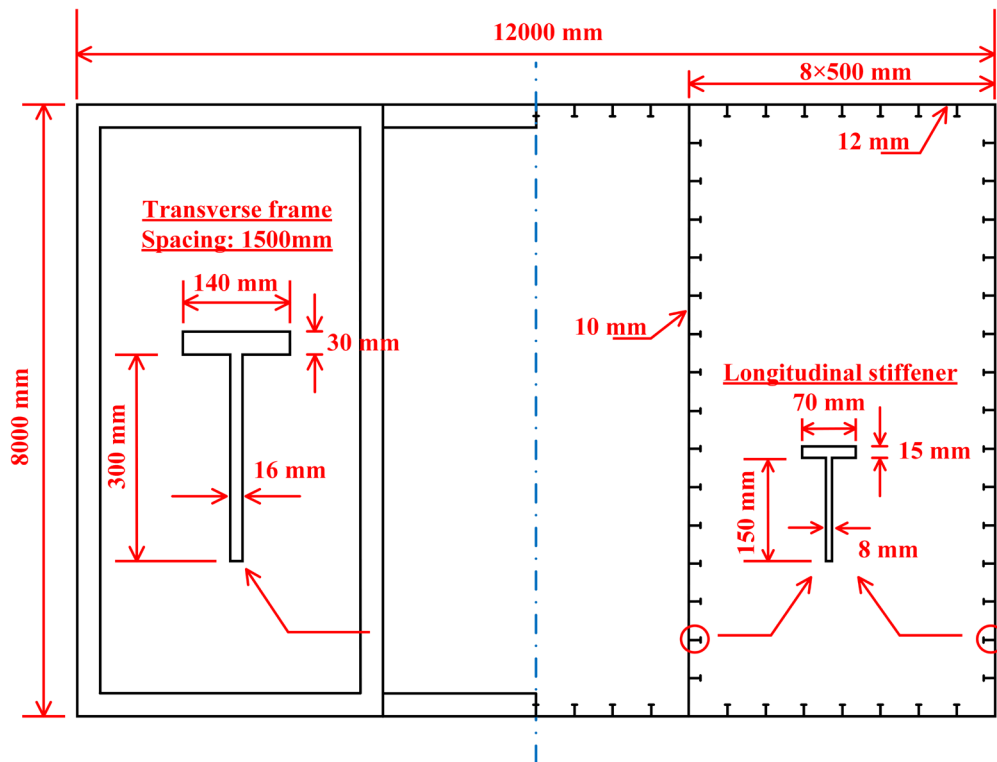


Figure 5-6 Cross section of the single hull model for numerical validation

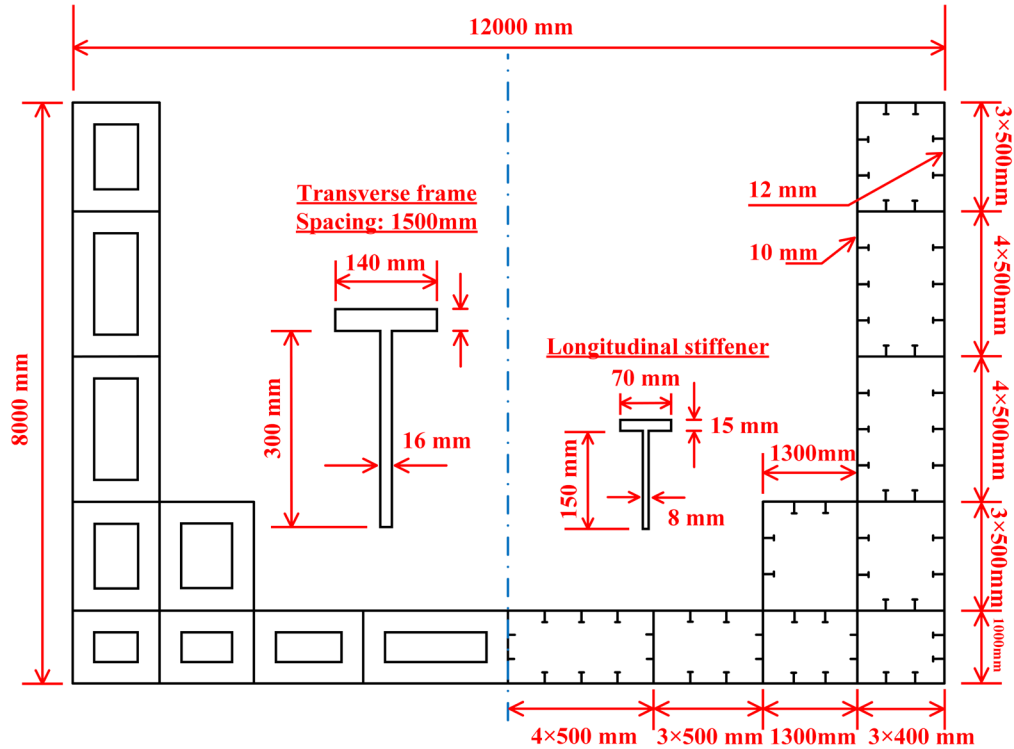


Figure 5-9 Cross section of the container ship model for numerical validation

5.3.2 Comparison of Load-Shortening Responses

- **Premises**

To validate the prediction of structural component load-shortening response under cyclic loading, a comparison of load-shortening curves of the critical stiffened panels of the case study models under cyclic loading is conducted, i.e. deck/bottom panels. As introduced in Section 5.2, the initial compressive load-shortening curve (LSC) of structural elements must be pre-defined as an input of the overall calculation methodology. Three different ways of predicting this initial LSC are used in the following analysis as summarised by Table 5-3. LSC 1 is generated using CSR method and LSC 2 is produced by static-Riks FEA. These two LSCs may be more comparable as both are static analysis-based and assume elastic-perfectly plastic material behaviour. On the other hand, LSC 3 is calculated with the same FEA model of producing LSC 2, but through the dynamic implicit finite element solver with consideration of Chaboche material hardening model. It is

used in two numerical test case (single hull and double hull under loading protocol 1) to elucidate the effect of material hardening.

As the scantling of transverse frame is not available in Cui and Yang (2018), a single bay plate–stiffener combination is utilised for the nonlinear FEA of stiffened panel elements of experimental model. In meshing the stiffened panel models, comparable numbers of shell elements are adopted and the ratio between the element numbers in longitudinal direction and transverse direction keeps as the same as the plating aspect ratio. The single–bay model is discretised with 50 four-node shell elements along its length, ten elements along its breadth and five elements along the height of stiffener’s web, resulting in a $10\text{mm} \times 10\text{mm}$ characteristic element size. On the other hand, a $\frac{1}{2} + \frac{1}{2}$ bay model with transverse frame is used for the stiffened panel elements of numerical models. The $\frac{1}{2} + \frac{1}{2}$ bay model is discretised with 60 four-node shell elements along its length, 20 elements in its breadth and 6 elements along the height of stiffener’s web, resulting in a $25\text{mm} \times 25\text{mm}$ characteristic element size. Boundary conditions of both models are illustrated in Figure 5-10. In the present NLFEM models, the pull-in of the long edges are restrained and the toe of the transverse frames are restricted on their transverse and vertical translations. The former may effectively lead to a biaxial loading condition on the panel due to Poisson’s effect, while the latter implies an infinitely rigid transverse support. These boundary conditions are liable to increase the initial stiffness and ultimate strength of the panels. Meanwhile, these may also induce an uncertainty in the capacity loss during post-collapse regime. However, this boundary condition may be equivalent to the CSR method, which adopts the Frankland formula (based on constrained plate data) for evaluating the effective width.

Table 5-3 Different LSCs used in the numerical validation

| No. | Methodology | Material behaviour |
|-------|----------------------|---------------------------|
| LSC 1 | CSR method | Elastic-perfectly plastic |
| LSC 2 | Static-Riks FEA | Elastic-perfectly plastic |
| LSC 3 | Dynamic implicit FEA | Chaboche hardening |

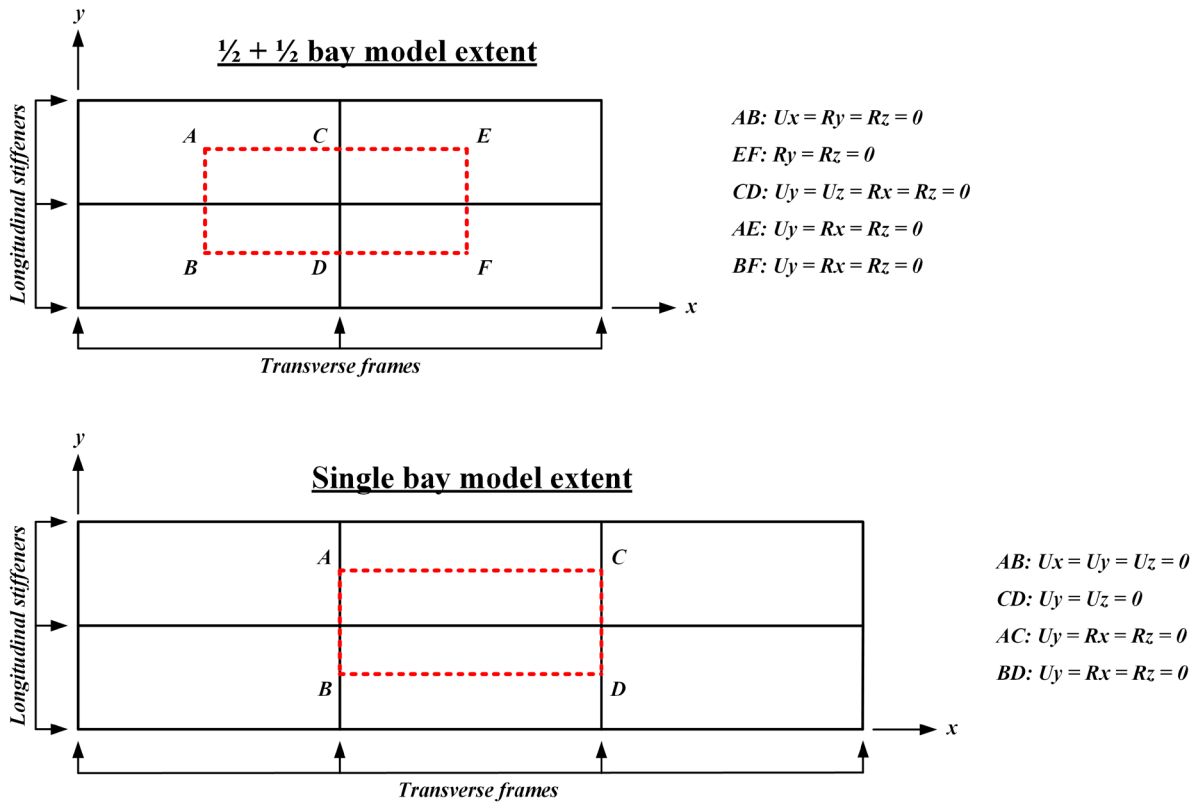


Figure 5-10 Model extent and boundary conditions of plate-stiffener combination model

• **Reduction factors**

To enable the modelling of compressive strength convergence and tensile strength reduction as found in the nonlinear FEA investigation, the use of reduction factors φ_1 and φ_2 are proposed in the updating rule 6 and 8. Whist these reduction factors are currently essential in the proposed method, they are also one of the limitations since there is not sufficient data to support a unified expression. In Chapter 4 validation, the former was specified as 0.3 and the latter was specified as 0.98 as

provisional values. The validation in Chapter 4 on plates and stiffened panels with emphasis on the reloading strength comparison showed a reasonable agreement with equivalent nonlinear FEA. However, these coefficients should be checked on a case-by-case basis at this stage. As demonstrated in Figure 5-11 which shows the load-shortening responses of the deck/bottom panels of present numerical box girder models under different cyclic loadings, it is more sensible to modify the reduction factor φ_1 as a function of the ultimate strain ε_u and unloading strain ε_{unload} . When the unloading in compression takes place far exceeding the ultimate limit point, a considerable change of post-ultimate strength stiffness may occur and the factor φ_1 can follow the recommendation in Chapter 4. By contrast, when the unloading takes place close to the onset of ultimate collapse, the reduction of post-collapse stiffness is less significant. Hence, a linear variation relationship is introduced to accommodate the difference led by the different unloading strain (Equation 5-8). Overall, the post-collapse compressive stiffness reduction factor φ_1 is specified according to Equation (5-8) to (5-10), while the tensile strength reduction factor φ_2 is specified as 0.98 following Chapter 5.

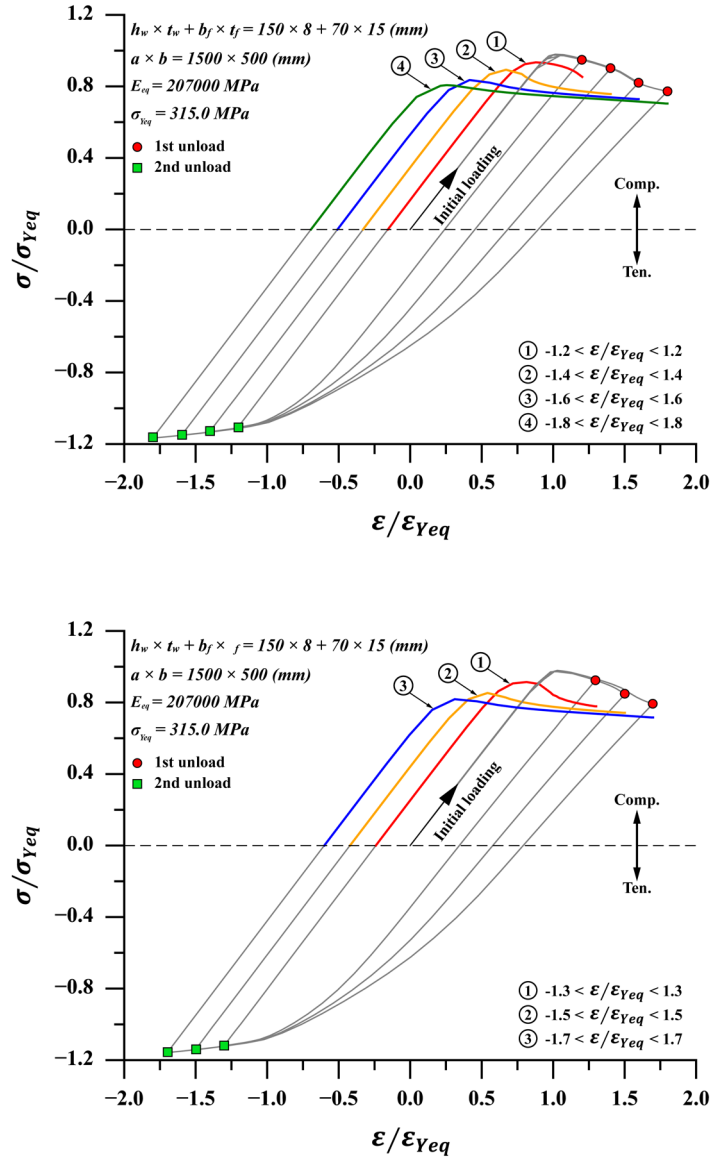


Figure 5-11 The effect of different cyclic loading on the post-ultimate strength stiffness in compression

$$\varphi_1 = 1 - 1.4 \times \bar{\varepsilon} \quad \text{for } \bar{\varepsilon} \leq 0.5 \quad (5-8)$$

$$\varphi_1 = 0.3 \quad \text{for } \bar{\varepsilon} > 0.5 \quad (5-9)$$

$$\bar{\varepsilon} = (\varepsilon_{unload} - \varepsilon_u) / \varepsilon_{Yeq} \quad (5-10)$$

- **Results and discussions**

Figure 5-12 and Figure 5-13 shows the load-shortening curve comparison under cyclic loading protocol $-1.8 < \varepsilon/\varepsilon_{Yeq} < 1.8$ for the critical stiffened panel of experimental model and numerical model respectively. The collapse modes of two models are shown in Figure 5-14. The results predicted by the method developed in Chapter 4 is depicted by as “Proposed” with the bracket indicating the embedded initial compressive LSC. The nonlinear FEA herein refers to the dynamic implicit solver prediction with consideration of Chaboche hardening. The issues of the structural member analysis under cyclic load with regard to the FE solver and material property have been highlighted in Chapter 4. It was found that numerically reliable prediction of cyclic load-shortening curve can only be made by the use of dynamic implicit solver with consideration of hardening. A satisfactory agreement may be found in these comparison, as the principle collapse behaviours of a stiffened panel under extreme cyclic load are well captured. The in-plane stiffness of the unloading path closely correlates with the nonlinear FEA results. As a conventional practice, the tensile ultimate strength is assumed as the material yield stress in the proposed method which therefore leads to certain discrepancy with respect to the FEA estimation. Meanwhile, the comparison also highlights the uncertainty on the compressive reloading strength prediction due to the use of different initial LSC. As suggested by Figure 5-12(c) and 5-13(c), the use of LSC 3 as an input results in a remarkably good correlation with nonlinear FEA, as both are based on dynamic implicit analysis considering material hardening. Despite LSC 1 and LSC 2 are more comparable in terms of their analysis assumptions (static-based and elastic-perfectly plastic), the former presents a better correlation of the reloading strength. This is primarily attributed to the difference in the post-collapse behaviour, as the reloading strength is taken as the same as the previous unloading stress from compression (Updating rule 7).

A further validation on the compressive reloading strength is shown in Figure 5-15 for regular loading protocols with seven magnitudes ($-C < \varepsilon/\varepsilon_{Yeq} < C$ with $C = 1.2\sim 1.8$). A reasonable correlation is obtained as indicated by the statistical analysis with a mean of 0.9621 and COV of 0.0812 for all test cases. Overall, the analytical method proposed in Chapter 4 could be concluded as a rational approach to simulate the collapse behaviour of structural component of the present case study box girder under extreme cyclic load and to be combined with the hull girder progressive collapse analysis.

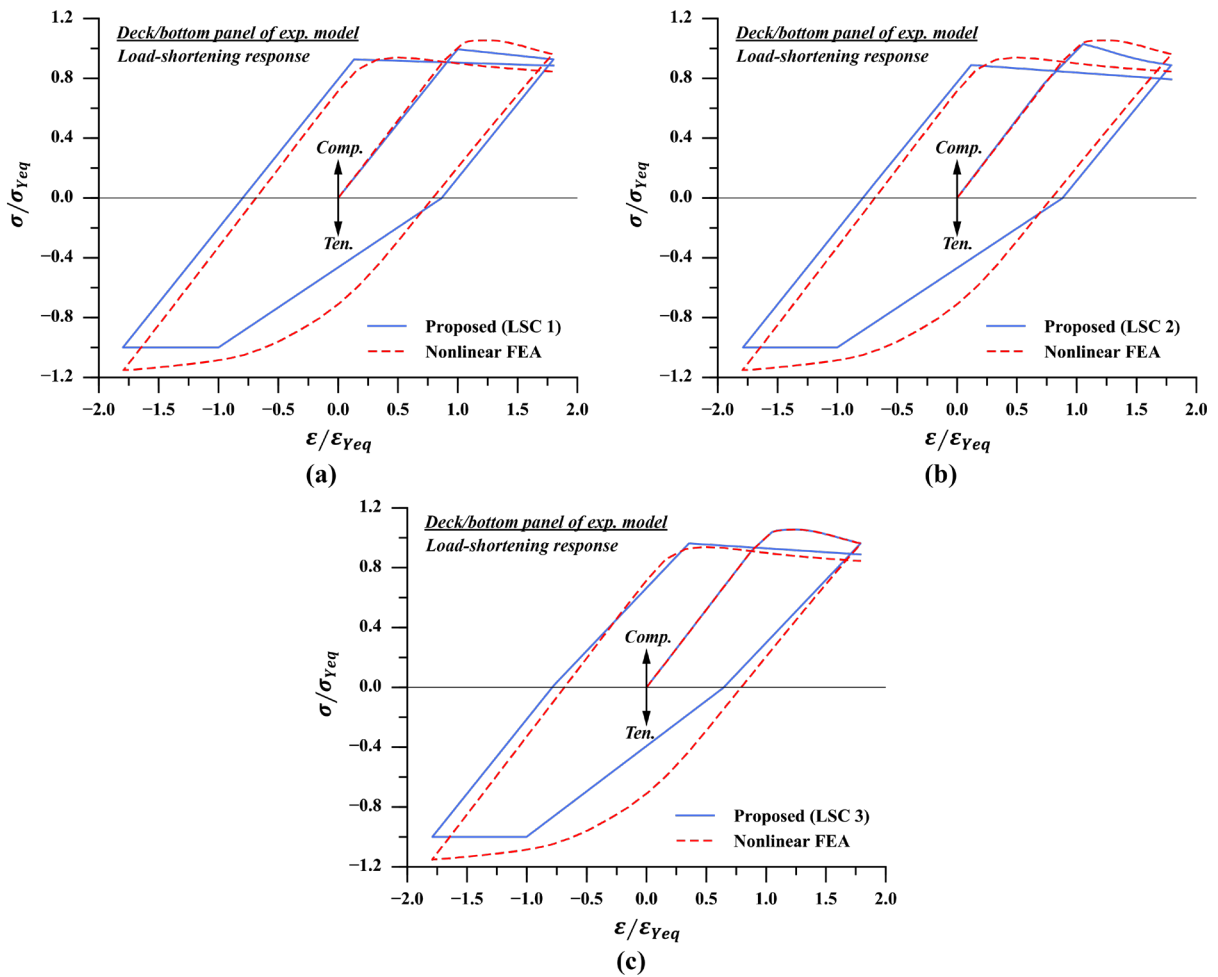


Figure 5-12 Load-shortening curve comparison of deck/bottom stiffened panel (Experimental box girder model)

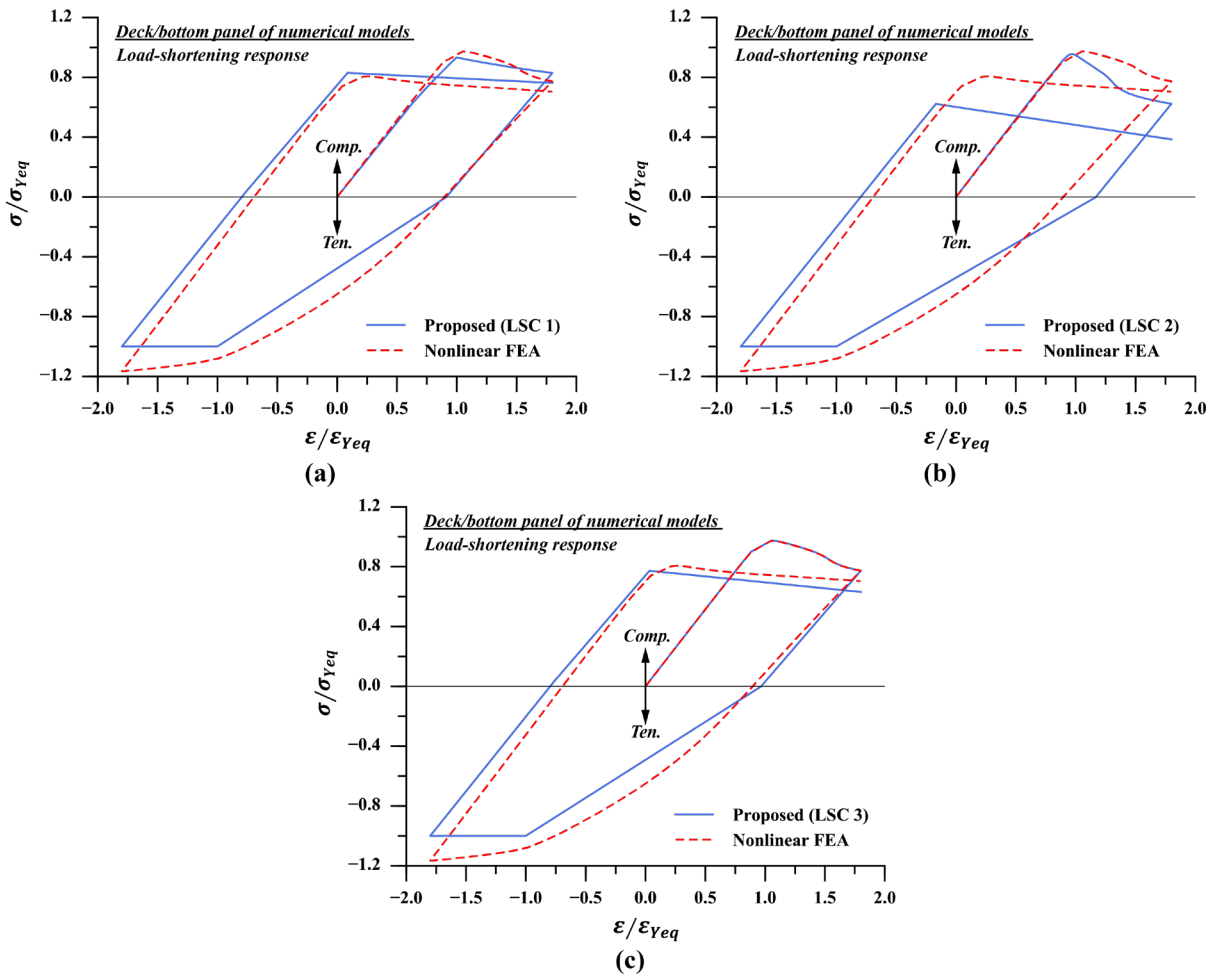
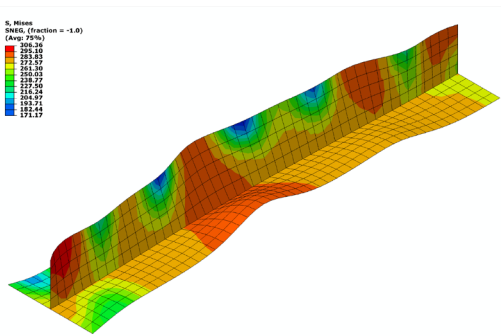


Figure 5-13 Load-shortening curve comparison of deck/bottom stiffened panel (Numerical box girder model)

a) Experimental model



b) Numerical model

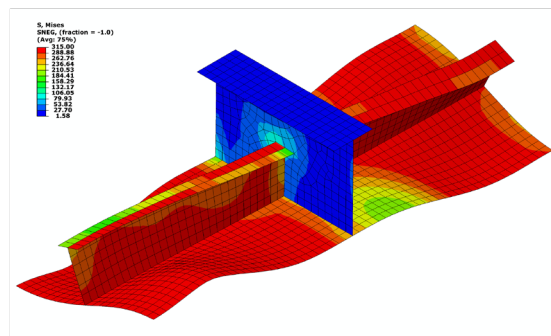


Figure 5-14 Collapse modes of the stiffened panels of experimental and numerical models

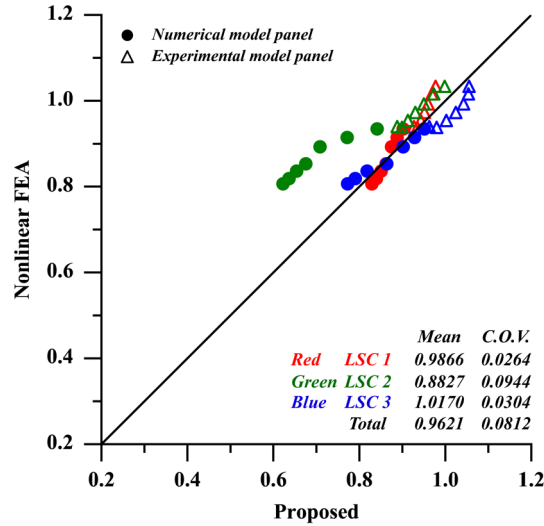


Figure 5-15 Correlation of the compressive reloading strength prediction

5.3.3 Comparison of Bending Moment Versus Curvature Relationship (Experimental Box Girder)

The prediction of bending moment/curvature curves of experimental model are compared in Figure 5-16. In general, a reasonable agreement is obtained. A higher initial ultimate bending strength is predicted by the proposed cyclic progressive collapse method, which might be attributed to the effect of welding-induced residual stress. In terms of the reloading to hogging at the first cycle, it appears that the reduction of ultimate bending strength is negligible, as indicated by the experimental measurement. This is consistent with Chapter 3 which shows that the pre-loading of structural component in compression or tension would not lead to a substantial capacity loss against the re-loading in an opposite direction. However, a significant strength reduction is experienced in the second cycle. This is due to the residual inelastic deformation of the structural components, developed by the previous loading in sagging where the nominal ultimate capacity has been surpassed. The sagging strength reduction of the second cycle is well correlated, whereas the prediction of hogging reloading strength in the second cycle by the cyclic progressive collapse method is relatively optimistic. The

proposed method with LSC 1 gives a higher strength prediction in both cycles, which is primarily a result of the difference in the post-collapse response of load-shortening curve. The LSC 2 has a steeper post-collapse response, in comparison to the gentle capacity loss of LSC 1 as reflected by Figure 5-12. The correlation of the bending strength between the predictions by the proposed method and experimental measurement is illustrated in Figure 5-17. Note that strength shown in Figure 5-17 are the max./min. values occurred at each loading cycle with the prescribed protocol. Owing to the effect of residual stress and uncertainty in initial distortion, the prediction by the proposed method is acceptably higher than the experimental measurement with an overall mean of 1.1468 and COV of 0.0841.

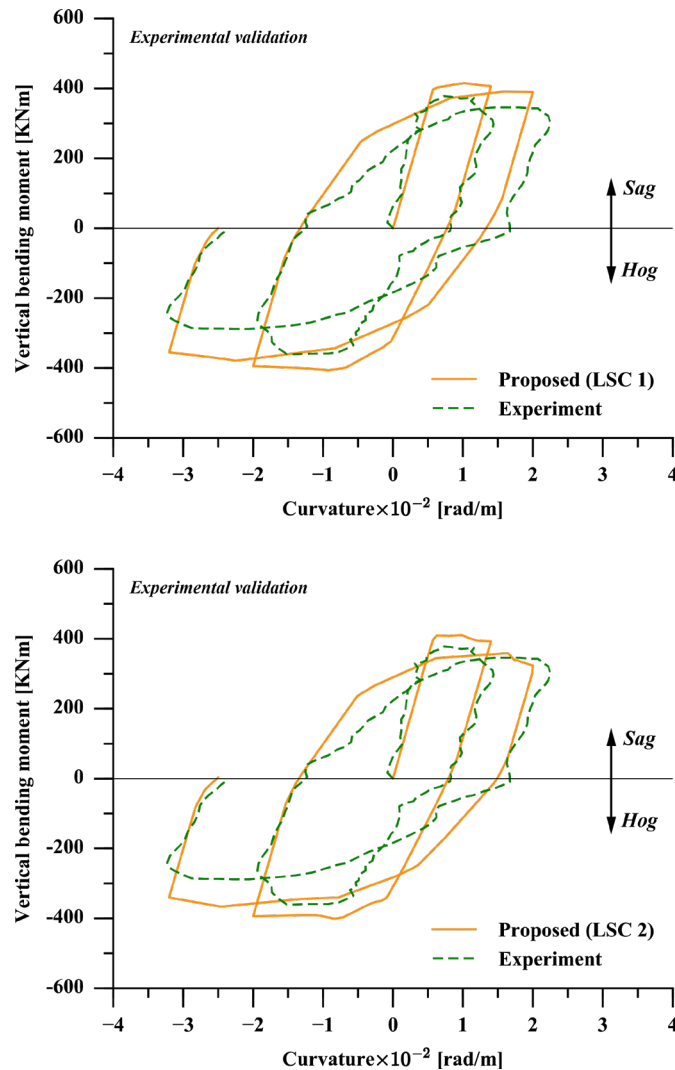


Figure 5-16 Bending moment versus curvature relation of experimental model

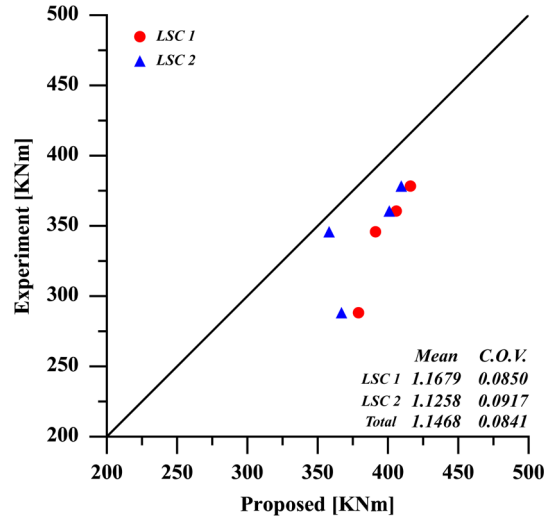


Figure 5-17 Correlation of the reloading strength of experimental model

5.3.4 Comparison of Bending Moment Versus Curvature Relationship (Numerical Box Girder)

Two cyclic loading protocols are analysed for the numerical models. The applied curvature is started in sagging followed by an equal magnitude hogging load, after which a further reloading to sagging is carried out. The magnitudes of each loading protocol are 0.6 rad/km and 0.4 rad/km respectively. The former case corresponds to the condition where the ship hull girder is monotonically loaded exceeding the ultimate collapse state, whereas the latter case corresponds to the condition in which the ship hull girder is monotonically loaded close to the ultimate collapse state.

The hull girder NLFEA is completed with dynamic explicit solver at a simulation time of 500 seconds (equivalent to a curvature rate of 6×10^{-3} rad/km per second) for each case to achieve quasi-static condition, as demonstrated by the small kinetic energy in all cases. Elastic–perfectly plastic material behaviour is assumed. The overall mesh size is 100mm \times 100mm. Rotational controlled loading is applied via a reference point coupled with one end of the model. The opposite end is constrained in six degrees of freedom. The progressive collapse analysis using the

proposed method is performed with the input of LSC 1 and 2. In addition, to elucidate the cyclic hardening and Bauschinger effect, an extra nonlinear FEA with Chaboche hardening is carried out for single hull model and a comparison is made with the proposed method based on LSC 3. Figure 5-18 and 5-19 illustrates the typical deformation contour plots of the case study models at three limit states under two loading protocols where max./min. values occurred in the bending moment curves, namely the first-cycle sagging, first-cycle hogging and the second-cycle sagging. At the first-cycle sagging ultimate collapse state, the deck and top shell panels fail in a combination of beam-column and local plate buckling accompanied with plastic permanent set. The failure mode of the first-cycle hogging is similar to that under monotonic hogging, in which the deck panel experiences a gross yielding while the bottom panel is slightly buckled. For the second-cycle ultimate collapse state in sagging, the buckling shapes of deck and top shell panels remain the same with an increase of the out-of-plane deflection. However, there is a change of the stress distribution in the top side shell panel when the hull girder is subjected to loading protocol 1. At the first-cycle ultimate sagging collapse state, a high stress level is experienced throughout the three-bay extent for both loading protocols. At the second-cycle, the high stress nucleates at the middle bay while the remaining part experiences a relatively low stress level when loading protocol 1 is applied.

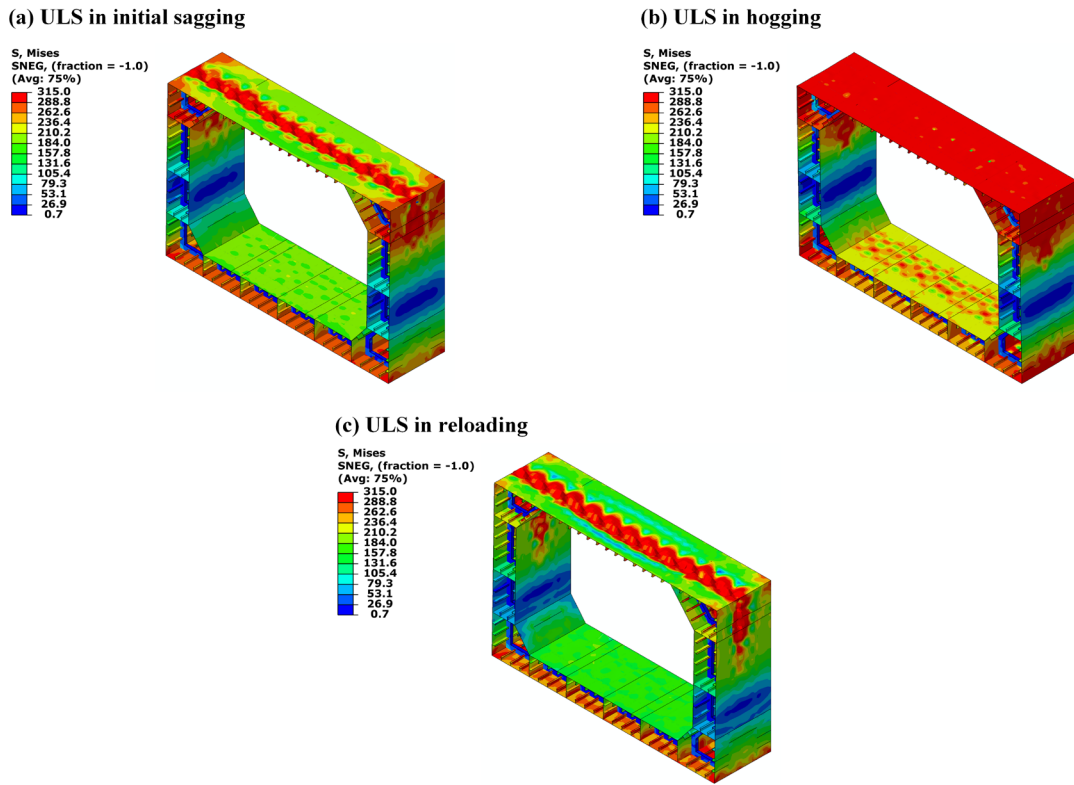


Figure 5-18 Contour plot of double hull model under loading protocol 1

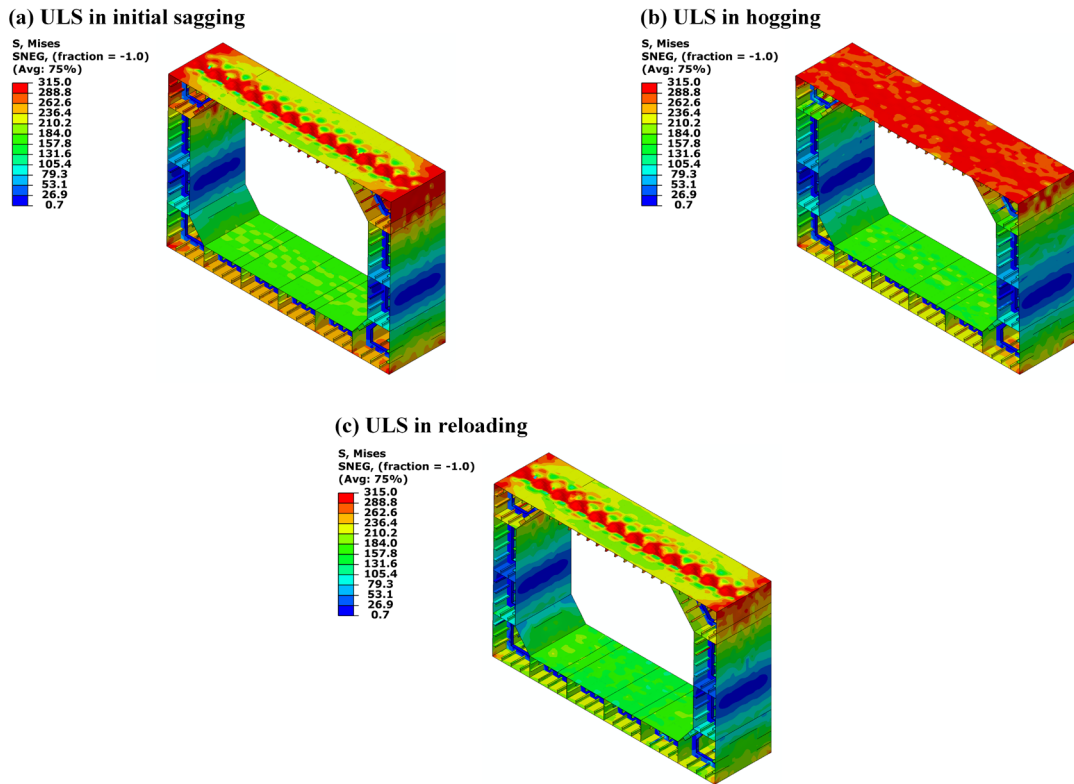


Figure 5-19 Contour plot of double hull model under loading protocol 2

All the bending moment/curvature curve comparisons are shown from Figure 5-20 to Figure 5-24. For loading protocol 2, the cyclic progressive collapse analysis is only carried out using LSC 2 (Figure 5-24), since it is found that there is only an insignificant strength reduction when LSC 1 is used. When the cross section is initially loaded in sagging up to or beyond the ultimate limit state of sagging, there is a considerable strength reduction in the sagging reload. On the other hand, the nonlinear FEA also predicts a reduction of the ultimate hogging strength. The cross sections with double side shell suffer from a larger strength reduction compared with the cross sections with single side shell. Under loading protocol 1 the bending stiffness is lower than the monotonic hogging stiffness when reloading from sagging to hogging. This differs from the hydro-elastoplastic approach developed in by Iijima et al. (2011) because a circular solid bar was used as test specimen to model the nonlinear structural behaviour, and hence no effect of cyclic buckling/plasticity of plate members was taken into account. The present analysis suggests that the structural stiffness of a thin-walled box girder would be reduced in the reloading phase because of the residual buckling deformation and residual stress.

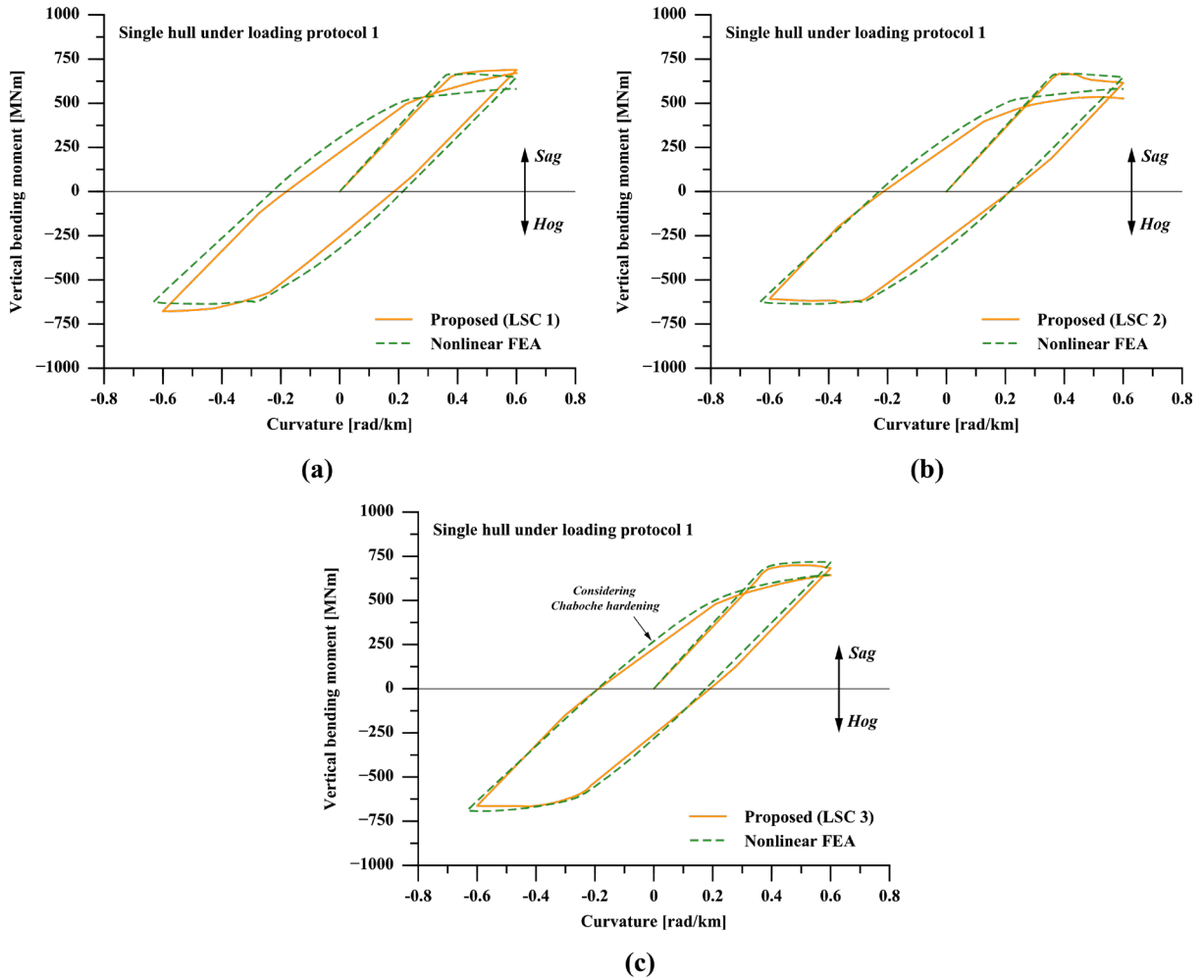


Figure 5-20 Bending moment versus curvature relation of single hull model under loading protocol 1

In the progressive collapse analysis using the proposed method, the reduction of sagging strength is primarily attributed to the reduction of ultimate compressive strength of structural components during cyclic loading. When LSC 2 is adopted, a better reloading sagging strength is predicted compared with the use of LSC 1. However, during the reloading in hogging at the first loading cycle, the strength of each compressed component remains the same as the initial condition. Any variation of hogging strength is caused by the differing in-plane stiffness of the structural components under tensile loading, which leads to a difference of the neutral axis position and consequently a change in the hogging strength.

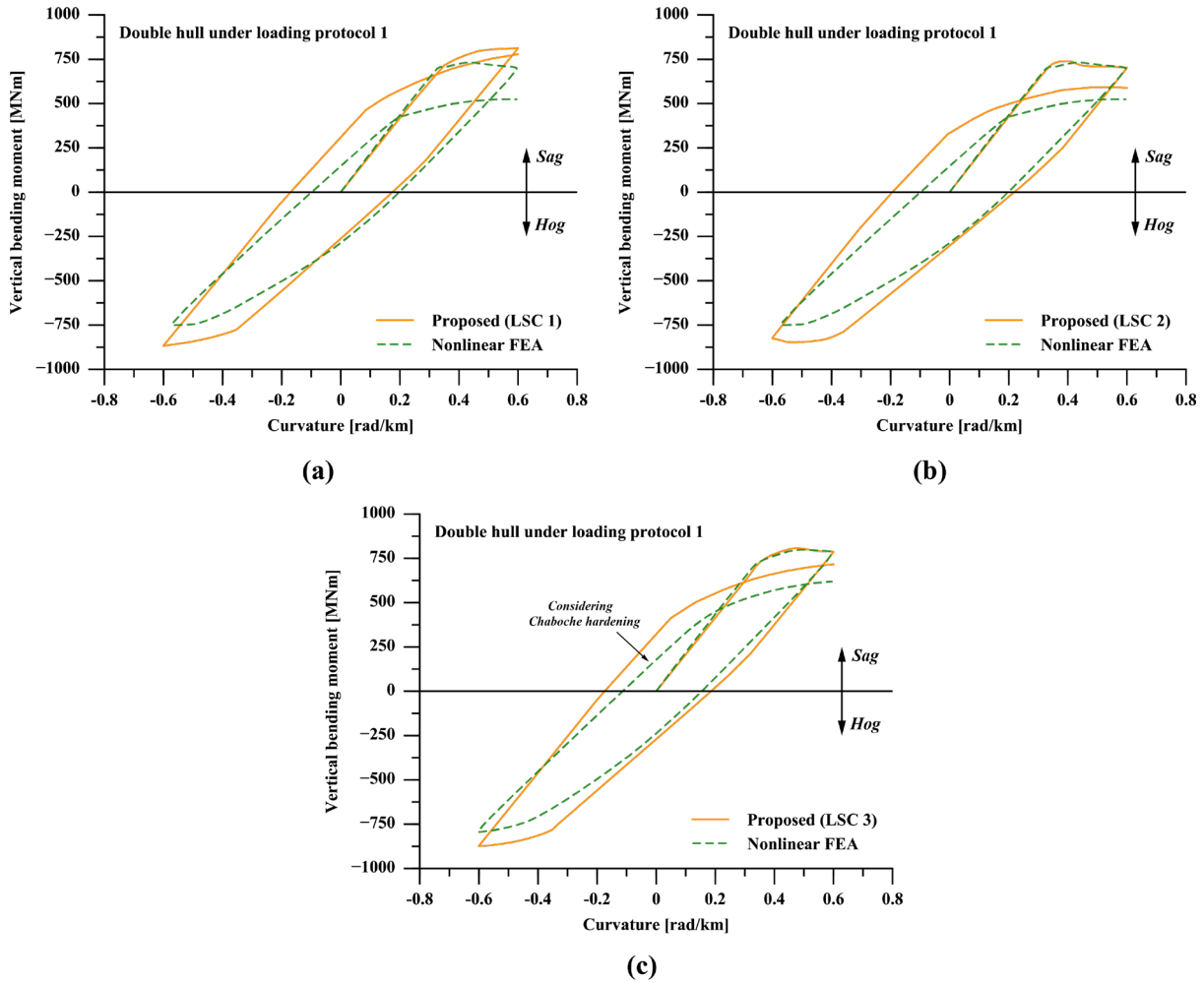


Figure 5-21 Bending moment versus curvature relation of double hull model under loading protocol 1

The effect of material hardening is shown in Figure 5-20(c) and Figure 5-21(c) which compare the bending moment/curvature curves predicted by NLFEM with Chaboche hardening and the proposed method based on LSC 3. The results correlate closely and suggest that the material hardening does not impose significant change on the overall bending response of a ship hull girder, but does cause an increase of the bending strength.

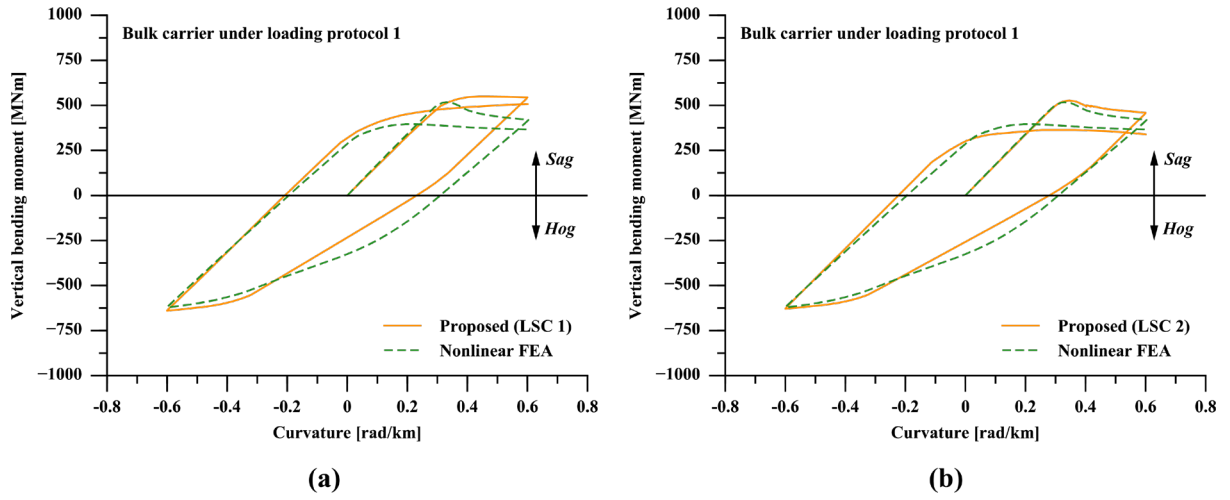


Figure 5-22 Bending moment versus curvature relation of bulk carrier model under loading protocol 1

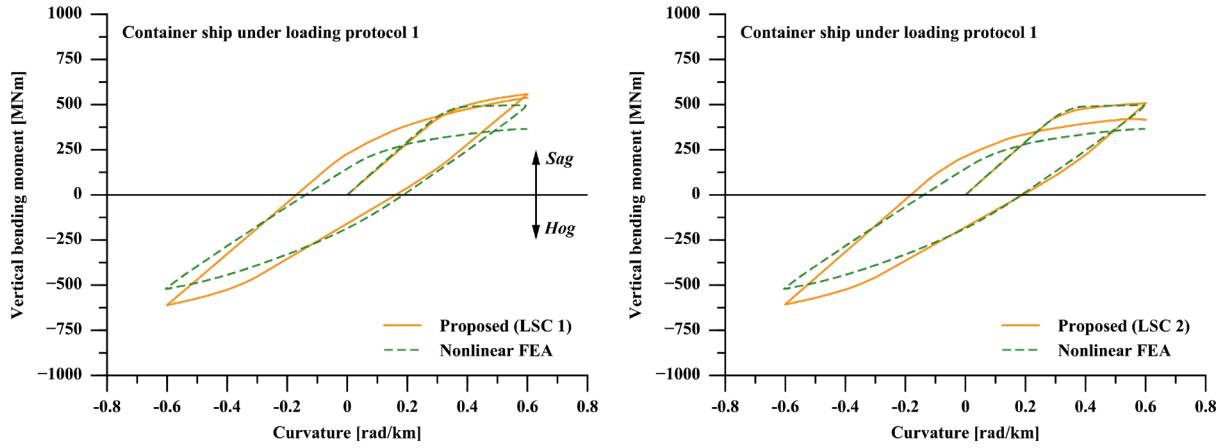


Figure 5-23 Bending moment versus curvature relation of container ship model under loading protocol 1

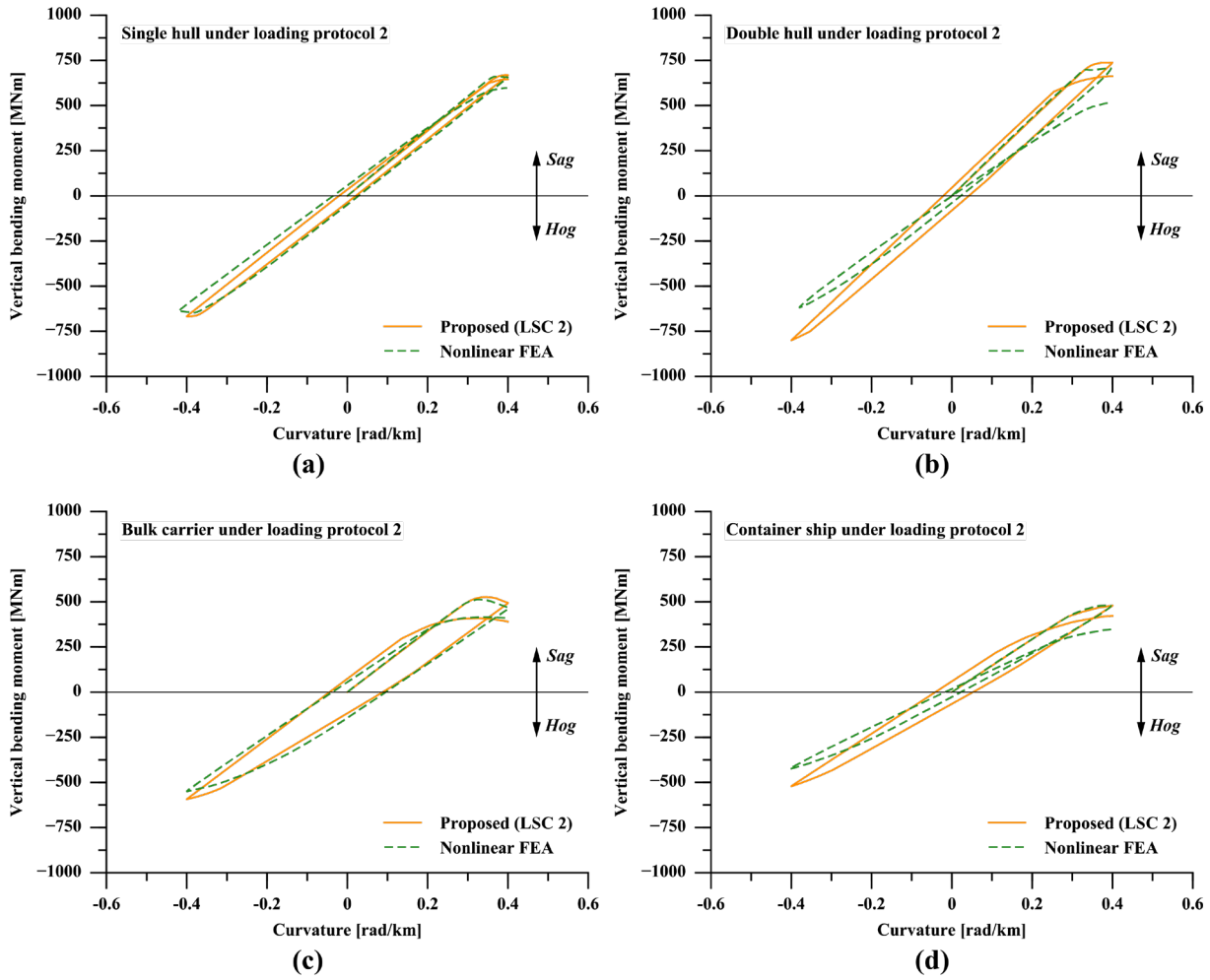


Figure 5-24 Bending moment versus curvature relation of case study models under loading protocol 2

As shown in Figure 5-25, the reloading strength predicted by the proposed method using LSC 2 is reasonably correlated with the nonlinear FEA results giving a mean value of 1.1002 and COV of 0.1080. Nevertheless, if LSC 1 is used, the predictions by the proposed method are optimistic with a mean value of 1.2252 and COV of 0.1396. The discrepancy is also related to the difference of the post-collapse response of structural components, the effect of which has already been highlighted in the validation of structural component load-shortening response in previous section. The statistical deviation is mainly associated with the results of double hull and container ship models, which have a double side shell cross section design. Apart from the fact that the present cyclic progressive collapse method might give

a higher prediction on the hogging reloading strength, another source of discrepancy may be related to the uncertainty of nonlinear FEA. For example the loading protocol 2 corresponds to the condition where the hull girder is loaded close to the ultimate limit point, a significant difficulty might be encountered in the numerical analysis, which leads to a convergence issue.

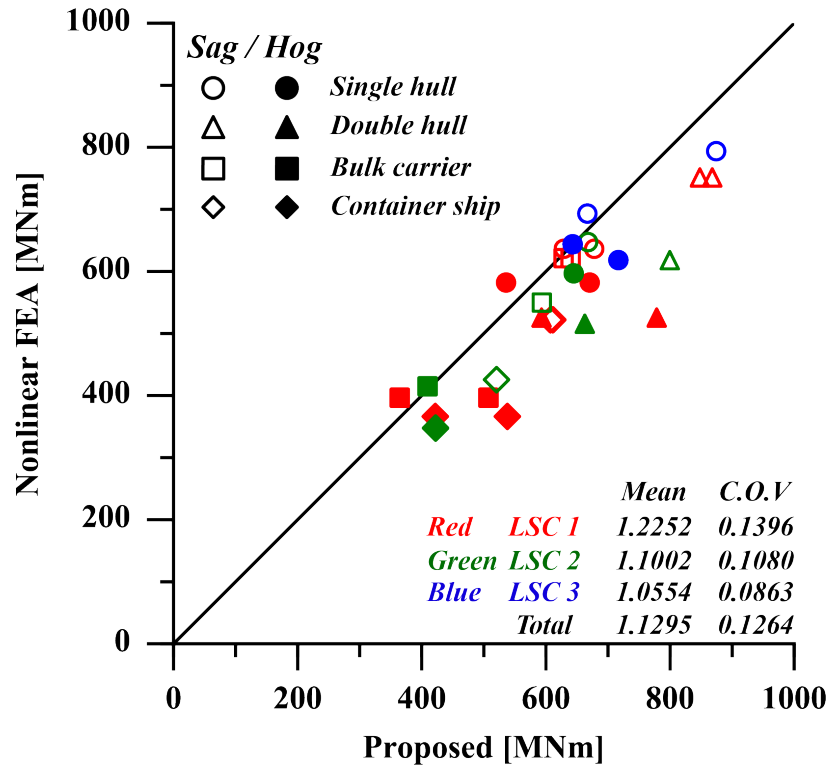


Figure 5-25 Correlation of the reloading bending moment with numerical simulation

5.3.5 Discussions

As presented above, the proposed cyclic progressive collapse method provides a reasonable prediction of the cyclic bending response of a ship hull girder when compared to equivalent nonlinear FEA. The analyses completed in this study are applied to simple representations of ship structures and are limited to a single extreme loading protocol which represents a more severe scenario than would be predicted by design guidelines such as the CSR. Nevertheless, the validation analyses indicate that the cyclic progressive collapse method is appropriate as a

framework to assess the post-ultimate strength behaviour following a complex series of extreme load events.

Additionally, uncertainty may be induced because of a different LSC input. When an FEA-based LSC is utilised within the cyclic progressive collapse method, a close correlation is obtained in comparison with NLFEM of the hull girder. When a CSR-based LSC is utilised in the cyclic progressive collapse method, the cyclic bending response prediction tends to be optimistic for the case studies analysed here. The discrepancy is mainly related to the difference in the post-collapse response of structural components. Whilst the proposed cyclic progressive collapse method is reasonably validated with the use of FEA-based LSC, it is necessary to further investigate the uncertainty caused by the different input of initial LSC, particularly the post-collapse response. According to the response and updating rule within the proposed method, the compressive reloading behaviour of structural components is highly affected by the post-collapse response of the previous cycle. A significant uncertainty may therefore be propagated into the prediction of hull girder reloading response. For instance, as shown in Section 5.3.2, the NLFEM models of stiffened panel elements are imposed with a rather conservative boundary condition in respect to their post-collapse response, which may then lead to an underestimation of hull girder strength. The influence of alternative LSCs based on different boundary conditions needs further investigation. Future work should also be conducted to investigate the effects of initial distortion and residual stress on the behaviour of structural components under extreme cyclic loading.

Meanwhile, the reduction factors φ_1 and φ_2 also contribute to the prediction uncertainty. The compressive post-collapse stiffness reduction factor φ_1 determines the post-collapse stiffness in the subsequent cycle and may significantly affect the hull girder strength prediction of the next cycle. The reduction factor

φ_2 may be relatively less important since the tensile response would not dominate the overall hull girder response.

5.4 Chapter Summary

This chapter describes an extended Smith method for predicting the collapse response of ship hull girders against cyclic longitudinal bending. The method follows the same assumption and general procedure of the original Smith-type progressive collapse method, with an extended capability to re-formulate the structural member's load-shortening curve when load reversal takes place. A series of validation is conducted with experimental data and finite element simulation. A reasonable correlation is obtained. Besides, it is showed that different initial LSC inputs would lead to significant variation of the reloading strength prediction. The CSR-based prediction is a non-conservative measure as compared with the FEM-based prediction in this case study.

Chapter 6 Uncertainty Evaluation of the Extended Smith Method

6.1 Rationale

An uncertainty evaluation of the extended Smith method is conducted in this chapter. The rationale of this evaluation is summarised as follows:

- 1) As indicated in the validation section of Chapter 5, the initial LSC input is the most important contributor to the prediction uncertainty of cyclic response;
- 2) From the collapse analysis's point of view, a structural component's LSC is governed by four major features, i.e. elastic stiffness, ultimate compressive strength, ultimate strain and post-collapse stiffness. It is necessary to investigate the respective influence of all these critical features on the overall collapse behaviour of ship hull girder;
- 3) To facilitate the uncertainty evaluation, a new LSC formulation should be developed, which is able to incorporate specific critical features as mentioned above;
- 4) The effect of LSC has always been an issue in predicting the ship hull girder strength, as different analysts have their preferred LSC prediction approach. The proposed uncertainty evaluation procedure is not only valuable for the extended Smith method, but also the original approach as well as its associate and all the other extensions.

6.2 Methodology

The overall procedure of the uncertainty evaluation is illustrated by Figure 6-1. The core of this methodology is the adaptable LSC algorithm. This algorithm is introduced to derive the LSC of a stiffened panel from four characteristics: elastic stiffness, ultimate strength, ultimate strain and post-collapse stiffness. With this

algorithm, the influences of each critical features are investigated independently in a deterministic manner.

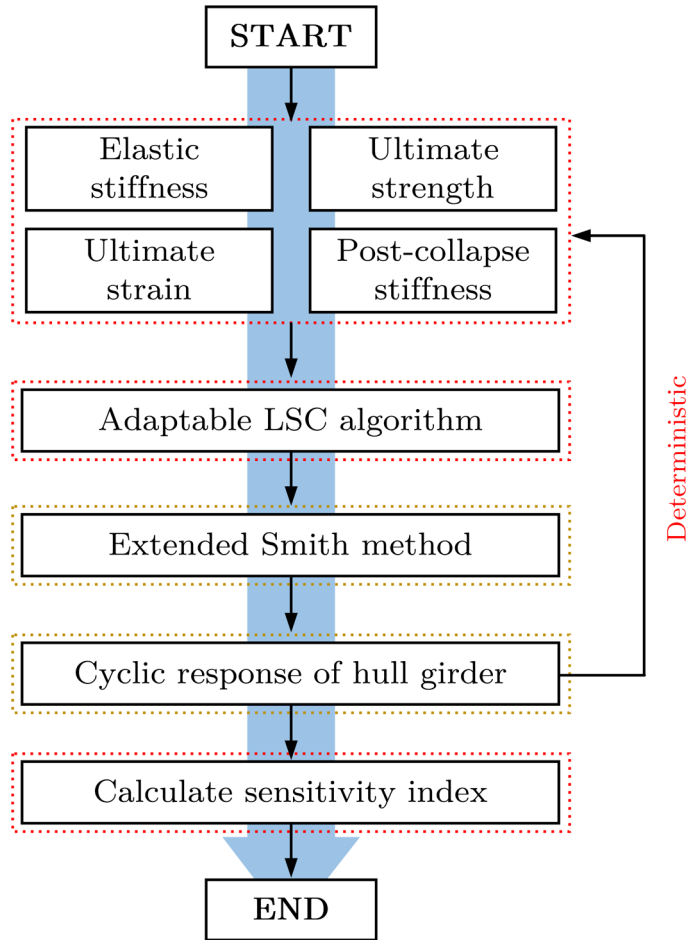


Figure 6-1 Overall procedure of uncertainty evaluation

Whilst a schematic illustration is shown in Figure 6-2, the formulation of the adaptable algorithm are given by Equation (6-1) to Equation (6-6) where E_{T_o} is the elastic stiffness, E_{T_p} is the post-collapse stiffness and E_T is the instantaneous tangent stiffness of the nonlinear arc-shaped response. Three components are proposed forming the complete load-shortening curve in the adaptable algorithm, namely linear elastic initial response (Equation 6-1), arc-shaped ultimate response (Equation 6-2) and linear post-collapse response (Equation 6-3).

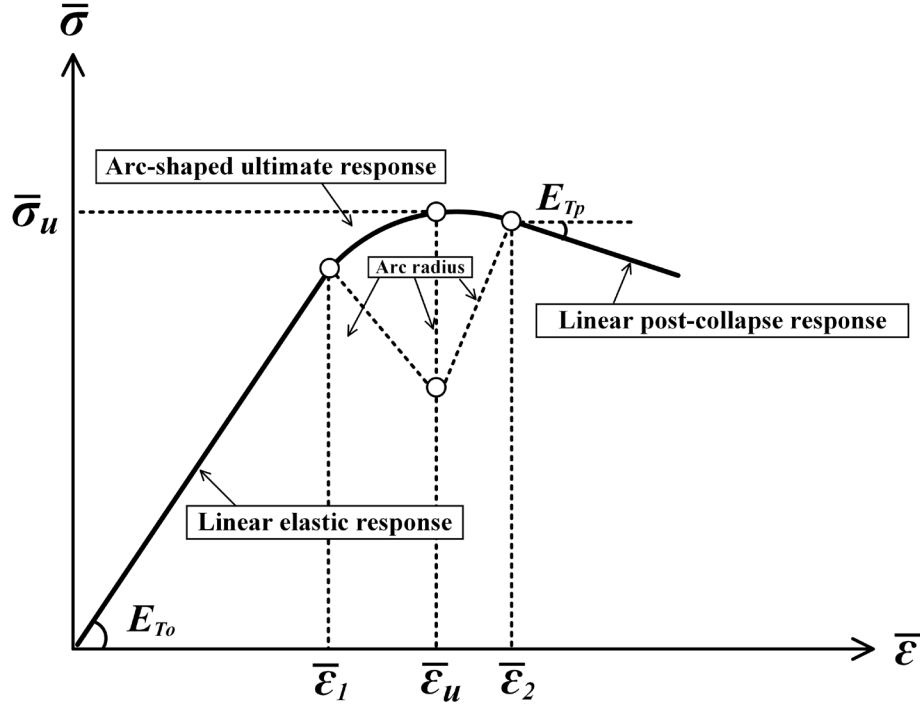


Figure 6-2 Schematic illustration of the adaptable algorithm

$$\frac{\sigma_x}{\sigma_{Yeq}} = E_{To} \frac{\epsilon_x}{\epsilon_{Yeq}} \quad (6-1)$$

$$\frac{\sigma_x}{\sigma_{Yeq}} = \frac{\sigma_{xu}}{\sigma_{Yeq}} - R + R \cos(-\tan^{-1}(E_T)) \quad (6-2)$$

$$\frac{\sigma_x}{\sigma_{Yeq}} = \frac{\sigma_2}{\sigma_{Yeq}} + \left(\frac{\epsilon_x}{\epsilon_{Yeq}} - \bar{\epsilon}_2 \right) E_{Tp} \quad (6-3)$$

$$R = \frac{\cos(\tan^{-1}(E_{To})) (E_T \epsilon_{xu} / \epsilon_{Yeq} - \sigma_{xu} / \sigma_{Yeq})}{1 - \cos(\tan^{-1}(E_{To}))} \quad (6-4)$$

$$\bar{\epsilon}_1 = \epsilon_{xu} / \epsilon_{Yeq} + R \sin[-\tan^{-1}(E_{To})] \quad (6-5)$$

$$\bar{\epsilon}_2 = \epsilon_{xu} / \epsilon_{Yeq} + R \sin[-\tan^{-1}(E_{Tp})] \quad (6-6)$$

6.3 Scope of Evaluation

The uncertainty evaluation is conducted for the double hull model in Chapter 5. Parametric progressive collapse analyses are performed for the loading protocol 1 and monotonic loading as a comparison. The four critical features of LSC are systematically varied as follows:

- Ultimate strength: a base ultimate strength (UltStr) is calculated by the empirical formula proposed by Paik and Thayamballi (1997). With this base ultimate strength, a strength ratio varied from 1.06 to 0.92 at an increment of 0.02 is applied so that eight different ultimate strength values are obtained;
- Elastic stiffness: eight different elastic stiffness values varying from unity to equal to the normalised base ultimate strength with equal increment are analysed;
- Ultimate strain: a base ultimate strain, normalised by material yield strain, is taken as the same as the normalised base ultimate strength. Eight ultimate strain values varying from the base ultimate strain to 1.20 with equal increment are utilised;
- Post-collapse stiffness: eight different post-collapse stiffness values are adopted from 0.00 to -0.35 at an increment of -0.05.

Each of these parameters are varied independently. If not under examination, the normalised ultimate strength, normalised ultimate strain, elastic stiffness and post-collapse stiffness are taken as the base ultimate strength, 1.0, 1.0 and -0.20 respectively. Examples of parametric load-shortening curves in relative coordinate are shown in Figure 6-3.

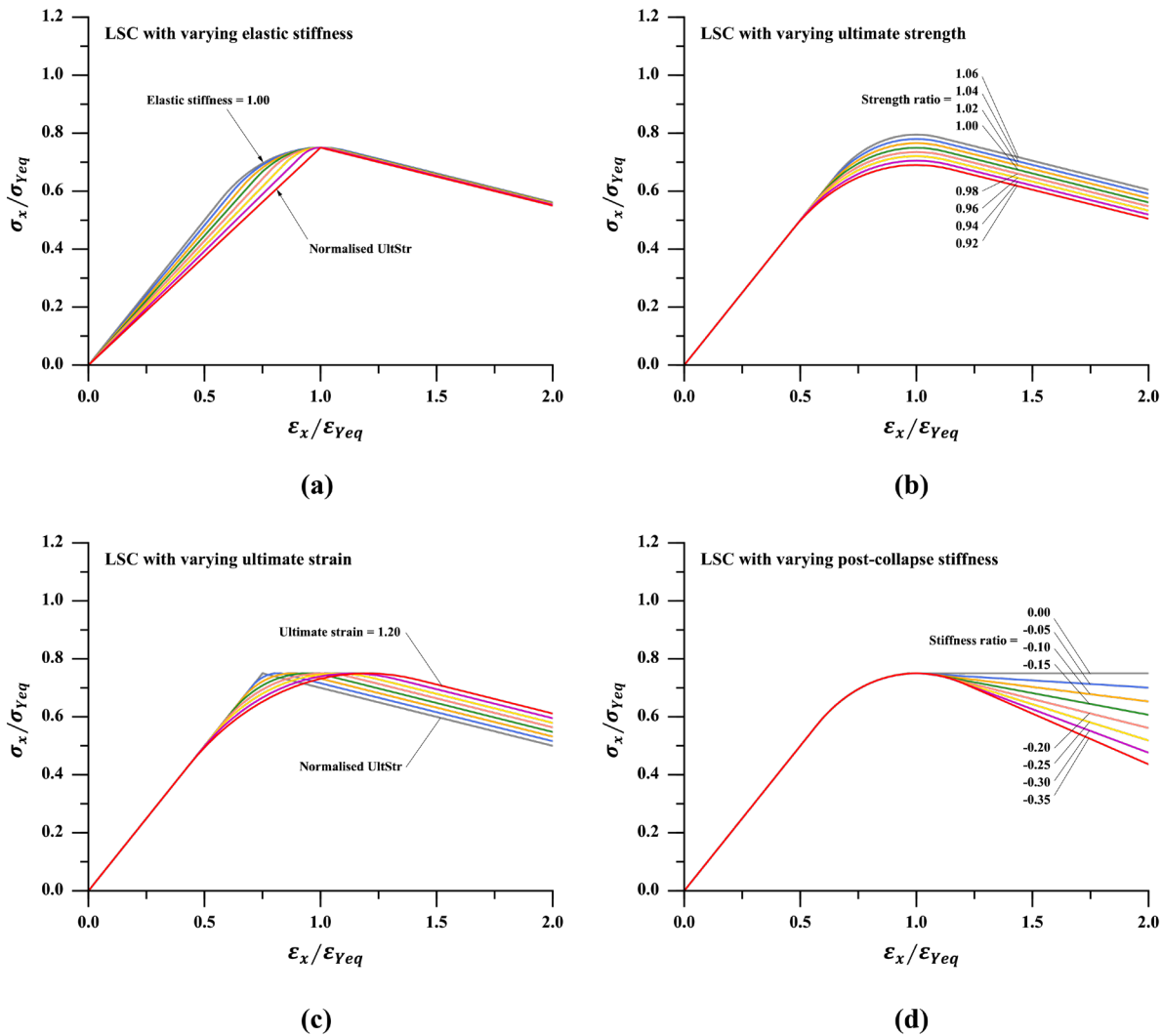


Figure 6-3 Example load-shortening curve developed by the adaptable algorithm

6.4 Effect of Elastic Stiffness

As shown in Figure 6-4, a relatively small deviation on both overall bending response and ultimate hull girder strength is resulted by the variance in elastic stiffness under both cyclic and monotonic bending. The rather negligible effect of elastic stiffness may also be validated by a preliminary case study presented by Li et al. (2019), in which a reasonable correlation was obtained between the prediction by nonlinear finite element analysis and simplified progressive collapse method incorporated with a linearized load-shortening curve which has a conservative elastic stiffness.

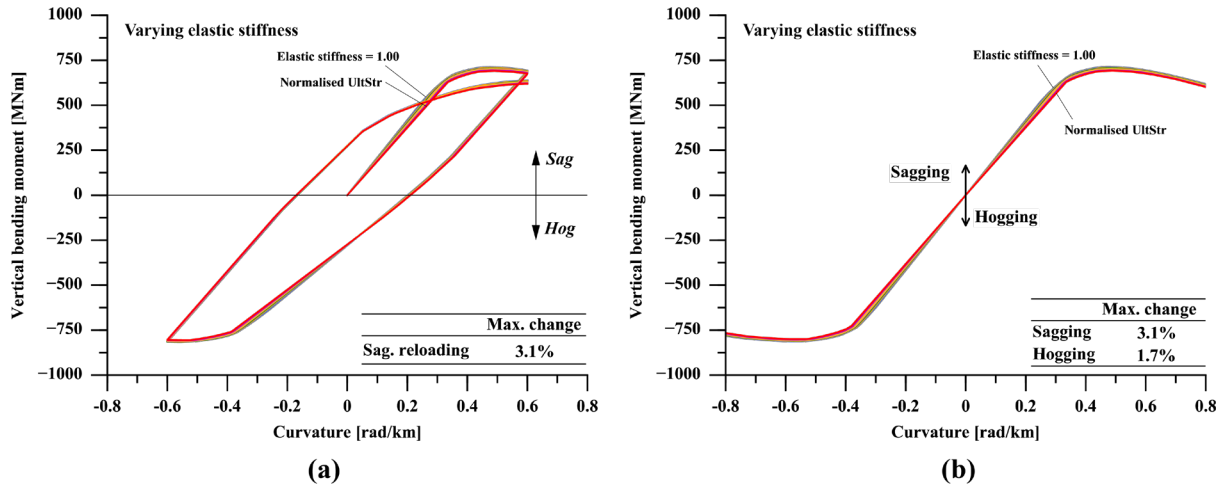


Figure 6-4 The effects of elastic stiffness on the cyclic and monotonic bending moment versus curvature response of double hull model

6.5 Effect of Ultimate Compressive Strength

With the change of structural element’s ultimate compressive strength, the overall shapes of the bending moment/curvature response is unaffected, as shown in Figure 6-5. The variation of ultimate compressive strength only results in a change of the ultimate hull girder moment. Under pure vertical bending, a maximum change of 8.9% and 5.6% is induced in sagging and hogging respectively. The variation is slightly amplified in the case of cyclic bending. According to the formulation introduced in Chapter 4, the unloading and reloading compressive stiffness are calculated as the ratio between ultimate compressive strength and ultimate strain before the unloading takes place. Thus, different compressive reloading stiffness is established between parametric load-shortening curves and thereby introduces further uncertainty to the hull girder strength calculation.

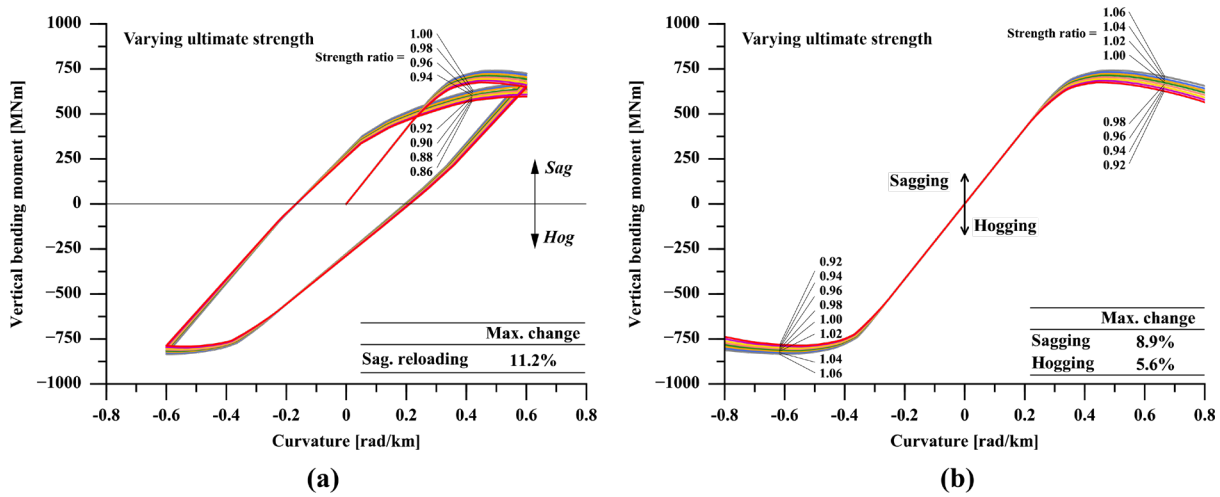


Figure 6-5 The effects of ultimate compressive strength on the cyclic and monotonic bending moment versus curvature response of double hull model

6.6 Effect of Ultimate Strain

As shown in Figure 6-6, the overall bending moment/curvature path experiences a slightly larger tangent stiffness at the onset of nonlinear bending behaviour with a smaller ultimate strain value. The bending rigidity then reduces rapidly and the ultimate collapse takes place. An intermediate effect on the ultimate hull girder strength is brought by the variation of ultimate strain of structural component, in which a maximum change of 6.4% and 4.0% is estimated for sagging and hogging respectively. In comparison to the effect of ultimate strength, a larger amplification caused by cyclic loading is obtained where a 12.2% of variation is induced on the reloading sagging strength prediction.

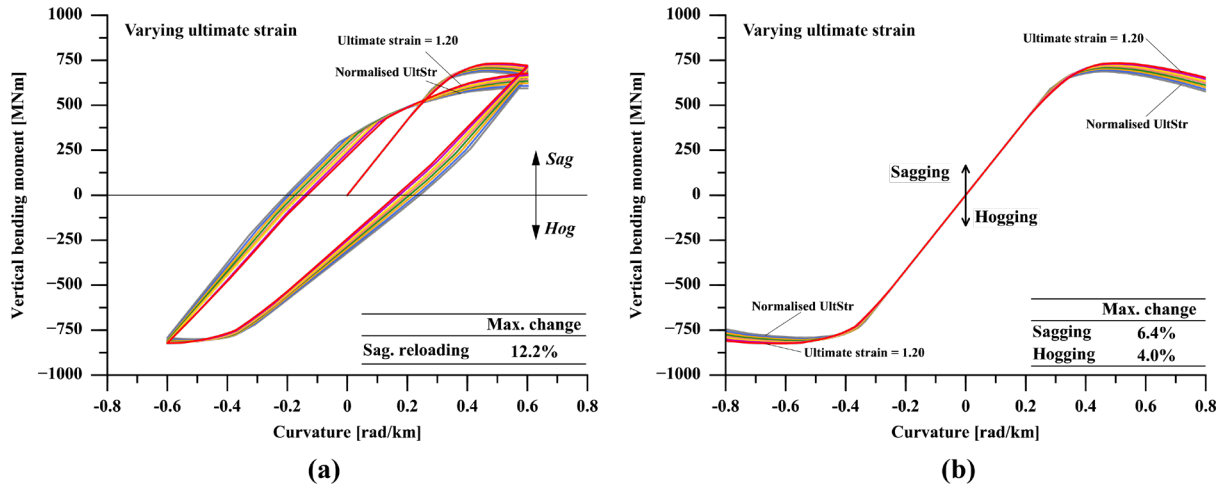


Figure 6-6 The effects of ultimate strain on the cyclic and monotonic bending moment versus curvature response of double hull model

6.7 Effect of Post-Collapse Stiffness

As shown in Figure 6-7, there is a significant change of the overall bending moment/curvature curve resulted by the variation of post-collapse stiffness of structural elements. In the case of $E_{Tp}/E = 0$, a distinct ultimate peak does not exist in the bending moment/curvature curve, as there is no load shedding between structural components. By contrast, a sharp ultimate limit point can be found in the case of steep post-collapse stiffness structural elements where a considerable load shedding would take place. A maximum change of 14.4% and 5.1% is shown under pure vertical sagging and hogging respectively. The cyclic bending greatly amplifies the effect of structural component's post-collapse stiffness. This is because the post-collapse stiffness has a direct impact on both the ultimate strength and post-collapse stiffness in the reloading regime. Following Chapter 4, the ultimate compressive reloading strength is assumed as the same as the stress where the previous compressive unloading is initiated. Thus, a steeper post-collapse stiffness would result in a lower reloading strength in the subsequent loading cycle, which introduces further variation on the hull girder strength.

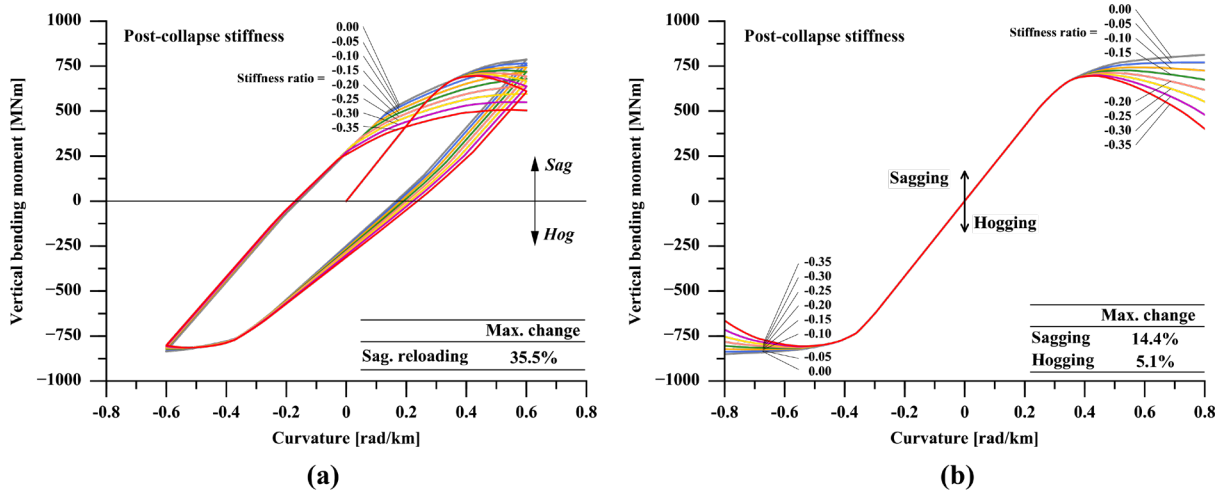


Figure 6-7 The effects of post-collapse stiffness on the cyclic and monotonic bending moment versus curvature response of double hull model

6.8 Sensitivity Index

The sensitivity of the ultimate bending strength of ship hull girder with respect to the i^{th} parameter is evaluated using a sensitivity index defined by Equation (6-7), following the method employed by 14th ISSC (2000) where M_u is the ultimate hull girder strength and x^i is the parameter under consideration. In the present study, the sensitivity index is modified to take into account the difference of variational range between each variable. Therefore, the i^{th} variable should be scaled from its original range to a fixed range between zero and unity. The sensitivity index can be further normalised by multiplying μ_{x_i}/μ_{M_u} as given by Equation (6-8).

$$S_i = \frac{\partial M_u}{\partial x_i} \quad (6-7)$$

$$\bar{S}_i = \frac{\mu_{x_i}}{\mu_{M_u}} \times S_i \quad (6-8)$$

where μ_{x_i} and μ_{M_u} are the mean value of the i^{th} variable and ultimate hull girder strength respectively. The mean value of each variable is given in Table 6-1. The

provisional mean values are calculated based on the variation of each parameter analysed in the present study. The mean value of the ultimate hull girder strength is evaluated using the mean value of the considered variables. The normalised sensitivity index defined by Equation (6-8) can be numerically evaluated as given by Equation (6-9) where $M_u^{+5\%}$ and $M_u^{-5\%}$ are the ultimate hull girder strength by changing the scaled variables by +5% and -5% respectively.

$$\bar{S}_i = \frac{\partial M_u / \mu_{M_u}}{\partial x_i / \mu_{x_i}} = \frac{(M_u^{+5\%} - M_u^{-5\%}) / \mu_{M_u}}{(1.05\mu_{x_i} - 0.95\mu_{x_i}) / \mu_{x_i}} = \frac{(M_u^{+5\%} - M_u^{-5\%})}{0.1\mu_{M_u}} \quad (5-11)$$

Table 6-1 Mean values of each critical features

| Variable | Mean values |
|-------------------------|---|
| Ultimate strength | $0.99\sigma_{xu} / \sigma_{Yeq}$ |
| Ultimate strain | $(1.20 + \sigma_{xu} / \sigma_{Yeq}) / 2$ |
| Elastic stiffness | $(1.00 + \sigma_{xu} / \sigma_{Yeq}) / 2$ |
| Post-collapse stiffness | -0.175 |

Note: $\sigma_{xu} / \sigma_{Yeq}$ = normalised base ultimate strength

The results of sensitivity index evaluation is summarised in Table 6-2. The sensitivity index in all cases are positive, indicating an increase of the hull girder strength with an increase of the variable. It can be seen that the ultimate compressive strength and post-collapse stiffness of structural components are the most influential parameters to the hull girder strength calculation. Also, the hull girder sagging strength is generally more sensitive than the hogging strength with respect to the load-shortening relationship, except for the variation of elastic stiffness. Meanwhile, the sensitivity index is generally amplified by the application of cyclic load, in which the effect of post-collapse stiffness has the largest amplification.

Table 6-2 Summary of the sensitivity index ($\times 10^{-2}$)

| Load type | σ_{xu}/σ_{Yeq} | $\varepsilon_{xu}/\varepsilon_{Yeq}$ | E_{To}/E | E_{Tp}/E |
|-------------|----------------------------|--------------------------------------|------------|------------|
| Mono. sag | 4.50 | 3.59 | 1.31 | 5.94 |
| Mono. Hog | 2.25 | 1.74 | 1.42 | 1.72 |
| Reload sag. | 6.54 | 6.01 | 1.25 | 20.8 |

6.9 Chapter Summary

It is demonstrated in Chapter 5 that the different initial LSC inputs would lead to significant variation of the reloading strength prediction using extended Smith-type calculation, especially caused by variability in the compressive post-collapse behaviour of structural components. In this regard, a deterministic procedure is proposed in this chapter for uncertainty evaluation of the extended Smith method. It is estimated that the maximum variation of the sagging reloading due to the variance in compressive post-collapse stiffness of structural members may be around 35.5% with a sensitivity index of 20.8.

Chapter 7 Conclusions and Recommendations

7.1 Thesis Summary

Ships and ship-type floating structures are subjected to time-varying longitudinal bending load. Ultimate limit state principle is currently adopted to guarantee the ship structural safety against the failure due to excessive longitudinal bending. The assessment of the extreme scenario based on ultimate limit state philosophy usually assumes monotonic loading.

However, ships and ship-type floating structures are exposed to cyclic loading when in service. In a rough sea state, they are likely to encounter a series of storm waves leading to cyclic loading with extreme magnitude. Each cycle may be detrimental to the structural integrity. In an unusual but possible situation, a series of extreme cyclic load may lead to the final destructive “breaking its back” failure, even if the extreme loads do not surpass the nominal ultimate limit state. Hence, it might be important to predict the progressive collapse of ship hull girder and structural members under cyclic load.

Within this context, the aim of this thesis is to better predict the collapse behaviours of ship structures under extreme cyclic load. Overall, four contributions are achieved, namely

- a) The nonlinear finite element study on the collapse behaviour of ship plating under extreme cyclic loading provides a new quantification of the cyclic response, including several distinctive features as compared with the responses under monotonic loads;
- b) A response and updating rule methodology, developed to predict the load-shortening response of structural components under cyclic loading, provides an enhanced approach to develop the load-shortening curves for implementing in an extended Smith-type progressive collapse analysis. The

enhancement includes three aspects: an ability to modify the existing monotonic load-shortening curve, a computationally efficient algorithm and the inclusion of all distinctive features with close correlation to equivalent finite element results;

- c) An extension to the Smith-type progressive collapse method for estimating the bending moment versus curvature relationship of ship hull girders is developed, which has a potential to be combined with a hydrodynamic approach;
- d) A methodology to evaluate the computational uncertainty of ultimate hull girder strength using a Smith-type progressive collapse method is introduced, which shows the influence structural member's load-shortening curve on the overall hull girder response.

7.2 Conclusions

The key conclusions of this thesis may be summarised as follows.

From the structural component analysis work in Chapter 3, it can be concluded that a consistent pattern of ultimate strength degradation occurs on ship type plating under extreme in-plane compression and tension. The analysis work in Chapter 4 extends this conclusion to more complex stiffened panel structural components. For plates and stiffened panels the degradation of compressive strength experiences convergence after two or three cycles of loading. Conversely, the tensile strength linearly degrades in each cycle. The degradation of compressive strength and its convergence phenomenon is shown to be associated with the change in compressive post-collapse stiffness, which also undergoes a convergence as approaching to zero (i.e. response plateau) after several cycles of loads.

The analysis work in Chapters 3 and 4 confirm, for the first time, the following specific characteristics within the component load shortening curves (**Contribution a**):

- A degradation of the ultimate strength is observed on the structural component under extreme in-plane compression and tension;
- The degradation of compressive strength experiences convergence after two or three cycles of loading, but a complete convergence is not observed. Conversely, the tensile strength linearly degrades in each cycle;
- The degradation of compressive strength and its convergence phenomenon is associated with the change in compressive post-collapse stiffness, which also undergoes a convergence as approaching to zero (i.e. response plateau) after several cycles of loads;
- The reloading strength of structural component is closely correlated with the unloading stress where the discharge of applied load is started;
- The stiffness of unloading in compression is slightly reduced as compared with the initial stiffness, whereas the stiffness of unloading in tension is close to the initial stiffness;
- The stiffness of reloading in compression is close to its unloading stiffness, whereas the stiffness of reloading in tension depends on the previous unloading history in tension may be substantially reduced;

In Chapter 4, these specific characteristics are shown to be sufficient to develop a robust methodology to predict the load-shortening curve (LSC) of structural component under cyclic load. Based on updating the critical points, the methodology is demonstrated to be an efficient and novel approach which is suitable for further implementation in the Smith-type progressive collapse method (**Contribution b**). It is shown that:

- As represented by the applied strain range and the cycle number, the loading protocol of structural components is formalized. With this definition, the loading history of structural components can be clearly described;
- The proposed method can be used with different monotonic load-shortening curves, including those derived by the NLFEM and CSR. Different base LSCs may lead to a substantial deviation of the cyclic response prediction, which is mainly due to the difference in the compressive post-collapse characteristics.
- As verified by the equivalent analysis using NLFEM, the method adequately represents the specific characteristics discovered in Contribution (a), such as the strength reduction and compressive post-collapse stiffness convergence.

In Chapter 5, an extension to the Smith-type progressive collapse method is devised in combination with the response and updating LSC methodology. It is shown that this is a feasible approach to estimate the collapse response of ship hull girders under cyclic bending (**Contribution c**). It is found that:

- Under extreme cyclic loads with magnitude surpassing the nominal maximum load-carrying capacity, a degradation of ship hull girder strength is found in experimental measurement, finite element simulation and extended Smith method computation;
- The comparison between extended Smith method calculation is reasonably correlated with the experimental measurement. The discrepancy may be due to the effect of residual stress. The finite element simulation appears to be more conservative than the extended Smith method in terms of the strength degradation;

To evaluate the calculation uncertainty of the extended Smith method, the evaluation using the procedure developed in Chapter 6 is informative (**Contribution d**). It is indicated that:

- As revealed by the computational uncertainty evaluation, the extended Smith method computation is sensitive the input of initial LSC of structural components, including the ultimate compressive strength, ultimate strain and post-collapse response, as demonstrated by the sensitivity index. However, the effect of the elastic stiffness is negligible;
- In particular, the post-collapse response has the largest influence, since it will affect both of the ultimate compressive strength and post-collapse response in the subsequent cycle.

The research presented in this thesis provides a useful framework for assessing the collapse behaviours of ship structures under extreme cyclic loads. This may improve the conventional assessment of the maximum load-carrying capacity by enabling to:

- i. Assess the post-ultimate strength behaviour of ship structures and evaluate the consequence of a failure event, i.e. assessing the collapse extent. This may be conducted in association with the risk assessment of ship structures while being based upon the current structural assessment code, as most of the developments in this thesis are the extensions to the CSR;
- ii. Evaluate the effect of local buckling and permanent deformation on the ultimate strength in the reloading regime;

7.3 Recommendations

7.3.1 Further Improvement (Numerical Study)

- **Test Matrix**

Although case studies on stiffened panels are also conducted, the numerical study in this thesis is focused on the load-shortening behaviour of ship plates. It is therefore necessary to expand the numerical simulation programme for both plates and stiffened panels. The objective of an extensive numerical campaign is to a) further confirm the validity of the proposed response and updating rule; b) collect extra data for formulating the expression of reduction factors. This further work should be completed by analysing an extensive range of plate slenderness ratio and column slenderness ratio. Comprehensive numerical studies on monotonic compression were conducted by Smith et al. (1991), Tanaka et al. (2014) and Kim et al. (2017), which may provide example test cases in terms of the stiffened panel scantling.

- **Loading Protocols**

Regarding the loading protocol, two further analyses, namely the repeated compression (tension) and the arbitrary cyclic load, would supplement the loading protocol test matrix analysed in this thesis. The former case may be a consequence of ship hull girder bending in either repeated sagging or repeated hogging. The latter case attempts to simulate the behaviour under a more realistic load, as compared with the simplified representation in this thesis. To complete this further improvement, the format of loading protocol in present test matrix may be revised from $-C\varepsilon_{Yeq} \leq \varepsilon \leq C\varepsilon_{Yeq}$ to $-C\varepsilon_{Yeq} \leq \varepsilon \leq 0$ or $0 \leq \varepsilon \leq C\varepsilon_{Yeq}$. In terms of the cyclic load with arbitrary magnitude, it might be difficult to justify a realistic loading history. A very recent study by Jagite et al. (2020) employed hydro-elastic analysis to generate the loading protocol of stiffened panels. This

might be the solution to the aforementioned challenge. However, it should be aware of the fact a hydro-elastic omits the plastic/buckling effects, which may thus be questionable in terms of predicting an extreme loading protocol for local components.

- **Material Hardening Model**

The combined hardening model (Chaboche model) is adopted in part of the NLFEM analysis of this thesis. Although the main reason for considering material hardening in this thesis is to achieve a reliable numerical prediction, it is important to better understand the effects of alternative coefficients in the Chaboche model, which is at present not rigorously for the constructional material of ship structures. The objective of this future work is to analyse the sensitivity of structural response to various material constants. Most experimental data calibrated for the combined hardening model refer to a specific grade of steel. It has been well recognized that material yield stress and Young's modulus would not lead to significant change on the collapse strength of ship structural component, as long as the overall structural slenderness is equivalent (Smith et al., 1987). Hence, it is recommended that the dimensions of the tested structures are scaled properly to ensure that the slenderness ratio remains the same even with different grade of steel.

- **Initial Deflection**

As discussed in Section 3.5.2 of Chapter 3, the compressive strength convergence phenomenon is associated with the accumulation of out-of-plane deflection at each cycle. This finding implies that the initial deflection of structural members may significantly affect the converged compressive strength after multiple loading. Particular attention should be paid to the deflection localisation in the post-collapse regime, which is greatly related to the post-collapse load-shedding. As revealed by Dow and Smith (1984), the localisation of out-of-plane deflection will

not occur if the critical buckling mode is assumed in the numerical simulation, whereas a more realistic deflection profile would lead to deflection localisation. As reflected in the load-shortening curve, the former case usually has a less significant load-shedding than the latter. Further analysis work should be devoted to resolving this, in which the three most common initial deflection profiles, i.e. critical buckling mode, A.R.E mode and the thin-horse mode, are compared in terms of the compressive converged strength and the development of out-of-plane deflection.

- **Welding Residual Stress**

The effects of residual stress is neglected throughout this thesis. There were a few studies in the literature investigating the effects of residual stress on the ultimate strength of structural members under monotonic compression (Khan and Zhang, 2011; Gannon et al., 2016). These studies illustrated a reduced ultimate strength and in-plane stiffness of stiffened panels. However, the residual stress may be shake out due to the cyclic load. This relaxation would probably impose uncertainty on the magnitude of the residual stress. Whilst this is the main reason to omit the residual stress in this thesis, it is beneficial to investigate effects of residual stress on the collapse behaviour under cyclic load. In this future work, apart from analysing the strength performance, the main emphasis may be placed on the comparison of the residual stress field and deflection field after discharge of in-plane load at each cycle between the cases with and without initial residual stress.

- **Boundary Condition**

Numerical case study may be conducted to show the effects of alternative boundary conditions, i.e. simple support versus clamped support and free transverse pull-in versus constrained transverse pull-in. It is commonly recognised

that simple support and free transverse pull-in boundary conditions would correspond a lower buckling strength. However, under the application of cyclic load, an uncertainty may be induced on the post-collapse response, which can influence the strength performance against the subsequent loading. The influence of boundary conditions also has a connection with the model extent (multi-bay and multi-span) and the initial deflection field (number of half-wave). Analysis concerning this issue may refer to Xu et al. (2013) where numerical study was conducted on stiffened panels under monotonic compression.

7.3.2 Further Improvement (Methodology for Predicting Load-Shortening Curve)

- **Reduction Factor φ_1**

Reduction factor φ_1 is introduced to simulate the compressive strength convergence phenomenon of structural members. Whilst this is an essential coefficient for predicting the load-shortening curve and therefore should remain in the methodology, it is necessary to improve the calibration of this coefficient. The most obvious improvement could be to extend the provisional φ_1 expression to be slenderness/aspect ratio dependent, since the coefficient is highly affected by the localisation of the out-of-plane deflection in the post-collapse regime. This can be completed in conjunction with the extensive numerical study as recommended above. In addition, the unloading strain dependency may be revised from the piece-wise form to a polynomial form, which again should be completed with the aid of an extensive numerical data.

- **Reduction Factor φ_2**

Reduction factor φ_2 is introduced to simulate the continuous deterioration of the tensile strength. The challenge is similar to those summarised for reduction factor φ_1 . The solution to the future improvement should be achieved with the help of a

more systematic numerical study. However, one particular issue might be specific attention, which is to investigate, within the assumption of buckling or gross yielding failure, if the “continuous deterioration” is still valid with cycles numbering more than ten.

- **In-Plane Stiffness**

The prediction of in-plane stiffness, including the unloading stiffness and the reloading stiffness, is not fully resolved. It appears that the in-plane stiffness in tension may not require any further enhancement. Instead, the major effort should be devoted to the in-plane stiffness in compression. In the current formulation, the in-plane stiffness after the first unloading is modified as the secant stiffness between the ultimate point and the permanent deformation point. Ever since this modification, it is assumed that the unloading stiffness and the reloading stiffness are the same and will not be subjected to any further revision. Two issues should be tackled: a) it is more reasonable that the unloading stiffness is correlated with the unloading point. In other words, if the unloading takes place further exceeding the ultimate point, the unloading stiffness should be less than that where the unloading occurs closer to the ultimate point; b) the reloading stiffness appears to be reduced at each cycle as shown in the numerical study. Although the in-plane stiffness may not significantly affect the overall hull girder strength prediction, as demonstrated in Chapter 6, a different in-plane stiffness would in the meantime lead to the change of the ultimate strain value in the current formulation. This probably induces a considerable hull girder strength prediction uncertainty. Hence, it is recommended that the reloading stiffness may be revised, perhaps by an additional reduction factor, with an emphasis of achieving better correlation on the ultimate strain. It is known that the unloading stiffness should be equivalent with the elastic stiffness of a buckled structural member, which is dominated by its imperfection. Different amounts of imperfection are accumulated by loading

protocols (e.g. different unloading points and loading cycles). Thus, a good starting point of this research is to investigate the relation between unloading stiffness and the instantaneous distortion within the structural member.

- **Correlation between Unloading and Reloading Strength**

An important assumption in the proposed methodology is that the compressive reloading strength is taken as the same as the unloading strength. It seems that this assumption may be revised as slenderness dependent. As illustrated in Section 4.7.3, the present assumption is reasonable for column slenderness ratio close to 0.2. However, the reloading strength is less correlated with the unloading strength for high column slenderness ratio. In addition, the compressive reloading strength may also be affected by the tensile loading, which is applied before the reloading in compression. As shown in Section 3.4.3, a large tensile loading would lead to a considerable increase of the subsequent compressive reloading strength. Hence, apart from slenderness dependency, it might be necessary to consider the extent of the “pre-tensile loading”.

- **Cyclic Response in Pre-Collapse Regime**

The current methodology is not able to evaluate the strength reduction due to cyclic load that is not surpassed the nominal ultimate point. However, so long as the magnitude of cyclic load is larger than the linear elastic limit, it has a potential of causing strength reduction of the panels. Future efforts should be devoted to this challenge.

7.3.3 Further Improvement (Extended Smith Method)

- **Credible Load Reversal Scenarios**

In this thesis, a nominal load reversal scenario (i.e. unloading point) is specified in terms of the curvature for hull girder and a few test cases are conducted for

methodology validation. However, a more realistic unloading point should be justified in the future research, which can be a fraction/multiple of the nominal ultimate collapse curvature. In the field of earthquake engineering, a design excitation time history is provided based on the past extreme earthquake records. However, equivalent wave train records are lacking in ocean engineering. This may be tackled in combination with a few hydroelasticity or hydro-elastoplasticity simulations.

Meanwhile, the load reversal scenarios can be associated with certain probability levels. This again should be aided by the simulations based on hydroelasticity or hydro-elastoplasticity theory to generate different loading scenarios and to evaluate their probabilities of occurrence. Once these information are available, the safety assessment of ship hull girders can be completed regarding its reloading strength under credible scenarios corresponding to different probability levels, in addition to a conventional monotonic ultimate strength evaluation.

- **Equivalent Loading Protocol**

Regarding the unloading point and loading protocol of ship hull girder, another future challenge may be to justify if it is appropriate to use curvature as the only mean of describing the loading history. This is an issue due to the fact that the overall progressive collapse behaviours may deviate considerably between different methods, such as NLFEM and Smith method. The discrepancy is primarily attributed to the difference in the underpinning algorithm for predicting the collapse behaviours involving geometric and material nonlinearities. In NLFEM, the nonlinearity is tackled by considering the change in deformation and three dimensional stress state when formulating the global stiffness matrix and setting up the equilibrium equation. In the Smith-type method, the nonlinearity is treated in a more efficient way by evaluating the local load-shortening response. It may

also be argued that the difference in the longitudinal model extent should be accounted in the discrepancy. Defining the unloading point only by curvature may correspond to a different status of different methods in relation to the ultimate collapse. Hence, it might be important to propose a different way to define the load reversal point.

7.3.4 Further Improvement (Uncertainty Evaluation)

The uncertainty evaluation in this thesis follows a deterministic procedure. It would be useful to extend the evaluation as a probabilistic approach. The adaptable algorithm is still the core of the probabilistic approach. Instead of a deterministic variation, the critical features are assigned with a probability distribution. Through appropriate sampling technique, a population of the hull strength prediction can be generated. The sensitivity of each critical features to hull girder strength is assessed by evaluating the mean value and coefficient of variation, as compared with the sensitivity index in the deterministic procedure. The benefit of this further improvement is to provide a systematic evaluation of the strength model uncertainty, which can be combined into the reliability analysis.

7.3.5 Potential Development (Structural Dynamic Analysis)

Smith-type progressive collapse analysis is fundamentally a static/quasi-static approach. It is advantageous to extend it into a dynamic analysis due to a) inertia effects may be dominant with high-frequency load, such as the whipping load. A dynamic analysis is therefore needed; b) Once a dynamic structural model is available, it provides a possibility to incorporate with hydrodynamic analysis. This potential development may be achieved in the following ways:

- **Single-Degree-Of-Freedom Approach**

In this approach, the bending moment versus curvature curve is directly used for formulating the nonlinear dynamic equilibrium relationship with single degree of freedom in vertical bending. The bending capacity curve is employed as an evaluation of the internal reaction. Example development refers to Derbanne et al. (2016). Similar approach refers to the plastic hinge method by Iijima et al. (2011). The former example is a true single-degree-of-freedom formulation, whereas in the latter only the nonlinear part is single-degree-of-freedom. However, these previous works only employed the monotonic bending capacity curve. Future development may attempt to utilise cyclic bending moment versus curvature curve, which may then be able to simulate the dynamic collapse behaviour under multi-cycle load.

- **Multi-Degree-Of-Freedom Approach**

A multi-degree-of-freedom approach can be formulated by combining the finite element method with the Smith-type progressive analysis. This concept was originated by Tanaka et al. (2015) for solving the combined vertical bending and torsional bending problem, and was later extended into performing dynamic analysis (Ko et al., 2018). The finite beam element is employed. In the formulation of beam element, the elastic modulus is replaced with the nonlinear tangent stiffness, which is evaluated by the Smith-type progressive collapse analysis at each incremental step. The average stress-strain curve is converted to the average stress-plastic strain curve. Taking the obtained stress-plastic strain curve as pseudo strain-hardening/softening behaviour, the elastoplastic stiffness of the beam element is calculated. Decomposing the strain into elastic and plastic components is essential for detecting unloading. The extended Smith method has

not yet been incorporated in this multi-degree-of-freedom approach, which is recommended as a most important and promising future research.

7.3.6 Potential Development (Hydro-Structural Dynamic Analysis)

Once the dynamic structural model is available, a hydro-structural dynamic analysis methodology may be developed. The coupling between structural analysis and hydrodynamic analysis can be completed by one-way or two-way scheme. In one-way coupling, the external load is first evaluated and then input into the dynamic structural model. The structural response will not affect the hydrodynamics. Conversely, in two-way coupling, the evaluation of external load is conducted considering the effects of instantaneous structural response on the fluid domain. Example developments may be found in Iijima et al. (2011) and Xu et al. (2015) where one-way coupling between structural beam model and hydrodynamic strip theory was adopted. The fluid domain was tackled using boundary element method by Iijima and Fujikubo (2018) where a two-way coupling was achieved. The instantaneous structural response (deflection of the beam) was considered in solving the potential flow problem at each time step.

7.3.7 Potential Development (Fracture and Cracking)

In a conventional ultimate limit state assessment, an elastoplastic buckling failure is evaluated. However, under the application of extreme cyclic load, it is likely that cracking would occur in the highly loaded part of the structures after several cycles of loading. This is also reflected by the ship hull girder failure that a “breaking of its back” could take place, in which a hull girder breaks into two parts due to the fracture at midship section. In this regards, further research should be devoted to incorporate the ultra low-cycle fatigue as another failure mode in the extended Smith method proposed in Chapter 5.

7.3.8 Prospective Application of the Cyclic Method

A prospective application of the cyclic methods developed for structural members and ship hull girder is to be employed in the real-time monitoring of the ultimate ship hull girder strength, which is denoted as the real-time capacity in the following for brevity. As a clarification, the ultimate ship hull girder strength calculated with the nominal properties and scantlings refers to be the as-built capacity. By contrast, the real-time capacity indicates the ultimate ship hull girder strength at the instantaneous moment (or a certain time slot in practice). It may differ from the as-built capacity due to the changes in imperfection, an extreme load event, corrosion and/or accidental damages.

The degradation caused by corrosion or accidental damages can be assessed by the conventional monotonic approach through a scantling reduction and damaged component removal respectively. Application examples of this kind include Kim et al. (2014), Benson et al. (2013) and Fujikubo et al. (2012).

However, to account for the influence of an extreme load event, the cyclic method should be employed as it has the potential to be integrated with the hydrodynamic analysis as introduced in Section 7.3.5 and Section 7.3.6. In terms of the real-time monitoring, a few strain gauges may be installed on the ships. The measurements could then be used to generate the load history of the ships at specific time slots, which can become the input into the cyclic method to update the real-time ultimate ship hull girder strength. This cannot be completed with the monotonic method, as it is unable to deal with the load reversal and hence the corresponding structural response.

Similarly, the variation of the ultimate ship hull girder strength due to the changes in imperfection can be evaluated with this prospective concept. With the application of cyclic load, the imperfection in the plating and stiffener may be

permanently altered from their as-built configurations. These may include the cumulatively growing of the imperfection magnitude and the change in the imperfection shape. Both could render a difference in the ultimate ship hull girder strength. Although this aspect could be accounted using the monotonic approach, much more measurements relating to the imperfection are required. However, with an improved cyclic method, the influence in the variation of imperfection may be treated only with the strain gauge data. This research could benefit the development of an on-board decision-making tool, in which case an efficient and reasonable computational method is necessary.

References

- 14th ISSC, 2000. Report of Ultimate Strength Committee III.1, Nagasaki, Japan.
- 15th ISSC, 2003. Report of Ultimate Strength Committee III.1, San Diego, United States.
- 18th ISSC, 2012. Report of Ultimate Strength Committee III.1, Rostock, Germany.
- Amlashi, J., Moan, T., 2008. Ultimate strength analysis of a bulk carrier hull girder under alternate hold loading condition – A case study Part 1: Nonlinear finite element modelling and ultimate hull girder capacity. *Marine Structures*, 21, 327 – 352.
- Antoniou, A.C., 1980. On the maximum deflection of plating in newly built ships. *Journal of ship research*, 24.
- Bishop, R.E.D., Price, W.G., 1979. *Hydroelasticity of ships*, Cambridge University Press.
- Benson, S., Downes, J., Dow, R.S., 2013. Compartment level progressive collapse analysis of lightweight ship structures. *Marine Structures* 31, 44–62.
- Benson, S., Abubakar, A., Dow, R.S., 2013. A comparison of computational methods to predict the progressive collapse behaviour of a damaged box girder. *Engineering Structures*, 48, 266-280.
- Bishop, R.E.D., Price, W.G., Wu, Y.S., 1986. A general linear hydroelasticity theory of floating structures moving in a seaway. *Philosophy Transaction of Royal Society*, 316, 375-426.
- Bradfield, C.D., 1980. Tests on plates loaded in in-plane compression. *Journal of Constructional Steel Research*, 1, 27-37.

- Benson, S., Collette, M.D., 2017. Finite element methods and approaches. Encyclopedia of Maritime and Offshore Engineering, John Wiley & Sons, Ltd.
- Benson, S., Downes, J., Dow, R.S., 2015. Overall buckling of lightweight stiffened panels using an adapted orthotropic plate method. *Engineering Structures*, 85, 107–117.
- Benson, S., 2011. Progressive collapse assessment of lightweight ship structures. PhD thesis, Newcastle University, UK.
- Class NK, 2014. Investigation report on structural safety of large container ships.
- Cui, H., Yang, P., 2018. Ultimate strength and failure characteristics research on steel box girders under cyclic-bending moments. *Journal of Marine Science and Technology*, 23, 926–936.
- Caldwell, J.B., 1965. Ultimate longitudinal strength. *Trans., RINA*, 107, 411 – 430.
- Chalmers, D.W., 1993. Design of ship's structures. London: HMSO.
- Caldwell, J.B., 1965. Ultimate longitudinal strength. *Trans RINA*.
- Carlsen, C.A., Czujko, J., 1978. The specification of post-welding distortion tolerances for stiffened plates in compression. *The Structural Engineer*, 54A, 133-141.
- Chen, Y., Kutt, L., Piaszczyk, C., Bienek, M., 1983. Ultimate strength of ship structures. *SNAME Trans.*, 91, 149–168.
- Chaboche, J.L., 1986. Time-independent constitutive theories for cyclic plasticity. *International Journal of Plasticity*, 2(2), 149–188.
- Collette, M., 2005. Strength and reliability of aluminium stiffened panels. PhD thesis, Newcastle University, UK.

- Dow, R.S., 1991. Testing and analysis of a 1/3 scale frigate model. In: *Advances in Marine Structures 2*. Dunfermline, Scotland: Elsevier, 749–773.
- Dow, R.S., Smith, C.S., 1986. FABSTRAN: A computer program for frame and beam static and transient response analysis (Nonlinear), ARE report TR86205.
- Dwight, J.B., Ractliffe, A.T., 1967. The strength of thin plates in compression.. In: *Symposium on thin walled steel structures*.
- Dowling, P.J., Chatterjee, S., Frieze, P.A., 1973. Experimental and predicted collapse behaviour of rectangular steel box girders. In: *International Conference on Steel Box Girder Bridges*, London.
- Dow, R.S., Smith, C.S., 1984. Effects of localized imperfections on compressive strength of long rectangular plates. *Journal of Construal Steel Research*, 4, 51–76.
- Dowling, P.J., Frieze, P.A., Harding, J.E., 1977. Imperfection sensitivity of steel plates under complex edge loading. In: *2nd International Colloquium on stability of steel structures*, Liege.
- Dow, R.S., 1997. Structural redundancy and damage tolerance in relation to ultimate ship hull strength. In: *Advances in Marine Structures 3*, DERA, Dunfermline, Scotland.
- Derbanne, Q., Lauzon, J. de, Bigot, F., Malenica, S., 2016. Investigations of the dynamic ultimate strength of a ship's hull girder during whipping. *Proceedings of International Symposium on Practical Design of Ships and others Floating Structures (PRADS)*, September 4–8, Copenhagen, Denmark.
- Darie, I., Rörup, J., 2017. Hull girder ultimate strength of container ships in oblique sea. In: *6th International Conference on Marine Structures*, Lisbon, Portugal.

- Fukumoto, Y., Itoh, Y., 1984. Basic compressive strength of steel plates from test data. *Proceeding Japan Society of Civil Engineers*, 334, 91.
- Fukumoto, Y., Kusama, H., 1985. Cyclic bending tests of thin-walled box beams. In *Proceedings of JSCE, Structural engineering/Earthquake engineering*, 2.
- Faulkner, D., 1977. Compression tests on welded eccentrically stiffened plate panels. *Steel Plated Structures*, Dowling P.J. (Eds), 581-617, London.
- Fukumoto, Y., Usami, T., Itoh, T., Nethercot, D.A., 1983. A numerical database approach to the ultimate compressive strength of unstiffened plates. In: 3rd ECCS International Conference on Stability of Metal Structures, Paris, France.
- Frankland, J.M., 1940. The strength of ship plating under edge compression. EMM report, US.
- Faulkner, D.A., Adamchak, J.C., Snyder, G.J., Vetter, M.F., 1973. Synthesis of welded grillages to withstand compression and normal loads. *Computers and Structures*, 3, 221–246.
- Fujikubo, M., Kaeding, P., Yao, T., 2000. ISUM rectangular plate element with new lateral shape function (1st report): Longitudinal and transverse thrust. *Journal of Society of Naval Architect of Japan*, 187, 209-219.
- Fujikubo, M., Zubair Muis Alie, M., Takemura, K., Iijima, K., Oka, S., 2012. Residual hull girder strength of asymmetrically damaged ships. *Journal of Japan Society of Naval Architects and Ocean Engineers*, 16, 131-140.
- Frieze, P.A., Lin, Y.T., 1991. Ship longitudinal strength modelling for reliability analysis. In: *Marine Structural Inspection, Maintenance and Monitoring Symposium*, Arlington, Virginia.

- Fukumoto, Y., Kusama, H., 1985. Cyclic behaviour of plates under in-plane loading. *Engineering Structures*, 7, 56–63.
- Gordo, J.M., Guedes Soares, C., 1993. Approximate load shortening curves for stiffened plates under uniaxial compression. *Integrity of Offshore Structures* (Faulkner et al, Eds.), UK.
- Gordo, J.M., Guedes Soares, C., 2013. Experiments on three mild steel box girders of different spans under pure bending moment. In: 4th International Conference on Marine Structures, Helsinki, Finland.
- Gordo, J.M., 2015. Effect of initial imperfections on the strength of restrained plates. *Journal of Offshore Mechanics and Arctic Engineering*, 137.
- Gannon, L., Liu, Y., Pegg, N., Smith, M.J., 2016. Nonlinear collapse analysis of stiffened plates considering welding-induced residual stress and distortion. *Ships and Offshore Structures*, 11, 228–244.
- Goto, Y., Toba, Y., Matsuoka, H., 1995. Localization of plastic buckling patterns under cyclic loading. *Journal of Engineering Mechanics*, 121, 493–501.
- Horne, M.R., Narayanan, R., 1976. Ultimate capacity of stiffened plates used in girders. *Proceeding of Institution of Civil Engineers*, 61(2), 253-280.
- Horne, M.R., Montague, P., Narayanan, R., 1977. Influence of strength of compression panels of stiffener section, spacing and welded connection. *Proceeding of Institution of Civil Engineers*, 63(2), 1-20.
- Hess, P.E., Adamchak, J.C., Falls, J., 1997. Failure analysis of an inland waterway oil bunker tanker. Survivability, structures and material directorate technical report. Naval surface warfare centre, Carderock division.

- Hughes, O.F., 1988. Ship structural design: A rationally-based, computer-aided optimization approach. SNAME.
- International Association of Classification Societies (IACS), 2019. Common Structural Rules for Bulk Carriers and Oil Tankers.
- International Association of Classification Societies (IACS), 2015. Longitudinal Strength Standard for Container Ships.
- Iijima, K., Fujikubo, M., 2015. Cumulative collapse of a ship hull girder under a series of extreme wave loads. *Journal of Marine Science and Technology*, 20 (3): 530–541.
- Iijima, K., Kimura, K., Xu, W., Fujikubo, M., 2011. Hydroelastoplasticity approach to predicting the post-ultimate strength behaviour of a ship's hull girder in waves. *Journal of Marine Science Technology*, 16(4): 379–389.
- Iijima, K., Fujikubo, M., 2018. Hydro-elastoplastic behaviour of VLFS under extreme vertical bending moment by segmented beam approach. *Marine Structures*, 57, 1-17.
- John, W., 1874. On the strength of iron ship. *Transaction of Institute of Naval Architects*, 15, 74-93.
- Jagite, G., Bigot, F., Derbanne, Q., Malenica, S., Sourne, Lauzon J., Cartraud, P., 2019. Numerical investigation on dynamic ultimate strength of stiffened panels considering real loading scenarios. *Ships and Offshore Structures*, 14: sup1, 374-386.
- Jagite, G., Bigot, F., Derbanne, Q., Malenica, S., Sourne, Lauzon J., Cartraud, P., 2020. A parametric study on the dynamic ultimate strength of a stiffened panel subjected to wave- and whipping-induced stresses. *Ships and Offshore Structures*, DOI: 10.1080/17445302.2020.1790985.

- Jia, L., J., Kuwamura, H., 2015. Ductile fracture model for structural steel under cyclic large strain loading. *Journal of Constructional Steel Research* 106, 110–121.
- Johnson, G. R., and W. H. Cook, 1985. Fracture Characteristics of Three Metals Subjected to Various Strains, Strain rates, Temperatures and Pressures. *Engineering Fracture Mechanics*, 21, 31–48.
- Kaminski, M., L., 1992. Cyclic compression of imperfect plates. PhD thesis, Delft University of Technology.
- Krolo P, Grandić D, Smolčić Ž., 2016. Experimental and numerical study of mild steel behaviour under cyclic loading with variable strain ranges. *Advances in Materials Science and Engineering*, 2016, 1–13.
- Kim, D.K., Kim, H.B., Park, D.H., Hairil, M., Paik, J.K., 2019. A practical diagram to determine the residual longitudinal strength of grounded ship in Northern Sea Route. *Ships and Offshore Structures*, 15, 683-700.
- Kim, D.K., Lim, H.L., Kim, M.S., Hwang, O.J., Park, K.S., 2017. An empirical formulation for predicting the ultimate strength of stiffened panels subjected to longitudinal compression. *Ocean Engineering*, 140, 270–280.
- Kim, D.K., Kim, H.B., Zhang, X.M., Li, C.G., Paik, J.K., 2014. Ultimate strength performance of tankers associated with industry corrosion addition practices. *International Journal of Naval Architecture and Ocean Engineering*, 6, 507-528.
- Kmieciak, M., 1981. Factors affecting the load-carrying capacity of plates. Technical University of Szczecin, Ship Research Institution, Report No. 115.
- Khan, I., Zhang, S.M., 2011. Effects of welding-induced residual stress on ultimate strength of plates and stiffened panels. *Ships and Offshore Structures*, 6, 297–309.

- Ko, H., Tatsumi, A., Iijima, K., Fujikubo, M., 2018. Collapse analysis of ship hull girder using hydro-elastoplastic beam model. In: 37th International Conference on Ocean, Offshore and Arctic Engineering (OMAE), Madrid, Spain.
- Lin, Y.T., 1985. Ship longitudinal strength modelling. PhD thesis, University of Glasgow, Scotland.
- Lee, Y.W., White, N., Wang, Z.H., Zhang, S.M., Hirdaris, S.E., 2012. Comparison of springing and whipping responses of model tests with predicted nonlinear hydro-elastic analyses. *International Journal of Offshore and Polar Engineering*, 22, 1-8.
- Lee, Y.W., White, N., Wang, Z.H., Hirdaris, S.E., 2012. Time domain analysis of springing and whipping responses acting on a large container ship. In: 30th International Conference on Ocean, Offshore and Arctic Engineering (OMAE), Rotterdam, Netherlands.
- Moxham, K.E., 1971. Buckling tests on individual welded steel plates in compression. Cambridge University, Report: CUED/C-Struct/TR3.
- Masaoka, K., Nagao, M., Shibahara, M., Tsubogo, T., 2006. Experimental study on collapse behaviour of a stiffened box-section girder under cyclic loading. In: *Symposium on welded structure*.
- Nishihara, S., 1983. Analysis of ultimate strength of stiffened rectangular plate (4th report): on the ultimate bending moment of ship hull girder. *Journal of the Society of Naval Architect of Japan*, 154, 367-375 (In Japanese).
- Nielsen, J.A., Johnsen, F., Gimsing, N.J., 1980. The strength of plates in compression. Report R122, Technical University of Denmark (in Danish).
- Niho, O., 1978. Ultimate strength of plated structures. PhD thesis, University of Tokyo (In Japanese).

- Nishihara, S., 1983. Analysis of ultimate strength of stiffened rectangular plate (4th report): on the ultimate bending moment of ship hull girder. *Journal of Society of Naval Architect of Japan*, 154, 367-375 (in Japanese).
- Paik, J.K., Thayamballi, A., 1997. An empirical formulation for predicting the ultimate compressive strength of stiffened panels. *Proceeding of 7th International Offshore and Polar Engineering Conference*, Honolulu, US.
- Paik, J.K., Lee, D.H., Park, D.K., Ringsberg, J.W., 2020. Full-scale collapse testing of a steel stiffened plate structure under axial-compressive loading at a temperature of -80°C . *Ships and Offshore Structures*.
- Paik, J.K., Lee, D.H., Noh, S.H., Park, D.K., Ringsberg, J.W., 2020. Full-scale collapse testing of a steel stiffened plate structure under cyclic axial-compressive loading. *Structures*, 26, 996-1009.
- Paik, J.K., Hughes, O.F., 2010. *Ship Structural Analysis and Design*. SNAME.
- Paik, J.K., Seo, J.K., 2009a. Nonlinear finite element method models for ultimate strength analysis of steel stiffened-plate structures under combined biaxial compression and lateral pressure actions: Part I: Plate elements. *Thin-Walled Structures*, 47, 1008–1017.
- Paik, J.K., Seo, J.K., 2009b. Nonlinear finite element method models for ultimate strength analysis of steel stiffened-plate structures under combined biaxial compression and lateral pressure actions: Part II: Stiffened panels. *Thin-Walled Structures*, 47, 998–1007.
- Paik, J.K., Mansour, A.E., 1995. A simple formulation for predicting the ultimate strength of ships. *Journal of Marine Science and Technology*, 1(1), 52–62.

- Paik, J.K., Kim, D.K., Park, D.H., Kim, H.B., Mansour, A.E., Caldwell, J.B., 2013. Modified Paik–Mansour formula for ultimate strength calculations of ship hulls. *Ships and Offshore Structures*, 8, 245-260.
- Paik, J.K., Thayamballi, A.K., 2003. Ultimate limit state design of steel-plated structures.
- Reckling, K., 1979. Behaviours of box girders under bending and shear. Proceeding of ISSC, Paris, France.
- Reckling, K.A., 1979. Preliminary report on box girder experiments (included report of Committee II.2 on nonlinear structural response). In: 7th International Ship Structures Conference, Paris, France.
- Rutherford, S.E., Caldwell, J., 1990. Ultimate longitudinal strength of ships - a case study. *Transactions of the Society of Naval Architects and Marine Engineers*, 98, 441-471.
- Smith, C.S., 1975. Compressive strength of welded steel ship grillages. *Trans. RINA*, 117.
- Smith, C.S., Davidson, P.C., Chapman, J.C., Dowling, P.J., 1987. Strength and stiffness of ship's plating under in-plane compression and tension. *Trans. RINA*, 130, 277-294.
- Smith, C.S., Dow, R.S., 1986. Ultimate strength of a ship's hull under biaxial bending. ARE TR 86204, Admiralty Research Establishment, Dunfermline, Scotland.
- Smith, C.S., 1977. Influence of local compressive failure on ultimate longitudinal strength of a ship's hull. In: International Symposium on Practical Design of Ships and others Floating Structures (PRADS), Tokyo, Japan.

- Smith, C.S., 1981. Imperfection effects and design tolerances in ships and offshore structures. *Transaction of the Institution of Engineers and Shipbuilders in Scotland*, 124, 37-46.
- Smith, C.S., Anderson, N., Chapman, J.C., Davidson, P.C., Dowling, P.J., 1991. Strength of stiffened plating under combined compression and lateral pressure. *Trans RINA*, 134, 131-147.
- Syrigou, M., Benson, S.D., Dow, R.S., 2018. Progressive collapse assessment of intact box girders under combined bending and torsional loads. In: *International Conference on Ships and Offshore Structures*, Gothenburg, Sweden.
- Syrigou, M.S., Dow, R.S., 2018. Strength of steel and aluminium alloy ship plating under combined shear and compression/tension. *Engineering Structures*, 166, 128–141.
- Salvesen, N., Tuck, E.O., Faltinsen, O., 1970. Ship motions and sea loads. *Trans SNAME*, 78, 250-287.
- Sumi, Y., Fujikubo, M., Fujita, H., Kawagoe, Y., Kidogawa, M., Kobayashi, K., Nakano, T., Iwano, J., Takahira, T., Tamura, K., Ueda, N., 2015. Final Report of Committee on Large Container Ship Safety, Japan.
- Tanaka, Y., Endo, H., 1988. Ultimate strength of stiffened plates with their stiffeners locally buckled in compression. *Journal of the Society of Naval Architects of Japan*, 164, 456-467 (In Japanese).
- Tanaka, S., Yanagihara, D., Yasuoka, A., Harada, M., Okazawa, S., Fujikubo, M., Yao, T., 2014. Evaluation of ultimate strength of stiffened panels under longitudinal thrust. *Marine Structures*, 36, 21-50.

- Tanaka, Y., Ogawa, H., Tatsumi, A., Fujikubo, M., 2015. Analysis methods of ultimate hull girder strength under combined loads. *Ships and Offshore Structures*, 10, 587-598.
- Timoshenko, S., Woinowsky-Krieger, S., 1959. *Theory of plate and shell*. McGraw-Hill, New York.
- Tatsumi, A., Fujikubo, M., 2020. Ultimate strength of container ships subjected to combined hogging moment and bottom local loads part 1: Nonlinear finite element analysis. *Marine Structures*, 69, 102683.
- Tatsumi, A., Ko, H., Fujikubo, M., 2020. Ultimate strength of container ships subjected to combined hogging moment and bottom local loads, Part 2: An extension of Smith's method. *Marine Structures*, 71, 102738.
- Ueda, Y., Rashed, S.M.H., 1984. The idealized structural unit method and its application to deep girder structures. *Computers & Structures*, 18, 277–293.
- Ueda, Y., Rashed, S.M.H., 1984. The idealized structural unit method and its application to deep girder structures. *Computers & Structures*, 18, 277–293.
- Ueda, Y., Masaoka, K., 1995. Ultimate strength analysis of thin plated structures using eigen-function (2nd report): rectangular plate element with initial imperfection. *Journal of Society of Naval Architect of Japan*, 178, 463-471.
- Ueda, Y., Yao, T., Nakacho, K., Tanaka, Y., Handa, K., 1983. Compressive ultimate strength of rectangular plates with initial imperfection due to welding (3rd report). Prediction method of compressive ultimate strength. *Journal of Society of Naval Architect of Japan*, 154, 345-355 (in Japanese).
- Ueda, Y., Yao, T., 1985. The influence of complex initial deflection modes on the behaviour and ultimate strength of rectangular plate in compression. *Journal of Constructional Steel Research*, 5, 265-302.

- Wong, Y.L., 1977. Some considerations in the ultimate strength of ships. MSc Thesis, University of Glasgow.
- Winter, G., 1947. Performance of thin steel compression flanges. Transactions of the American Society of Civil Engineers, 112, 527-554.
- Xu, M.C., Song, Z.J., Zhang, B.W., Pan, J., 2018. Empirical formula for predicting ultimate strength of stiffened panel of ship structure under combined longitudinal compression and lateral loads. Ocean Engineering, 162, 161–175.
- Xu, M.C., Yanagihara, D., Fujikubo, M., Guedes Soares, C., 2013. Influence of boundary conditions on the collapse behaviour of stiffened panels under combined loads. Marine Structures, 34, 205-225.
- Xu, W.J., Duan W.Y., Han, D.F., 2015. Investigation into the dynamic collapse behaviour of a bulk carrier under extreme wave loads. Ocean Engineering, 106, 115-127.
- Yao, T., 1980. Ultimate compressive strength of ship plating. PhD thesis, Osaka University, Japan.
- Yao, T., Nikolov, P., I., 1990. Buckling/plastic collapse of plates under cyclic loading. Journal of the Society of Naval Architects of Japan, 168.
- Yao, T., Fujikubo, M., Nie, C., Kamiyama, S., 1995. Development and application of simple plate model to simulate collapse behaviour under thrust. Journal of the Society of Naval Architects of Japan, 178, 439-449 (in Japanese).
- Yao, T., Fujikubo, M., 2016. Buckling and ultimate strength of ship and ship-like floating structures. Elsevier.

- Yao, T., Nikolov, P.I., Miyagawa, Y., 1992. Influence of welding imperfections on stiffness of rectangular plate under thrust. In: Karlsson, L., Lindgren, L.E., Jonsson, M., editors. Mechanical effects of welding. Springer-Verlag, 261-268.
- Yao, T., 1980. Compressive ultimate strength of structural members in ship structure. PhD thesis, Osaka University, Japan (in Japanese).
- Yao, T., Fujikubo, M., Yanagihara, D., Varghese, B., Niho, O., 1998. Influences of welding imperfections on buckling/ultimate strength of ship bottom plating subjected to combined bi-axial thrust and lateral pressure. In: International symposium on thin-walled structures, Singapore.
- Yao, T., Nikolov, P.I., 1990. Buckling/plastic collapse of plates under cyclic loading. Journal of the Society of Naval Architects of Japan, 168, 449–462.
- Yao, T., Fujikubo, M., Nie, C., Kamiyama, S., 1995. Development and application of simple plate model to simulate collapse behaviour under thrust. Journal of the Society of Naval Architects of Japan, 178, 439–449.
- Zhang, S.M., Khan, I., 2009. Buckling and ultimate capability of plates and stiffened panels in axial compression. Marine Structures, 22, 791-808.